1987

The Effect of Steel Fibers and Compressive Reinforcement on the Plastic Rotation Capacity and Properties of Reinforced Concrete Continuous Beams

Nizam A. Qassem

THE EFFECT OF STEEL FIBERS AND COMPRESSIVE REINFORCEMENT ON THE PLASTIC ROTATION CAPACITY AND PROPERTIES OF REINFORCED CONCRETE CONTINUOUS BEAMS

by

NIZAM A. QASSEM

A thesis submitted
in partial fulfillment of the requirements for the
Degree Master of Science
Major in Civil Engineering
South Dakota State University
1987

THE EFFECT OF STEEL FIBERS AND COMPRESSIVE REINFORCEMENT ON THE PLASTIC ROTATION CAPACITY AND PROPERTIES OF REINFORCED CONCRETE CONTINUOUS BEAMS

This thesis is approved as a creditable and independent investigation by a candidate for the degree, Master of Science, and is acceptable for meeting the thesis requirements for this degree. Acceptance of this thesis does not imply that the conclusions reached by the candidate are necessarily the conclusions of the major department.

Dr. M. Nadim Hassoun — Date
Major Advisor

Dr. Dwayne A. Rollag — Date
Head, Civil Engineering Department

DEDICATION

I wish to dedicate this thesis to my family for their encouragement, support and patience throughout my study.

ACKNOWLEDGEMENTS

The author wishes to express sincere appreciation to Dr. M. Nadim Hassoun for his assistance and guidance throughout the course of this study.

Acknowledgements are extended to Dr. Dwayne A. Rollag, Head of the Civil Engineering Department for his support and encouragement, Dr. Robert J. Lacher for his assistance with the statistical analysis of the data. Marilyn Eighmy for expertly typing this thesis, Roger M. Tolrud, laboratory technician for his help in handling the necessary laboratory equipment, Jeanne Lesinski for correcting this manuscript, and to Bekaert Steel Wire Corporation for supplying the steel fibers.

The author wishes to thank the faculty and students for their suggestions and assistance during testing.

NAQ

TABLE OF CONTENTS

TABLE OF CONTENTS (Continued)

LIST OF TABLES

LIST OF TABLES (Continued)

LIST OF TABLES (Continued)

LIST OF TABLES (Continued)

LIST OF TABLES (Continued)

LIST OF TABLES (Continued)

LIST OF FIGURES

LIST OF FIGURES (Continued)

LIST OF FIGURES (Continued)

LIST OF FIGURES (Continued)

LIST OF FIGURES (Continued)

LIST OF FIGURES (Continued)

NOTATIONS

a = depth of the equivalent rectangular stress block

a_1, a_2 = the length over which curvature is measured at middle support

A = effective tension area of concrete surrounding one bar (this value is used for control of cracking)

ACI = American Concrete Institute

A_s = area of main steel (tension steel)

A_s' = area of compression steel

ASTM = American Society for Testing Materials

A_v = cross section area of one stirrup

b = width of the beams

c = distance from extreme compression fibers to neutral axis

C_c = compression force in a concrete compression block

c_s = compression force in compression steel

d = distance from the extreme compression fibers to the centroid of the tension steel

d' = distance from the extreme compression fibers to the centroid of the compression steel

d_c = distance from tension extreme fiber to center of closest bar (used in crack control)

D = diameter of standard cylinder

E_c = modulus of elasticity of concrete = $33w^{1.5}\sqrt{f'_c}$

E_{ca} = actual modulus of elasticity from testing

E_{cs} = predicted modulus of elasticity of fibrous concrete

$E_c I_e$ = flexural stiffness of the beams

E_s = modulus of elasticity of steel = 29,000 ksi

f = flexure stress = MC/I

f_c = concrete stress at working load

f_{ct} = split cylinder strength = $6.7\sqrt{f'_c}$

f_{ctai} = actual initial split cylinder tensile strength

f_{ctau} = actual ultimate split cylinder tensile strength

f_{cts} = predicted ultimate split cylinder tensile strength of fibrous concrete

f'_c = 28-day compressive strength of concrete (Standard Cylinder Strength)

f_r = modulus of rupture of concrete = $7.5\sqrt{f'_c}$

f_{ri} = actual first modulus of rupture from testing

f_{rsi} = predicted first modulus of rupture of fibrous concrete

f_{ru} = actual ultimate modulus of rupture from testing

f_{rsu} = predicted ultimate modulus of rupture of fibrous concrete

f_s = main steel stress

f'_s = compression steel stress

f_y = yield strength of steel reinforcement

h = total depth of the section

H_L = plastic hinge length

I = moment of inertia

I_{cr} = moment of inertia of a cracked transformed section

I_{cr1}, I_{cr2} = moment of inertia of a cracked transformed doubly and singly reinforced section respectively

I_e = effective moment of inertia to compute deflection

I_{e1}, I_{e2} = effective moment of inertia to compute deflection for doubly and singly reinforced sections respectively

I_{ef} = regression multiplier factor for predicting effective moment of inertia of fibrous concrete

I_g = moment of inertia of cross section of concrete neglecting steel

k = a factor relality the position of neutral axis to d

k_1 = k for doubly reinforced section

$k_1 d$ = depth of neutral axis for doubly reinforced section

k_2 = k for singly reinforced section

$k_2 d$ = depth of netural axis for singly reinforced section

k_u = k at ultimate

$k_u d$ = depth of neutral axis at ultimate

kips = kilopounds (1000 pounds)

L = span length, length of the cylinder

L_1 = limit state when steel yields

M = design bending moment

M_a = moment of service load at midspan

M_A, M_B = plastic moment at A and B

M_{FA}, M_{FB} = fixed end moment at A and B

M_{cr} = cracking moment

M_p = plastic moment

M_u = ultimate moment capacity at a section

M_{y1} = yield moment at section 1 (middle support)

M_{y2} = yield moment at section 2 (midspan)

m = regression multiplier for predicting the modulus elasticity of fibrous concrete

n = modular ratio = E_s/E_c

p = applied load

p_u = ultimate load

p_y = yield load

p_{y1} = yield load of section 1 (middle support)

p_{y2} = yield load of section 2 (midspan)

p'_y = actual yield load

p'_u = actual ultimate load

psi = pounds per square inch

pcf = pounds per cubic foot

r' = experimental load redistribution factor p'_u/p'_y

R = radius of curvature

s_{min} = minimum distance between stirrups

S.F. = steel fiber

T = tension force in main steel

V_u = maximum shearing force

v_c = concrete shearing strength $2\sqrt{f'_c}$

v_s = shear strength resisted by shear reinforcement

v_u = ultimate shear stress V_u/bd

w = width of crack; unit weight of concrete

w_1, w_2 = calculated crack width for doubly and singly reinforced section

w_E = external work

w_I = internal work

w/c = water cement ratio

x = the distance from the load to outside supports

y_t = distance from centroidal axis of cross section, neglecting reinforcement, to extreme top fiber

z = factor related to crack width = $f_s \sqrt[3]{Ad_c}$

α = regression multiplier factor for predicting curvature distribution factor of fibrous concrete

γ = regression multiplier factor for predictor ductility index of fibrous concrete

β = curvature distribution factor

β', β'' = ratio of all distances from netural axis $k_1 d$, $k_2 d$ to tension face and to the steel centroid respectively

Δ_{a1} = change in length a_1 due to rotation

Δ_{a2} = change in length a_2 due to rotation

ΔL = axial deformation

Δ = deflection at service load

Δp = plastic deflection

$\varepsilon = \Delta L/L$

ε_c = concrete strain

ε_s = main steel strain

ε'_s = compression steel strain

ε_{sy} = compression steel strain at limit state L_1

ε = plastic strain = $\varepsilon_{cu} - \varepsilon_{cy}$

ε_{cu} = ultimate concrete strain

ε_{cy} = concrete strain when main steel yield

ε_{c1} = concrete strain at limit state L_1

ε_{s1} = steel strain at limit state L_1 (yield strain of main steel)

σ = stress load/area

ϕ = curvature ε_c/kd

ϕ_e = elastic curvature

ϕ_u = ultimate curvature

ϕ_y = yield curvature

θ = rotation in radian

θ_c = total rotation in radians when concrete started to fail at middle support

θ_e = elastic rotation

θ_p = calculated rotation capacity

θ_{pc} = magnitude of plastic rotation capacity = $\theta_u - \theta_y$

θ_{ps} = predicted plastic rotation capacity of fibrous concrete beams

θ_r = total rotation in radians prior to rupture

θ_y = total rotation in radians at linear limit (first yield)

θ_u = total rotation in radian at utlimate (second yield)

θ_1, θ_2 = calculated required rotations for doubly and singly reinfroced section

λ = regression multiplier for predicting plastic hinge of fibrous concrete beams

μ = ductility index ϕ_u/ϕ_y

μ' = ductility index for fibrous concrete

ρ = ratio of main steel = A_s/bd

ρ_b = balanced steel ratio

ρ' = ratio of compression steel

% = percentage

$\int$ = integration symbol

CHAPTER 1

INTRODUCTION

1.1 A General Overview

A reinforced concrete structure must satisfy adequate strength at ultimate load stage and serviceability at service load, and it must meet the ductility requirements. Unfortunately reinforced concrete, unlike steel, tends to fail in a relatively brittle manner due to its limited ductility, which has led to a limitation in steel quantities to be used by the ACI Code. An over-reinforced concrete section will fail by crushing of concrete before the yielding of steel, whereas in under-reinforced section the steel will yield before the crushing of concrete. Ductility plays a significant role in structures, especially those built in seismic zones or those subjected to blast or suddenly applied loads. Numerous investigations have dealt with ductility in reinforced concrete structures, thus leading to improved economy, and sometimes to simplified design procedures. New design concepts have been developed, especially the use of the limit state design concept, which relies heavily on the inelastic behavior of reinforced concrete. For the limit state design concept to be valid, a concrete structure must have adequate rotation capacity that exceeds what is required by the plastic hinges. Plastic hinge rotation depends primarily on concrete compression failure. A low compressive strain in concrete will reduce the degree of moment redistribution;

therefore, a collapse mechanism will develop without reaching the ultimate load capacity, unless the ultimate strain can be increased in some way, as adding fibers to the concrete mix.

1.2 Concept of Limit State Design

A reinforced concrete structure remains in the elastic range when loaded under low stress. But when loads are increased to higher stages, it deviates from elastic behavior. Therefore, more theories were developed to describe such behavior, and the theory that received the most attention is the concept of limit state design, which gives a realistic idea of the strength of the structure at failure. A great deal of research on plastic concepts was done by many investigators, such as Baker (7), as early as 1949.

For the limit design method to be valid, it should satisfy the following conditions:

1. Mechanism condition: sufficient plastic hinges are formed to convert the structure to a mechanism.
2. Limit equilibrium: the bending moments must be in equilibrium with the applied loads.
3. Yield condition: the ultimate moment is not exceeded at any point in the structure.
4. Rotation compatibility: the rotation required by the plastic hinge is less than the rotation available for the member to allow the structure to develop a mechanism.

The advantage of limit design method over the conventional elastic method is twofold: First, it reduces the amount of reinforcement so as to achieve economy; second, it reduces the congestion of reinforcement which often occurs in high-moment areas, such as at the junction of girders with columns.

1.3 Historical Background

Reinforced concrete has been recognized to behave inelastically for a long time, and a considerable research effort was established to describe such behavior. In the 1940's, Professor A.L.L. Baker (7), studied the concept of inelastic behavior of reinforced concrete. He showed that structures are able to support additional loads after first yielding, especially in under-reinforced concrete sections.

Since that time, many researchers have concurred with the concept of plastic analysis in reinforced concrete and proposed hypotheses on control and evaluation of the behavior of plastic hinges in concrete.

In 1955, Chan (16) concluded that the plastic rotations may be increased by using lateral binding. He also concluded that under-reinforced sections tend to develop high plastic rotation. Similar conclusions were drawn by Nawy, Danesi and Crasko (40). In 1963, Cohn (19) established a test program on redundant reinforced concrete beams and concluded that as long as the main steel (ρ) is less than 2 and the distribution factor P_u/P_y does not exceed 1.6,

full moment redistribution can be obtained. In 1980, Kauskik, Ramamurthy and Kokeuja (32) concluded that ultimate load capacity can be attained as long as percentage of reinforcement is less than 2 and the ratio of test and calculated ultimate load is greater than or equal to 1.25. In 1984 Hassoun and Sahebjam (28) concluded that the plastic rotations is substantially improved by using steel fibers as secondary reinforcement.

1.4 Effect of Reinforcement on Ductility of Concrete

Ductility is an important factor in the design of reinforced concrete structures. Many investigators have concluded that ductility can be improved by using three different types of reinforcement: compression steel, stirrups and fibers.

1.4.1 Compression Steel

Compression steel has been used in certain concrete sections where the dimensions are limited and applied moments exceed the internal moment capacity for singly reinforced section. Compression steel reduces the long time deflection and holds stirrups, which are used to resist shear forces.

On work related to improvement of ductility, A.L.L. Baker (7) suggested that the use of short lengths of compression steel can significantly increase rotation capacity. Researchers (12,52) have concluded that addition of secondary steel to the main reinforcement

adds greatly to the ductility of reinforced concrete members and can ensure the redistribution of moments. Thomas Hsu (30) concluded that the ductility factor decreases with the increase of tensile steel, but it increases with the increase of compression steel.

1.4.2 Stirrups

Although stirrups are used to resist shear, they have been found to be a very effective reinforcement for improving ductility. Shah (52) concluded that the use of closely spaced stirrups significantly increases ductility. Burns (12) also concluded that closely spaced closed stirrups in the zone where plastic action is concentrated play a key role. He also found that these stirrups are effective in supporting the compression steel against buckling. Baker (7) indicates that if special binding is used, the ultimate crushing strain in bound concrete may be as high as 0.012.

1.4.3 Steel Fibers

Use of steel fibers in concrete is known to improve the strength and ductility of concrete in flexure.

Swamy and Al-Noori (59) studied the behavior of reinforced concrete beams with fiber concrete and concluded that fiber concrete in tension zones controls the width of cracks and deflection and enables the beam to develop plastic deformations at failure. Tests (60) have shown that the strain of concrete on the compressive face at

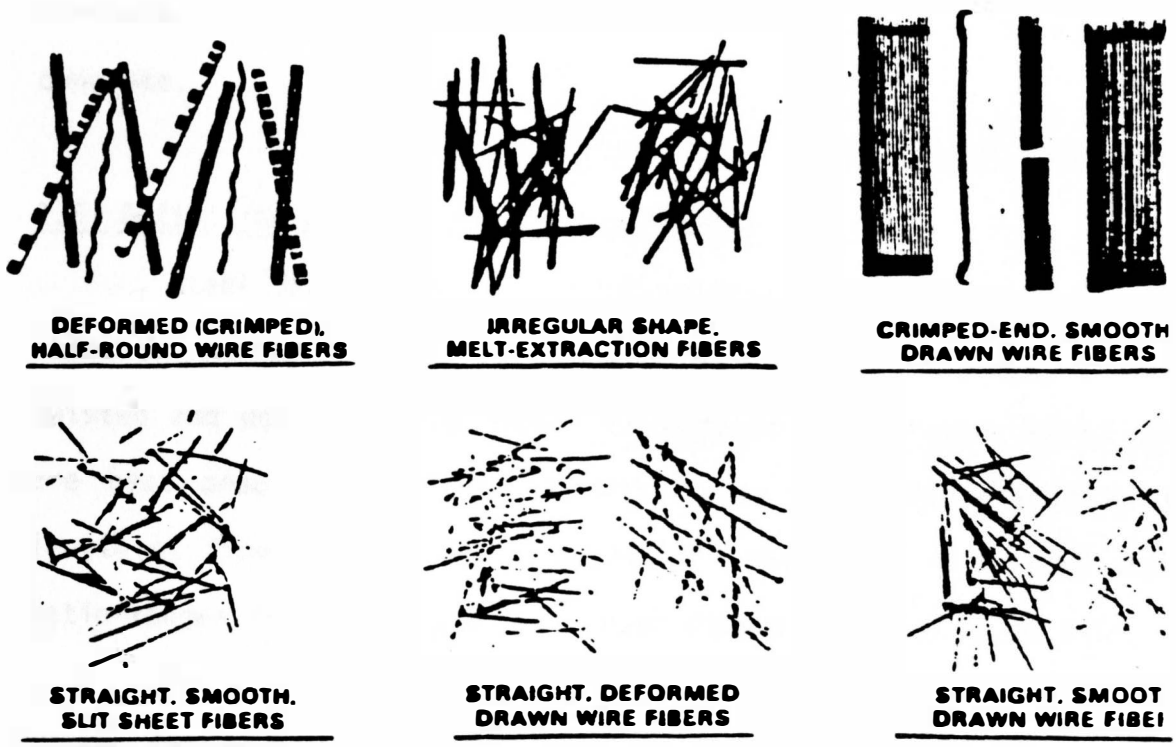

Figure 1.2 Typical commercially available steel fibers.

loads prior to failure have ranged from 524 to 6620 x 10^{-6} (in/in) for beams reinforced with steel fibers. Sahebjam (50) concluded that fibrous concrete can have maximum strain of up to 5800 x 10^{-6} in/in.

Therefore, it is important to study the properties of fibrous concrete and to describe the role of steel fiber in reinforced concrete.

1.5 Definition of Steel Fibers and Fibrous Concrete

Steel fibers are small thin materials that are produced from steel in various shapes and sizes. They can be straight, crimped, twisted and deformed with hooked or paddled ends (Figure 1.2). They are best described by their aspect ratio, which is defined as the length of fiber divided by an equivalent diameter. A typical aspect ratio ranges from 30 to 150 for length dimensions of 0.25 to 3 in.

Fibrous concrete is a composite material that is made of fine, coarse aggregate cement, water and discontinuous discrete fibers. In general, concretes having steel fibers differ from conventional concrete in having a higher cement content and a smaller aggregate size. In most applications considered to date, fiber content has ranged from about 0.3 to 2 volume percent.

The idea of using fibers to strengthen concrete is not new. It began with Porter in 1910, and the major turning point was achieved by Romnaldi and Batson (49) in 1963, who showed that by using steel fibers in concrete the cracking strength is increased. They concluded

that this strength is inversely proportional to square root of the fiber spacing. Since that time, research was carried out by many investigators, and the following aspects were tested using steel fibers.

1.6 Compressive Strength of Fibrous Concrete

The effect of steel fibers on the compressive strength of concrete has been tested by many investigators during the past two decades. In June 1979, Halvorsen and Kesler (25) concluded that the compressive strength is unaffected by fiber type or content.

Anil (33) in 1972 also concluded that the increase in compressive strength of fibrous concrete was not appreciable. Similar observations were made by Sahebjam (50) in 1984. That same year, Ravindrarajah (47) and Tam (47) concluded that the compressive cube strength of concrete is not significantly affected by the addition of steel fibers.

1.7 Deflection and Crack Control

Two important factors affecting the serviceability of reinforced concrete flexural members include cracks and deflection. Excessive deflection will lead to large cracks, thus damaging the structure. Therefore the ACI Code recognizes the use of steel up to a yield strength of 80 ksi and the use of high strength concrete.

The presence of steel fibers in concrete improves serviceability. Tests reported by Swamy and Al-Noori (59) showed that the presence of steel fibers enables high-strength steel, much higher than currently allowed by ACI Code, to be used without excessive cracking and deflection under service load. Swamy, Al-taan and Ali (60) also concluded that the addition of steel fibers to concrete beams will increase the stiffness at service load thus resulting in a substantial decrease in deflection. They also concluded that the presence of steel fiber transforms the inherently unstable and uncontrolled cracking in plain concrete into slow, controlled crack width.

1.8 Stiffness (flexural rigidity)

Stiffness of a flexural member can be determined by the product of the moment of inertia and the modulus of elasticity. Cracked and uncracked sections can occur along the length of flexural member, resulting in variable moment of inertia EI; therefore it is necessary to use a proper value of EI. The ACI adopted an average value for the flexural rigidity using an effective moment of inertia, I_e.

Swamy and Al-Noori (59) reported in 1975 that the addition of steel fiber to concrete will increase its stiffness due to crack control in fibrous concrete. A similar conclusion was reported in 1979 by Swamy, Al-taan and Ali (60). They concluded that the stiffness of the beams at service loads is increased, resulting in a reduction of deflection.

1.9 Applications of Steel Fibers

Continued research and utilization of the properties of fiber reinforced concrete have led to a growing acceptance of this material as an alternative to conventionally reinforced concrete. Steel fibers are used in many applications, such as the following:

1. Bridge deck overlays and construction: steel fibers were used in these overlays to take advantage of increased strength and to improve the performance.
2. Highway, street and airfield pavements: fiber overlays were used on such applications to resist the impact loads, to improve crack control and to reduce thickness, thus leading to improved economy.
3. Maintenance and repairs: steel fibers are found to be efficient in repairing deteriorated portions of concrete slabs, pavements, culverts and many others.
4. Concrete pipes: the benefits of steel fibers in concrete pipes include increase in strength, reduced wall sections and better performance.
5. Industrial floors: the benefits of steel fibers in this application include a reduction in concrete volume per unit floor area and a reduction in construction and repair costs.
6. Structural units: the benefits of steel fibers in this application are increased crack resistance,

ductility at failure, higher load capacity and smaller concrete sections.

7. Other applications: steel fibers are used in such applications as mining and tunneling, rock slope stabilizations, concrete piles and several precast products.

It is likely to see new applications of steel fibers in the future due to continued research and improved testing methods.

1.10 Objectives and Scope of Investigation

The main objectives of this investigation are to study the effect of both compression steel and steel fibers in addition to the main steel on the plastic rotation of reinforced concrete in continuous beams. This study is limited to the case of bending, utilizing two-span, continuous beams loaded at the middle of each span to failure. This research also studies the effect of steel fibers on cracking and deflection behavior of these beams and the physical properties of fibrous reinforced concrete. The emphasis will mainly be on the modulus of elasticity, compressive strength, tensile strength (modulus of rupture test and split cylinder test), crack width distribution, ductility and deflection.

For the purpose of this research, nine beams were cast and tested to failure. The beams were under-reinforced and had the same compression steel and different combinations of main steel and steel

fibers. The effect of the variables, steel fibers ρ_s, compression steel ρ' and main steel ρ on the length of the plastic hinge, curvature distribution factor, ductility and plastic rotation capacity of reinforced concrete will be analyzed. In addition, concrete cylinders and small beams were cast and tested to determine the physical properties of plain and fibrous concrete used in this investigation.

CHAPTER 2

ELASTO-PLASTIC ROTATION OF REINFORCED CONCRETE BEAMS

2.1 Rotation Capacity of Reinforced Concrete Beams

Calculations of rotation capacity of reinforced concrete tend to be complex; therefore many researchers tried to develop methods with some reasonable assumptions in order to arrive at satisfactory results that could be compared to the actual rotations. In general, rotation can be expressed as the integral of curvature. The curvature can be calculated at any stage of loading and be integrated over a finite length to give the rotation accrued over a desired length.

The total rotation up to failure that occurs at a critical section can be approximated by the sum of two major parts:

1. Elastic rotation "θ_e" which is the rotation up to the first yield of main reinforcement (Figure 2.1).
2. Plastic rotation "θ_p" from first yield up to failure. The plastic rotation θ_p is a much greater amount when compared to elastic rotation simply because the section is not taking any extra moment, and therefore further loading merely produces excessive rotation (Figure 2.1).

The calculation of elastic rotation can be evaluated at any stage from the following equation:

$$\theta_e = (\phi_e)(\ell) \qquad (2.1)$$

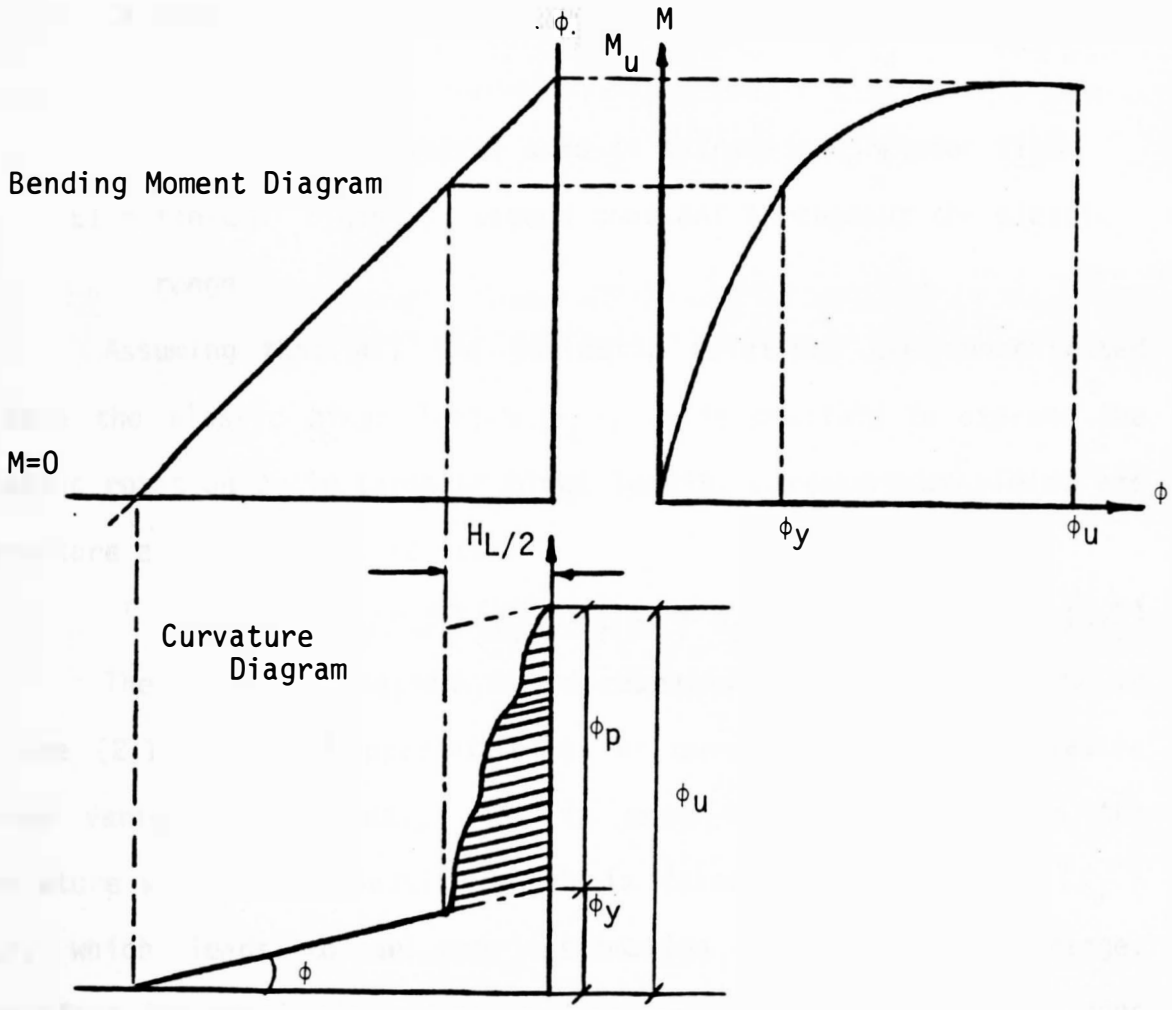

Figure 2.1. Plastic rotation from moment-curvature and moment gradient.

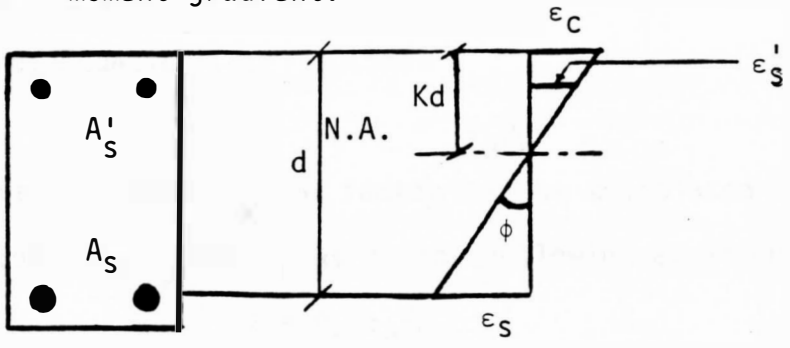

Figure 2.2. Typical relation between strain and curvature.

where ϕ_e = the elastic curvature (M/EI) or (ε_c/Kd) (Figure 2.2)

ℓ = desired length

ε_c = concrete strain

Kd = distance from neutral axis to extreme compression fiber

EI = flexural rigidity assumed constant throughout the elastic range

Assuming that all the inelastic relations are concentrated within the plastic hinge length (H_L), it is possible to express the plastic rotation θ_p in terms of hinge length, curvature at yield, and curvature at ultimate as follows:

$$\theta_p = \int_0^{H_L} (\phi_u - \phi_y) d\ell = \phi_p H_L \qquad (2.2)$$

The plastic rotation is represented by the shaded area in Figure (2.1). It is apparent that the curvature along the plastic hinge varies significantly, and in most rotation computation the curvature within the plastic length is taken uniformly to be (ϕ_u - ϕ_y), which leads to an over estimation of the plastic hinge. Therefore introducing a curvature distribution factor β must be done when calculating the plastic rotation.

Therefore, Equation (2.2) becomes

$$\theta_p = \beta(\phi_u - \phi_y) H_L = \beta \phi_p H_L \qquad (2.3)$$

The curvature distribution factor can be calculated from the experimental values θ_p, ϕ_p and H_L as in the following equation:

$$\beta = \theta_p / \phi_p H_L \qquad (2.4)$$

In order to have a complete redistribution of moments, the required plastic rotation at the assumed hinge positions must not exceed the rotation capacity of the section.

The required rotation for plastic hinges in an indeterminate reinforced concrete structure allow other plastic hinges to develop, and the structure to reach a mechanism can be determined by slope deflection as follows (26) (Figure 2.3):

$$\theta_{AB} = L[2(M_A - M_{FA}) + (M_B - M_{FB})]/6E_cI \qquad (2.5)$$

where: M_A and M_B = ultimate moments at A and B respectively

M_{FA} and F_{FB} = elastic fixed end moments at A and B

E_c = modulus of elasticity of concrete = $33W^{1.5}\sqrt{f'_c}$

I = moment of inertia of a cracked section

Baker (7) estimated that the angle of rotation as follows:

$$\theta_p = \phi_p H_L$$

$$\phi_p = \varepsilon_p / K_u d$$

Therefore:

$$\theta_p = \varepsilon_p H_L / K_u d$$

Assuming $H_L = d$ then $\theta_p = \varepsilon_p / K_u = \varepsilon_{cu} - \varepsilon_{cy} / K_u$

$\varepsilon_{cy} = \varepsilon_{sy}(K_u/1-K_u) = (f_y/E_s)(K_u/1-K_u)$ from Figure (2.4)

Therefore:

$$\theta_p = \varepsilon_{cu}/K_u - f_y/(E_s)(1-K_u) \qquad (2.6)$$

From Equation (2.6) the rotation capacity is inversely proportional, for a given moment distribution, to depth at neutral axis, where rotation capacity is insufficient to meet the required rotation.

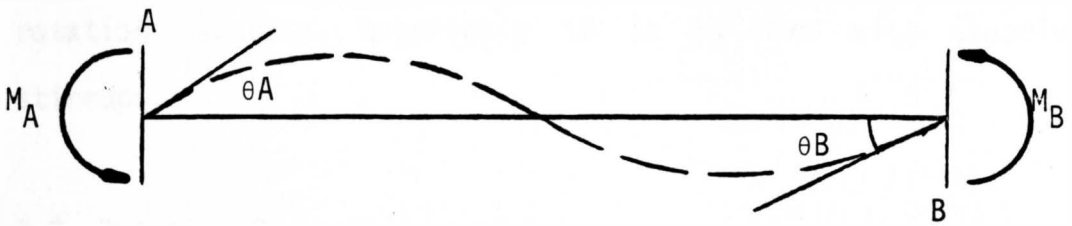

Figure 2.3. Typical flexural member.

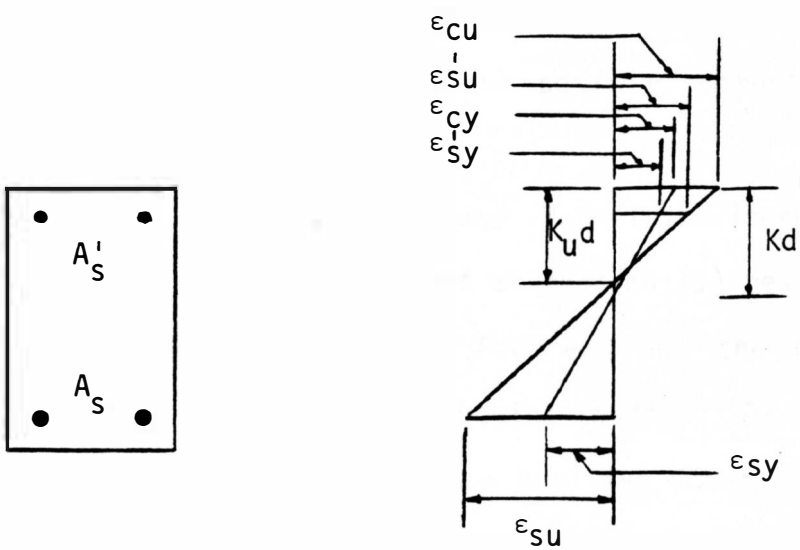

Figure 2.4. Ultimate strain diagram.

Addition of compression steel can be made at plastic hinges to reduce the neutral axis; therefore, it can bring a marked increase in rotation capacity, especially if it is used with closely spaced stirrups.

2.2 Rotation Compatibility

For the redistribution of moments, compatibility condition demands sufficient plastic rotation at critical sections to allow the member to sustain a further increase in curvature. Consider the two-span, continuous beam in Figure (2.5).

The beam is under symmetrical loading with a concentrated load at the midpoint of each span. This type of loading will produce a negative moment at section (1) higher than the positive moment at section (2).

Figure (2.5a) shows that both M_1 and M_2 first increase linearly in the elastic range. When the moment at section (1) reaches the yield moment (taken as M_{y1} according to Figure 2.5b) the corresponding load will be P_{y1}, a plastic hinge begins to form. At this stage of yield load P_{y1}, the sections of maximum positive moment have not failed and the reserve capacity M_{y2} can still be utilized. Further increase in load beyond P_{y1} requires a redistribution of moments. This means that moments at the maximum positive moment sections continue to increase, but the negative moment at section (1) remains constant (moment M_{y1}). Therefore, it is essential that the plastic rotation capacity of section (1) be adequate to permit M_2 to

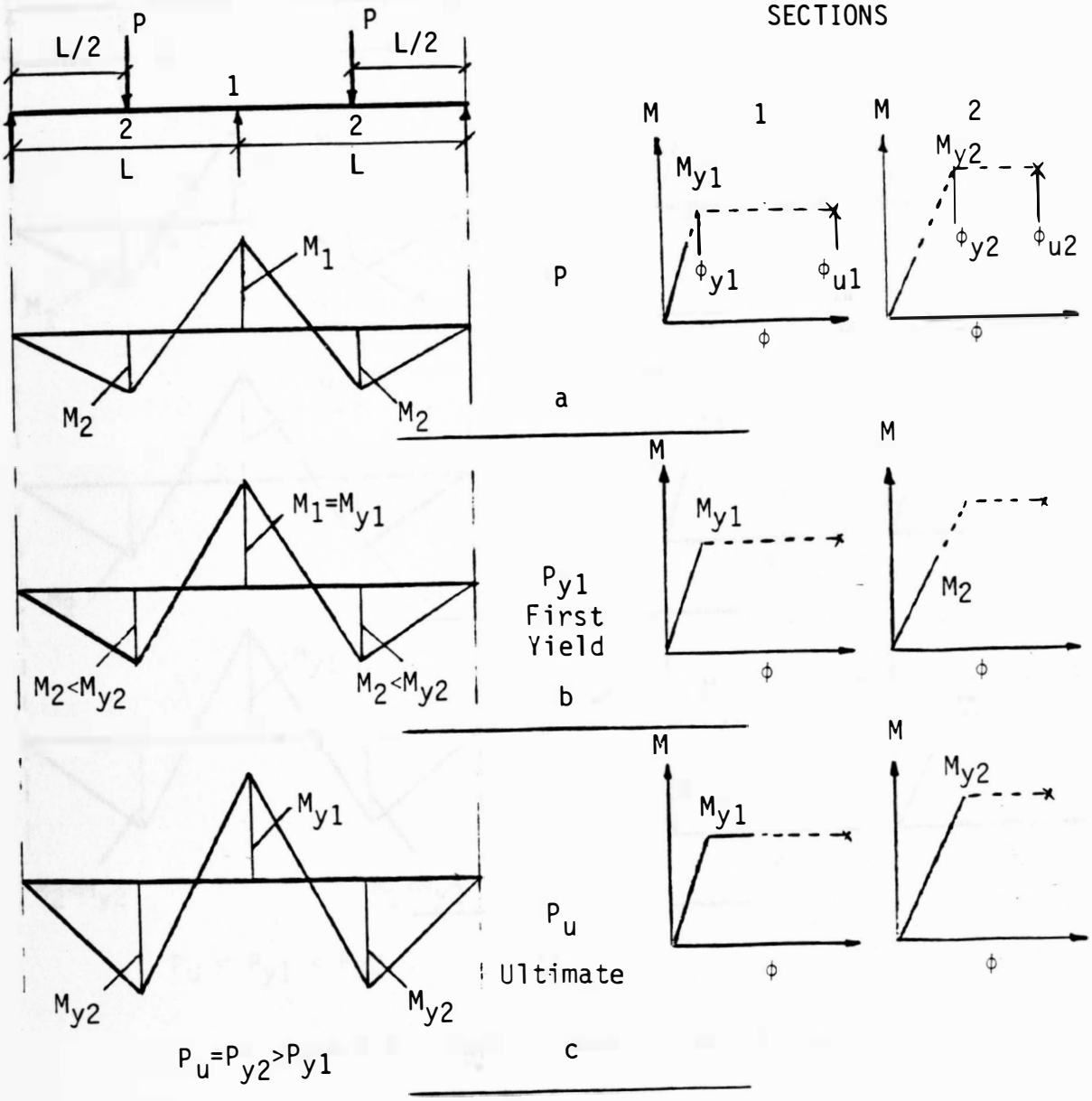

Figure 2.5. Full moment redistribution.

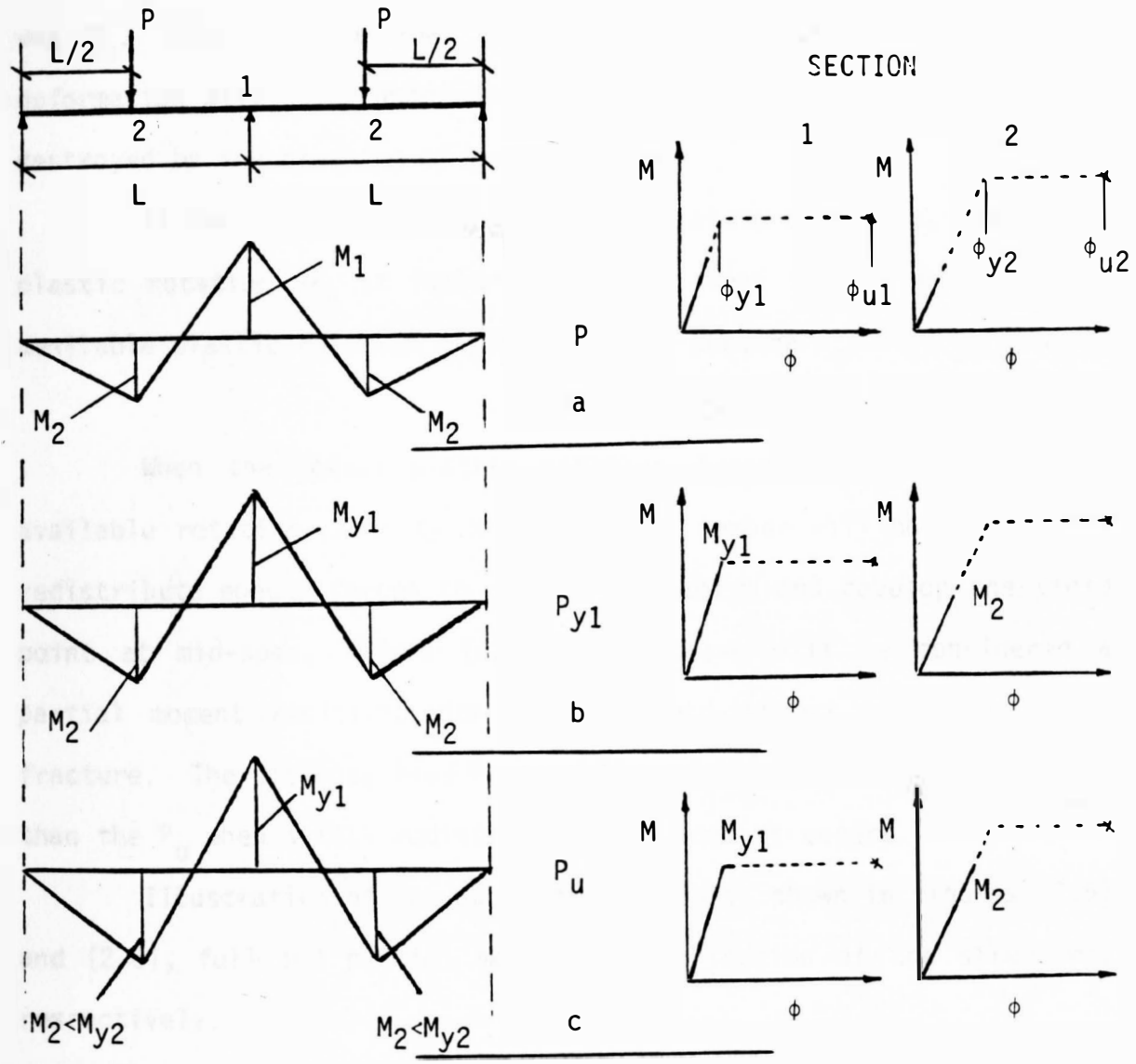

$P_u = P_{y1} < P_{y2}$

Figure 2.6. Partial moment redistribution.

reach M_{y2}. When section (2) yielded, M_{y2} in (Figure 2.5c), the load was P_u. The ultimate load capacity of the structure and further deformation will occur under constant load until one of the hinges is destroyed by the crushing of the concrete.

It can be seen that to achieve the above condition, the actual plastic rotation θP_u at failure has to be less than or equal to the available plastic rotation capacity of the section θ_p.

$$\theta P_u \leq \theta P$$

When the actual plastic rotation exceeds the calculated or available rotation capacity $\theta P_u > \theta P$, the member will not be able to redistribute enough forces to reach a mechanism and develop the yield point at mid-span, Figure (2.6). This case will be considered a partial moment redistribution and the mid-support undergoes local fracture. The ultimate load P_u that the structure can support is less than the P_u when a full redistribution of moments occurs.

Illustration of the above discussion is shown in figures (2.5) and (2.6), full and partial moment redistribution of the structure, respectively.

2.3 Moment Curvature Relationship

If a short segment of reinforced concrete member is subjected to a bending moment, curvature of the beam axis will result, as shown in Figure (2.7), and there will be a corresponding rotation of the one

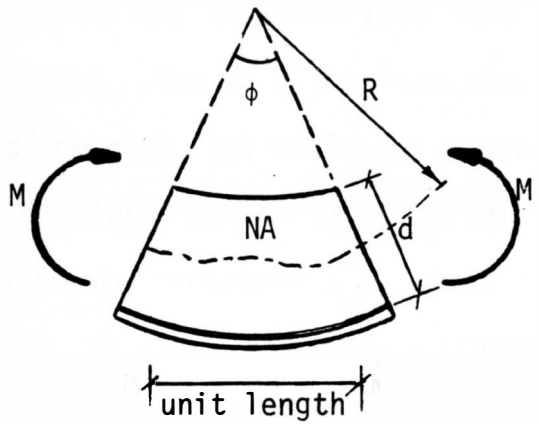

Figure 2.7. Unit rotation of flexural member.

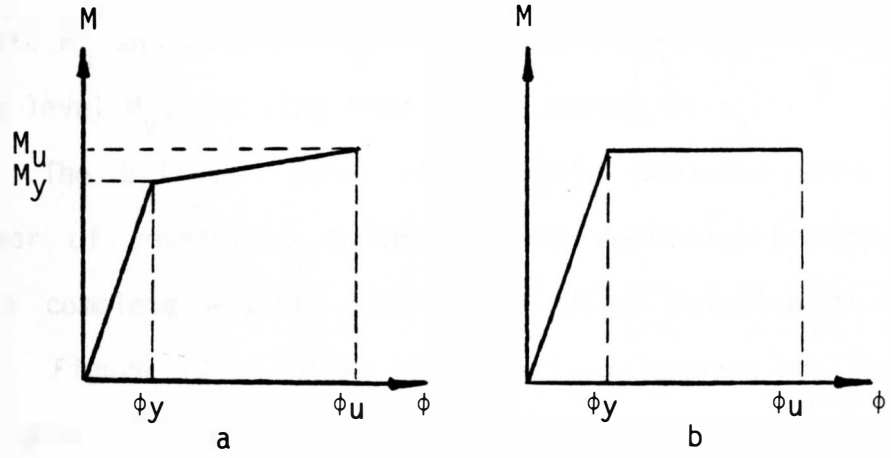

Figure 2.8. Idealized M-ϕ curve.

face of the segment with respect to another. Therefore, a representative relation between moment and curvature is an important aspect when studying the inelastic behavior of reinforced concrete.

The M-ϕ curve can be idealized into two straight lines as shown in Figure (2.8a). One straight line starts from the origin and ends at the yield moment M_y (or yield curvature ϕ_y). Another straight line with a small slope starts from M_y and ends at the ultimate moment, M_u (or ultimate curvature ϕ_u). Such a curve has been used by some investigators (32,29). However, a further simplification has commonly been made by assuming the second straight line to be horizontal (8), as shown in Figure (2.8b). The first straight line of this M-ϕ curve starts at the origin and ends at a point with an ordinate M_u and abscissa ϕ_y. The second straight line is horizontal at the level M_u, starting from ϕ_y and ending at ϕ_u.

The bilinear (M-ϕ) relationship deviates from the actual behavior of reinforced concrete since reinforced concrete does not have a complete elastic and linear (M-ϕ) relation in the elastic range. Figure (2.9) gives a comparison between an ideal bilinear elasto-plastic (M-ϕ) to the actual (M-ϕ) relationship of reinforced concrete.

The reinforced concrete beam in the actual (M-ϕ) curve behaves elastically up to the cracking moment. As the load increases the beam continues to behave elastically but with a flatter slope up to the yield moment. An additional increase in load will cause the beam to

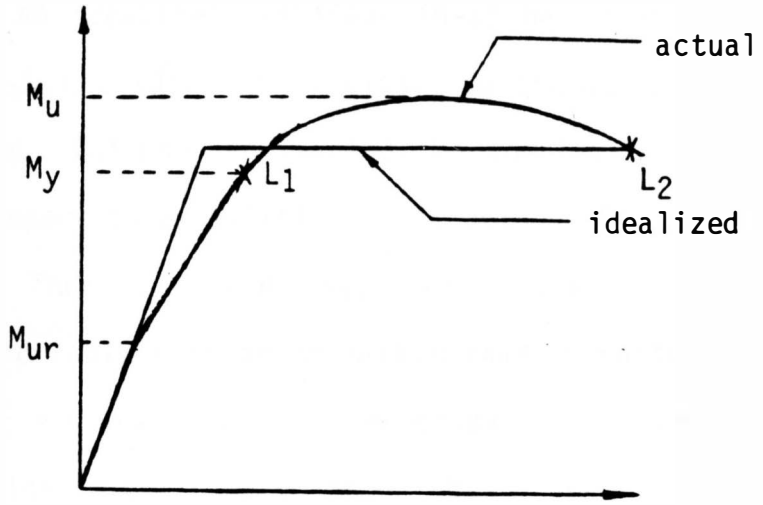

Figure 2.9. Actual and idealized moment-curvature.

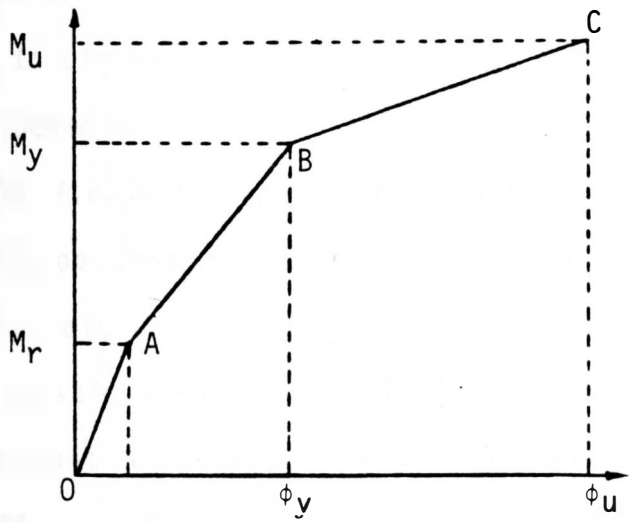

Figure 2.10. Trilinear Moment-Curvature.

behave disproportionately until it reaches its ultimate capacity, limit state L_2. An idealized trilinear (M-ϕ) has been used by some investigators (Figure 2.10). It is closer to the actual curve than a bilinear M-ϕ curve. But one can imagine the complexity of the actual M-ϕ curve with respect to calculation of EI between limit state L_1 and limit state L_2. Therefore, the idealized bilinear curve has been found to be considerably simpler to manage than the actual M-ϕ curve. Also the bilinear M-ϕ was found to overestimate the deformation of a given section, which is believed to be on the conservative side (8).

The curvature can be calculated from the strain diagram if the position of the neutral axis, represented by K, is known as shown in Figure (2.2), or from the equation $\phi = M/EI$.

It is obvious that the value of ϕ increases as loading is increased to ultimate load; consequently the compressive strain of the concrete increases.

The flexural rigidity of concrete decreases when excessive cracks develop beyond the yield point of steel. Evaluation of a correct and safe value of flexural rigidity is necessary when calculating the plastic deformation. Therefore the value of EI was assumed to be constant throughout the elastic and plastic stages in some experiments (7), which will lead to a conservative overestimating of the plastic rotation.

A.L.L. Baker (7) defines EI for cracked rectangular section in Equation (2.7), which is based on the properties of the material,

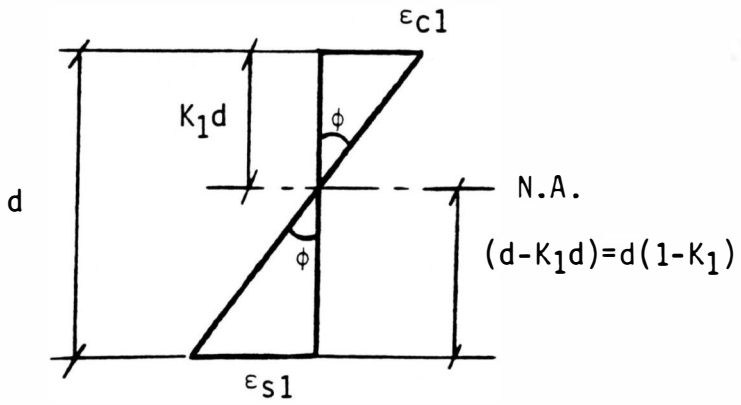

Figure 2.11. Curvature at limit state L_1.

geometry of the section, and the curvature at a particular limit state L_1 (Figure 2.11).

$$\phi = M_1/EI = 1/R$$

$$\phi = \varepsilon_{c1}/K_1 d = \varepsilon_{s1}/d(1-K_1)$$

Therefore:

$$EI = M_1 K_1 d/\varepsilon_{c1} \text{ or } EI = M_1(1-K_1)d/\varepsilon_{s1} \qquad (2.7)$$

where: K_1 = ratio of the neutral axis depth to the effective depth

M_1 = moment limit state L_1

2.4 Plastic Hinge

The idealized assumption of inelastic rotation concentrated at this point is only theoretical. In fact, the plastic deformations are concentrated over a finite length called "plastic hinge length, H_L". This length is dependent on the shape of the bending moment diagram at the ultimate stage. Specifically it is found to vary with the distance between point of contraflexure when the first hinge forms over the support; and in the case when the hinge forms first in the span, it varies with the distance from end support to the point of contraflexure (32).

Referring to Figure (2.1), the length $H_L/2$ represents the plastic hinge length on one side of the center of support. Therefore H_L can be calculated from moment-curvature and bending moment diagram. The experimental values of H_L that have been proposed by several investigators are summarized in Table (2.1).

TABLE 2.1

COMPARISON OF PLASTIC HINGE LENGTH VALUES

REFERENCE	PLASTIC HINGE LENGTH (H_L)
Baker 1956	$H_L = 1.0d$
Chan 1955	$H_L <$ span/10
Chan 1962	$H_L = 0.4d - 2.4d$
Cohn and Petcu 1963	$H_L = 0.3d - 0.9d$
Wright and Berwanger 1960	$H_L = 1.0d$
I.C.E. 1962	$H_L = K_1K_2K_3d\ (Z/d)^{0.25}$
Corley 1967	$H_L = 0.5d + 0.2\sqrt{d}(Z/d)$
Mattock 1967	$H_L = 0.5d + 0.05Z$
Sawyer 1964	$H_L = 0.25d + 0.075Z$
Kaushik et al 1980	$H_L = 0.25d - 1.0d$
Sahebjam 1984	$H_L = 1.06d$

where d = effective depth of beam

Z = distance from the section of maximum moment to the section of zero moment

K_1 = 0.7 (mild steel); 0.9 (cold form steel)

K_2 = 1 influence of axial load

K_3 = 0.6 (f'_c=6000 psi), 0.75 (f'_c=4000 psi), 0.9 (f'_c=2000 psi)

CHAPTER 3

SPECIMENS, MATERIALS, AND FABRICATION

3.1 Test Specimens

A total of nine rectangular reinforced concrete continuous beams were tested in this research. All the beams were 5 x 8 in. in cross section, 11 ft. long, with two spans of 5 ft. each. The beams were reinforced with three different main steel reinforcements and with three different steel fiber percentages. All the beams also contained two #3 bars as top steel. The beams were arranged as shown in Table 3.1 and Figures 3.6 through 3.8. All tests were conducted under symmetrical loading with a concentrated load at the midpoint of each span.

3.2 Materials

3.2.1 Concrete Constituents

Concrete is basically a mixture of two parts: aggregates and paste. The paste is comprised of Portland cement and water.

Aggregates are generally divided into two groups: fine and coarse. The fine aggregates consist of natural or manufactured sand with particle sizes up to 1/4 in. and should meet the gradation requirements given in ASTM C33. The coarse aggregates are those with particles retained on the No. 16 sieve and should be ASTM C33 size no.

TABLE 3.1

BEAM ARRANGEMENT

Beam No.*	% Steel Fiber (ρ_s)	Tension Steel (A_s)	d in.	Top Steel (A'_s)	d' in.
1	0.0	2 #4	6.5	2 #3	1.44
4	0.8	2 #4	6.5	2 #3	1.44
7	1.2	2 #4	6.5	2 #3	1.44
2	0.0	2 #5	6.31	2 #3	1.56
5	0.8	2 #5	6.31	2 #3	1.56
8	1.2	2 #5	6.31	2 #3	1.56
3	0.0	2 #6	6.25	2 #3	1.56
6	0.8	2 #6	6.25	2 #3	1.56
9	1.2	2 #6	6.25	2 #3	1.56

*b = 5 in. and h. = 8 in for all beams.

8 or equivalent for nominal 3/8 in. maximum size aggregate mixtures and should be size no. 67 or equivalent for 3/4 in. maximum size aggregate mixtures. Aggregate of 3/8 in. maximum size is generally used in steel fibrous reinforced concrete (17).

Portland cements are hydraulic cements; that is, they set and harden by reacting chemically with water. They are available in different types to meet different physical and chemical requirements, for specific purposes such as: Type I normal, Type II moderate, Type III high early strength, Type IV low heat of hydration and Type V sulfate resisting. High cement content is generally used in steel fibrous reinforced concrete.

3.2.2 Steel Fibers

The steel fibers used in this experiment were provided by Bekaert Steel Wire Corporation and made from low carbon steel with a tensile strength of 181-232 ksi, elastic modulus of 28-30 ksi and specific gravity of 7.8 lb/ft^3.

Individual fibers were 2 in. long and 0.02 in. in diameter, giving the fiber an aspect ratio of 100. The steel fibers were hooked with 65 degree bends at each end and shipped glued together side by side in bundles of 25. When steel fibers are added to the water in the mix, the glue dissolves and the fibers will be separated and distributed uniformly throughout the concrete mix during mechanical mixing.

Figure 3.1. Steel fibers.

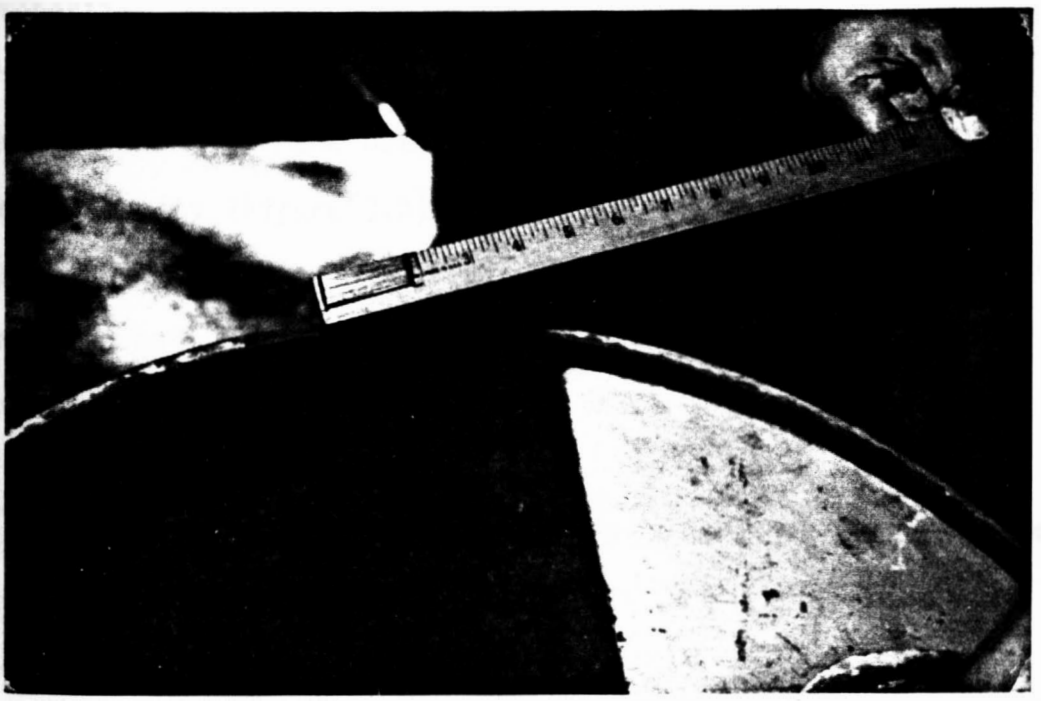

Figure 3.2. Steel fiber length.

The hooked end steel fibers were used to allow a proper anchorage between fibers and concrete (Figures 3.1 and 3.2).

3.2.3 Mixes

All concrete mixes contained the following:

1. Type I Portland cement.
2. Fine aggregate with a finess modulus of 2.90.
3. Coarse aggregate maximum size of 3/8 inch.
4. Water.

Three mixes were made in this experiment. Each mix was made in five batches of 2.7 cubic foot; therefore each mix was approximately 13.5 cubic foot of concrete. Two steel fiber mixes were made using different fiber percentages, 0.8% and 1.2%. To compare the properties of fibrous concrete with plain concrete, one plain concrete mix was also made. All three mixes were made using the same mix proportions. All the batches were mixed in a drum mixer of 3 cubic foot capacity (Figure 3.3). For each batch of the steel fiber mixes, the aggregates, cement and water were mixed thoroughly for about 4 minutes and the steel fibers were subsequently added in small quantities in order to minimize balling and interlocking between fibers.

The following specimens were made from each concrete mix: three (5 x 8 x 132 in.) main beams, six (6 x 12 in.) cylinders for the compressive strength, modulus of elasticity and split cylinder tests, and two (6 x 6 x 24 in.) small beams for the modulus of rupture test.

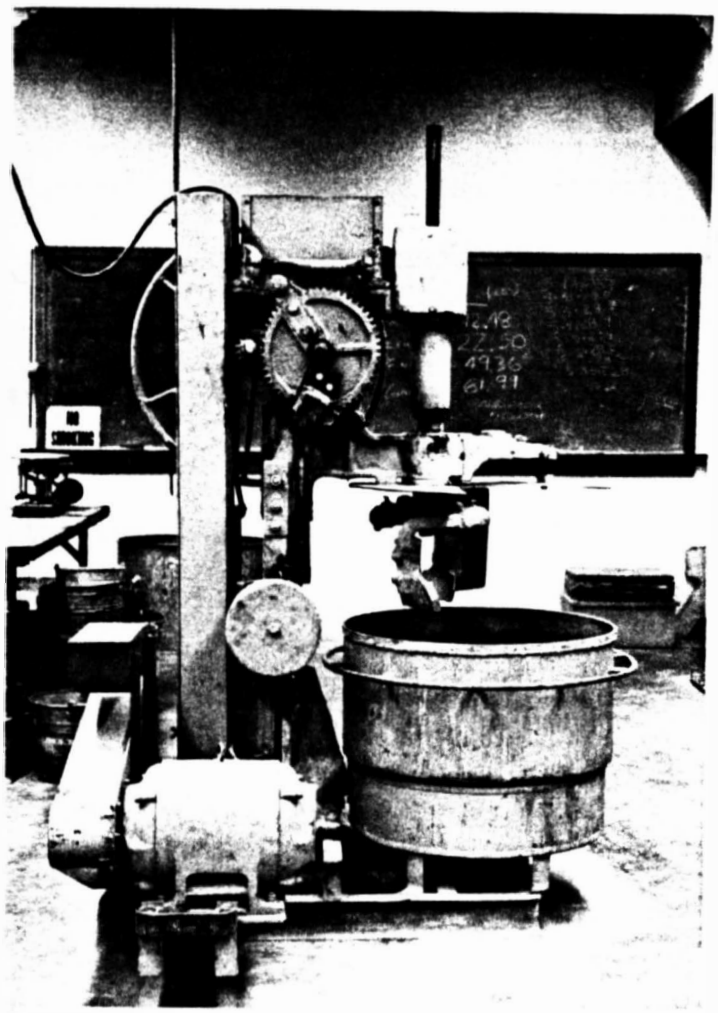

Figure 3.3. 3.0 cubic foot mixer.

For each batch of fresh concrete, a slump test was performed in accordance with ASTM standards (C-143). The concrete mix was scooped into the wooden forms and molds. The forms were fabricated for a variable uniform width and length (up to 11 feet) and a maximum depth of 10 inches. The wooden frames were supported by steel brackets for lateral support against concrete pressure. The use of a vibrator was necessary to ensure dispersion and penetration of the aggregates and steel fibers within the steel reinforcement gage. One-inch cement blocks were wired to steel reinforcement gage to ensure a one-inch concrete cover and to prevent movement during placement of the concrete. The excess concrete was then scraped off the surface and smoothed by using a trowel (Figures 3.4 and 3.5).

3.2.4 Mix Design

The method used for the concrete mix design was the absolute volumetric method. The calculations were based on a cubic yard basis. Depending on the volume required, all calculations were converted to pounds per cubic foot. The calculations are as follows:

Specific Gravity (from testing ASTM C-127, 128)

Fine Aggregate	= 2.62
Coarse Aggregate	= 2.63
Portland Cement Type I	= 3.15

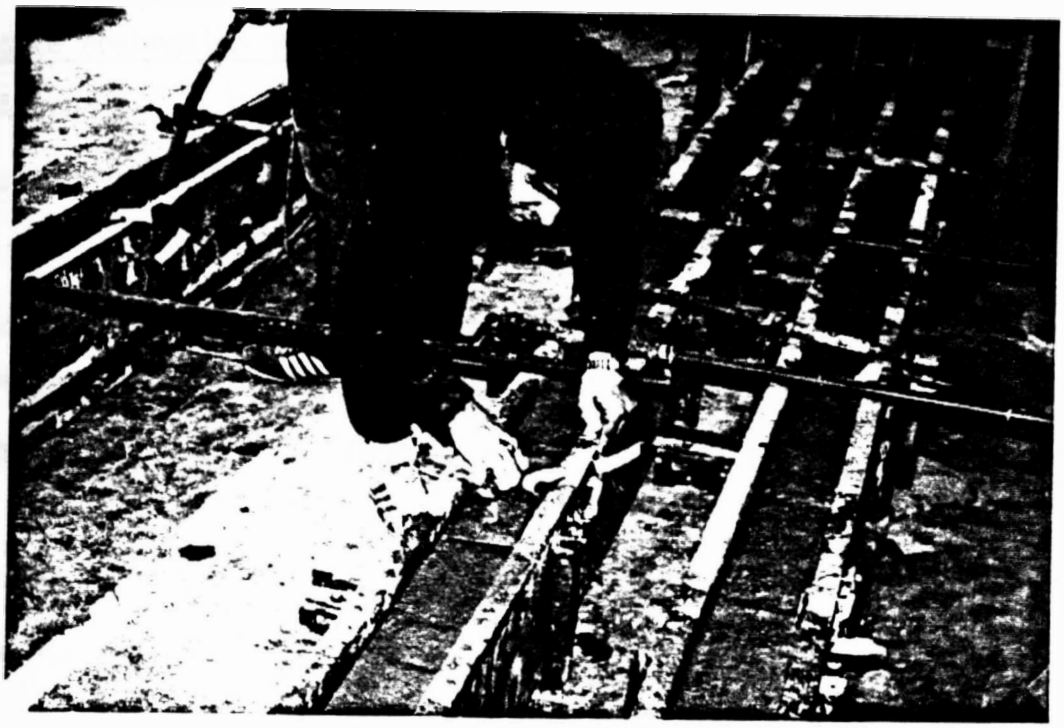

Figure 3.4. Concrete finishing.

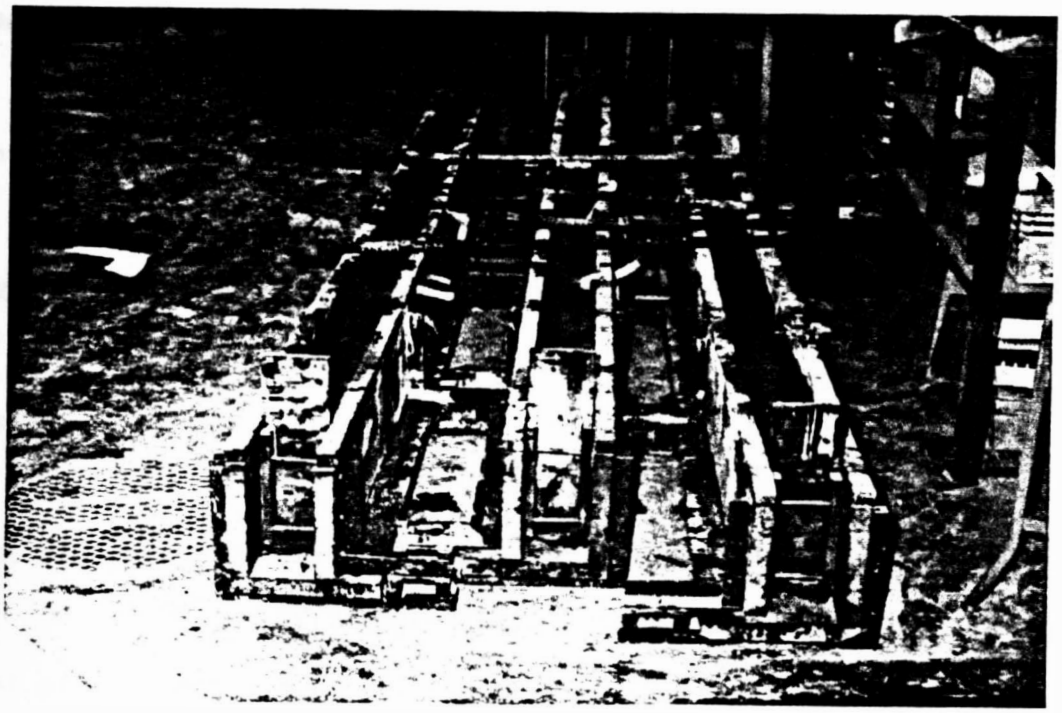

Figure 3.5. Complete work.

Aggregate Absorption (from testing ASTM C-127, 128)

Fine Aggregate = 1.45%

Coarse Aggregate = 1.9%

Moisture Content of Aggregates and Known Parameters

Fine Aggregate = 3.0%

Coarse Aggregate = 0.35%

Water Content = 285 lb/yd^3

W/C = 0.65

% Fine Aggregate = 45%

Calculations

Volume of Water = unit weight/unit weight of water

= (285 lb/yd^3)/(62.4 lb/ft^3) = 4.57 ft^3/yd^3

Weight and Volume of cement:

C = W/0.65 = 285/0.65 = 438.46 lb/yd^3

Volume of Cement = weight/[(sp.gr.)(62.4lb/ft^3)] = 438.46/(3.15x62.4)

= 2.23 ft^3yd^3

Volume of Aggregate = (27 ft^3/yd^3) - V water - V cement

= 27-4.57-2.23 = 20.2 ft^3/yd^3

Weight of Aggregate = (V agg)x(62.4 lb/ft^3)x(sp. gr. of aggregate)

x(% aggregate)

Weight of Fine Agg = (20.2 ft^3/yd^3)x(62.4 lb/ft^3)x(2.62)x(0.45)

= 1486.11 lb/yd^3

Weight of Coarse Agg = (20.2 ft^3/yd^3)x(62.4 lb/ft^3)x(2.63)x(0.55)

= 1823.28 lb/yd^3

Moisture Corrections

Correction Weight = [moisture content - absorption]

x[weight of aggregate/(1 + absorption)]

Fine Correction = [0.03-0.0145][1486.11/(1+0.0145)] = 22.71 lb/yd^3

Coarse Correction = [0.0035-0.019][1823.28/(1+0.019)] = -27.73 lb/yd^3

Component	Weight (lb/yd^3)	Correction (lb/yd^3)	Corrected Weight (lb/yd^3)
Cement	438.46	-----	438.46
Water	285.00	+5.02	290.02
Fine Aggregate	1486.11	+22.71	1508.82
Coarse Aggregate	1823.28	-27.73	1795.55

Calculations for Steel Fiber Weights

Specific Gravity of Steel Fibers = 7.8

Unit Weight of Fibers = (sp. gr.)x(62.4 lb/ft^3)

= 7.8x62.4 = 486.72 lb/ft^3

Volume of Each Concrete Mix = 13.5 ft^3

Weight of steel fibers used in each mix:

a) when 0.8% is used:

= (486.72 lb/ft^3)x13.5 ft^3x(0.8/100) = 52.57 lbs

b) when 1.2% is used:

$$= (486.72\ lb/ft^3) \times 13.5\ ft^3 \times (1.2/100) = 78.85\ lbs$$

Therefore the total weight of steel fibers used:

% Steel Fibers	Wt. of Steel Fiber per Cubic Yard	Wt. of Steel Fiber per Mix (0.5 cy^3)
0	0	0
0.8	105.14	52.57
1.2	157.7	78.85
		Total Weight = 131.4 lbs

Batch Weight

Three mixes were used in this experiment; each mix has 0.5 cubic yards of concrete. Therefore, a total of 1.5 cubic yards of concrete was used.

Component	Weight lbs/yd^3	Overall Weight (lbs/1.5 yd^3)
Cement	438	658
Water	290	435
Fine Aggregate	1509	2263
Coarse Aggregate	1796	2693

3.3 Fabrication

3.3.1 Steel Reinforcement

Adequate reinforcement was provided to resist the two main stresses, shear and flexure. All the beams in this experiment were made with top and bottom bars. Equal percentages of steel were provided at span and support critical sections.

Two #4, two #5 and two #6 deformed bars were used as the main reinforcement on the tension side. Two #3 deformed bars were used as compression steel or stirrup supports on the compression side. The steel reinforcement details are shown in Figures 3.6 through 3.8.

The top and bottom bars were marked and cut off with an acetylene torch at the proper points. A two-inch cover was allowed between the end of the bars and the end of the concrete beams (Figures 3.6 through 3.8).

A 20 inch long test sample was cut from each bar reinforcement and a tension test was conducted on each sample. Yield and ultimate strengths were determined and tabulated in Table 3.2.

For beams reinforced with two #5 and two #6, higher shear was expected, therefore, two kinds of stirrups were used: #3 over the expected plastic hinge region and #2 beyond the expected plasticity zone. For beams reinforced with two #4, #2 stirrups were adequate and were used throughout.

TABLE 3.2

TENSION TEST RESULTS

Bar Size	Yield Stress f_y (ksi)	Ultimate Strength f_u (ksi)
#2	51.0	66.0
#3	72.4	115.0
#4	64.9	99.8
#5	63.2	105.8
#6	67.0	103.2

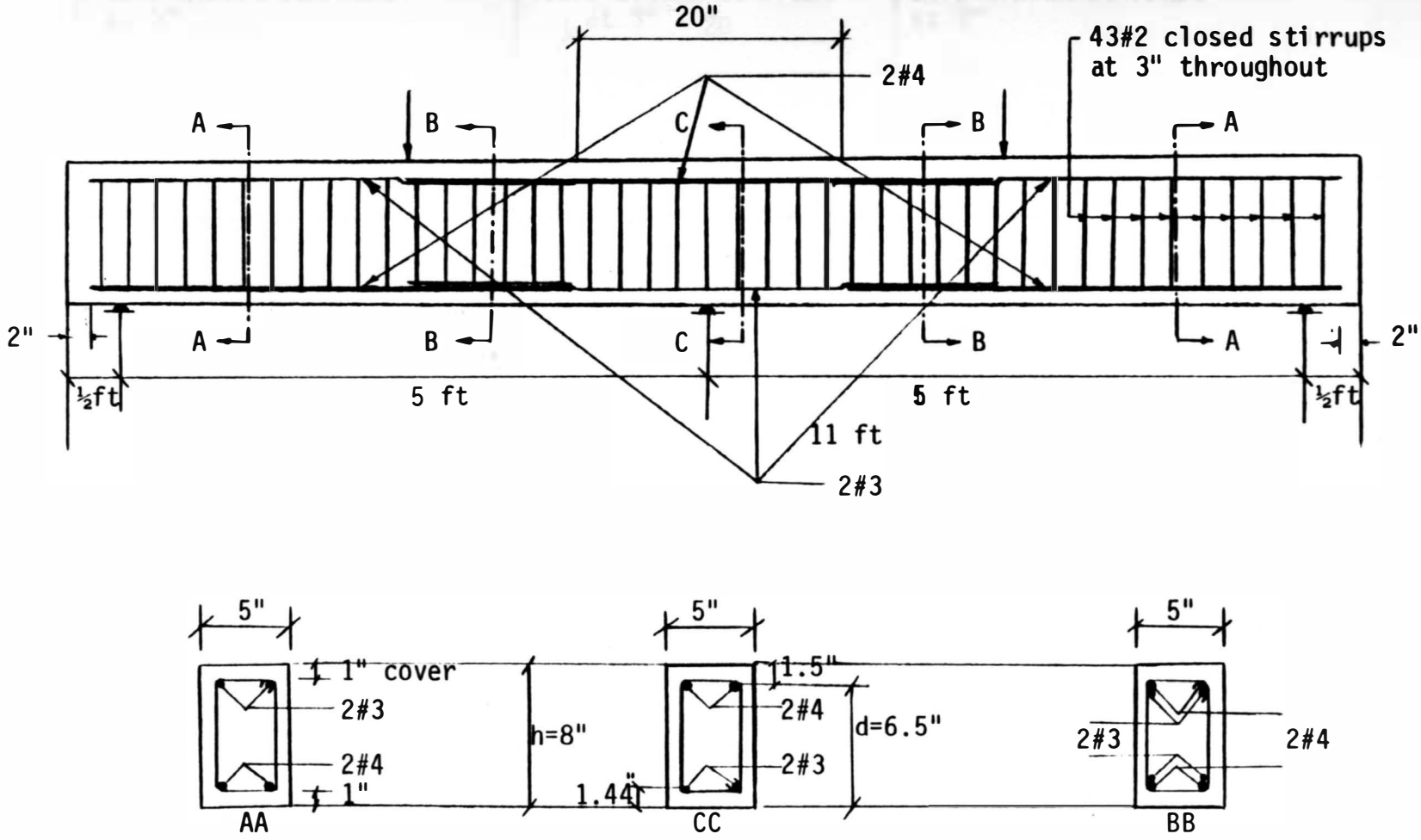

Figure 3.6. Reinforcement details of continuous beams 1, 4 and 7.

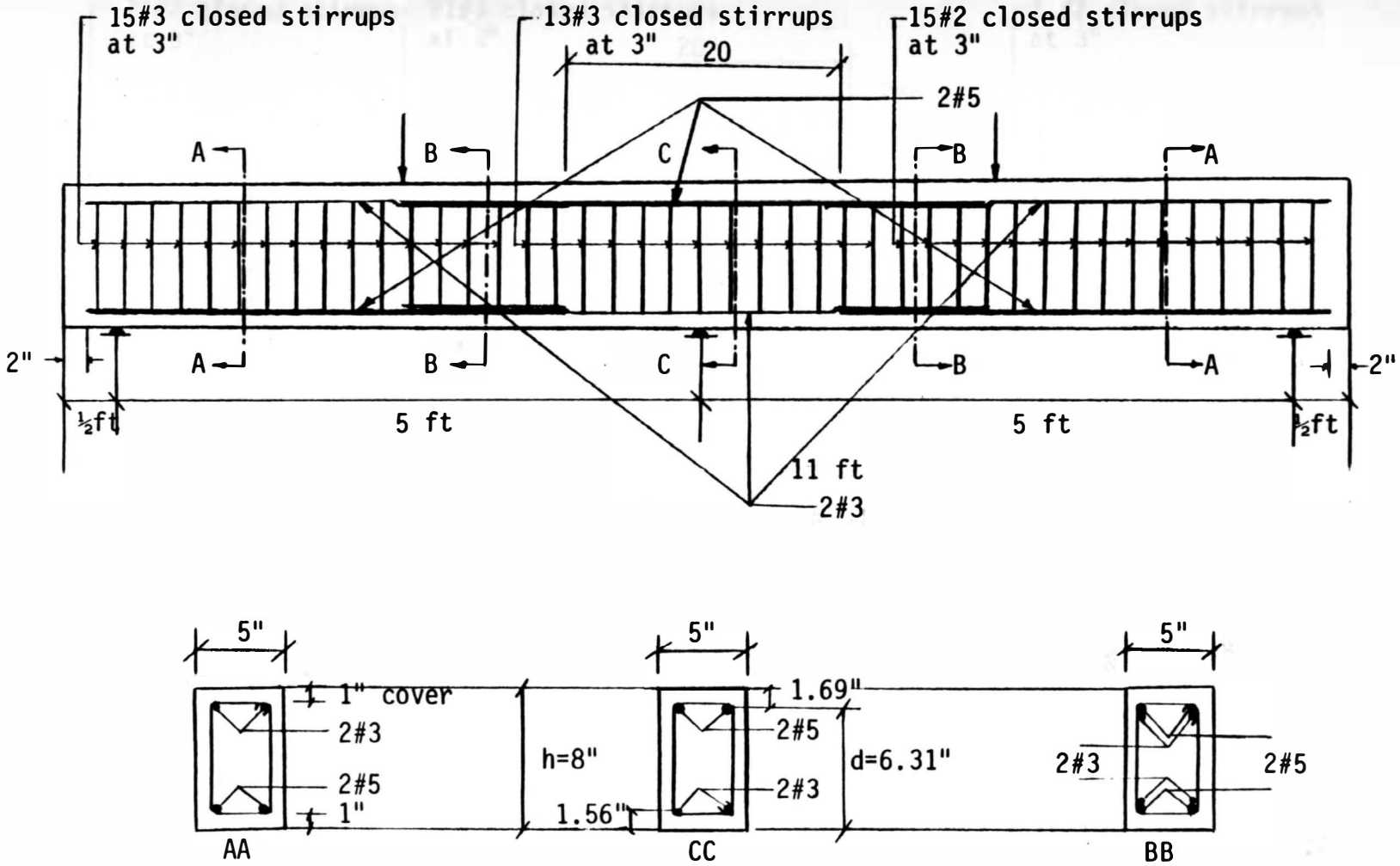

Figure 3.7. Reinforcement details of continuous beams 2, 5 and 8.

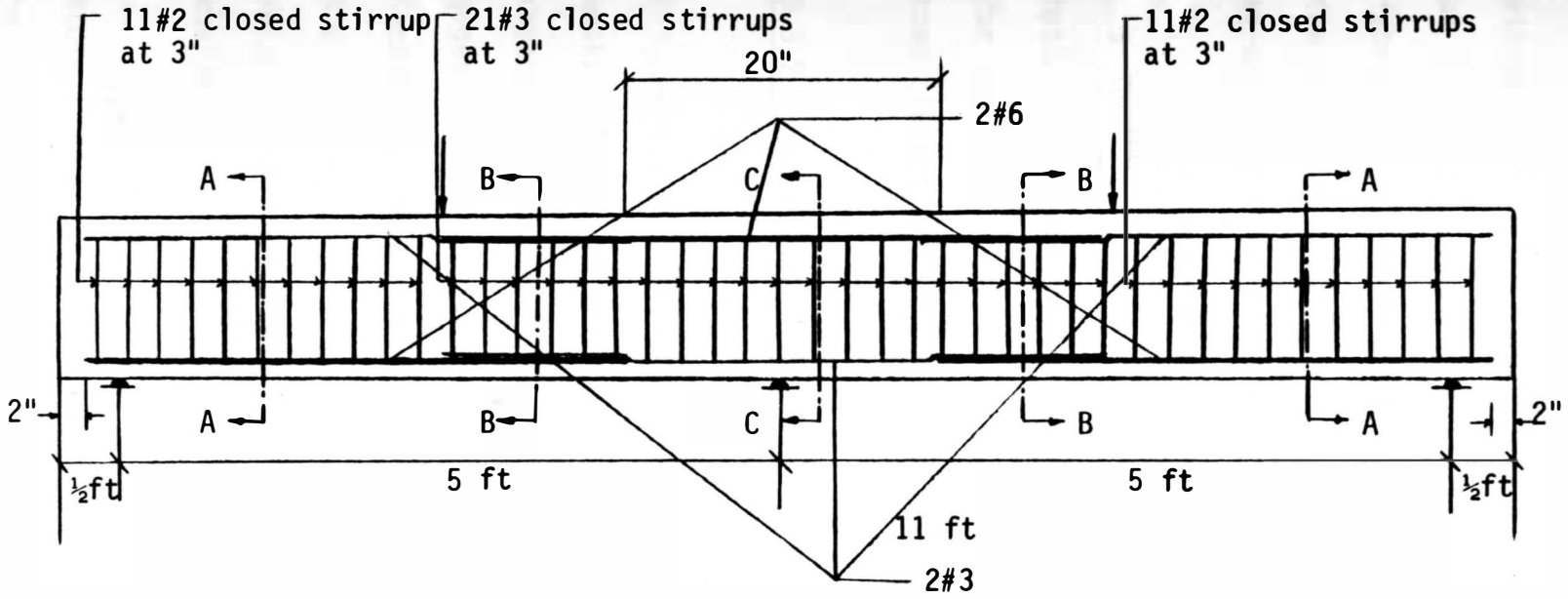

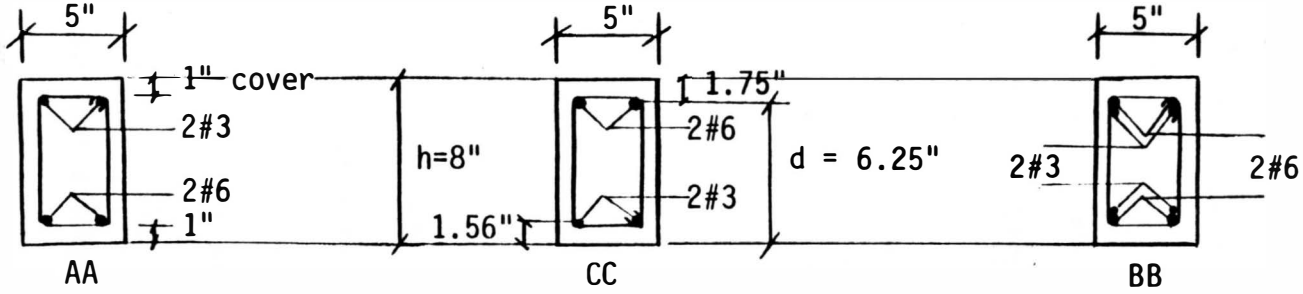

Figure 3.8. Reinforcement details of continuous beams 3, 6 and 9.

All shear reinforcements were made into closed rectangular stirrups which were spaced at 3 in. intervals. The stirrups were cut at 21 inch lengths and bent manually on especially designed and fabricated equipment. Adequate shear reinforcements were provided in the region of plastic hinging to avoid any shear failure. Figures 3.6 through 3.8 show the stirrup arrangement and beam cross sections.

The longitudinal bars and stirrups were tied manually using 5.5 inch long tie wires (Figure 3.9). The surface of the top and bottom bars were filed and smoothed at the points of maximum moments for the purpose of attaching strain gages. The smoothed surface was then cleaned and degreased (Figure 3.10)

3.3.2 Beam Preparation

The beams were demolded at 2 days and covered with wet burlap (Figure 3.11). The curing was done by sprinkling water during three weeks. The beams were carefully placed in a loading frame of 120 ton capacity. Concrete strains were obtained from electrical resistance gages type A-1 attached to the top of concrete compression zone located at middle of each span and on the under surface an inch from the mid-reaction bearing plate. All connecting wires were then soldered to the strain gages and connected to the automatic strain analyzer.

Crack measurements on beams were done using cylindrical brass studs (3/8 x 3/8) with conical holes. The brass studs were glued at one inch intervals over the 20-inch length on a straight line

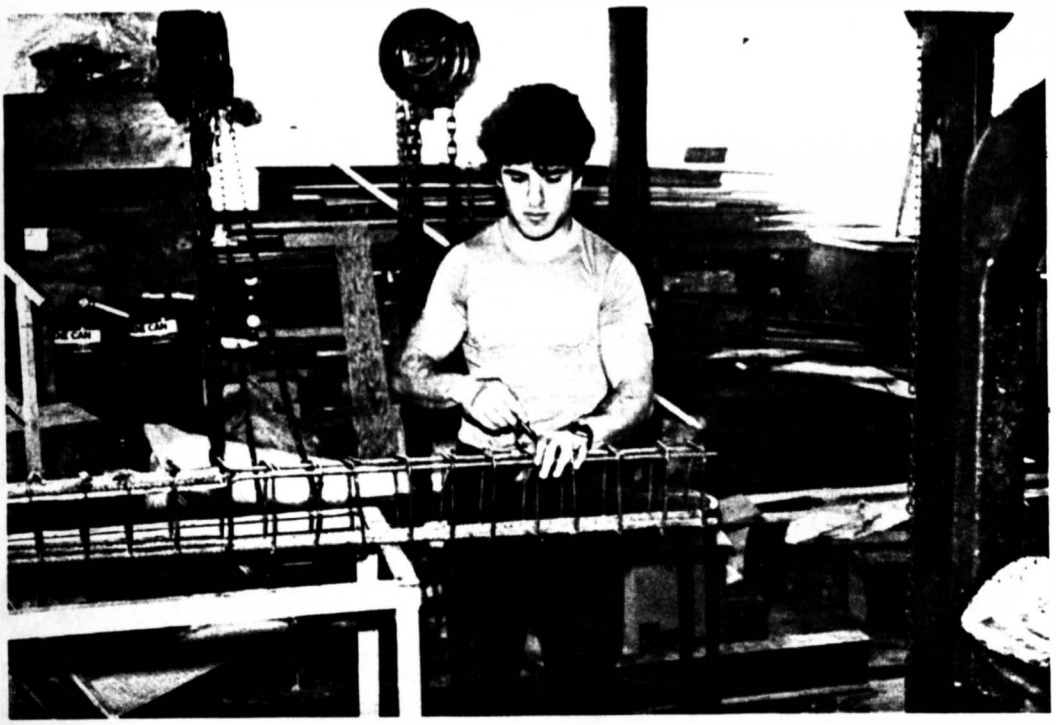

Figure 3.9. Manual tying of steel gage.

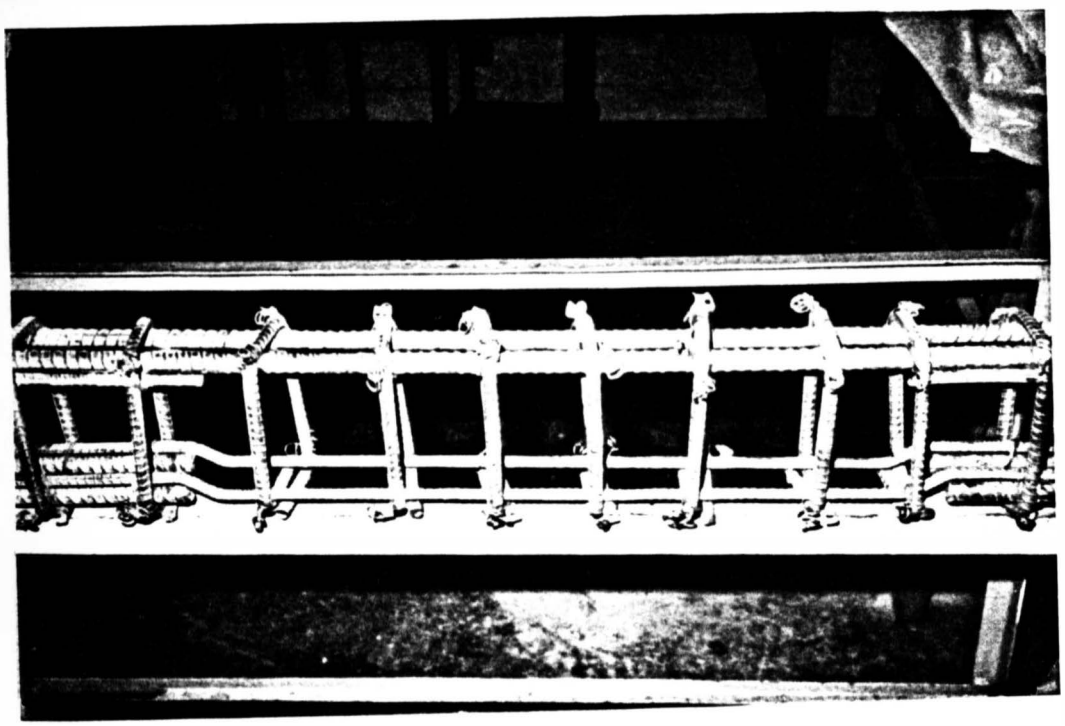

Figure 3.10. Polished steel surface.

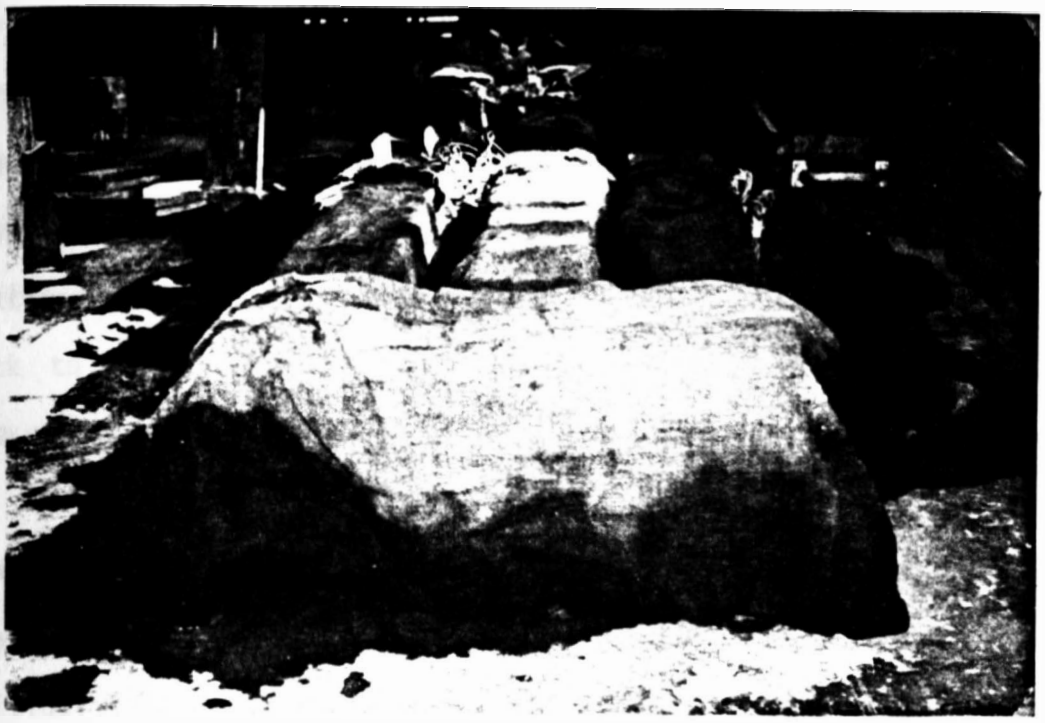

Figure 3.11. Concrete curing.

drawn on the center of the beam at the critical section over the middle support. The same brass arrangements were used on the under surface of the beam (under the applied loads). The brass studs were also glued on the side at the middle support for curvature measurements. A complete illustration of brass studs arrangement is shown in Figure 3.12. The vertical loads were applied on a steel platform that has a concave seat that allows the point head of each jack to hit uniformly. High strength dental plaster of paris or gypsum was used under the loading plates to ensure a uniform bearing.

The beams were marked at ten points for level readings. A scale with an accuracy of 1/100 of an inch was used to read the actual elastic curves and in particular the plastic deformation of the critical section up to failure. The beams were marked at the point of maximum deflection. A dial gage with an accuracy of 1/1000 of an inch was used to read the actual deflection.

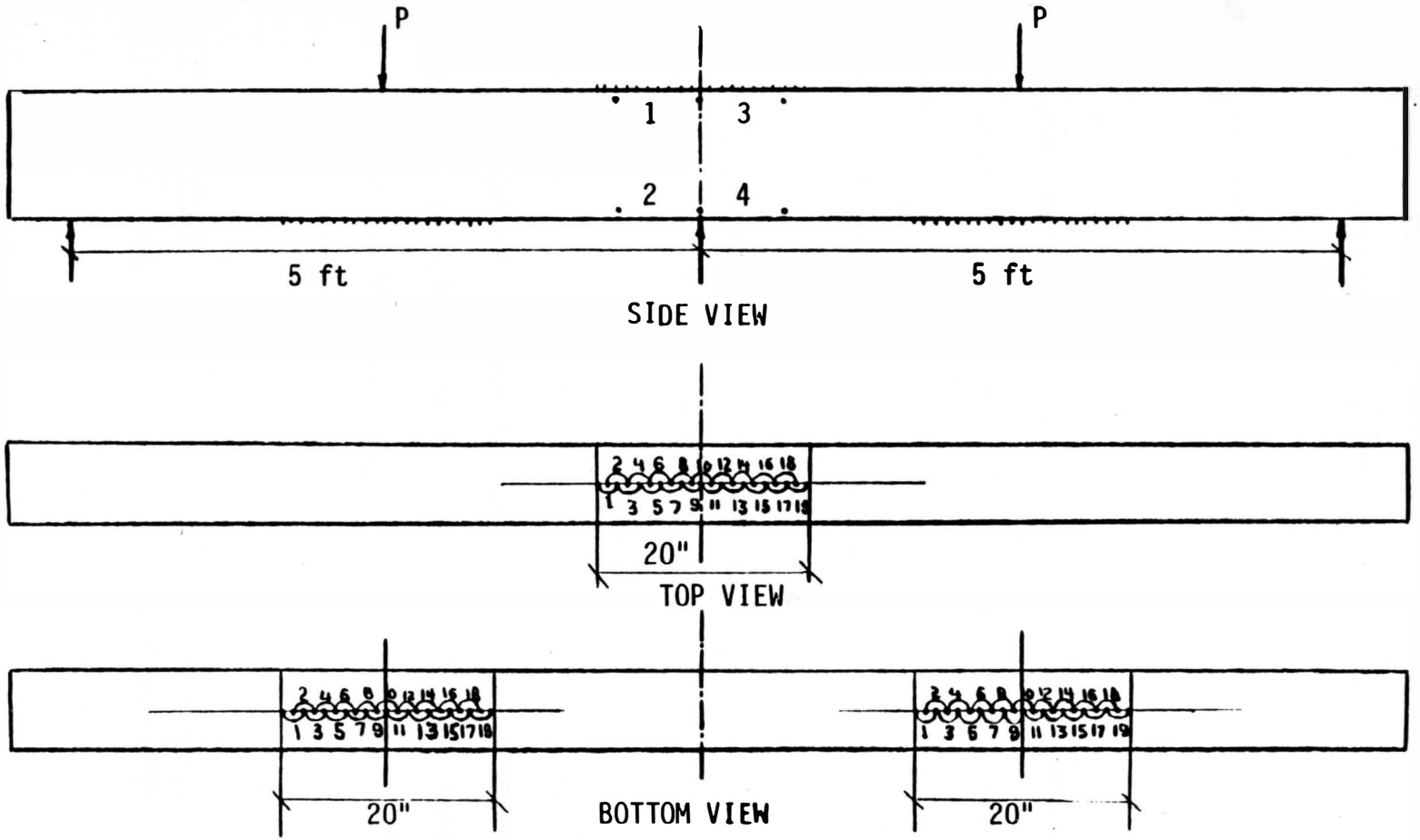

Figure 3.12. Brass studs arrangement for crack reading.

CHAPTER 4

INSTRUMENTATION AND TEST PROCEDURE

4.1 Instrumentation

4.1.1 Testing Frame

The steel girder frame used in the experiment has a capacity of 120 tons with a maximum end reaction of 60 tons, and it has a capacity of handling specimens up to twenty feet in length, five feet in width, and three feet in depth (Figure 4.1).

4.1.2. Hydraulic Console

A low and high dual range hydraulic console with a capacity of 10,000 psi was used. The low range is from zero to 2000 psi with an increment of 20 psi. The high range is from zero to 10000 psi, with an increment of 100 psi. An air pressure system was connected to the hydraulic console to release the load from the beams. This pressure system is energized by the building's air supply system, with an air pressure of about 120 pounds per square inch (Figure 4.2).

4.1.3 Hydraulic Jacks

All beams were tested in a loading frame with a manually pumped 30 ton hydraulic jack at each span (Figure 4.1). The jacks were connected with high pressure hydraulic hoses with a self-sealing

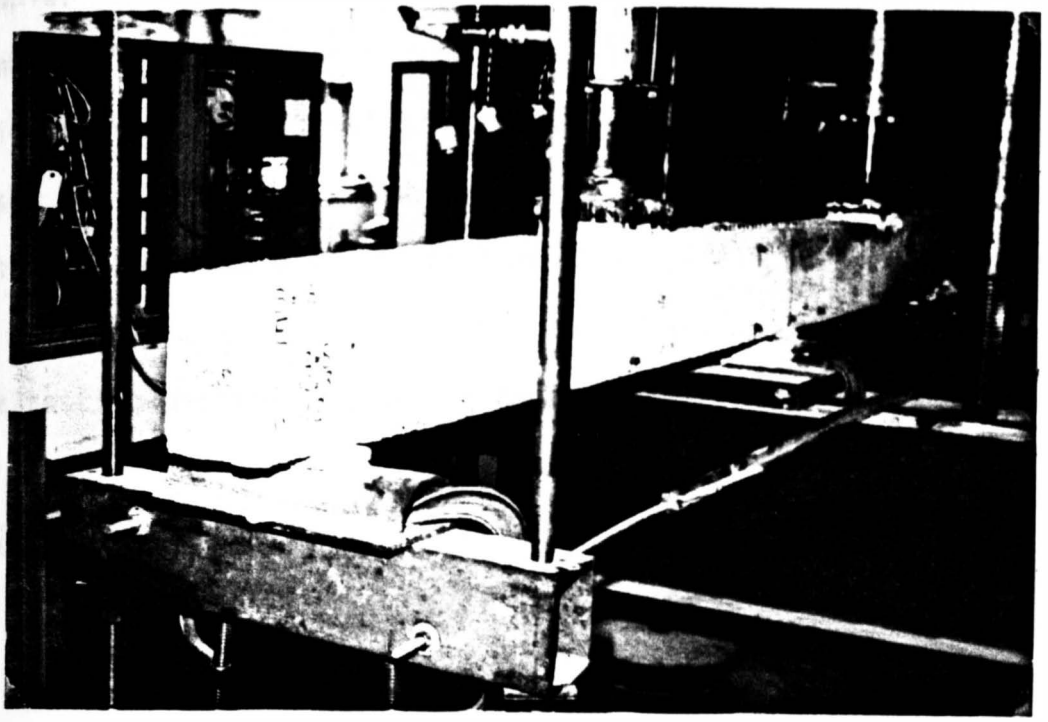

Figure 4.1. Testing frame.

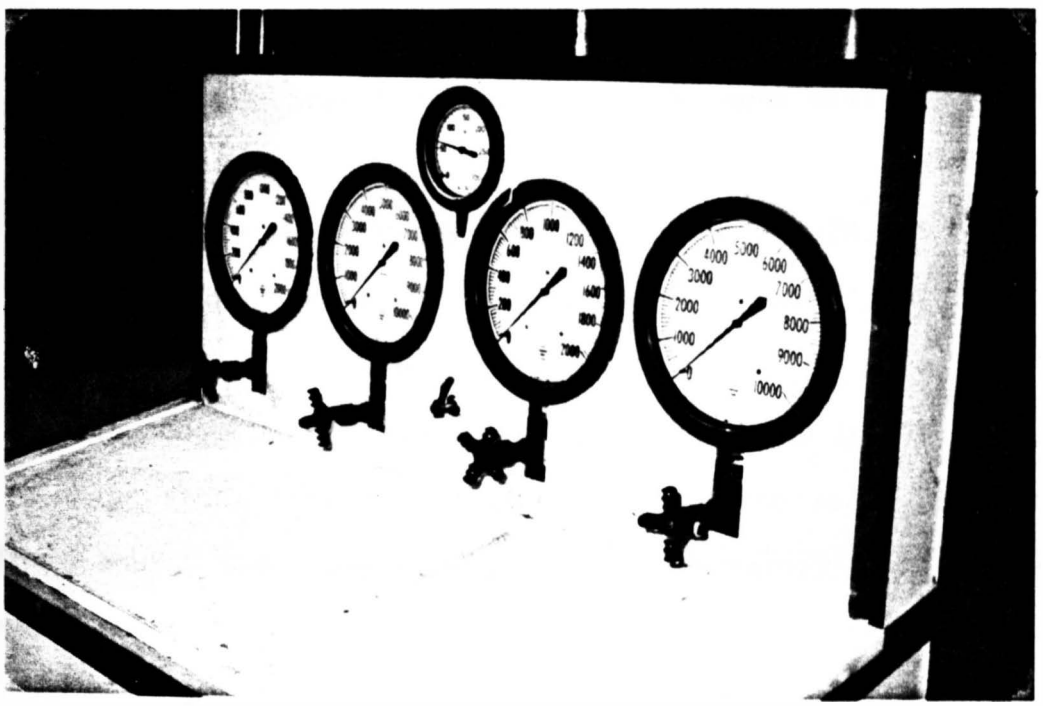

Figure 4.2. Hydraulic console.

coupler to the outlets on the loading frame. The oil was pumped manually into the jacks from the main hydraulic control console. Prior to the actual testing the jacks were calibrated by using a Tinus Olsen testing machine. The two jacks proved to behave identically. Testing the Tinus Olsen testing machine against a proving ring showed an accuracy of about 0.15%. The calibration chart of the jacks vs. the testing machine is shown in Appendix E.

4.1.4 Strain Gages

Three different types of SR-4 strain gages were used:

1. A-8 strain gages with a resistance of 1195 $\pm$ 0.3 ohms and a gage factor of 1.73 $\pm$ 2% when used for main bars.
2. A-19 strain gages with a resistance of 60.0 $\pm$ 0.5 ohms and a gage factor of 1.66 $\pm$ 3% were used for #3 bars.
3. A1-S6 strain gages with resistance of 120.4 $\pm$ 0.2 ohms and a gage factor of 1.94 $\pm$ 1% were used for concrete compression strains.

The locations of the strain gages are shown in Figure 4.3.

The steel strain gages were glued at the polished points and left 24 hours, then covered with a special material SR-4 carrier E to prevent moisture penetration to the strain gages (Figure 4.4). A

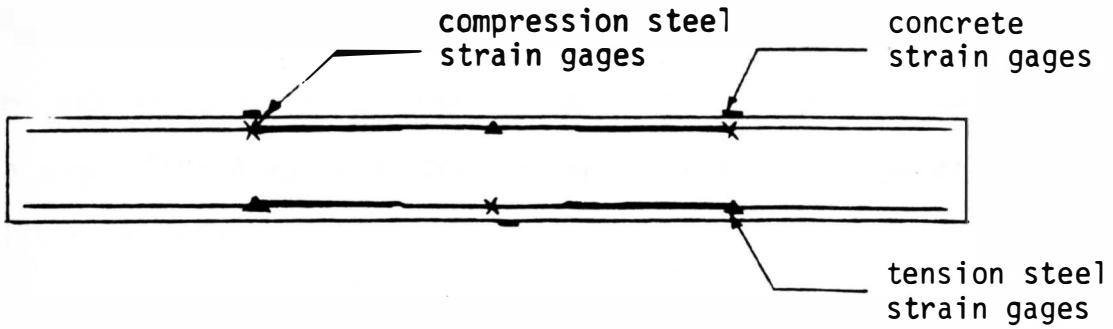

Figure 4.3. Location of strain gages.

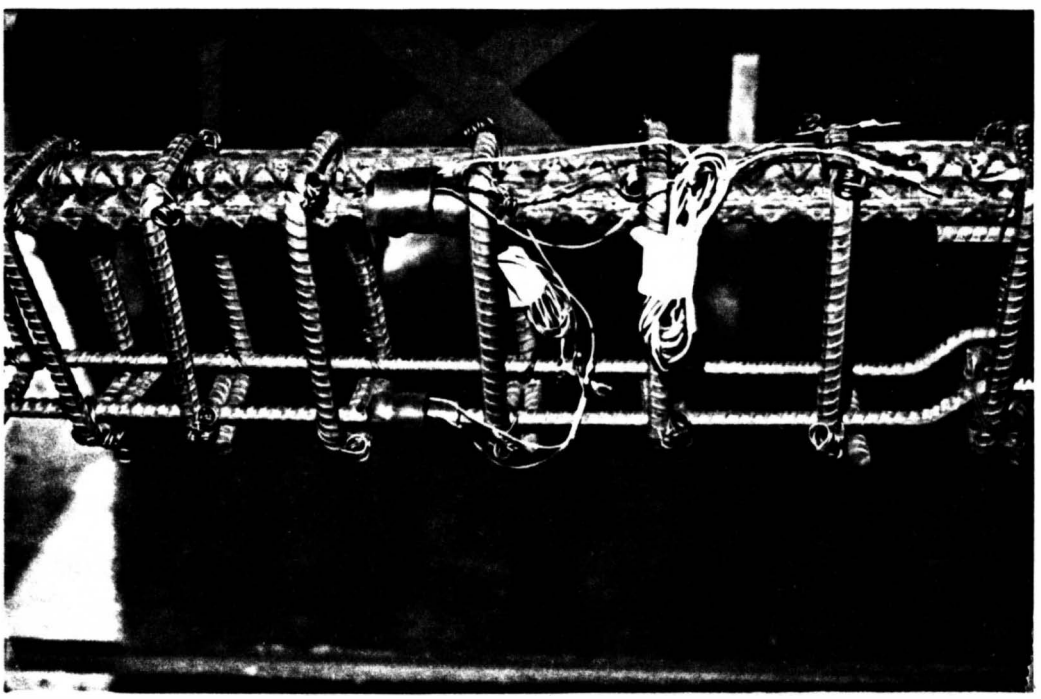

Figure 4.4. Covered strain gages at negative moment section.

hot melt glue was used to seal and protect this carrier and the strain gages from any damage or moisture seepage (Figure 4.5). Special standard #22 wires were soldered to the strain gages. Figure 4.6 shows a simplified diagram of the wiring from the strain gages to the digital strain indicator.

4.1.5 Portable Digital Strain Indicator

Concrete and steel strain gage readings were obtained by using a strain gage scanning system (Figure 4.7). It consists of four main parts:

1. Digital strain indicator which gives the direct strain readings from the channel being used. The corresponding gage factor is also set on this unit.
2. A printer which could be set to print all the strain readings.
3. Scanning module unit to which all the strain gage wires are hooked. The channels are also on this unit.
4. A controller with a three-way position mode switch and four push button switches for manual stop, stop, reset and start. The mode switch selects one of the three scanning modes:
    a. Manual mode used for individual readings.
    b. Single scan mode cycles through every channel and stops.

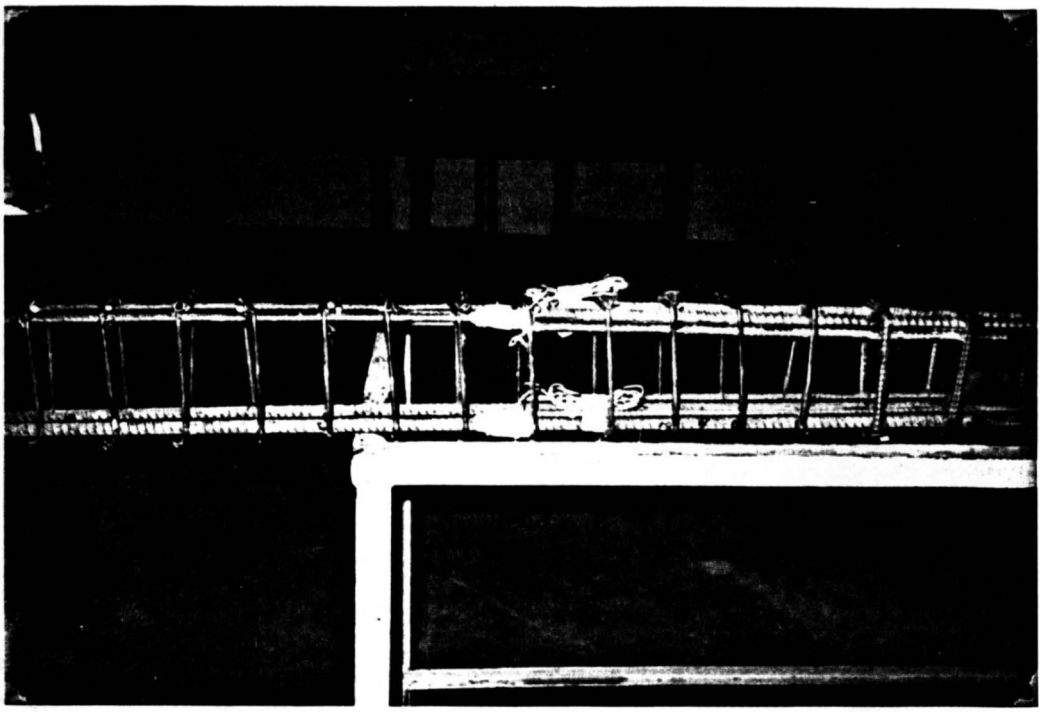

Figure 4.5. Waxed strain gages.

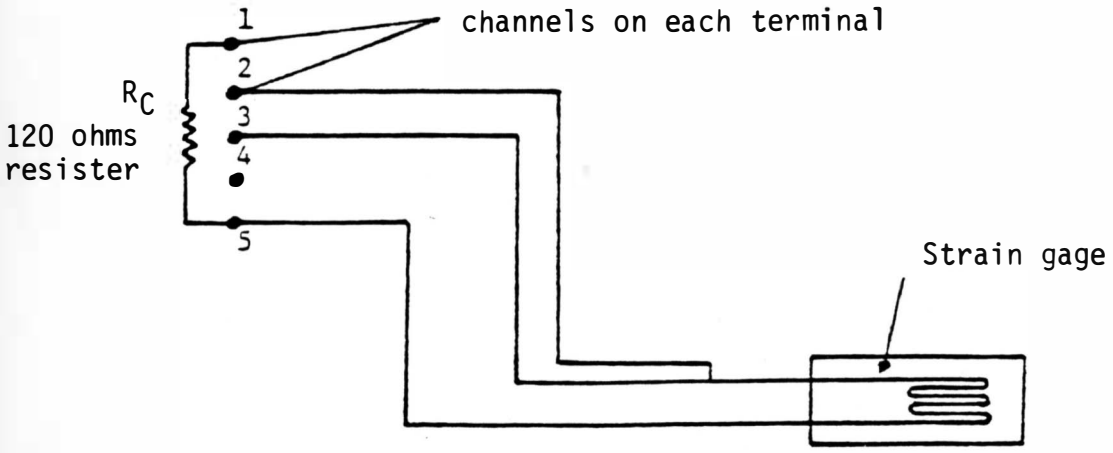

Figure 4.6. Wiring system.

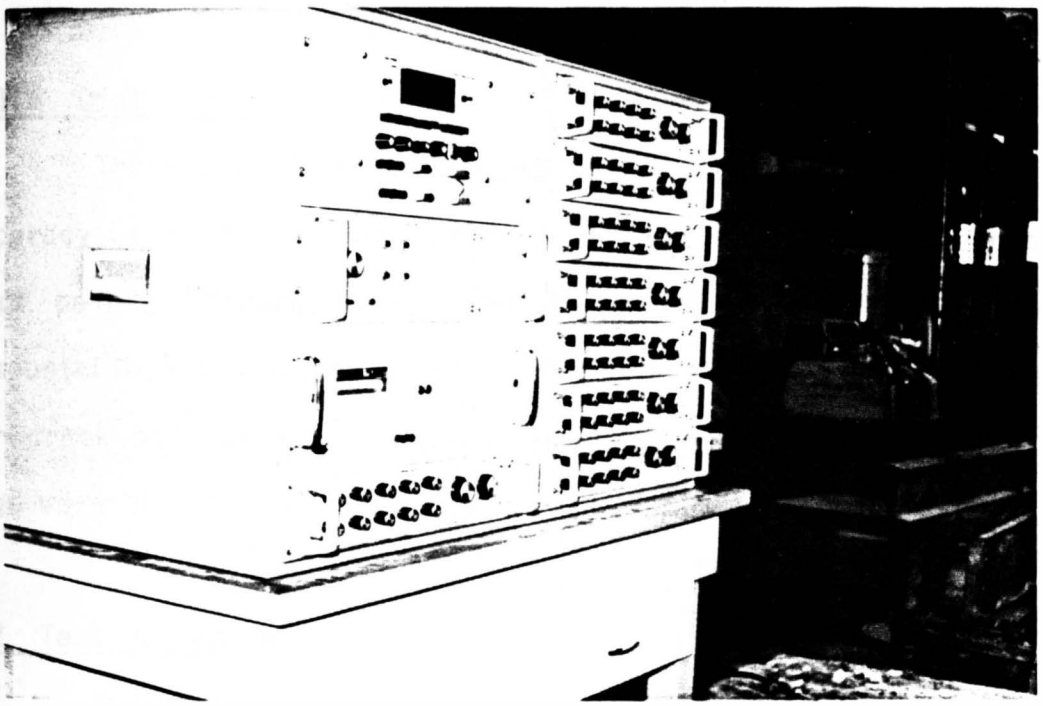

Figure 4.7. Portable digital strain indicater.

c. Automatically scans and stops after the last channel reading has been printed out.

4.1.6 Dial Gages

Three dial gages were used in the beam testing. Two with an accuracy of 1/1000 in. were used for deflection readings under the two load points (Figure 4.8). The third dial, which has mechanical demountable extensometer gages of 2 and 8 in. gage lengths, was used for crack and curvature measurements, respectively. Readings of this gage were observed with an accuracy of 1/1000 in. (Figure 4.9).

4.2 Test Procedure

The same test procedure was adopted to test all beams. Before commencing the tests, all the equipment was rechecked and zero readings were taken for strain gages, deflections, cracks, level and curvature. The load was applied gradually by increments of 1.02 kips. The following measurements were recorded during the test:

1. The strains of the steel and the concrete at critical sections.
2. Deflections in the span critical sections (under the concentrated loads).
3. Curvature along the beam side at critical sections (middle supports).
4. Level readings at marked points.
5. Crack width at critical sections.

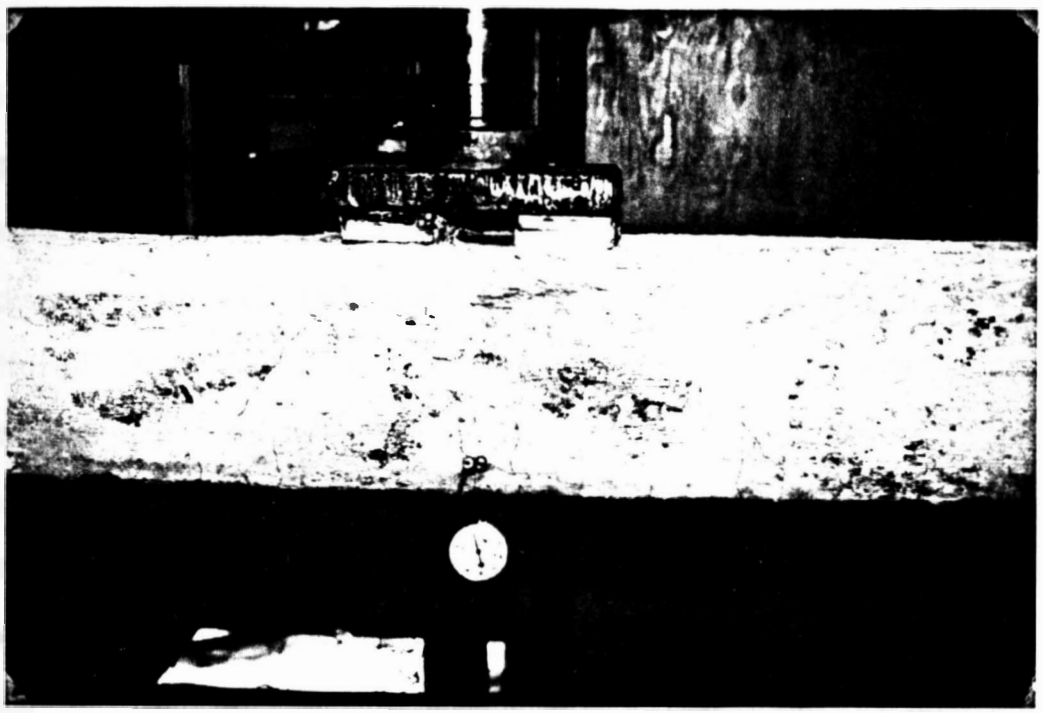

Figure 4.8. Deflection dial gage.

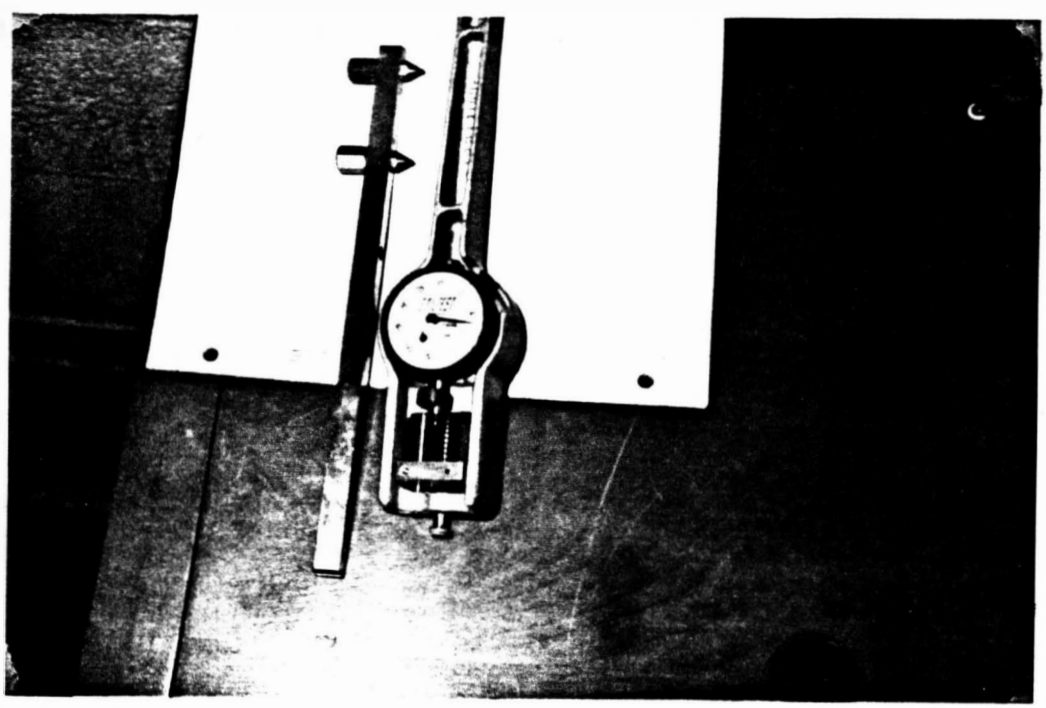

Figure 4.9. Crack width dial gage.

CHAPTER 5

BEAM DESIGN

5.1 Beam Loading System

The loading system used in this research project is shown in Figure 5.1. It shows a continuous beam with two identical spans. A concentrated load is applied on the midpoint of each span. Three different loading possibilities were considered before choosing the optimum case:

1. Load at x = 0.45L when maximum positive moment is obtained.
2. Load at x = 0.55L when maximum negative moment at midsupport is obtained.
3. Load at midspan (x = 0.50L).

The moments at B and C were computed and tabulated in terms of P, where L = 60 inches (Table 5.1).

The redistribution factor r was determined for each case. As it is obvious when x = 0.45L, r = 1.07 where there is not enough redistribution of moments to discuss the plastic rotation capacity of the critical section. When x = 0.35L the value of r = 1.35, meaning 35% moment redistribution is required for the critical section to develop a collapse mechanism that is relatively high.

Therefore, an optimum x value at 0.5L was chosen to result in a reasonable 20% moment redistribution, so the rotation capacity of the middle support can be determined without a premature failure.

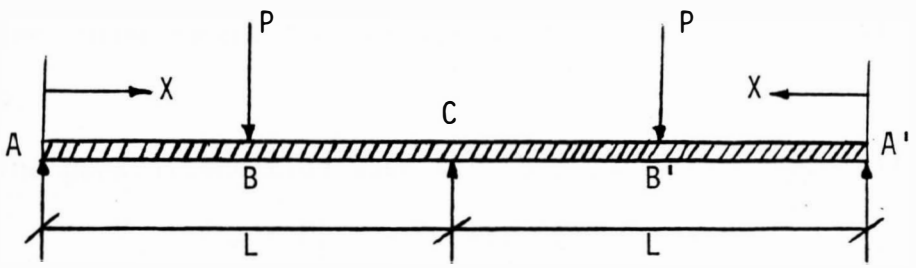

Figure 5.1. Loading system.

TABLE 5.1

MOMENT DISTRIBUTION FOR DIFFERENT LOADING SYSTEMS

X	0.45L	0.55L	0.50L
MB	10P	8.53P	9.38
MC	10.76P	11.6P	11.25P
r	1.07	1.35	1.2

5.2 Beam Analysis

5.2.1 Elastic Analysis of Beams

The three-moment theorem was used for the elastic analysis of the beams.

The general equation used for this analysis is as follows:

$$M_A + 4M_C + M_E = -\Sigma P_1 L(K_1 - K_1^3) - \Sigma P_2 L(K_2 - K_2^3)$$

In this case equal concentrated loads exist as well as equal spans and the load is at the center of the span ($K_1 = K_2 = 0.5$) (Figure 5.2). Therefore, the above equation is reduced as follows:

$$M_A + 4M_C + M_E = -2PL(0.5 - 0.5^3)$$

$$M_A + 4M_C + M_E = -2PL(0.375)$$

$$M_A = M_E = 0$$

Therefore $4M_C = -0.75PL$

for L = 60"

$$M_C = -11.25P$$

Reactions were calculated by statics (refer to Figure 5.2)

$$R_A = R_E = 0.313P$$

$$R_C = 0.688P + 0.688P = 1.38P$$

Shear force and bending moment diagrams are shown in Figure 5.2.

5.2.2 Plastic Analysis

The virtual displacement principle is used to analyze the two-span continuous beam with the concentrated loads at the center of the spans.

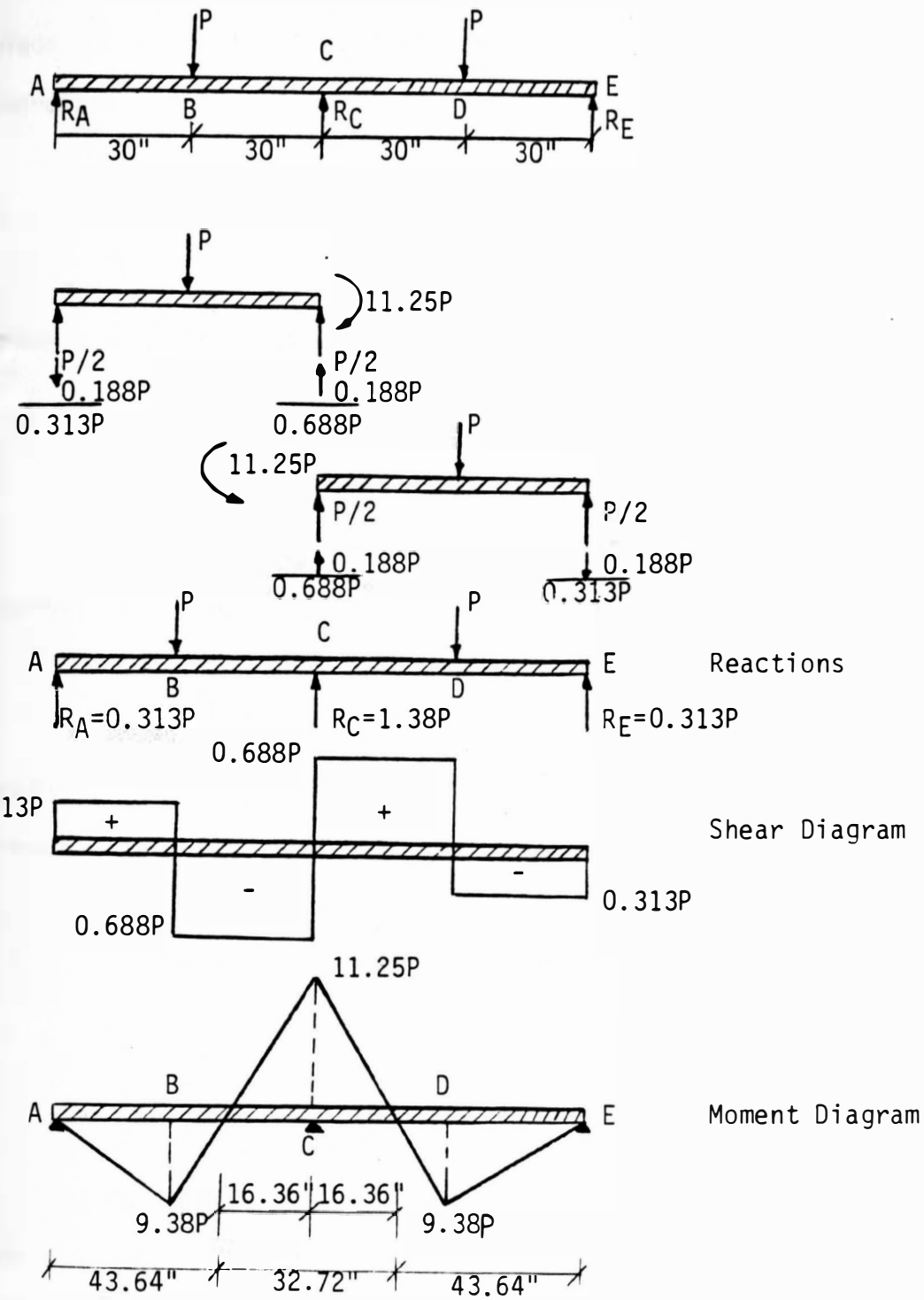

Figure 5.2. Elastic analysis.

In the virtual work method, the external work done by applied loads is equal to the internal work absorbed by the plastic hinges. Therefore

$$W_E - W_I$$

$$W_E = \sum_{i=1}^{K} P_i \Delta_i$$

where Δ = vertical displacement of hinges

$$\Delta_2 = \Delta_4 = L/2(\theta)$$

$$W_E = P(L/2)(\theta) + P\ (L/2)(\theta) = 2P(L/2)(\theta)$$

The internal work in the structure will be the sum of the virtual work done at the plastic hinges.

$$W_I = \Sigma M_P \theta_i = M_P \sum_{i=1}^{K} \theta_i$$

where θ_i = the angle through which the hinges rotate.

From Figure 5.3 the following is obtained:

$$W_I = M_P \times 2\theta \ + \ M_P \times 2\theta \ + \ M_P \times 2\theta$$

Section 2 Section 3 Section 4

$$W_I = 3M_P \times 2\theta$$

$$W_I = W_E$$

$$2P(L/2)\theta = 3M_P \times 2\theta$$

$$Pu = 6M_P/L$$

where L = 60 inches

Therefore $M_P = 10\ P_u$

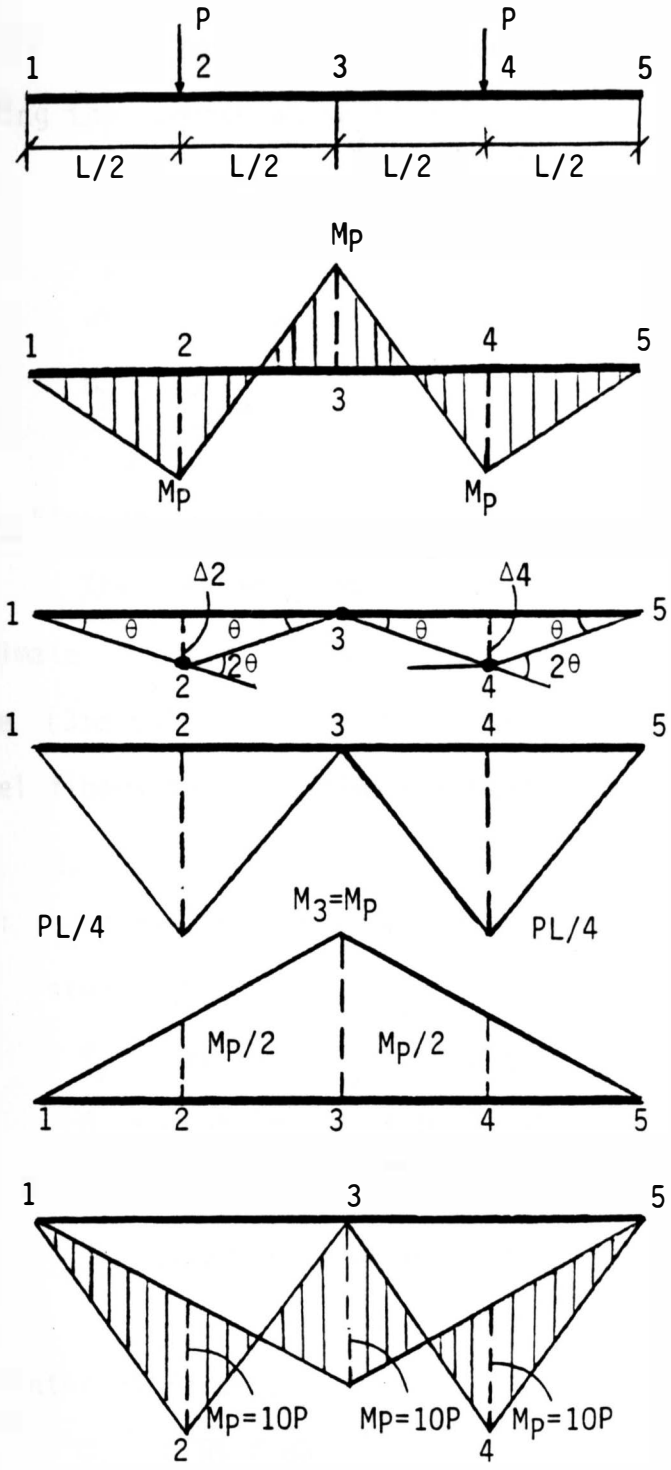

a) Bending Moment Diagram

b) Mechanism

c) Moment due to determinate loading

d) Moment due to reduntant loading

e) Composite moment diagram

Figure 5.3. Plastic analysis.

This result can be checked by the equilibrium equation by adding the moments at section 2 on Figure 5.3 (c,d,e).

$P_u L/4 = M_P + M_P/2$

$P_u = 6M_P/L$

where L = 60 in.

$M_P = 10\ P_u$

5.3 Flexure Design of the Beams

The method used for design of the beams is based on the ultimate strength theory of reinforced concrete according to the ACI Code (318-83). In the following calculations the contribution of steel fibers to the ultimate moment capacity of the beam is neglected.

B#1: A_s = 2#4 tension steel, A_s' = 2#3 compression steel and 0.0% steel fibers.

$f_c' = 4970$ psi, $f_y = 64.9$ ksi, $f_y' = 72.4$ ksi

$A_s = 0.39\ in^2$, $A_s' = 0.22\ in^2$

d = 6.5 in, d' = 1.44 in

Ultimate moment capacity M_u is calculated according to Figure 5.4.

1. Internal forces:

$C_c = 0.85\ f_c' ab$

$C_c = 0.85(4.97)(a)(5) = 21.123a$ kips

C_s = the force in compression steel

$= A'_s f'_s$ - force in displaced concrete

$= A'_s f'_s - A'_s(0.85f'_c) = 0.22 f'_s - 0.22 \times 0.85 \times 4.97$

$= 0.22 f'_s - 0.929$

$T = T_1 + T_2 = A_s f_y = 0.39 \times 64.9 = 25.31$ kips

Since $T = C_c + C_s$

Therefore:

$$26.24 = 0.22 f'_s + 21.123a$$

By trial and error $c = 1.505$ in

$a = \beta(c)$ where $\beta = 0.8$ since $f'_c \approx 5000$ psi

$a = 0.8 \times 1.505 = 1.204$ in

From force triangles (Figure 5.5)

$$f'_s = \{[(c - d')(\varepsilon_c)]/c\}E_s =$$

$$\{[(1.505-1.44)(0.003)]/1.505\}29000 = 3.76 \text{ ksi}$$

$T_2 = C_s$

$A_{s2} f_y = A'_s f'_s$

$A_{s2} = A'_s f'_s / f_y = (0.22 \times 3.76)/64.9 = 0.01275 \text{ in}^2$

$A_{s1} = A_s - A_{s2} = 0.39 - 0.01275 = 0.3773 \text{ in}^2$

2. Check if section is underreinforced:

$\rho_{balance} = 0.85 \times \beta[f'_c/f_y][87/(87 + f_y)]$

$\rho_{balance} = 0.85x0.8[4.97/64.9][87/(87+64.9)] = 0.02989 = 2.99\%$

$\rho_{max} = 0.75\ \rho_{balance} = 0.75 \times 0.02989 = 0.02242 = 2.24\%$

$\rho_{min} = 200/f_y = 200/64900 = 0.00308$

$\rho_1 = (A_s - A_{s2})/bd$

$= 0.3773/(5x6.5) = 0.01161 < \rho_{balance} = 0.02989 < \rho_{max}$

Therefore, the section is underreinforced

ρ/ρ_{max} = 0.01161/0.02242 = 0.518

$\rho/\rho_{balance}$ = 0.01161/0.02989 = 0.401

3. Calculate the ultimate moment using the following equation:

$M_u = [A_{s1}f_y][d - (a/2)] + (A'_s f'_s)(d-d')$

$= [0.3773x64.9][6.5-(1.204/2)]+(0.22x3.76)(6.5-1.44) =$

149.73 k.in

4. Calculate P_y and P_u

P_y = 149.73/11.25 = 13.31 k

$M_P = 1.2\ M_u$ (Table 5.1)

M_P = 1.2 (149.73) = 179.68 k in

But $M_P = 10\ P_u$

Therefore P_u = 179.68/10 = 17.97 k

B#2: A_s = 2#5 tension steel, A'_s = 2#3 compression steel and 0.0% steel fibers.

f'_c = 4970 psi, f_y = 63.2 ksi, f'_y = 72.4 ksi

A_s = 0.61 in^2, A'_s = 0.22 in^2

d = 6.31 in, d' = 1.56 in

Ultimate moment capacity M_u is calculated according to Figure 5.5.

1. Internal forces:

$C_1 = 0.85\ f'_c ab$

$C_1 = 0.85(4.97)(a)(5) = 21.123a$ kips

C_2 = the force in compression steel

$= A'_s f'_s$ - force in displaced concrete

$= A'_s f'_s - A'_s(0.85f'_c) = 0.22 f'_s - 0.22x0.85x4.97$

$= 0.22 f'_s - 0.929$

$T = T_1 + T_2 = A_s f_y = 0.61x63.2 = 38.55$ kips

Since $T = C_c + C_s$

Therefore:

$39.48 = 0.22 f'_s + 21.123a$

By trial and error $c = 2.061$ in.

$a = \beta(C)$ where $\beta = 0.8$ since f'_c 5000 psi

$a = 0.8x2.061 = 1.649$ in

From force triangles (Figure 5.6)

$f'_s = \{[(c - d')(\varepsilon_c)]/c\}E_s$

$f'_s = \{[(2.061-1.56)(0.003)]/2.061\}29000 = 21.16$ ksi

$T_2 = C_s$

$A_{s2} f_y = A'_s f'_s$

$A_{s2} = A'_s f'_s / f_y = (0.22x21.26)/63.2 = 0.074$ in^2

$A_{s1} = A_s - A_{s2} = 0.61 - 0.0737 = 0.536$ in^2

2. Check if section is underreinforced

$\rho_{balance} = 0.85(0.8)[4.97/63.2][87/(87+63.2)] = 0.03109 = 3.11\%$

$\rho_{max} = 0.75\ \rho_{balance} = 0.75x0.03109 = 0.02332 = 2.33\%$

$\rho_{min} = 200/f_y = 200/63200 = 0.00317$

$\rho_1 = (A_s - A_{s2})/bd$

$= 0.536/(5x6.31) = 0.01699 < \rho_{balance} = 0.03109$

$\rho/\rho_{max} = 0.01699/0.02332 = 0.729$

$\rho/\rho_{balance} = 0.01699/0.03109 = 0.546$

3. Calculate the ultimate moment using the following equation:

$$M_u = [A_{s1} f_y][d - (a/2)] + (A'_s f'_s)(d-d')$$

$$= [0.536 \times 63.2][6.31-(1.649/2)]+(0.22 \times 21.16)(6.31-1.56) =$$

207.9 k.in

4. Calculate P_y and P_u

$$P_y = 207.9/11.25 = 14.48 \text{ k}$$

$$M_P = 1.2(207.9) = 249.48 \text{ k. in}$$

$$M_P = 10\ P_u$$

$$P_u = 249.48/10 = 24.95 \text{ k}$$

B#3: A_s = 2#6 tension steel, A'_s = 2#3 compression steel and 0.0% steel fibers.

f'_c = 4970 psi, f_y = 67.0 ksi, f'_y = 72.4 ksi

$A_s = 0.88 \text{ in}^2$, $A'_s = 0.22 \text{ in}^2$

d = 6.25 in, d' = 1.56 in

Ultimate moment capacity M_u is calculated according to Figure 5.6.

1. Internal forces:

$$C_c = 0.85\ f'_c ab$$

$$C_c = 0.85(4.97)(a)(5) = 21.123a \text{ kips}$$

C_s = the force in displaced concrete

$$= A'_s f'_s - A'_s(0.85f'_c) = 0.22\ f'_s - 0.22(0.85 \times 4.97)$$

$$= 0.22\ f'_s - 0.929$$

$$T = A_s f_y = 0.88 \times 67 = 58.96 \text{ kips}$$

$$T = C_c + C_s$$

Therefore:

$$59.89 = 0.22\ f'_s + 21.123a$$

By trial and error $c = 3.0$ in

$a = \beta(c)$ where $\beta = 0.8$ since f'_c 5000 psi

$a = 0.8 \times 3.0 = 2.4$ in

From force triangles (Figure 5.6)

$$f'_s = \{[(c - d')(\varepsilon_c)]/c\}E_s =$$

$$\{[(3.0-1.56)(0.003)]/3.0\}29000 = 41.76 \text{ ksi}$$

$$T_2 = C_s$$

$$A_{s2}\ f_y = A'_s\ f'_s$$

$$A_{s2} = A'_s f'_s / f_y = (0.22 \times 41.76)/67.0 = 0.137 \text{ in}^2$$

$$A_{s1} = A_s - A_{s2} = 0.88 - 0.137 = 0.743 \text{ in}^2$$

2. Check if section is underreinforced

$$\rho_{balance} = 0.85(0.8)[4.97/67.0][87/(87+67.0)] = 0.02859 = 2.86\%$$

$$\rho_{max} = 0.75\ \rho_{balance} = 0.75 \times 0.02859 = 0.02144 = 2.14\%$$

$$\rho_{min} = 200/f_y = 200/67 = 0.00299$$

$$\rho_1 = (A_s - A_{s2})/bd = 0.743/(5 \times 6.25) = 0.02378$$

$$\rho' = A_{S2}/bd = 0.137/5 \times 6.25 = 0.438$$

$$\rho/\rho_{max} = 0.02378/0.02144 = 1.11$$

$$\rho/\rho_{balance} = 0.02378/0.02859 = 0.832$$

3. Calculate the ultimate moment using the following equation

$$M_u = [A_s f_y][d - (a/2)] + (A'_s f'_s)(d-d')$$

$$M_u = [0.743 \times 67.0][6.25-(2.4/2)]+(0.22 \times 41.76)(6.25-1.56) =$$

$$294.48 \text{ k.in}$$

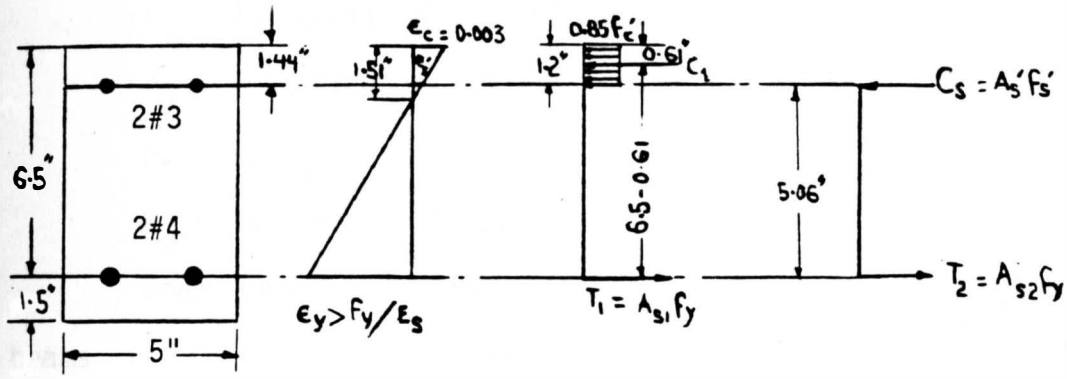

Figure 5.4. Stress and strain diagram for Beam #1.

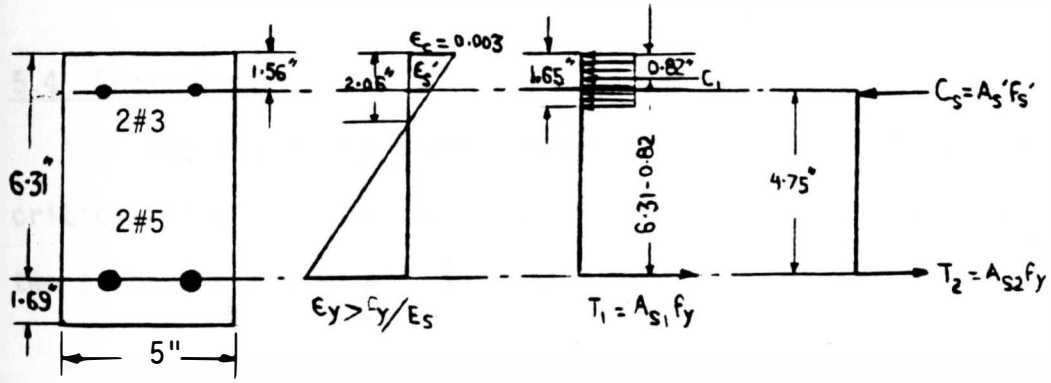

Figure 5.5. Stress and strain diagram for Beam #2.

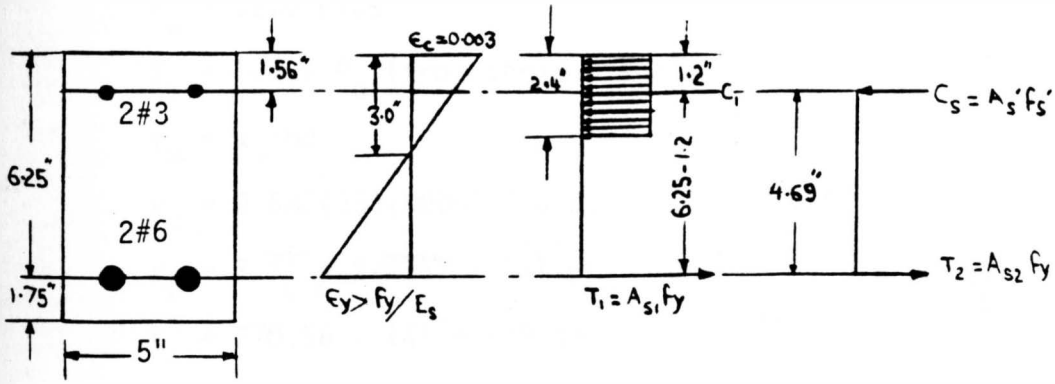

Figure 5.6. Stress and strain diagram for Beam #3.

4. Calculate P_y and P_u

$P_y = M_u/11.25$

$P_y = 294.48/11.25 = 26.18$ kips

$M_P = 1.2(294.48) = 353.38$

$M_P = 10\ P_u$

$P_u = 353.38/10 = 35.34$ kips

Beam properties and ultimate moment capacity of the tested beams in this experiment are summarized in Tables 5.2 and 5.3 respectively.

5.4 Shear Design

The following shear design calculation is done for the most critical case when two #6 bars are used as tension reinforcement and two #3 bars are used as compression reinforcement.

Beam #3 A_s = 2#6 bars, A_s' = 2#3 bars and 0.0 steel fibers

$P_u = 35.0$ kips

$V_u = 0.688\ P_u$ (from shear diagram Figure 5.2)

$v_u = V_u/bd$

$v_u = 0.688(35)(1000)/5(6.25) = 770.56$ psi

$v_c = 2\sqrt{f_c'} = 2\sqrt{4967} = 141$ psi

$V_s = 770.56 - 141 = 629.56$ psi

$S_{required} = A_v f_y/V_s b = 0.22(72.4)(1000)/629.56(5) = 5.06$ in

$d/2 = 6.25/2 = 3.13$ in

The spacing used for all beams was 3 in. Therefore, adequate shear reinforcement was provided in all beams. Shear reinforcement details are shown in Figures 3.6 through 3.8.

TABLE 5.2

BEAM PROPERTIES

Beam No.*	% Steel Fibers	TENSION STEEL Bars	TENSION STEEL Yield Stress f_y (ksi)	TENSION STEEL Ultimate Stress f_u (ksi)	TOP STEEL Bars	TOP STEEL Yield Stress f_y' (ksi)	TOP STEEL Ultimate Stress f_u (ksi)	Compressive Strength f'_c (psi)
1	0.0	2#4	64.9	99.8	2#3	72.4	115	4970
4	0.8	2#4	64.9	99.8	2#3	72.4	115	5180
7	1.2	2#4	64.9	99.8	2#3	72.4	115	5275
2	0.0	2#5	63.2	105.8	2#3	72.4	115	4970
5	0.8	2#5	63.2	105.8	2#3	72.4	115	5180
8	1.2	2#5	63.2	105.8	2#3	72.4	115	5275
3	0.0	2#6	67.0	103.2	2#3	72.4	115	4970
6	0.8	2#6	67.0	103.2	2#3	72.4	115	5180
9	1.2	2#6	67.0	103.2	2#3	72.4	115	5275

*b = 5 in. and h = 8 in. for all beams.

TABLE 5.3

ULTIMATE MOMENT CAPACITY

Beam No.	% Steel Fibers	b in inches	d in inches	d' in inches	$\rho = A_s/bd$	f'_s (psi)	$\rho' = A_{s2}/bd$ in (%)	M_u k.in.	P_y kips	P_u kips
1	0.0	5	6.5	1.44	1.20	3.76	*	149.73	13.31	17.97
4	0.8	5	6.5	1.44	1.20	2.35	*	152.41	13.55	18.29
7	1.2	5	6.5	1.44	1.20	1.54	*	153.87	13.68	18.46
2	0.0	5	6.31	1.56	1.93	21.16	*	207.9	18.48	24.95
5	0.8	5	6.31	1.56	1.93	19.81	*	209.2	18.60	25.10
7	1.2	5	6.31	1.56	1.93	19.14	*	209.56	18.63	25.15
3	0.0	5	6.25	1.56	2.82	41.76	0.438	294.48	26.18	35.34
6	0.8	5	6.25	1.56	2.82	40.69	0.427	296.65	26.37	35.60
9	1.2	5	6.25	1.56	2.82	40.04	0.421	297.5	26.44	35.70

*Bars act as stirrup holders only; stress is very low.

CHAPTER 6

TEST RESULTS

6.1 Compressive Strength

Concrete is a brittle material, and its ability to resist compressive stresses is much higher than tensile stresses. Therefore compressive strength that depends mainly on the water/cement ratio and curing condition is considered the main measure ofthe structural quality of concrete. The compressive strength of concrete is determined by testing a 28-day standard size cylinder of 6 in. across and 12 in. high at a specified loading rate. In present practice, compressive strength between 3000 and 6000 psi is usually specified for reinforced concrete structures, values between 3000 and 4000 psi being the most common. For prestressed concrete, higher strengths, between 4000 and 8000 psi are designated, with f'_c = 5000 to 6000 psi the most customary.

In this research 6" x 12" control cylinders were cast and tested according to ASTM standards (C39) in a specially manufactured loading machine. Compressive strength was determined for plain and fibrous concrete with different percentages of steel fibers. The results and comparisons are shown in Table 6.1.

6.2 Modulus of Elasticity

The modulus of elasticity of concrete, E_c, is defined as the ratio of normal stress to corresponding strain for tensile or

TABLE 6.1

COMPRESSIVE STRENGTH OF CONCRETE

Cylinder Number	% Steel Fiber	Designated for Beams	Actual Unit Weight (pcf)	Actual Average Unit Weight (pcf)	% Increase from 0.0% Fiber	Actual f'_c (psi)	Average f'_c (psi)	Relative Strength*
C11			145.2			4986		
C12			146.0			5023		
	0.0	B1,B2,B3		146.3	---		4970	1.0
C13			147.0			4925		
C14			147.0			4951		
C21			149.0			5182		
C22	0.8	B4,B5,B6	149.5	148.8	+1.7	5196	5180	1.04
C23			148.0			5160		
C31			150.0			5234		
C32	1.2	B7,B8,B9	150.5	150.2	+2.7	5305	5275	1.06
C33			150.0			5287		

*Relative Strength = $\frac{\text{compressive strength of concrete with fibers}}{\text{compressive strength of concrete without fibers}}$

compressive strength. It is important in designing members to resist deflection. Since concrete is not perfectly elastic, the stress-strain relationship is a curved line. The value of the modulus of elasticity depends on the strength of the concrete and the proportion and rigidity of the aggregate.

The modulus of elasticity of concrete can be described as the:

a) Initial tangent modulus, which is the slope of the stress-strain diagram at the origin.

b) Tangent modulus of elasticity, which is the slope of stress-strain diagram at given stress f'_c.

c) Secant modulus of elasticity, which is the slope of stress-strain diagram at a stress $f'_c/2$.

In this research, three groups of cylinders were cast with different percentages of steel fibers. Before testing, the cylinders were dried and capped to ensure parallel and smooth surfaces (Figure 6.1). Standard 6 in. gage length was marked on the cylinder side to read the deformation or change in the gage length (Figure 6.2). The readings were taken at regular intervals. The resulting stress and strain coordinates were plotted to determine the stress-strain diagram and modulus of elasticity of concrete (Figures 6.3 through 6.8).

The following formulas were used to calculate the modulus of elasticity considering the secant modulus a level of stress $f'_c/2$:

$$\sigma = P/A$$

$$\varepsilon = \Delta L/L$$

$$E_{ca} = 0.5\ f'_c/\varepsilon$$

Figure 6.1. Capping the cylinders.

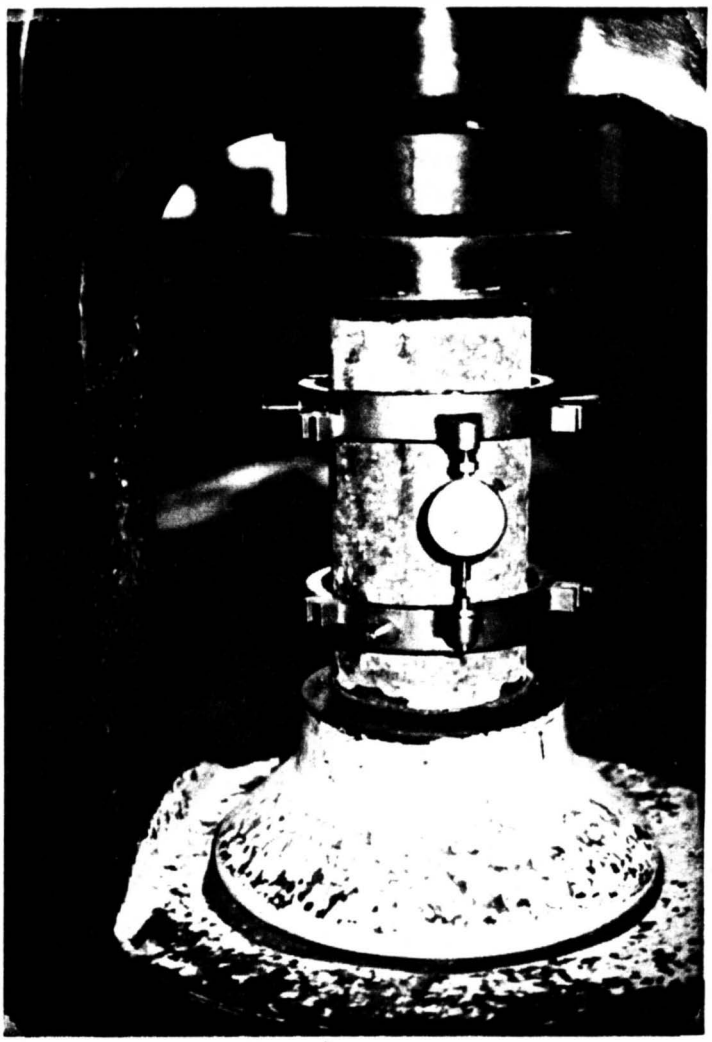

Figure 6.2. Compressometer to determine the modulus of elasticity.

FIGURE 6.3
MODULUS OF ELASTISITY OF CONCRETE
CYLINDER C11
% STEEL FIBRES = 0.0 FC'=4986 PSI

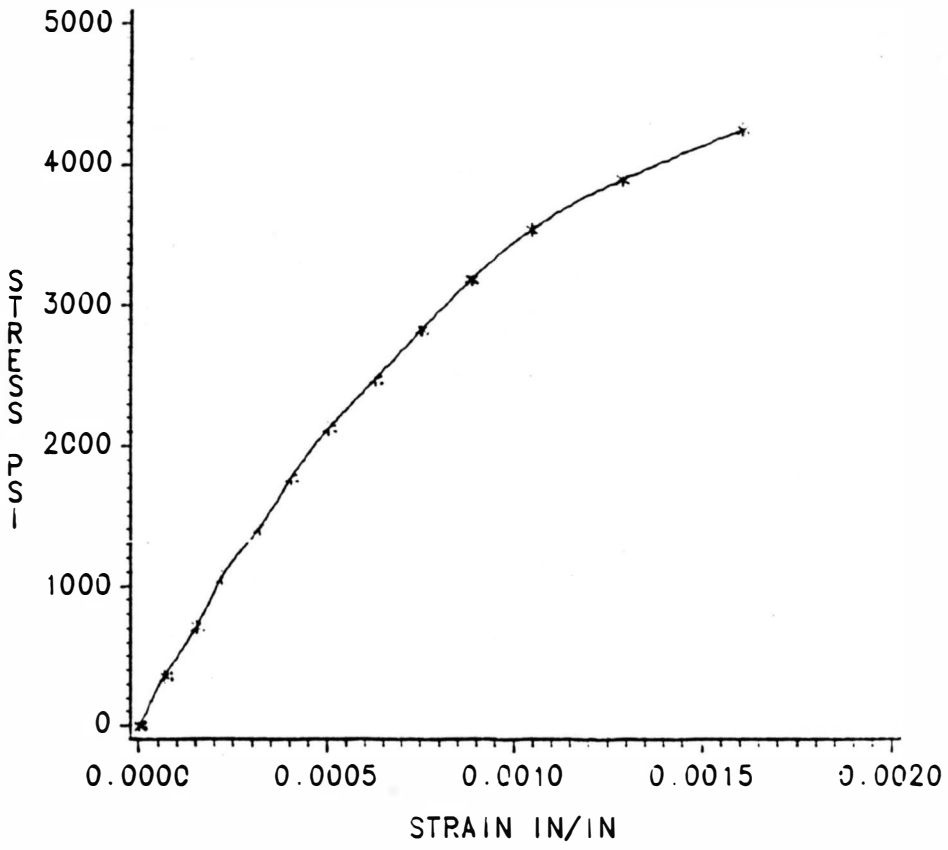

FIGURE 6.3 STRESS VS STRAIN

FIGURE 6.4
MODULUS OF ELASTISITY OF CONCRETE
CYLINDER C12
% STEEL FIBRES = 0.0 FC'=5023 PSI

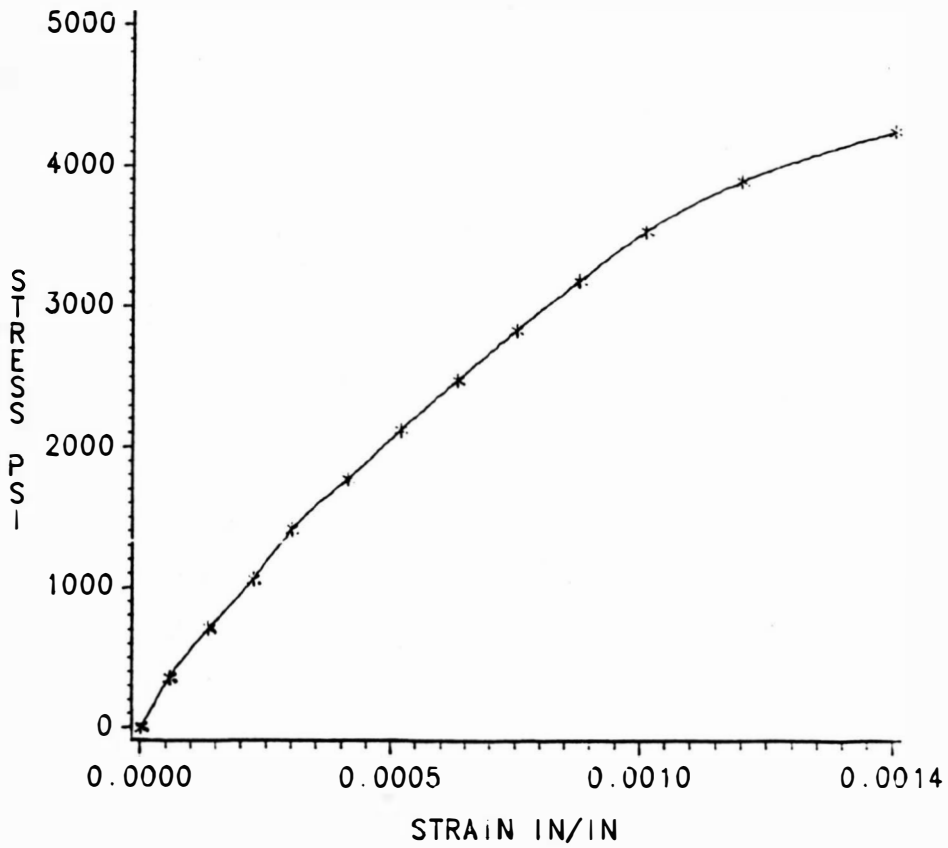

FIGURE 6.4 STRESS VS STRAIN

FIGURE 6.5
MODULUS OF ELASTISITY OF CONCRETE
CYLINDER C21
% STEEL FIBRES = 0.8 FC'=5182 PSI

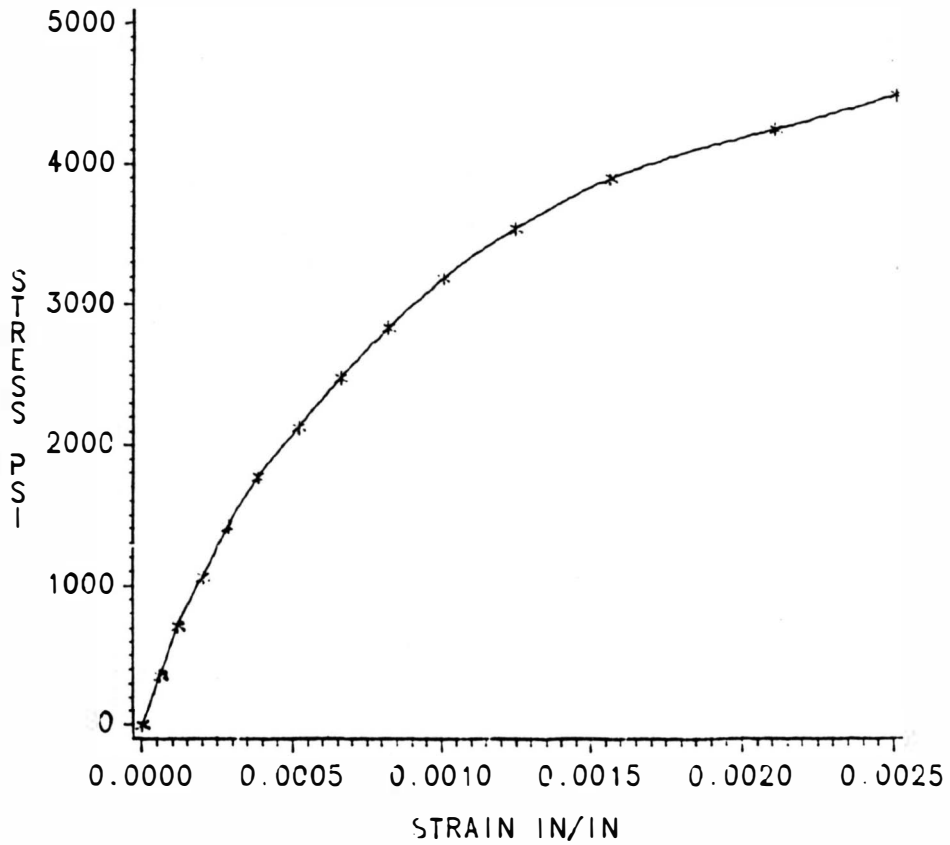

FIGURE 6.5 STRESS VS STRAIN

FIGURE 6.6
MODULUS OF ELASTISITY OF CONCRETE
CYLINDER C22
% STEEL FIBRES = 0.8 FC'=5190 PSI

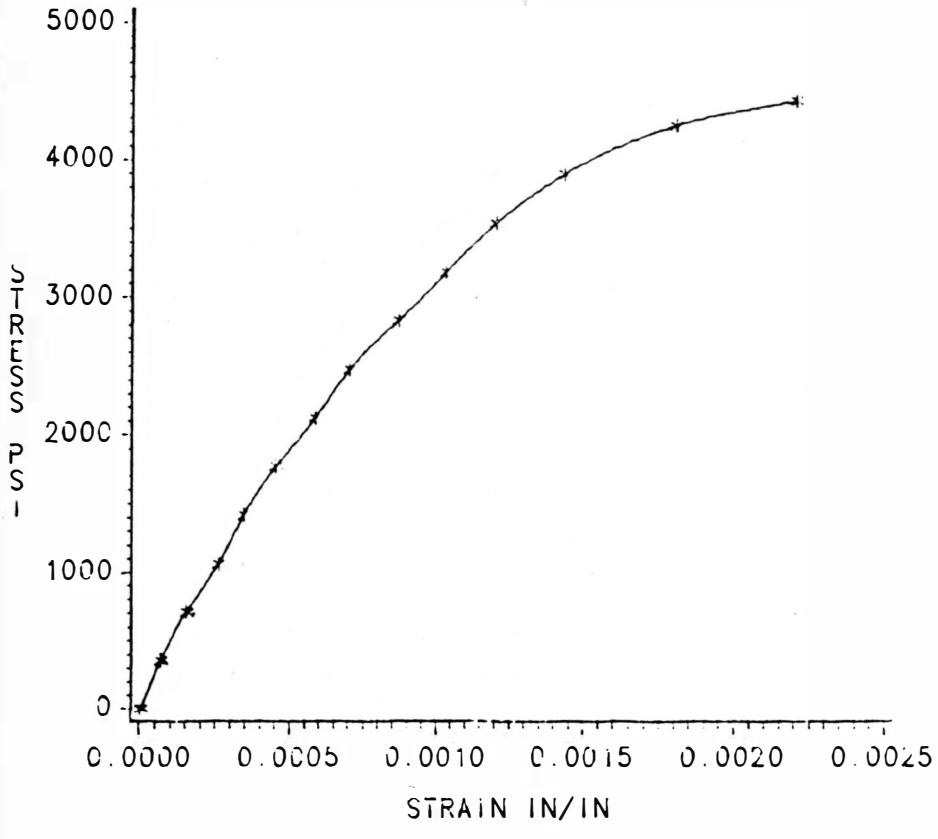

FIGURE 6.6 STRESS VS STRAIN

FIGURE 6.7
MODULUS OF ELASTISITY OF CONCRETE
CYLINDER C31
% STEEL FIBRES = 1.2 FC'=5234 PSI

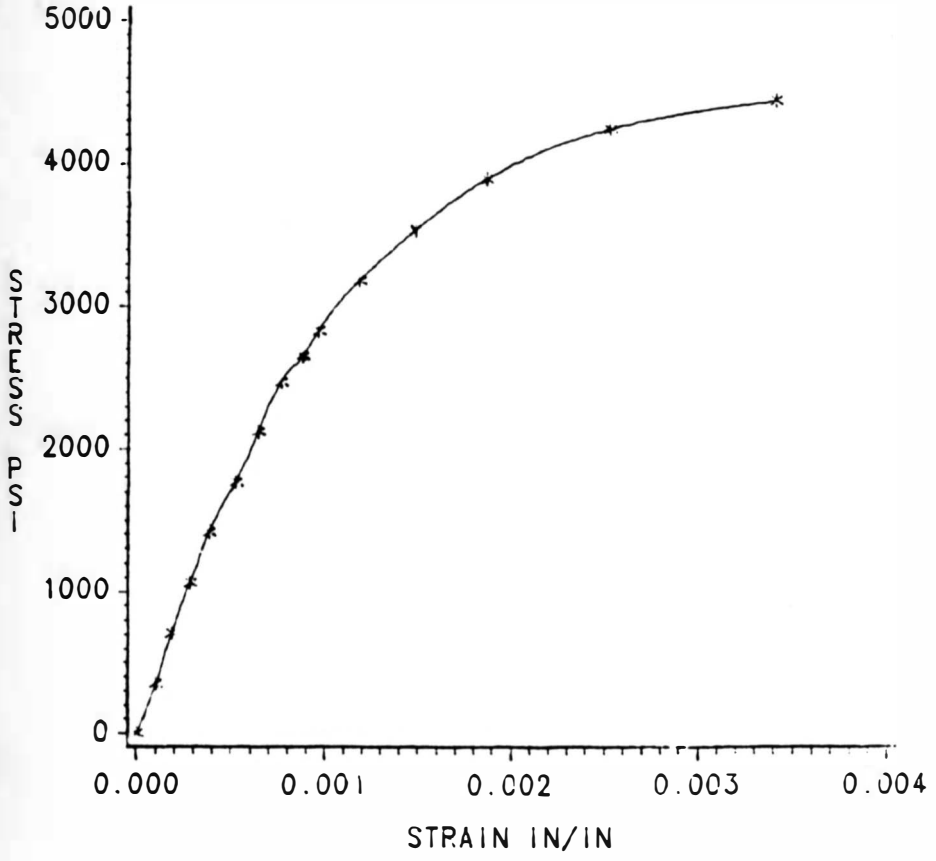

FIGURE 6.7 STRESS VS STRAIN

FIGURE 6.8
MODULUS OF ELASTISITY OF CONCRETE
CYLINDER C32
% STEEL FIBRES = 1.2 FC'=5305 PSI

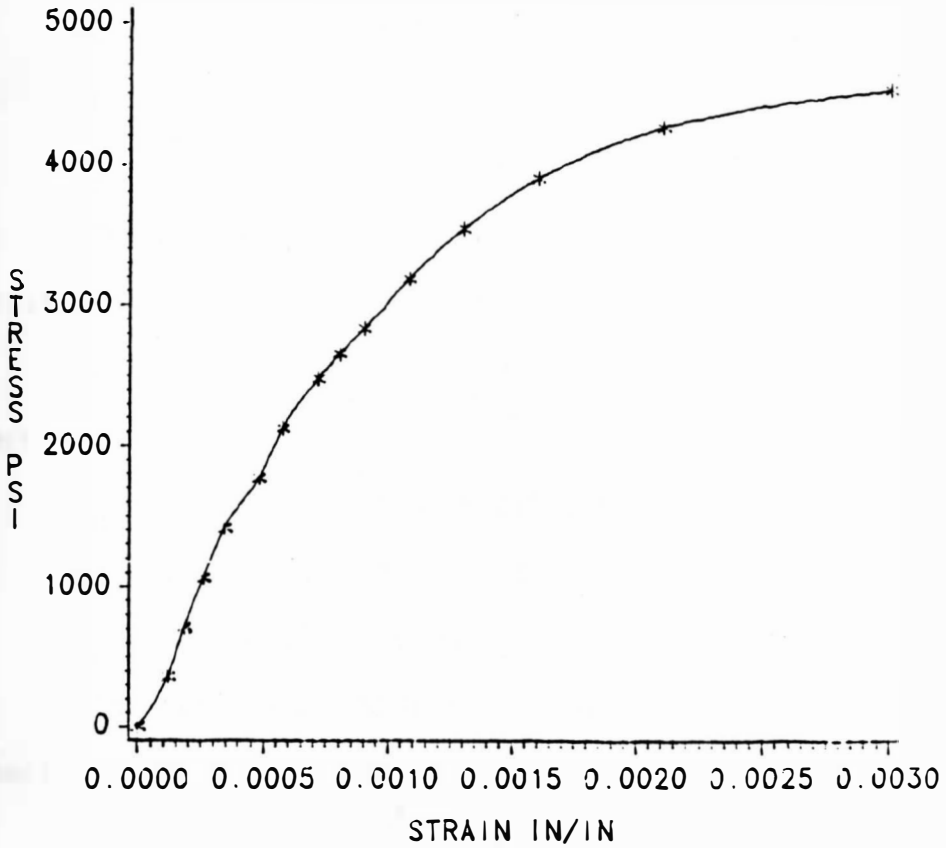

FIGURE 6.8 STRESS VS STRAIN

where:

σ = stress (psi)

P = applied load (lbs)

A = cross section area (28.27 in^2)

ε = average strain of a cylinder (in/in)

ΔL = deformation (in)

L = gage length (6 inches)

E_{ca} = actual secant Modulus of Elasticity (psi)

The ACI Code (318-83) Section 8.5 adopted a simple formula for calculating the modulus of elasticity at level of stress $f'_c/2$:

$$E_c = 33w^{1.5}\sqrt{f'_c} \qquad (6.1)$$

where:

E_c = secant Modulus of Elasticity (psi)

w = unit weight of concrete (pcf)

f'_c = compressive strength of concrete (psi)

The results of Modulus of Elasticity and the effect of steel fibers are tabulated in Table 6.2.

6.3 Split Cylinder

Although the tensile strength of concrete is much less than its compressive strength, it can be important as it influences the spacing and control of cracks in structures.

Tensile strength is measured indirectly by splitting a 6" x 12" cylinder (ASTM C-78), the same type of cylinders as used for the

TABLE 6.2

MODULUS OF ELASTICITY OF CONCRETE

Cylinder Number	% Steel Fibers	Designated for Beams	Unit Weight (PCF)	f'_c (PSI)	Actual $E_{ca} \times 10^6$ (PSI)	ACI Code $E_c \times 10^6$ $33w^{1.5}\sqrt{f'_c}$ (PSI)	Actual Average $E_{ca} \times 10^6$ (PSI)	ACI Code Average $E_c \times 10^6$ (PSI)	% Deviation from ACI Code	Relative Modulus of Elasticity*
C11	0.0	B1,B2,B3	145.2	4986	3.97	4.08	4.00	4.11	-2.7	1.00
C12			146.0	5023	4.02	4.13				
C21	0.8	B4,B5,B6	149.0	5182	3.80	4.32	3.71	4.34	-14.5	0.928
C22			149.5	5196	3.62	4.35				
C31	1.2	B7,B8,B9	150.0	5234	3.00	4.39	3.15	4.40	-28.4	0.788
C32			150.5	5305	3.30	4.40				

*Relative modulus of elasticity = $\frac{\text{Modulus of elasticity of concrete with fibers}}{\text{Modulus of elasticity of concrete without fibers}}$

compression test. The test is usually called the split-cylinder test. In this test the concrete cylinder is inserted in the horizontal position in a compression testing machine. The load is applied uniformly through two plywood pads along two opposite lines on the surface of the cylinder (Figure 6.9). Plain concrete cylinders as well as cylinders with different steel fiber percentages were tested until failure took place. It can be seen from Figure 6.10 that the tensile stress existing in the cylinder is nearly uniform. The tensile strength is calculated by the following formula:

$$f_{ct} = 2P/\pi DL \quad (26)$$

where:

P = applied load of failure (lbs)

D = diameter of cylinder (in)

L = length of cylinder (in)

The splitting strength can be related to the compressive strength of concrete in that it varies between 6 and 7 times $\sqrt{f'_c}$ for normal weight concrete. The ACI Code (318-83) Section 11.2 adopted an average value of

$$f_{ct} = 6.7\sqrt{f'_c} \quad (6.2)$$

where:

f_{ct} = the split-cylinder tensile strength (psi)

f'_c = 28-day compressive strength (psi)

The results of split-cylinder test and the effect of steel fibers are shown in Table 6.3.

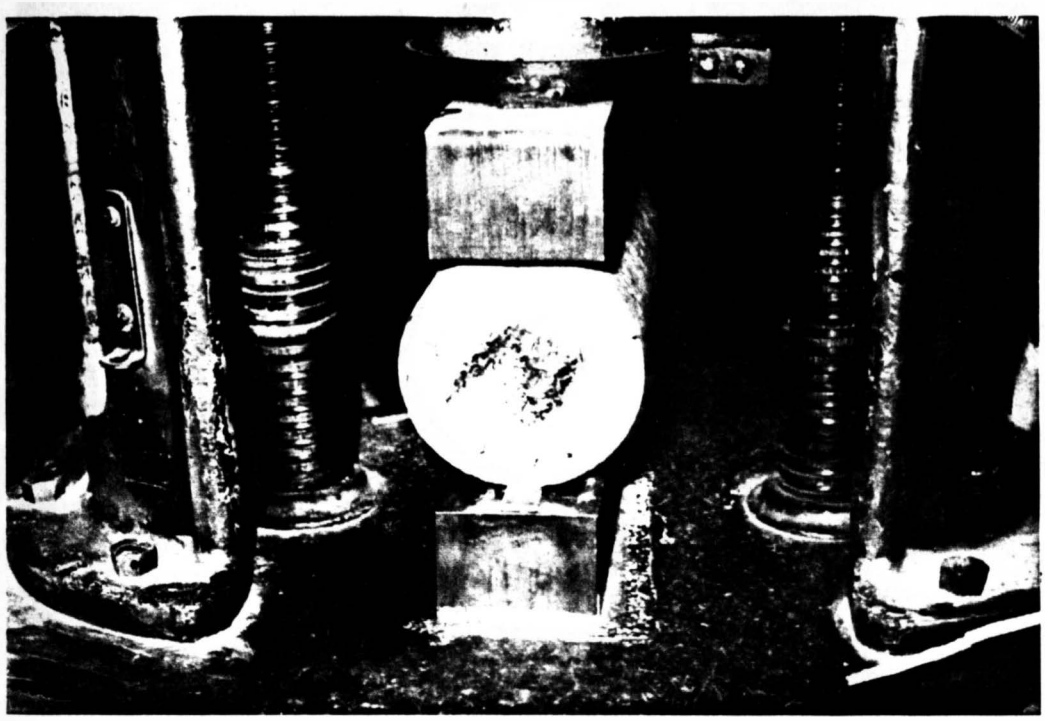

Figure 6.9. Split cylinder test set up.

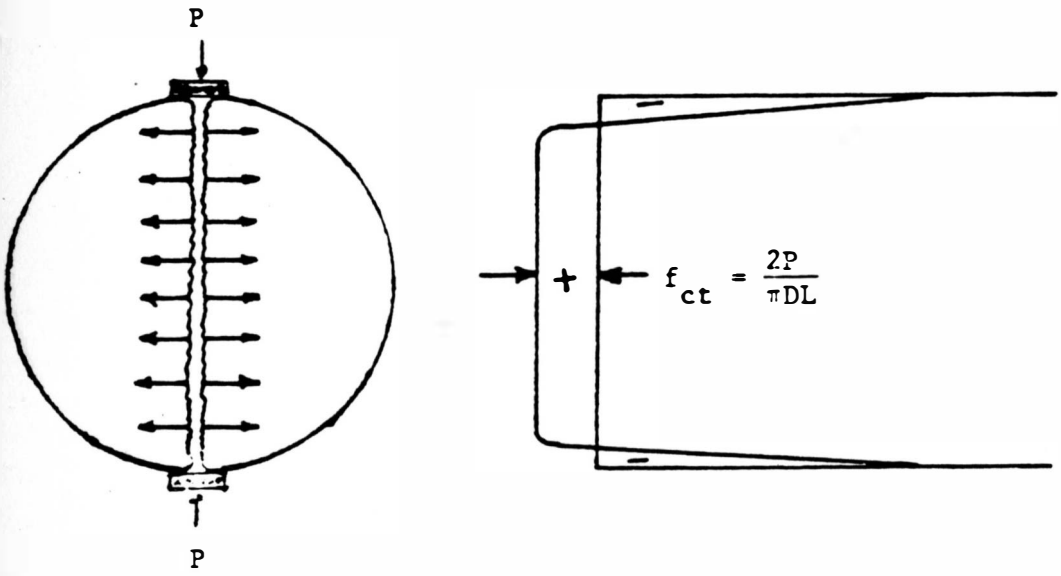

Figure 6.10. Stresses in a split cylinder.

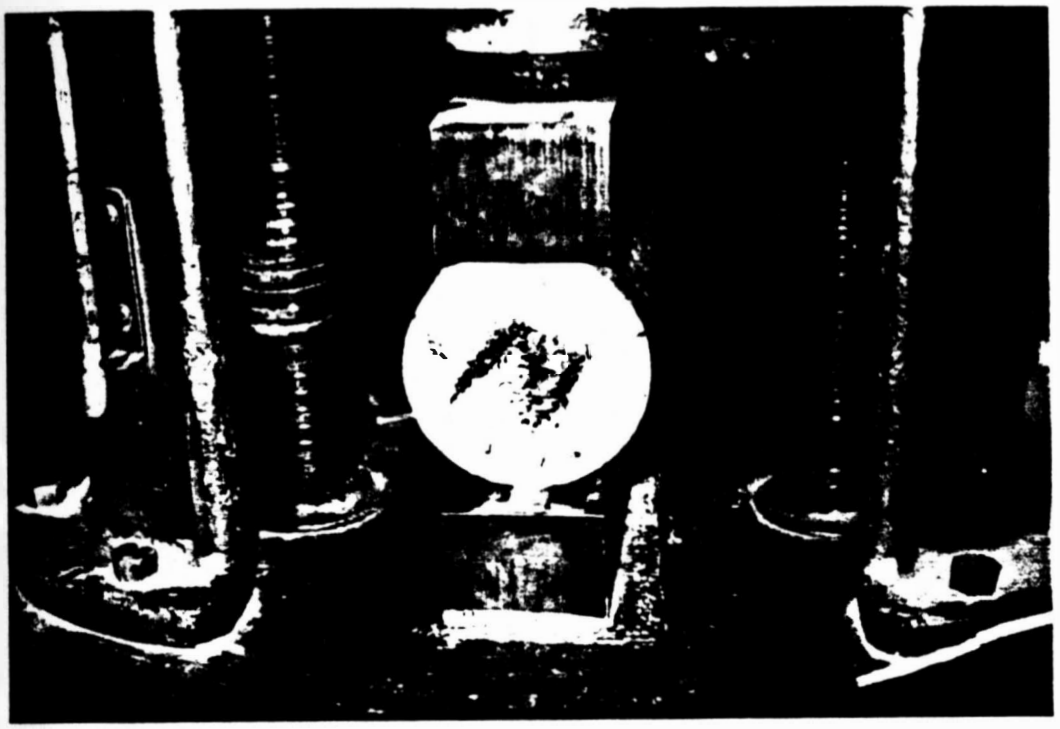

Figure 6.9. Split cylinder test set up.

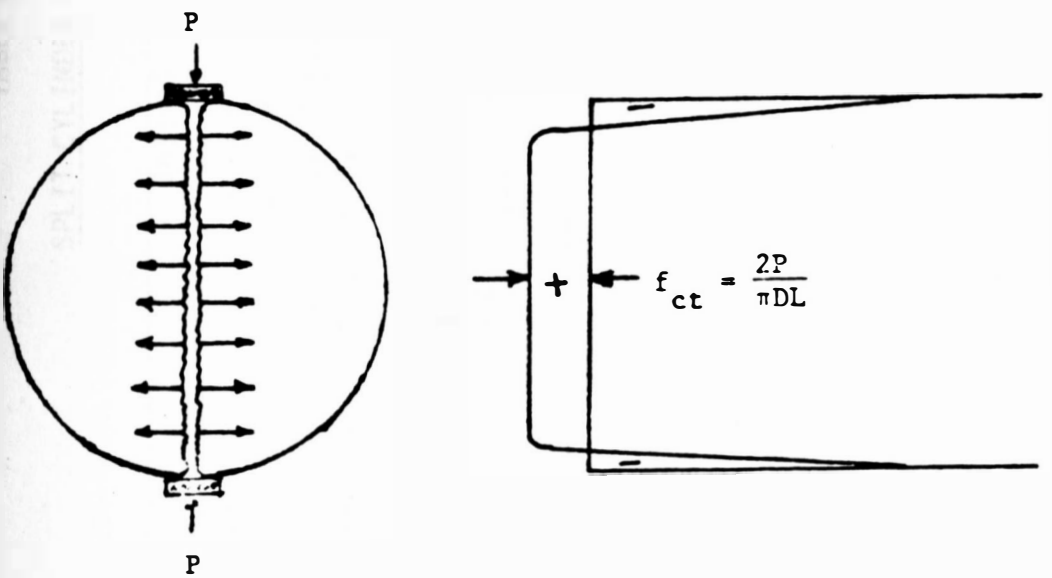

Figure 6.10. Stresses in a split cylinder.

TABLE 6.3

SPLIT CYLINDER TEST RESULTS

Cylinder Number	% Steel Fibers	Designated for Beams	Unit Weight (PCF)	f'_c (PSI)	Initial Tensile Strength f_{ctai} (PSI)	Initial Tensile Strength Average f_{ctai} (PSI)	Ultimate Tensile Strength f_{ctau} (PSI)	Ultimate Tensile Strength Average f_{ctau} (PSI)	ACI Code $f_{ct} = 6.7\sqrt{f'_c}$ (PSI)	% Deviation from Code f_{ctai}	% Deviation from Code f_{ctau}	Relative Tensile Strength* f_{ctai}	Relative Tensile Strength* f_{ctau}
C15	0.0	B1,B2,B3	147.0	4970	445	451	445	451	472	-4.4	-4.4	1.0	1.0
C16			146.5		457		457						
C24	0.8	B4,B5,B6	149.0	5180	542	546	573	575	482	13.3	+19.3	1.21	1.27
C25			148.5		550		577						
C34	1.2	B7,B8,B9	151.0	5275	574	583	671	681	487	19.7	+39.8	1.29	1.51
C35			150.0		592		691						

*Relative Tensile Strength = $\frac{\text{Tensile strength of concrete with fibers}}{\text{Tensile strength of concrete without fibers}}$

TABLE 6.3

SPLIT CYLINDER TEST RESULTS

Cylinder Number	% Steel Fibers	Designated for Beams	Unit Weight (PCF)	f'_c (PSI)	Initial Tensile Strength f_{ctai} (PSI)	Initial Tensile Strength Average f_{ctai} (PSI)	Ultimate Tensile Strength f_{ctau} (PSI)	Ultimate Tensile Strength Average f_{ctau} (PSI)	ACI Code $f_{ct} = 6.7\sqrt{f'_c}$ (PSI)	% Deviation from Code f_{ctai}	% Deviation from Code f_{ctau}	Relative Tensile Strength* f_{ctai}	Relative Tensile Strength* f_{ctau}
C15	0.0	B1,B2,B3	147.0	4970	445	451	445	451	472	-4.4	-4.4	1.0	1.0
C16			146.5		457		457						
C24	0.8	B4,B5,B6	149.0	5180	542	546	573	575	482	13.3	+19.3	1.21	1.27
C25			148.5		550		577						
C34	1.2	B7,B8,B9	151.0	5275	574	583	671	681	487	19.7	+39.8	1.29	1.51
C35			150.0		592		691						

*Relative Tensile Strength = $\frac{\text{Tensile strength of concrete with fibers}}{\text{Tensile strength of concrete without fibers}}$

6.4 Modulus of Rupture

Concrete maximum tensile stress in bending is known as the modulus of rupture. The modulus of rupture f_r is important when considering the cracking and deflection of beams. It is computed from the general formula f = MC/I, and it usually gives higher values for tensile strength than the split-cylinder test primarily because concrete compressive stress distribution is not linear when tensile failure is imminent, as it is assumed in the computation of the nominal MC/I stress.

In this experiment, 6 x 6 x 24 inch concrete beams reinforced with varying percentages of steel fiber were tested for flexure in a two point loading machine (S6 beam tester) with a clear span of 18 in. The beams were loaded to rupture according to ASTM Standard C-78. Direct readings in pound per square inch were recorded from the S6 model testing machine.

The ACI Code (318-83) Section 9.5.2.3 accepted an average value for the modulus of rupture f_r for normal weight concrete:

$$f_r = 7.5\sqrt{f'_c} \qquad (6.3)$$

where:

f'_c = 28-day compressive strength, psi

The results of modulus of rupture with the effect of steel fibers are tabulated in Table 6.4.

TABLE 6.4

MODULUS OF RUPTURE (f_r) FOR BEAMS (6 x 6 x 24 in)

Beam Number	% Steel Fibers	Designated for Beams	Unit Weight (PCF)	f'_c (PSI)	First Crack f_{ri} (PSI)	First Crack Average f_{ri} (PSI)	Ultimate f_{ru} (PSI)	Ultimate Average f_{ru} (PSI)	ACI Code $f_r = 7.5\sqrt{f'_c}$ (PSI)	% Deviation From Code f_{ri}	% Deviation From Code f_{ru}	Relative Modulus of Rupture* f_{ri}	Relative Modulus of Rupture* f_{ru}
BF11	0.0	B1,B2,B3	146.0	4970	500	508	500	508	529	-3.97	-3.97	1.0	1.0
BF12			146.5		516		516						
BF21	0.8	B4,B5,B6	148.0	5180	620	610	790	770	540	+13.0	+24.0	1.2	1.52
BF22			149.5		600		750						
BF31	1.2	B7,B8,B9	151.0	5275	750	715	940	890	545	+31.0	+63.0	1.41	1.75
BF32			150.5		680		840						

*Relative Modulus of Rupture = $\frac{\text{Modulus of rupture of concrete with fibers}}{\text{Modulus of rupture of concrete without fibers}}$

6.5 Load Carrying Capacity of Beams

The behavior of continuous beam to two identical spans under symmetrical loading in bending (Figure 2.5) was explained in Section 2.2 of Chapter 2. Calculated yield and ultimate loads of the beams were shown in Table 5.3 and presented in columns 5 and 6 of Table 6.5, where P_y is calculated on the assumption that the behavior of the beam is elastic up to the formation of the first hinge in the middle support, and P_u is calculated on the assumption of the formation of the second hinge in the mid-span (positive section). Experimental P'_y corresponding to the yield of main steel in the middle support and P'_u corresponding to yield of steel at mid span were both observed and presented in columns 7 and 8 of Table 6.5, respectively. The redistribution factor r, which is the ratio of ultimate to yield load both theoretically and experimentally was calculated and presented in columns 9 and 10. The ratio of experimental loads to theoretical loads was also presented in columns 11 and 12.

Actual moments at middle support using actual loads were computed and presented in Table 6.6. The ratio of actual to calculated negative moments is presented in column 7. The percent increase in the ultimate moment due to the presence of steel fibers is presented in column 8.

TABLE 6.5

LOAD CARRYING CAPACITY OF BEAMS

Beam No. (1)	% Steel Fibers (2)	Tension Steel A_s (3)	Top Steel A'_s (4)	CALCULATED P_y (Kips) (5)	CALCULATED P_u (Kips) (6)	TESTED P'_y (Kips) (7)	TESTED P'_u (Kips) (8)	$r=P_u/P_y$ (9)	$r'=P'_u/P'_y$ (10)	P'_y/P'_y (11)	P'_u/P_u (12)
1	0.0	2#4	2#3	13.31	17.97	17.00	21.80	1.35	1.28	1.28	1.21
4	0.8	2#4	2#3	13.55	18.29	18.40	24.80	1.35	1.36	1.36	1.36
7	1.2	2#4	2#3	13.68	18.46	20.79	28.90	1.35	1.39	1.52	1.56
2	0.0	2#5	2#3	18.48	24.95	23.93	28.00	1.35	1.17	1.29	1.12
5	0.8	2#5	2#3	18.60	25.10	25.92	32.40	1.35	1.25	1.39	1.29
8	1.2	2#5	2#3	18.63	25.15	27.16	34.50	1.35	1.27	1.46	1.37
3	0.0	2#6	2#3	26.18	35.34	28.00	35.00	1.35	1.25	1.07	0.99
6	0.8	2#6	2#3	26.37	35.60	30.00	38.28	1.35	1.27	1.14	1.07
9	1.2	2#6	2#3	26.44	35.70	33.60	43.40	1.35	1.29	1.27	1.21

TABLE 6.6

ULTIMATE MOMENT CAPACITY OF THE MIDDLE SUPPORT

Beam No. (1)	Tension Steel Bars (2)	Top Steel Bars (3)	% Steel Fibers (4)	Calculated Ultimate Negative Moment (K-in) (5)	Actual Ultimate Negative Moment (K-in) (6)	Ratio of Actual to Calculated Negative Moment (7)	% Increase of Actual Ultimate Moment From 0.0% S.F. (8)
1	2#4	2#3	0.0	149.73	191.25	1.28	-
4	2#4	2#3	0.8	152.41	207.00	1.36	8.24
7	2#4	2#3	1.2	153.87	233.90	1.52	22.30
2	2#5	2#3	0.0	207.90	269.20	1.29	-
5	2#5	2#3	0.8	209.20	291.60	1.39	8.32
8	2#5	2#3	1.2	209.56	305.60	1.46	13.52
3	2#6	2#3	0.0	294.48	315.00	1.07	-
6	2#6	2#3	0.8	296.65	337.50	1.14	7.14
9	2#6	2#3	1.2	297.50	378.00	1.27	20.00

6.6 Rotations

6.6.1 Introduction

The rotation capacity of the plastic hinge θp is defined as the inelastic rotation recorded from the first yield to the failure of the compressed concrete of the critical section. Because studying the rotation capacity of reinforced concrete is a primary aim of this research, it was explained thoroughly in Chapter 2.

Actual rotation was measured in this experiment and presented in this chapter and Appendix A.

The rotation at midsupport in the distance equal to the effective d was measured by the following methods:

1) Brass studs were glued on the side of the beam as shown in Figure (6.11). In this method the curvatures were calculated from measuring the length of the top side of the beam by the use of a mechanical dial of 8 in. gage length as discussed in Chapter 4.

The curvature was calculated as follows:

$$\phi = \sum_{i=1}^{2}[\Delta a_i/a_i][1/d] = [1/d]\sum_{i=1}^{2}\Delta a/a = [1/d][(\Delta a_1/a_1)+(\Delta a_2/a_2)]$$

where:

$\Delta a_i/a_i$ = the strain at the section

Δa = dial reading in 10^{-4} in.

a = 8 inches

d = effective depth of the section

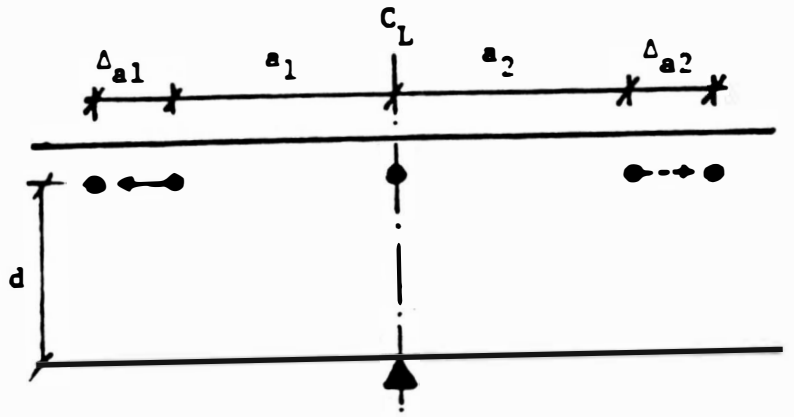

Figure 6.11. Curvature measurement (Method 1).

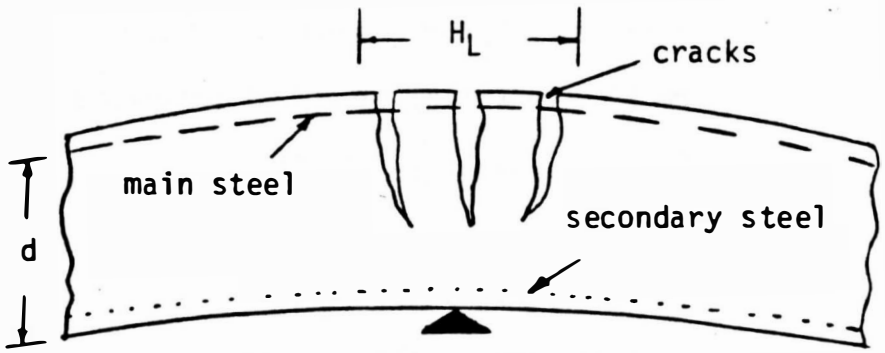

Figure 6.12 Plastic hinge at middle support of a continuous beam.

The plastic rotation θp occurs over a narrow region called the plastic hinge region. The length of the plastic hinge region is defined as the plastic hinge length, H_L.

In this research, a plastic hinge developed at middle support after the first yield of steel, and the spacing of cracks over the first critical hinge section will seem to indicate the plastic hinge length (Figure 6.12). Therefore θp, the plastic rotation over the hinge length is $\theta p = \phi p H_L$. Results are in Appendix A Tables A.1 through A.9.

2) By using a level and a scale the beams were marked at different sections and the deflection of each point was determined at each load increment. This method was most appropriate for determining the plastic deformation since level readings were taken at all load stages up to failure.

Using the above method the experimental rotation was calculated according to Figure (6.13) as follows:

$$\theta pc = (\Delta_{1p})/(L/2) + (\Delta_{2p})/(L/2)$$

where:

Δ_{1p}, Δ_{2p} = plastic deformation

Δ_1, Δ_2 = differential level readings at any stage

θ = the tangent line drawn to the curve at the critical section

Both the theoretical and experimental rotation capacity (Method 2) were determined and presented in Table 6.7, columns 13 and 14 respectively. The ratio of experimental to theoretical rotation

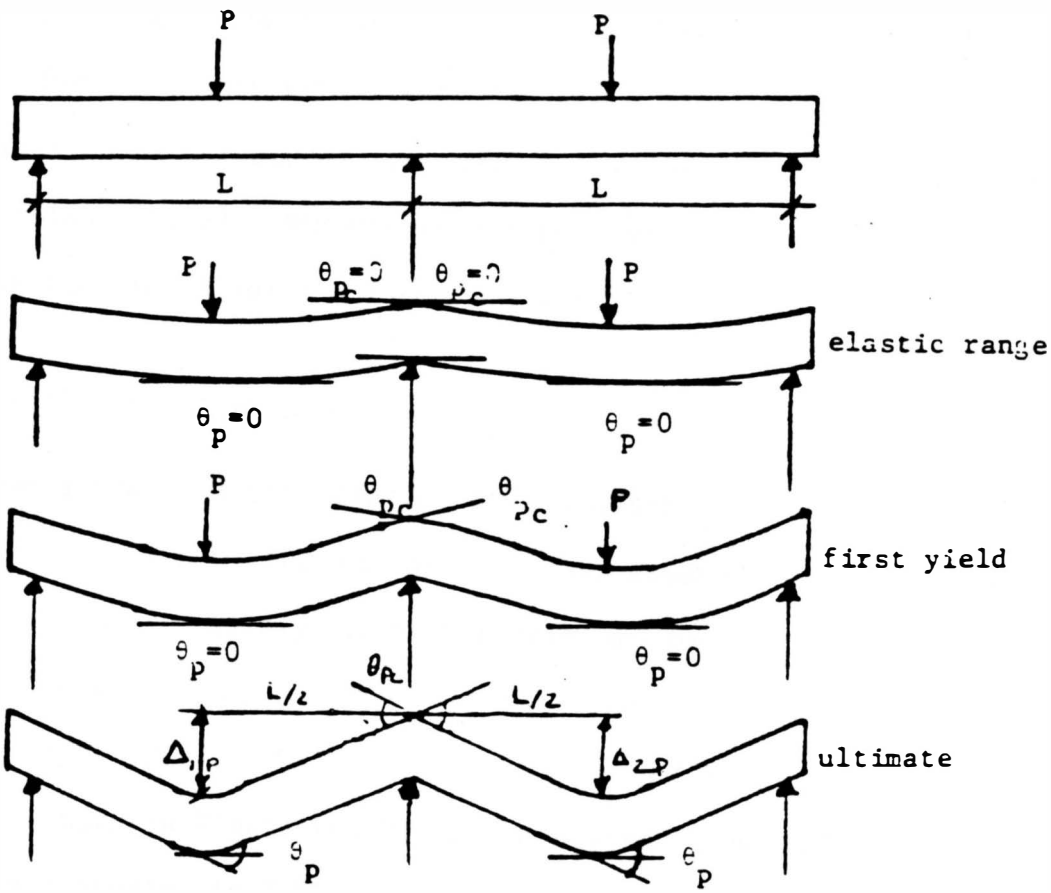

Figure 6.13. Deflection and rotation at different loading stages (Method 2).

capacity is shown in the last column of Table 6.7. Table 6.8 lists the values of total elastic rotation θy, the incremental plastic rotation θpc, and the total rotation $\theta u = \theta pc + \theta y$.

The actual moment-curvature diagrams are shown in Figures 6.14-6.22 for different main steel, secondary steel and steel fibers combinations. The curvatures were measured using actual strains using Method 1 (Figure 6.13). Moments were determined using the actual load applied on the beam (Tables A.1 through A.9).

6.6.2 Plastic Hinge Length (H_L)

The actual plastic rotation at a plastic hinge point develops over a short length in the vicinity of the assumed hinge position. This length varies mainly with the form of bending diagram (3). Several experimental values proposed by several investigators were shown in Table (2.1). In this research actual hinge lengths were measured as shown in Figure (6.12) to the nearest one-half inch. The results are presented in Table 6.9.

6.6.3 Curvature Distribution Factor (β)

The curvature distribution factor β was introduced in Chapter 2. This factor is ignored in most rotation estimation, which leads to over-estimation of the plastic rotation. Therefore, to give an actual value of plastic rotation in this research, the distribution factor was calculated from having experimental values ϕp, H_L and θpc Table

FIGURE 6.14
MOMENT-CURVATURE RELATIONSHIP
MAIN STEEL-2#4 TOP STEEL-2#3 %STEEL FIBERS-0.0
BEAM #1

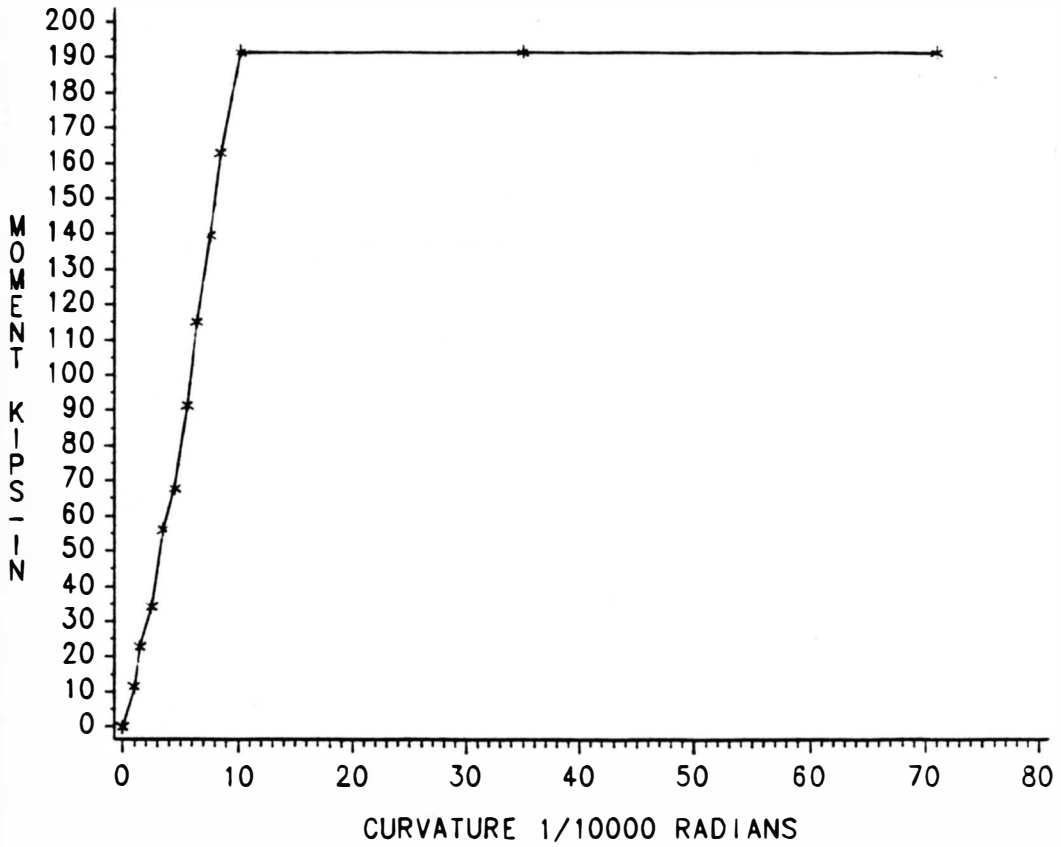

FIGURE 6.14 MOMENT-CURVATURE

FIGURE 6.15
MOMENT-CURVATURE RELATIONSHIP
MAIN STEEL-2#4 TOP STEEL-2#3 %STEEL FIBERS-0.8
BEAM #4

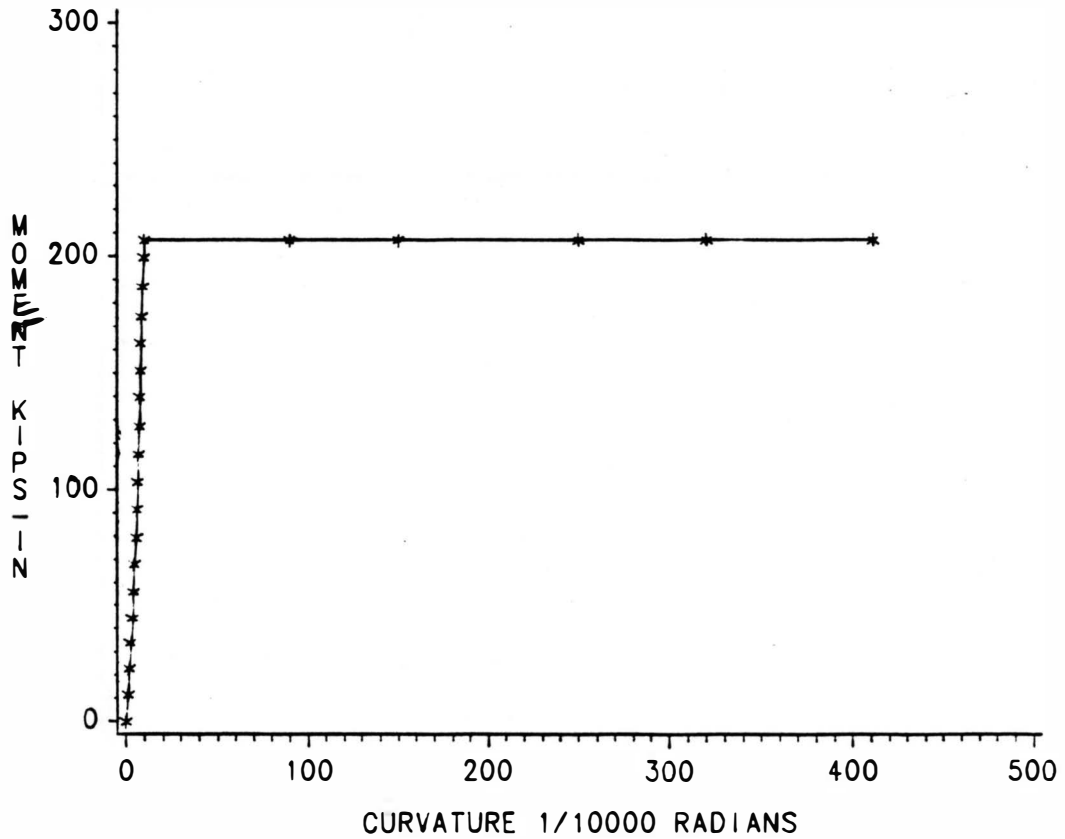

FIGURE 6.15 MOMENT-CURVATURE

FIGURE 6.15
MOMENT-CURVATURE RELATIONSHIP
MAIN STEEL-2#4 TOP STEEL-2#3 %STEEL FIBERS-1.2
BEAM #7

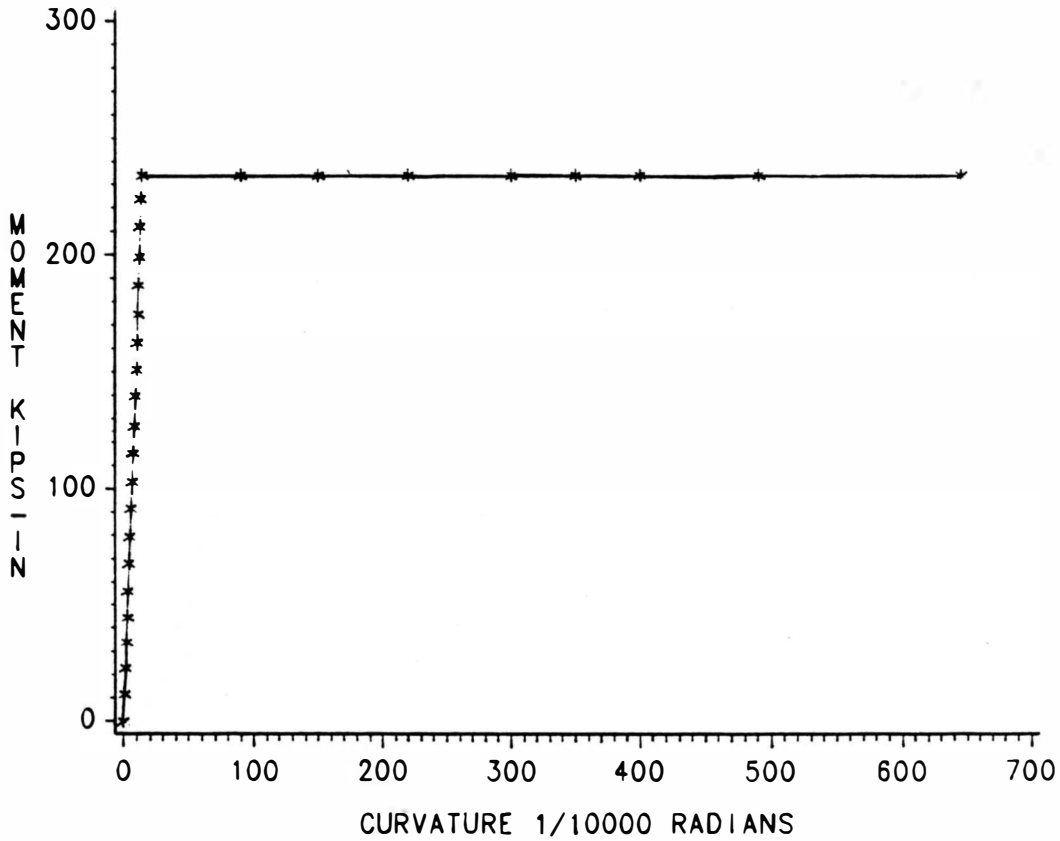

FIGURE 6.15 MOMENT-CURVATURE

FIGURE 6.17
MOMENT-CURVATURE RELATIONSHIP
MAIN STEEL-2#5 TOP STEEL-2#3 %STEEL FIBERS-0.0
BEAM #2

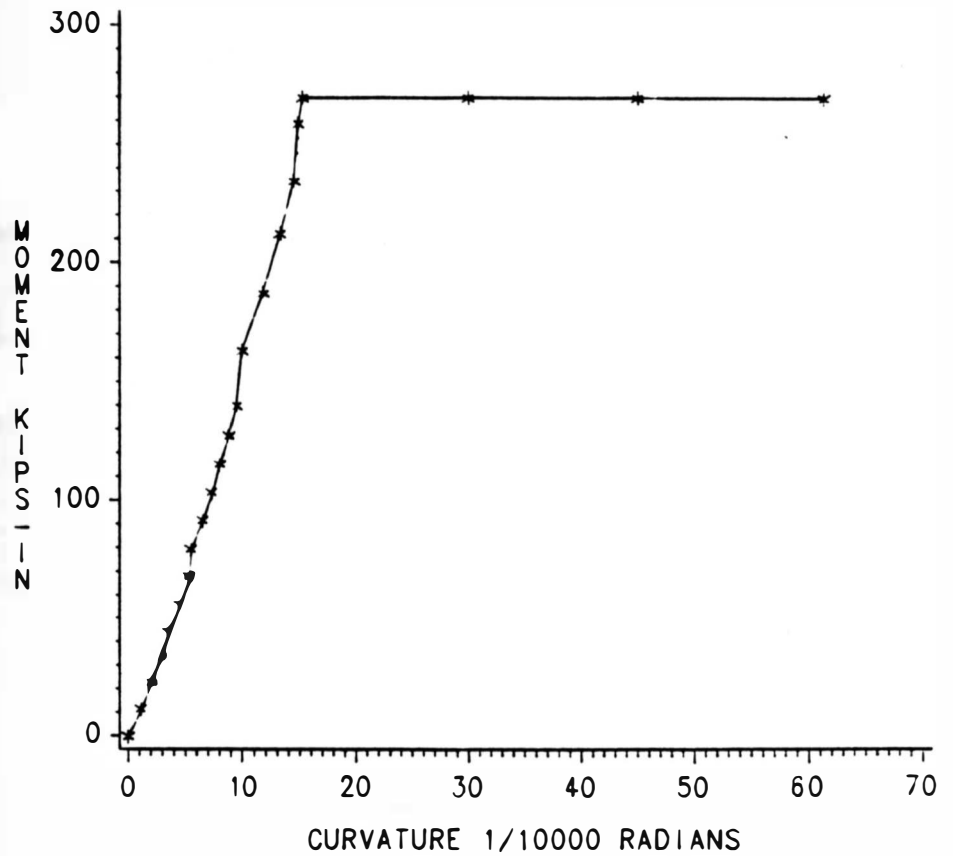

FIGURE 6.17 MOMENT-CURVATURE

FIGURE 6.18
MOMENT-CURVATURE RELATIONSHIP
MAIN STEEL=2#5 TOP STEEL=2#3 %STEEL FIBERS=0.8
BEAM #5

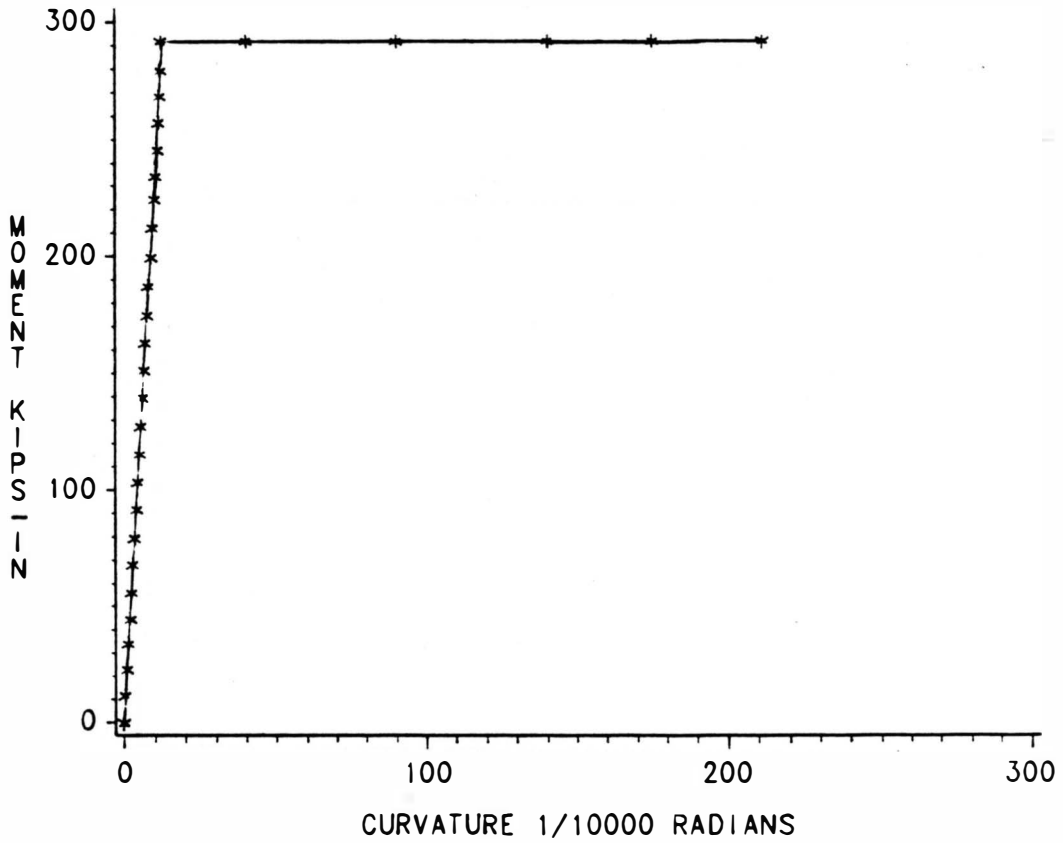

FIGURE 6.18 MOMENT-CURVATURE

FIGURE 6.19
MOMENT-CURVATURE RELATIONSHIP
MAIN STEEL-2#5 TOP STEEL-2#3 %STEEL FIBERS-1.2
BEAM #8

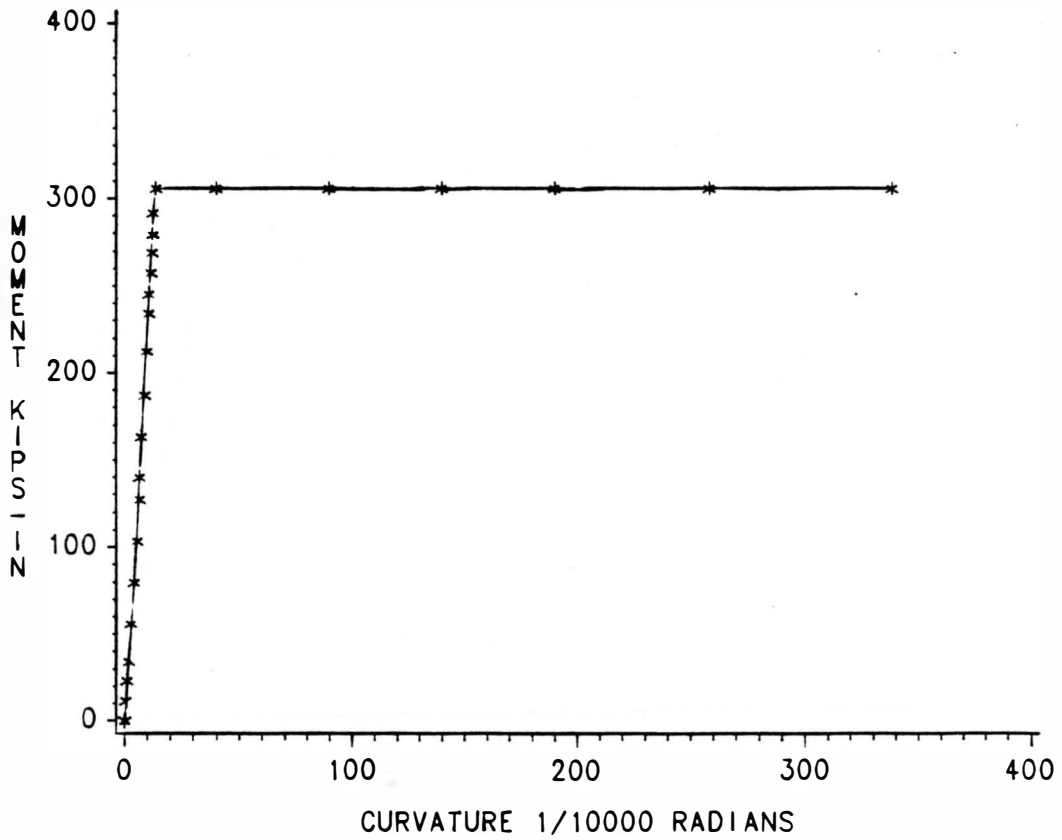

FIGURE 6.19 MOMENT-CURVATURE

FIGURE 6.20
MOMENT-CURVATURE RELATIONSHIP
MAIN STEEL-2#6 TOP STEEL-2#3 %STEEL FIBERS-0.0
BEAM #3

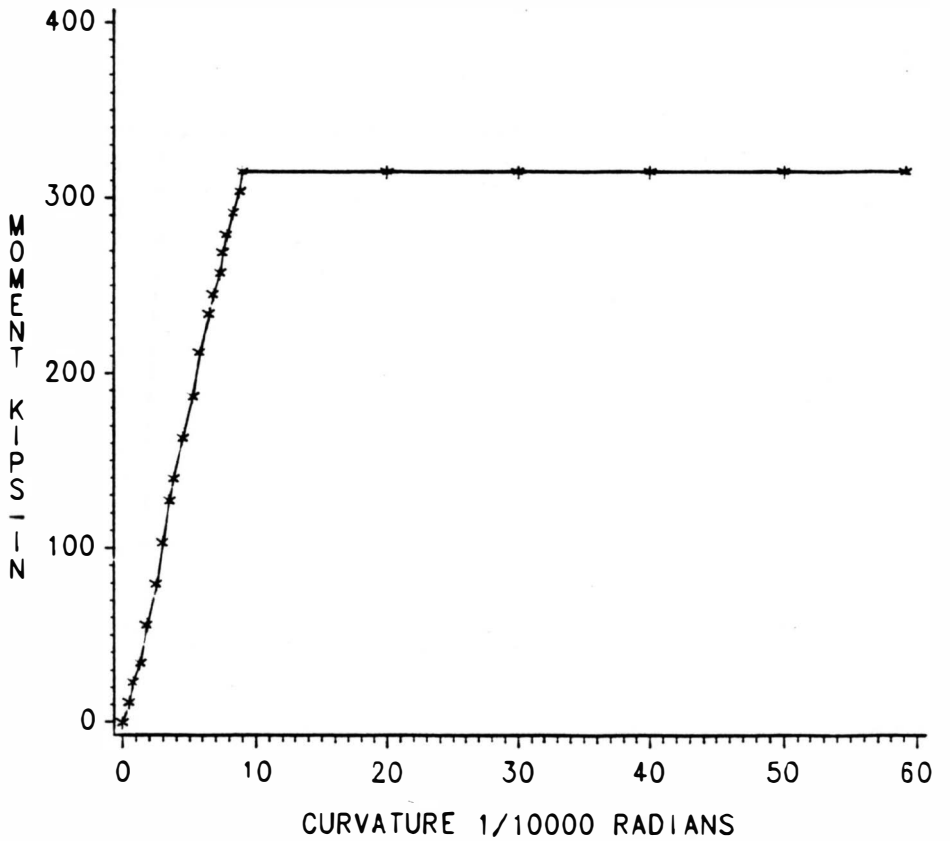

FIGURE 6.20 MOMENT-CURVATURE

FIGURE 6.21
MOMENT-CURVATURE RELATIONSHIP
MAIN STEEL=2#6 TOP STEEL=2#3 %STEEL FIBERS=0.8
BEAM #6

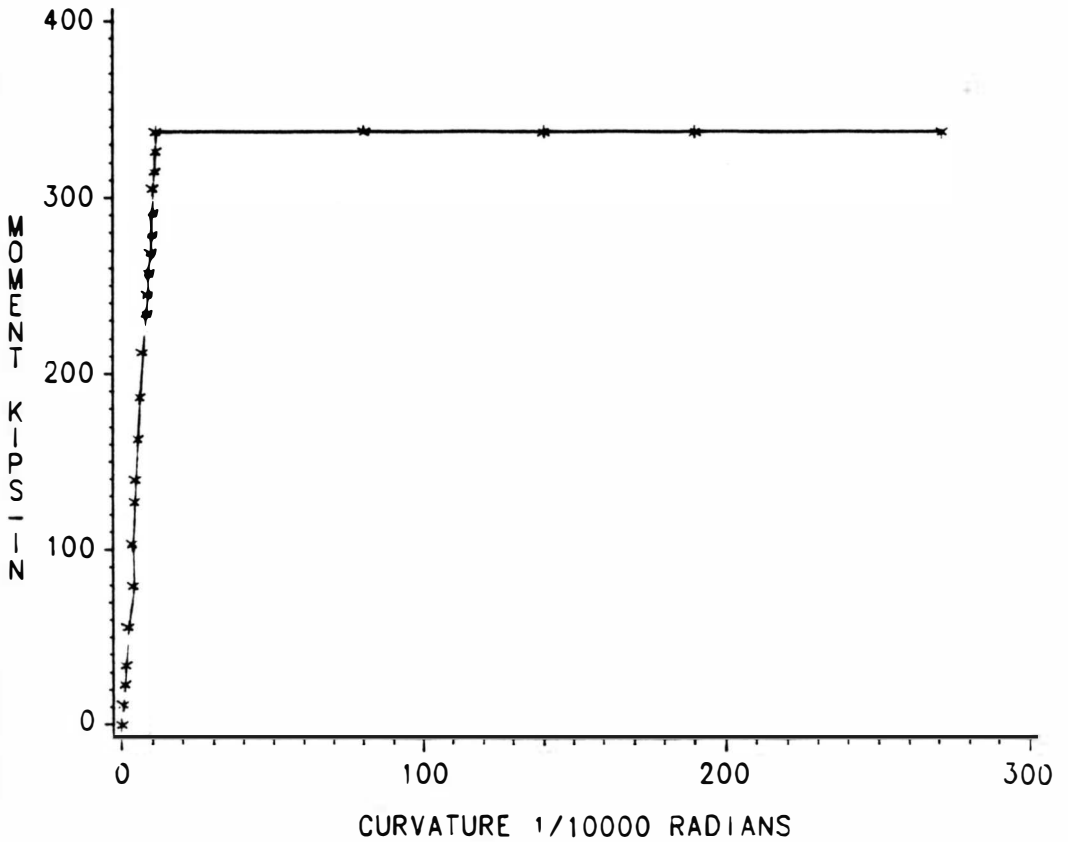

FIGURE 6.21 MOMENT-CURVATURE

FIGURE 6.22
MOMENT-CURVATURE RELATIONSHIP
MAIN STEEL=2#6 TOP STEEL=2#3 %STEEL FIBERS=1.2
BEAM #9

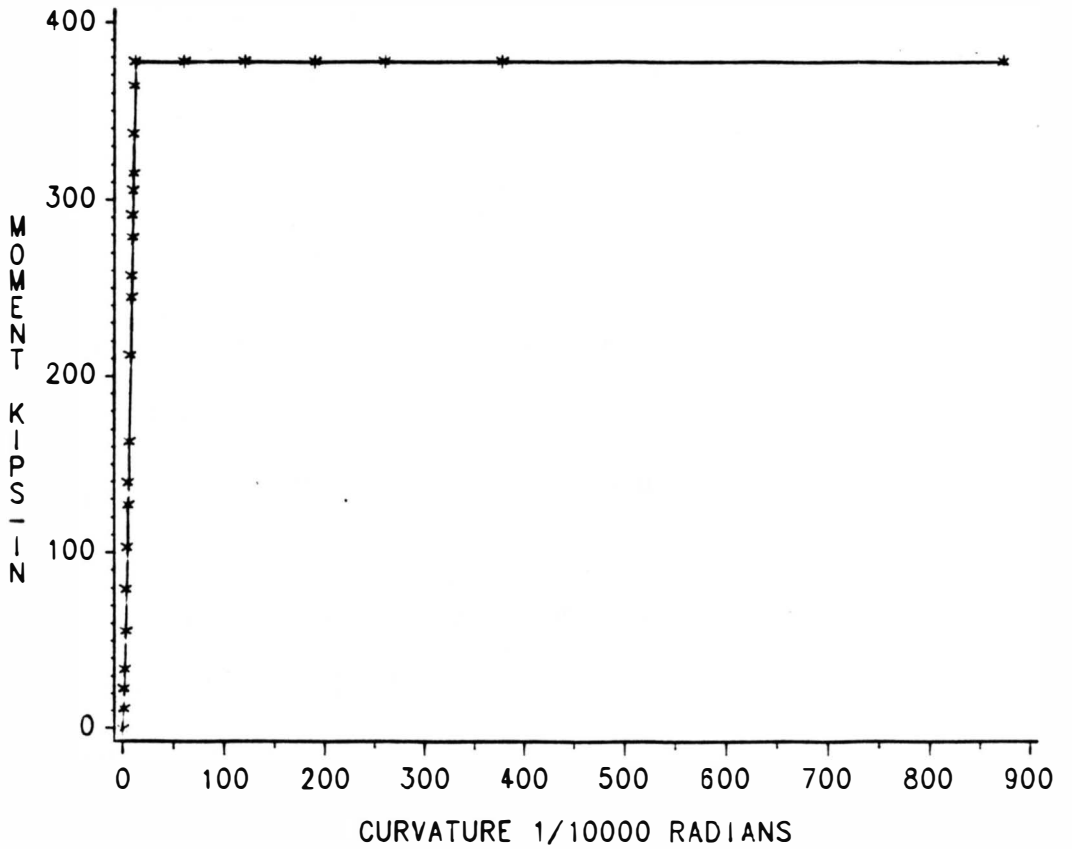

FIGURE 6.22 MOMENT-CURVATURE

6.10 as follows $\beta = \theta pc/\theta pH_L$. Where θpc was calculated using Method 2 (level and the scale). Values of β are shown in the last column of Table 6.10.

6.6.4 Calculations of Plastic Rotations (Table 6.7)

B#1: A_s = 2#4 main steel, 2#3 top steel, and 0.0% steel fibers

d = 6.5 in d' = 1.44 in n = 7.25

Plastic moment = 10 P'_u (P'_u is from Table 6.5)

= 10 x 21.8 = 218 k.in (column 3)

Fixed end moment = $P_uL/8$ = (21.8x60)/8 = 163.5 k.in (column 4)

k_1d = position of neutral axis when the top steel is considered

k_1 = k_1d/d (column 8)

k_1d is calculated from the following

$b(k_1d)^2/2+(2n-1)A'_s(k_1d-d')-nA_s(d-k_1d) = 0$

$5(k_1d)^2/2+(2x7.25-1)(0.22)(k_1d-1.44)-7.25(0.39)(6.5-k_1d) = 0$

$2.5k_1d^2+5.8k_1d-22.66$

k_1d = 2.07 in

k_1 = 2.07/6.5 = 0.318

k_2d = position of neutral axis when the top steel is neglected

k_2d is calculated from the following

$b(k_2d)^2/2-nA_s(d-k_2d) = 0$

$5(k_2d)^2/2-7.25(0.39)(6.5-k_2d) = 0$

$2.5(k_2d)^2+2.83(k_2d)-18.38$

k_2d = 2.2 in

k_2 = k_2d/d (column 9)

$k_2 = 2.2/6.5 = 0.338$

k_{ud} = position of neutral axis at ultimate stage

$k_{ud} = a/\beta_1$

k_{ud} = 1.51 in (from flexural analysis of beams, B#1, Chapter 5)

$k_u = k_{ud}/d$ (column 10)

$k_u = 1.51/6.5 = 0.232$

I_{cr1} = moment of inertia of cracked section when the top steel is considered (column 5)

$I_{cr1} = b(k_1d)^3/3+(2n-1)A'_s(k_1d-d')^2+nA_s(d-k_1d)^2$

$= 5(2.07)^3/c+(2x7.25-1)(0.22)(2.07-1.44)^2$

$+7.25(0.39)(6.5-2.07)^2 = 71.45\ in^4$

I_{cr2} = moment of inertia of cracked section when the top steel is neglected (column 6)

$I_{cr2} = b(k_2d)^3/3+nA_s(d-k_2d)^2$

$= 5(2.2)^3/3+7.25(0.39)(6.5-2.2)^2 = 70.42\ n^4$

Ip = moment of inertia of ultimate stage (column 7)

$= b(k_ud)^3/3+nA_s(d-k_ud)^2$

$= 5(1.51)^3/3+7.25(0.39)(6.5-1.51)^2 = 76.14\ in^4$

To calculate the required rotation using Equation (2.5), the smaller value of the moment of inertia is used to require higher rotations.

$\theta = L[2(M_A-M_{FA})+(M_B-M_{FB})]/6E_cI$

θ_1 = required plastic rotation when the top steel is considered (Column 11)

$\theta_1 = 60[2(-218.0+163.5)+(0+163.5)]/b(4x10^3)(71.45)$

$= 1.91 \times 10^{-3}$ radians

θ_2 = required plastic rotation when the top steel is neglected (column 12)

$\theta_2 = 60[2(218.0+163.5)+(0+163.5)]/6(4x10^3)(70.45)$

$= 1.94 \times 10^{-3}$ radians

Rotation capacity using Equation (2.6) (column 13)

$\theta p = \phi_{cu}/k_u - f_y/(E_s)(1-k_u)$

$\theta p = 0.0035/0.232 - 64.9/29000(1-0.232) = 12.27 \times 10^{-3}$ radians

B#2: A_s = 2#5 main steel, compression steel 2#3, and 0.0% steel fibers

d = 6.3 in d' = 1.56 in n = 7.25

Plastic moment = 10 P'_u (P'_u is from Table 6.5)

= 10 x 28 = 280 k.in

Fixed end moment = $P_uL/8$ = 28 x 60/8 = 210 k.in

$5(k_1d)^2/2+(2x7.25-1)(0.22)(k_1d-1.56)-7.25(0.61)(6.31-k_1d) = 0$

$2.5k_1d^2+4.42k_2d-27.91$

$k_2d = 2.57$

$k_2d = 2.57/6.31 = 0.407$

k_ud = 2.06 in (from flexural analysis of beam, B#2, Chapter 5)

$K_u = 2.06/6.31 = 0.326$

$I_{cr1} = 5(2.42)^3/3+(2x7.25-1)(0.22)(2.42-1.56)^2$

$+ 7.25(0.61)(6.31-2.42)^2 = 92.74$ in^4

$I_{cr2} = 5(2.57)^3/3+7.25(0.61)(6.31-2.57)^2 = 90.15$ n^4

$Ip = 5(2.06)^3/3+7.25(0.61)(6.31-2.06)^2 = 94.45$ in^4

Required rotation using Equation (2.5)

$\theta_1 = 60[2(-280.0+210.0)+(0+210)]/6(4x10^3)(92.74)$

$= 1.89 \times 10^{-3}$ radians

$\theta_2 = 60[2(-280.0+210.0)+(0+210)]/6(4x10^3)(90.15)$

$= 1.94 \times 10^{-3}$ radians

Rotation capacity using Equation (2.6)

$\theta p = 0.0035/0.326-63.2/29000(1-0.326) = 7.5 \times 10^{-3}$ radians

B#3: A_s=2#6 main steel, 2#3 compression steel, and 0.0% steel fibers

d = 6.25 in d' = 1.56 in n = 7.25

Plastic moment = 10 P'_u (P'_u is from Table 6.5)

= 10 x 35 = 350

Fixed end moment = $P'_uL/8 = 35(60)/8 = 262.5$ k.in

$5(k_1d)^2/2+(2x7.25-1)(0.22)(k_1d-1.56)-7.25(0.88)(6.25-k_1d)$

$2.5k_1d^2+9.35k_1d-44.51$

$k_1d = 2.75$ in

$k_1 = 2.75/6.25 = 0.44$

$k_ud = 3.0$ in (from flexural analysis of beam, B#3, Chapter 5)

$K_u = 3.0/6.25 = 0.0480$

$I_{cr1} = 5(2.75)^3/3+(2x7.25-1)(0.22)(2.75-1.56)^2$

$+7.25(0.88)(6.25-2.75)^2 = 117.0$ in^4

$Ip = 5(3.0)^3/3+(2x7.25)(0.22)(3.0-1.56)^2$

$+7.25(0.88)(6.25-3.0)^2 = 118.54$ in^4

TABLE 6.7

REQUIRED AND AVAILABLE ROTATION CAPACITY

Beam No. (1)	% Steel Fibers (2)	Plastic Moment k.in (3)	Fixed End Moment k.in (4)	I_{cr1} in^4 (5)	I_{cr2} in^4 (6)	I_p in^4 (7)	k_1 (8)	k_2 (9)	k_u (10)	Required Rotation by Eq. (2.5) $\upsilon_1 \times 10^{-4}$ radians (11)	Required Rotation by Eq. (2.5) $\upsilon_2 \times 10^{-4}$ radians (12)	Rotation Capacity by Eq. (2.6) $\theta_p \times 10^{-4}$ radians (13)	Actual Rotation from testing $\upsilon_{pc} \times 10^{-4}$ radians (14)	υ_{pc}/υ_p (14)/(13) (15)	Relative Actual Increase from 0.0% Steel Fiber (16)
1	0.0	218.0	163.5	71.45	70.14	76.31	0.318	0.338	0.232	19.4	19.4	121.7	164	1.35	1.0
4	0.8	248.0	186.0	75.9	74.18	82.26	0.326	0.349	0.228	22.0	22.5	124.5	1168	9.4	7.12
7	1.2	289.0	216.8	86.36	83.40	96.27	0.342	0.372	0.226	26.6	27.8	126.0	1615	12.8	9.85
2	0.0	280.0	210.0	92.74	90.15	94.45	0.384	0.407	0.326	18.9	19.4	75.0	120	1.6	1.0
5	0.8	324.0	243.0	99.80	94.92	105.53	0.393	0.418	0.320	21.9	23.1	77.3	527	6.8	4.39
8	1.2	345.0	258.8	110.77	105.80	117.70	0.412	0.445	0.317	24.8	25.9	78.5	762	9.7	6.35
3	0.0	350.0	262.5	117.0	---	118.54	0.440	---	0.480	18.7	---	28.3	137	4.8	1.0
6	0.8	382.8	287.1	123.45	---	123.82	0.450	---	0.469	24.6	---	31.1	722	23.2	5.27
9	1.2	434.0	325.5	138.45	---	138.50	0.470	---	0.462	24.9	---	32.8	840	25.6	6.13

TABLE 6.8

ELASTIC AND PLASTIC ROTATIONS

Beam No. (1)	% Steel Fibers (2)	Tension Steel A_s (3)	Top Steel A'_s (4)	θ_y 1×10^{-4} (Radians) (5)	θ_u 1×10^{-4} (Radians) (6)	θ_{pc} 1×10^{-4} (Radians) $(\theta_u - \theta_y)$ (7)	θ_c 1×10^{-4} (Radians) (8)	θ_r 1×10^{-4} (Radians) (9)
1	0.0	2#4	2#3	103	267	164	787	1050
4	0.8	2#4	2#3	354	1522	1168	1903	3031
7	1.2	2#4	2#3	156	1771	1615	2335	3811
2	0.0	2#5	2#3	86	206	120	670	839
5	0.8	2#5	2#3	197	724	527	1522	1785
8	1.2	2#5	2#3	419	1181	762	1522	2205
3	0.0	2#6	2#3	93	230	137	750	950
6	0.8	2#6	2#3	262	984	722	1676	1971
9	1.2	2#6	2#3	262	1102	840	1667	2257

θ_y = total rotation in radians at linear limit (first yield).

θ_u = total rotation in radians at ultimate (second yield).

θ_{pc} = magnitude of plastic rotation capacity = $\theta_u - \theta_y$.

θ_c = total rotation in radians when concrete started to fail at middle support.

θ_r = total rotation in radians prior to rupture.

TABLE 6.9

PLASTIC HINGE LENGTHS

Beam No.	% Steel Fibers	Tension Steel A_s	Top Steel A'_s	Plastic Hinge Length (in)	H_L/d
1	0.0	2#4	2#3	6.0	0.92
4	0.8	2#4	2#3	7.5	1.15
7	1.2	2#4	2#3	8.0	1.23
2	0.0	2#5	2#3	6.0	0.95
5	0.8	2#5	2#3	8.0	1.27
8	1.2	2#5	2#3	9.0	1.43
3	0.0	2#6	2#3	6.5	1.04
6	0.8	2#6	2#3	9.0	1.44
9	1.2	2#6	2#3	9.5	1.52

TABLE 6.10

CURVATURE DISTRIBUTION FACTOR

Beam No.	% Steel Fibers	Tension Steel A_s	Top Steel A'_s	$\theta pc \times 10^4$ Radians	$\phi p \times 10^{-4}$	H_L in.	$\phi pH_L \times 10^{-4}$ Radians	$\beta = \theta pc/\phi pH_L$
(1)	(2)	(3)	(4)	(5)	(6)	(7)	(8)	(9)
1	0.0	2#4	2#3	164	61	6.0	366	0.45
4	0.8	2#4	2#3	1168	401	7.5	3008	0.39
7	1.2	2#4	2#3	1615	631	8.0	5048	0.32
2	0.0	2#5	2#3	120	46	6.0	276	0.44
5	0.8	2#5	2#3	527	200	8.0	1600	0.33
8	1.2	2#5	2#3	762	324	9.0	2916	0.26
3	0.0	2#6	2#3	137	50	6.5	325	0.42
6	0.8	2#6	2#3	722	261	9.0	2349	0.31
9	1.2	2#6	2#3	840	366	9.5	3477	0.24

Required rotation using Equation (2.5)

$$\theta_1 = 60[2(-350.0+262.5)+(0+262.5)]/6(4x10^3)(117)$$

$$= 1.87 \times 10^{-4} \text{ radians}$$

Rotation capacity using Equation (2.6)

$$\theta p = 0.0035/0.48-67.0/29000(1-0.48) = 28.4 \times 10^{-4} \text{ radians}$$

6.7 Deflections

6.7.1 Introduction

A rigid body moves when it is subjected to a load and the resulting displacement of various points from their original portions are called deflection. Deflection is considered an important factor that affects the serviceability of reinforced concrete flexural members. Excessive beam and slab deflections can lead to objectionable cracking of partitions, poor fitting of door frames and windows, poor drainage, excessive vibrations, etc. Therefore, to minimize the preceding problems adequate stiffness of members is necessary to prevent excessive deflection. The stiffness, flexural rigidity, of reinforced concrete consists of the modulus of elasticity and the moment of inertia of the section. Therefore, it is important to use a correct and safe value for the moment of inertia when calculating the deflection. The ACI Code (318.83) Section 9.5.2.3 presents an equation to determine an effective moment of inertia to be used in calculating deflection in flexural members:

$$I_e = (M_{cr}/M_a)^3 I_g + [1-(M_{cr}/M_a)^3] I_{cr} I_g \qquad (6.4)$$

where:

I_e = effective moment of inertia

M_{cr} = cracking moment ($f_r I_g / Y_t$)

f_r = modulus of rupture at concrete ($7.5\sqrt{f'_c}$)

M_a = maximum moment in member at stage for which the deflection is computed

I_g = gross moment of inertia neglecting steel

I_{cr} = moment of inertia of cracked transformed section

6.7.2 Theoretical Deflection Calculations

If a beam is subjected to different types of loads or subjected to end moments, the deflection may be calculated separately for each type of loading or force applied on the beam and the total deflection is calculated by superposition.

In this research all the beams were loaded under symmetrical loading with a concentrated load at the midpoint of each span. The calculation of theoretical deflection for the preceding case is as follows:

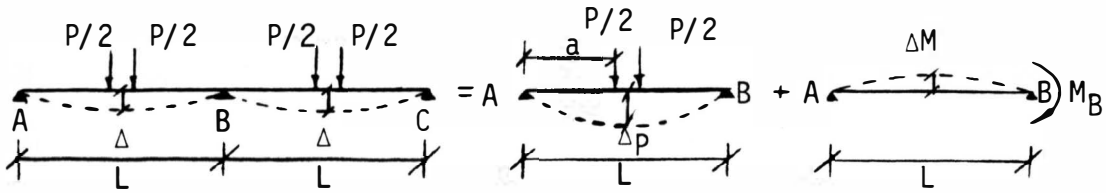

The correct value of deflection will be the summation of the deflection due to concentrated load P and due to M_B.

$$\Delta_p = \{(P/2)L^3[(3a/4L) - (a/L)^3]\}/6EI_e$$

where:

$$a = 0.45L$$

$$\Delta_p = \{(P/2)L^3[(3x0.45L/4L)-(0.45L/L)^3]\}/6EI_e$$

$$\Delta_p = (P/2)L^3(0.2464)/6EI_e$$

$$\Delta_M = (ML^2/16EI_e)$$

where:

M_B = 11.25P = 0.1875PL (Refer to moment diagram Figure 5.2)

$\Delta_M = -0.1875PL^3/16EI_e = 0.011PL^3/EI_e$

$\Delta_{net} = \Delta_p + \Delta_M = [(0.021 - 0.011)(PL^3]/EI_e = 0.01PL^3/EI_e$

Calculation of deflection at service load

B#1: A_s = 2#4 main steel, 2#3 top steel, and 0.0% steel fibers

d = 6.5 in d' = 1.44 in n = 7.25 $E_{ca} = 4x10^6$ psi

k_1d = 2.07 in (from Table 6.7) k_2d = 212 in (from Table 6.7)

I_{cr1}=71.45 in^4 (from Table 6.7) I_{cr2}=70.42 in^4 (from Table 6.7)

$I_g = bh^3/12 = (5 \times 8^3)/12 = 213.33\ in^4$

$M_{cr} = f_rI_g/Y_t = (508 \times 213.33)/4 = 21.1$ k.in

$M_a = 9.38(0.6\ P'_u) = 9.38(0.6 \times 21.8) = 9.38(13.08) = 122.7$ k.in

$(M_{cr}/M_a)^3 = (27.1/122.7)^3 = 0.0108$

$I_e = (M_{cr}/M_a)^3I_g+[1-(M_{cr}/M_a)^3]I_{cr}$

I_{el} = Effective moment of inertia when the top steel is considered

I_{e1} = 0.01008 (213.33) + (1-0.0108)(71.45) = 72.98 in^4

I_{e2} = Effective moment of inertia when the top steel is neglected

I_{e2} = 0.0108 (213.33) + (1 - 0.0108)(70.42) = 71.96 in^4

$\Delta = PL^3/100E_cI_e$

Δ_1 = calculated deflection when the top steel is considered

$\Delta_1 = (13.08x1000x60^3x1000)/(100x4x10^6x72.98) = 97.0 \times 10^{-3}$ in

Δ_2 = calculated deflection when the top steel is neglected

$\Delta_2 = (13.08x1000x60^3x1000)/(100x4x10^6x70.42) = 98.0 \times 10^{-3}$ in

B#2: A_s = 2#5 main steel, 2#3 top steel, and 0.0% steel fibers

d = 6.31 in d' = 1.56 in n = 7.25 $E_{ca} = 4x10^6$ psi

k_1d = 2.42 in (from Table 6.7) k_2d = 2.57 in (from Table 6.7)

I_{cr1}=92.74 in^4 (from Table 6.7) I_{cr2}=90.15 in^4 (from Table 6.7)

$I_g = bh^3/12 = (5 \times 8^3)/12 = 213.33$ in^4

$M_{cr} = f_rI_g/Y_t = (508 \times 213.33)/4 = 21.1$ k.in

$M_a = 9.38(0.6\ P_u') = 9.38(0.6 \times 28) = 9.38(16.8) = 157.58$ k.in

$(M_{cr}/M_a)^3 = (27.1/157.78)^3 = 0.0051$

$I_e = (M_{cr}/M_a)^3I_g+[1-(M_{cr}/M_a)^3]I_{cr}$

I_{e1} = (0.0051)(213.33) + (1-0.0051) 92.74 = 93.36 in^4

I_{e2} = (0.0051)(213.33) + (1 - 0.0051) 90.15 = 90.77 in^4

$\Delta_1 = (16.8x1000x60^3x1000)/(100x4x10^6x93.36) = 97.0 \times 10^{-3}$ in

$\Delta_2 = (16.8x1000x60^3x1000)/(100x4x10^6x90.77) = 100.0 \times 10^{-3}$ in

B#3: A_s = 2#6 main steel, compression steel 2#3, and 0.0% steel fibers

$d = 6.25$ in $\quad d' = 1.56$ in $\quad n = 7.25 \quad E_{ca} = 4 \times 10^6$ psi

$k_1 d = 2.75$ in (from Table 6.7) $\quad I_{cr1} = 117.0$ in^4 (from Table 6.7)

$M_{cr} = f_r I_g / Y_t = (508 \times 213.33)/4.0 = 27.1$ k.in

$M_a = 9.38(0.6\ P'_u) = 9.38(0.6 \times 35) = 9.38(21.0) = 196.98$ k.in

$(M_{cr}/M_a)^3 = (27.1/196.98)^3 = 0.0026$

$I_{el} = 0.0026\ (213.33) + (1-0.0026)\ 117.0 = 117.25$ in^4

$\Delta_1 = (21 \times 1000 \times 60^3 \times 1000)/(100 \times 4 \times 10^6 \times 117.25) = 97 \times 10^{-3}$ in

Theoretical and experimental deflection at service load are presented in Table 6.12. The percent decrease from 0.0% steel fiber is shown in the last column of Table 6.12. Typical experimental load-deflection curves are shown in Figures 6.23 through 6.31. Actual values of deflection at load increments are listed in Appendix B, Tables B.4 to B.7.

6.8 Cracks

6.8.1 Introduction

Excessive tension in the reinforcement can cause excessive cracking in the adjacent concrete. Due to the low tensile strength of concrete, beams subjected to flexural tension exhibit a series of distributed flexural cracks even at service load. In general, these cracks are harmless, unless the width becomes excessive. Therefore, the maximum crack width under service load must be limited to a

TABLE 6.11

CALCULATED BEAM PARAMETERS FOR DEFLECTION CALCULATIONS

Beam No. (1)	% Steel Fibers (2)	Tension Steel A_s (3)	Top Steel A'_s (4)	$k_1 d$ (in) (5)	$k_2 d$ (in) (6)	I_g (in^4) (7)	f_{ri} (psi) (8)	M_{cr} (k.in) (9)	M_a k.in) (10)	$(M_{cr}/M_a)^3$ (11)	I_{cr1} (in^4) (12)	I_{cr2} (in^4) (13)
1	0.0	2#4	2#3	2.07	2.2	213.33	508	27.10	122.7	0.0108	71.45	70.42
4	0.8	2#4	2#3	2.12	2.27	213.33	610	32.53	139.57	0.0125	75.90	74.10
7	1.2	2#4	2#3	2.22	2.42	213.33	715	38.13	162.65	0.0129	86.36	83.40
2	0.0	2#5	2#3	2.42	2.57	213.33	508	17.10	157.58	0.0051	92.74	90.15
5	0.8	2#5	2#3	2.48	2.64	213.33	610	32.53	182.35	0.0057	99.80	94.92
7	1.2	2#5	2#3	2.6	2.81	213.33	715	38.13	194.17	0.0076	110.77	105.8
3	0.0	2#6	2#3	2.75	---	213.33	508	27.10	196.98	0.0026	117.0	---
6	0.8	2#6	2#3	2.81	---	213.33	610	32.53	215.46	0.0034	123.45	---
9	1.2	2#6	2#3	2.94	---	213.33	715	38.13	247.63	0.0037	138.45	---

TABLE 6.12

CALCULATED AND ACTUAL DEFLECTION AT SERVICE LOAD

Beam No. (1)	% Steel Fibers (2)	Service Load $P=0.6P_u$ (kips) (3)	I_{e1} (in^4) (4)	I_{e2} (in^4) (5)	$E_{ca} \times 10^6$ (psi) (6)	$\Delta_1 \times 10^{-3}$ Calculated* (in) (7)	$\Delta_2 \times 10^{-3}$ Calculated** (in) (8)	$\Delta \times 10^{-3}$ Actual (in) (9)	% Decrease From 0.0% Steel Fibers (10)
1	0.0	13.08	72.98	71.96	4.00	97	98	95	---
4	0.8	14.88	77.62	75.84	3.71	112	115	85	-10.53
7	1.2	17.34	88.00	85.10	3.15	131	135	80	-15.79
2	0.0	16.80	93.36	90.77	4.0	97	100	85	---
5	0.8	19.44	100.45	95.59	3.71	113	118	84	-1.18
8	1.2	20.70	111.55	106.62	3.15	127	134	83	-2.35
3	0.0	21.00	117.25	---	4.0	97	---	95	---
6	0.8	22.97	123.75	---	3.71	110	---	88	-7.37
9	1.2	26.04	138.73	---	3.15	130	---	87	-8.42

*Calculated deflection corresponding to I_{e1}.

**Calculated deflection corresponding to I_{e2}.

FIGURE 6.23
P/PU-DEFLECTION RELATIONSHIP
MAIN STEEL-2#4 TOP STEEL-2#3 %STEEL FIBERS-0.0
BEAM #1

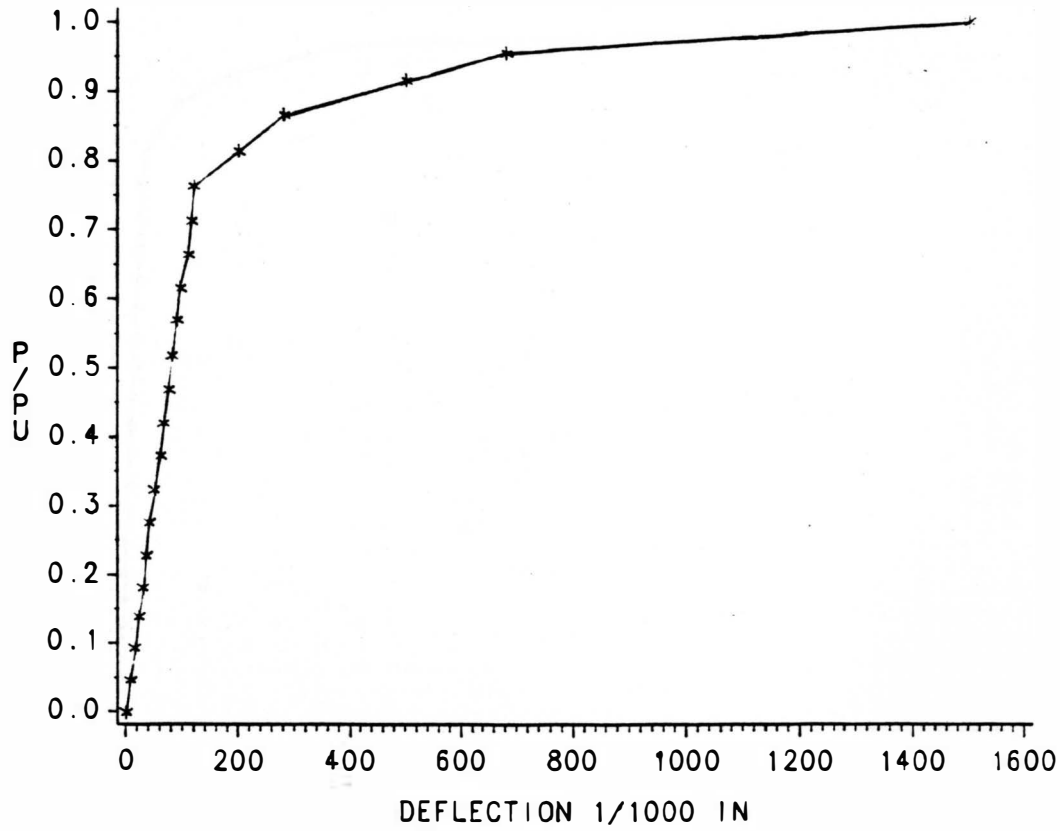

FIGURE 6.23 LOAD VS.DEFLECTION

FIGURE 6.24
P/PU-DEFLECTION RELATIONSHIP
MAIN STEEL-2#4 TOP STEEL 2#3 %STEEL FIBERS-0.0
BEAM #4

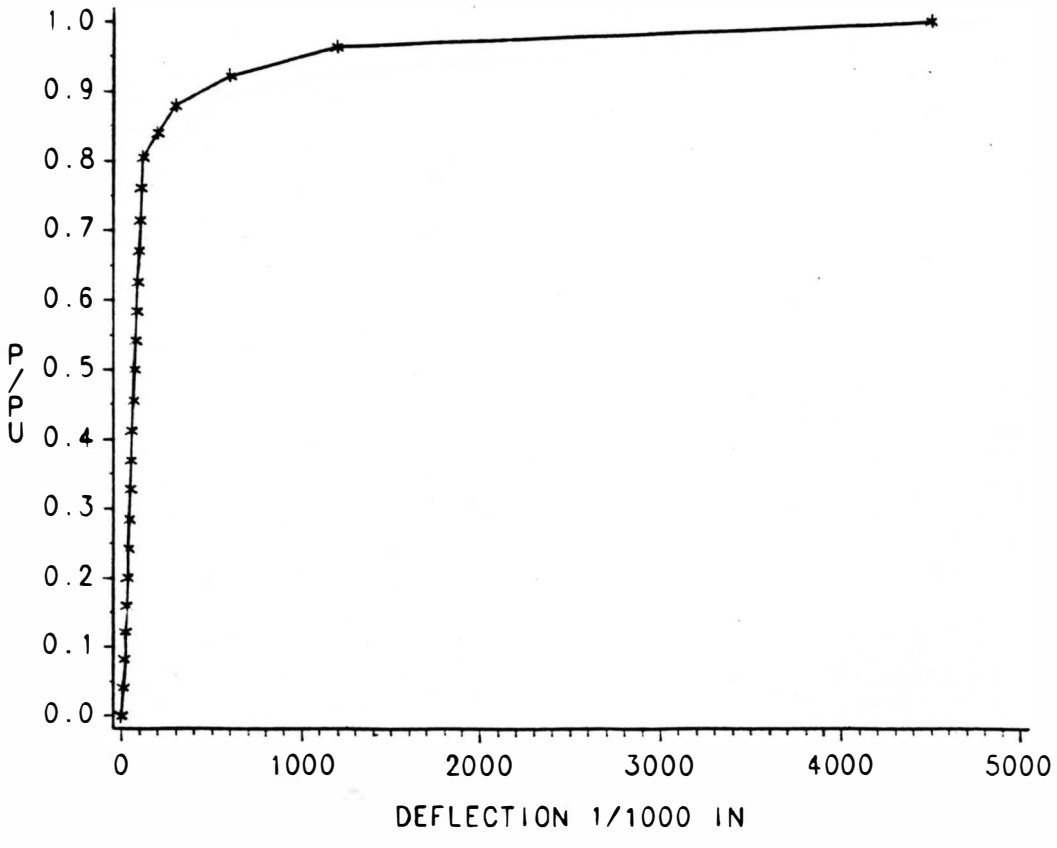

FIGURE 6.24 LOAD VS.DEFLECTION

FIGURE 6.25
P/PU-DEFLECTION RELATIONSHIP
MAIN STEEL=2#4 TOP STEEL=2#3 %STEEL FIBERS=1.2
BEAM #7

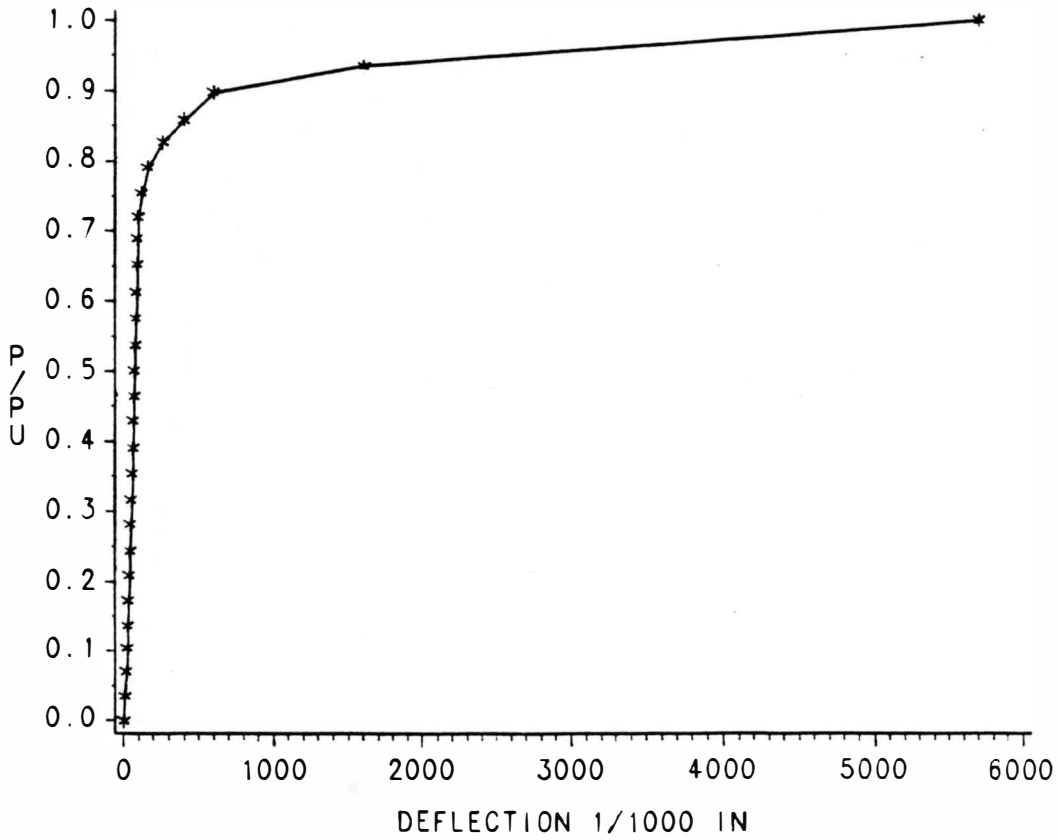

FIGURE 6.25 LOAD VS. DEFLECTION

FIGURE 6.26
P/PU-DEFLECTION RELATIONSHIP
MAIN STEEL-2#5 TOP STEEL-2#3 /STEEL FIBERS=0.0
BEAM #2

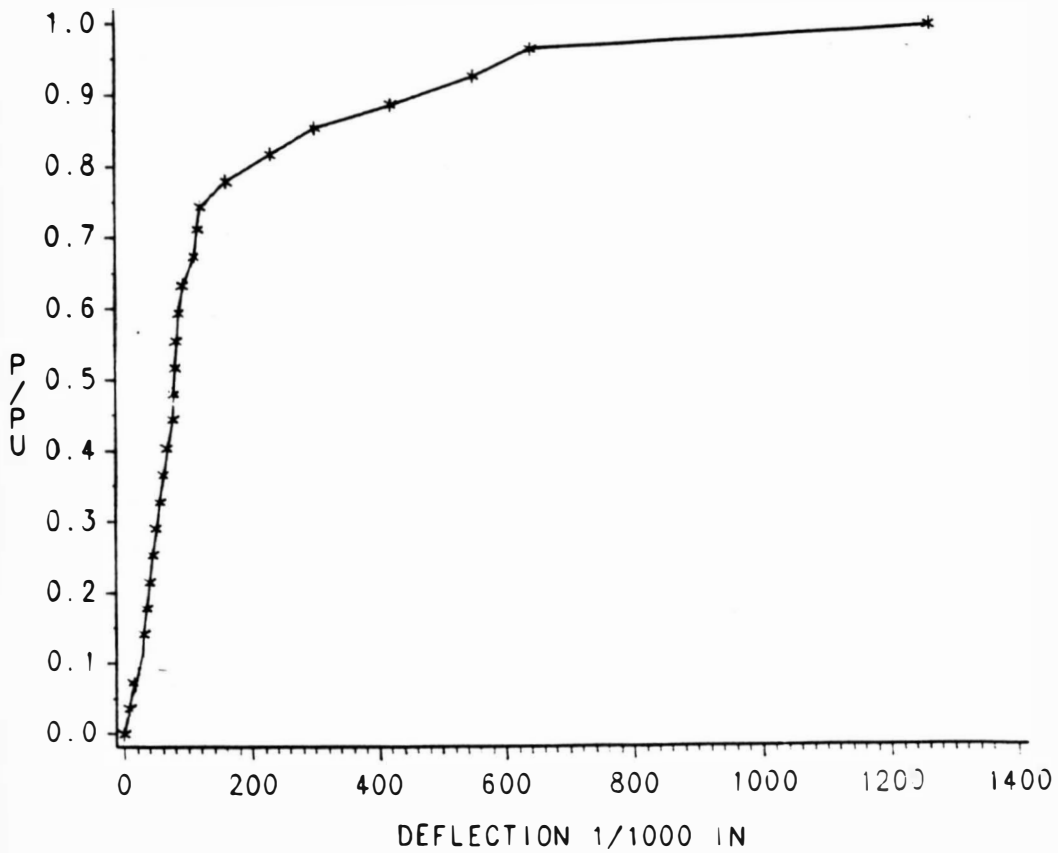

FIGURE 6.26 LOAD VS.DEFLECTION

FIGURE 6.27
P/PU-DEFLECTION RELATIONSHIP
MAIN STEEL=2#6 TOP STEEL=2#3 /STEEL FIBERS=0.8
BEAM #5

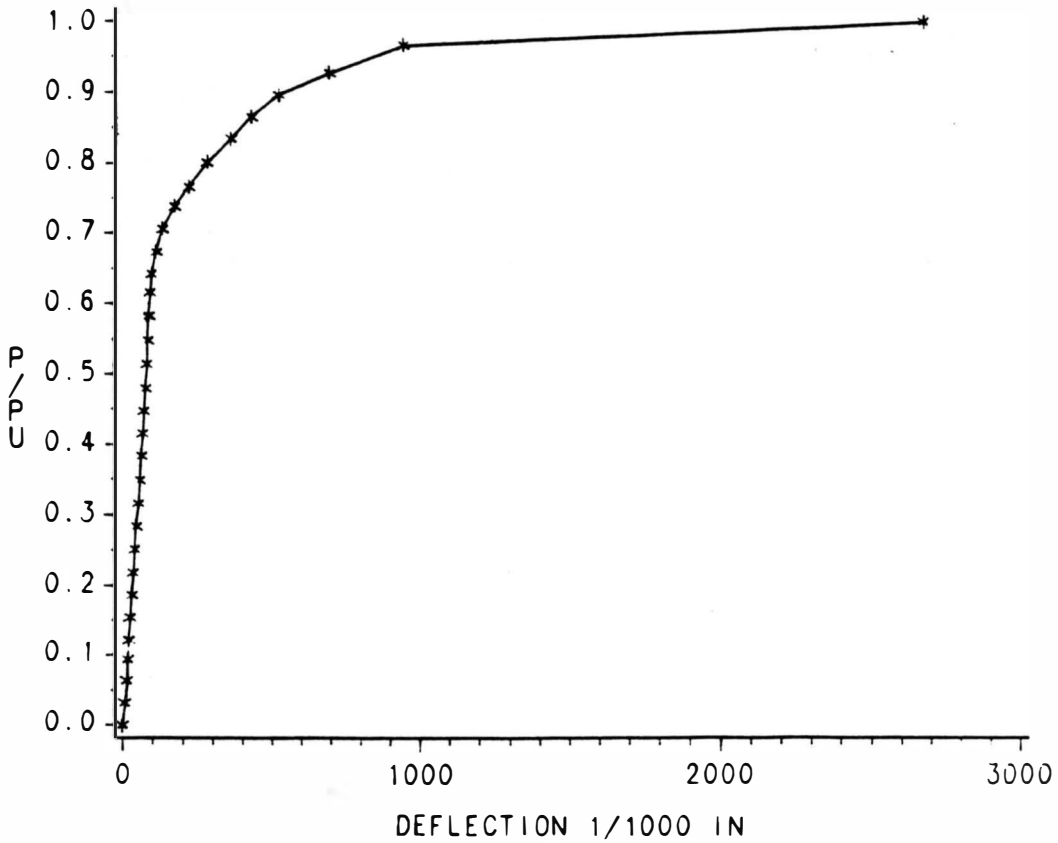

FIGURE 6.27 LOAD VS. DEFLECTION

FIGURE 6.28
P/PU-DEFLECTION RELATIONSHIP
MAIN STEEL=2#5 TOP STEEL=2#3 %STEEL FIBERS=1.2
BEAM #8

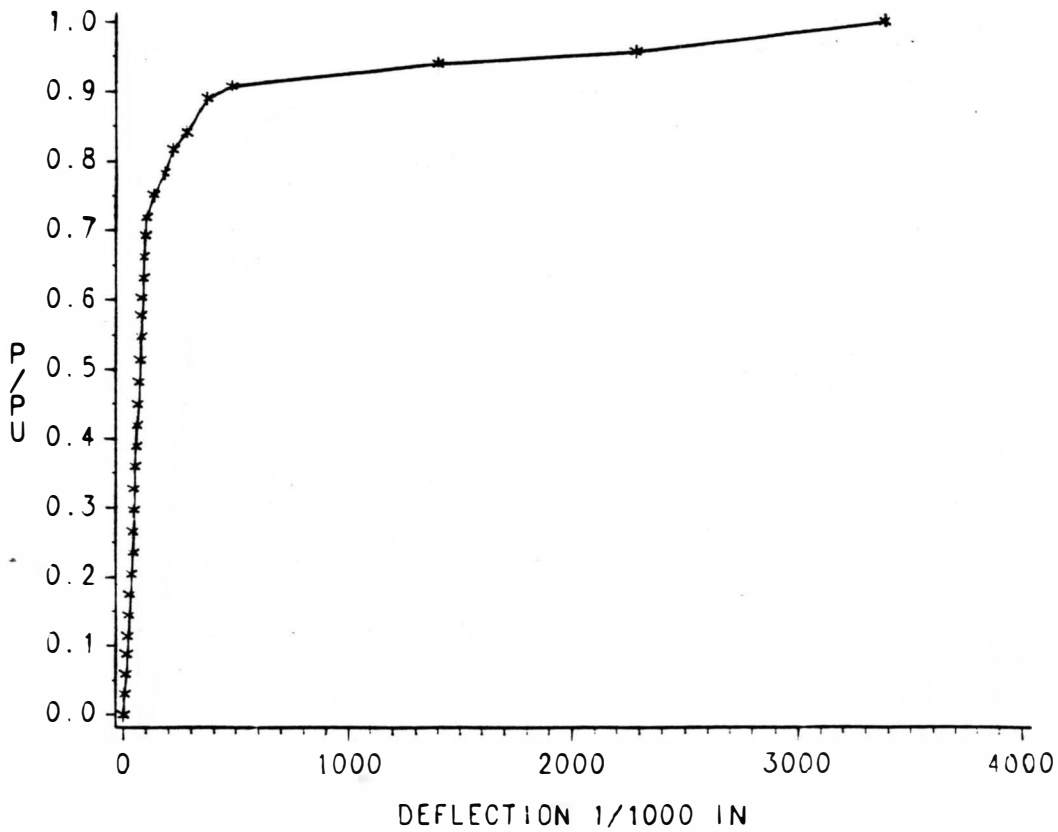

FIGURE 6.28 LOAD VS. DEFLECTION

FIGURE 6.29
P/PU-DEFLECTION RELATIONSHIP
MAIN STEEL=2#6 TOP STEEL=2#3 /STEEL FIBERS=0.0
BEAM #3

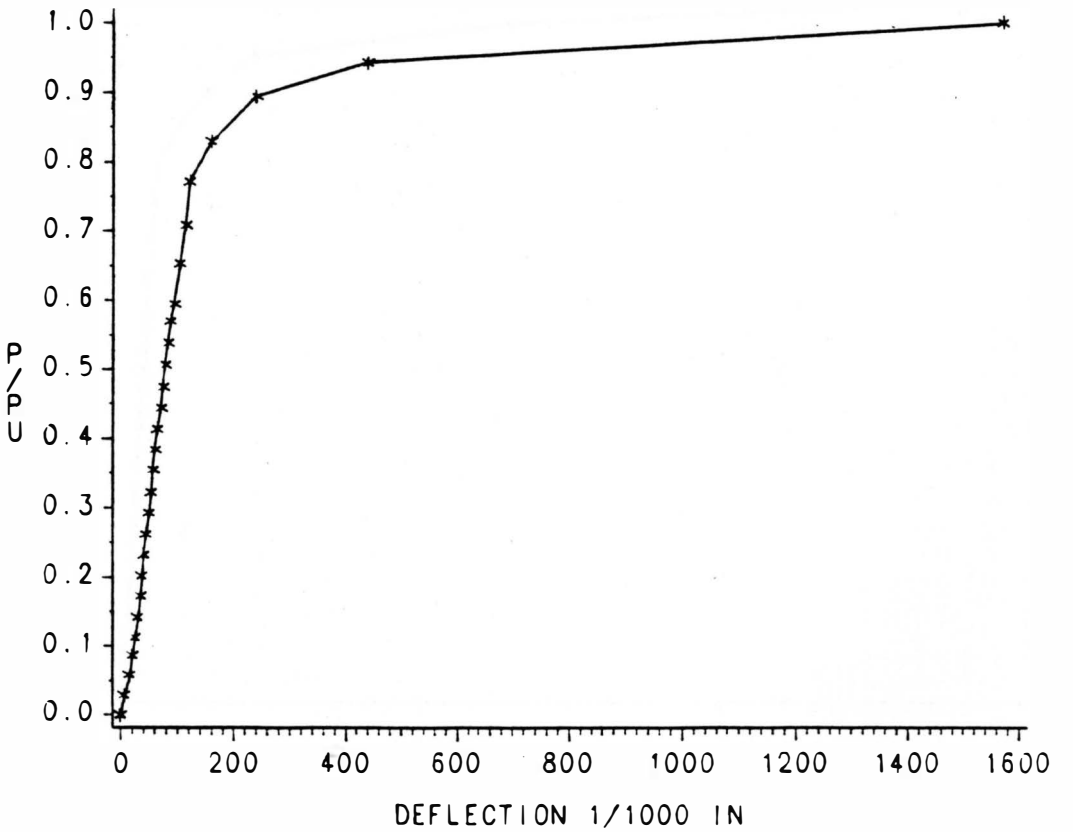

FIGURE 6.29 LOAD VS.DEFLECTION

FIGURE 6.30
P/PU-DEFLECTION RELATIONSHIP
MAIN STEEL=2#6 TOP STEEL=2#3 %STEEL FIBERS=0.8
BEAM #6

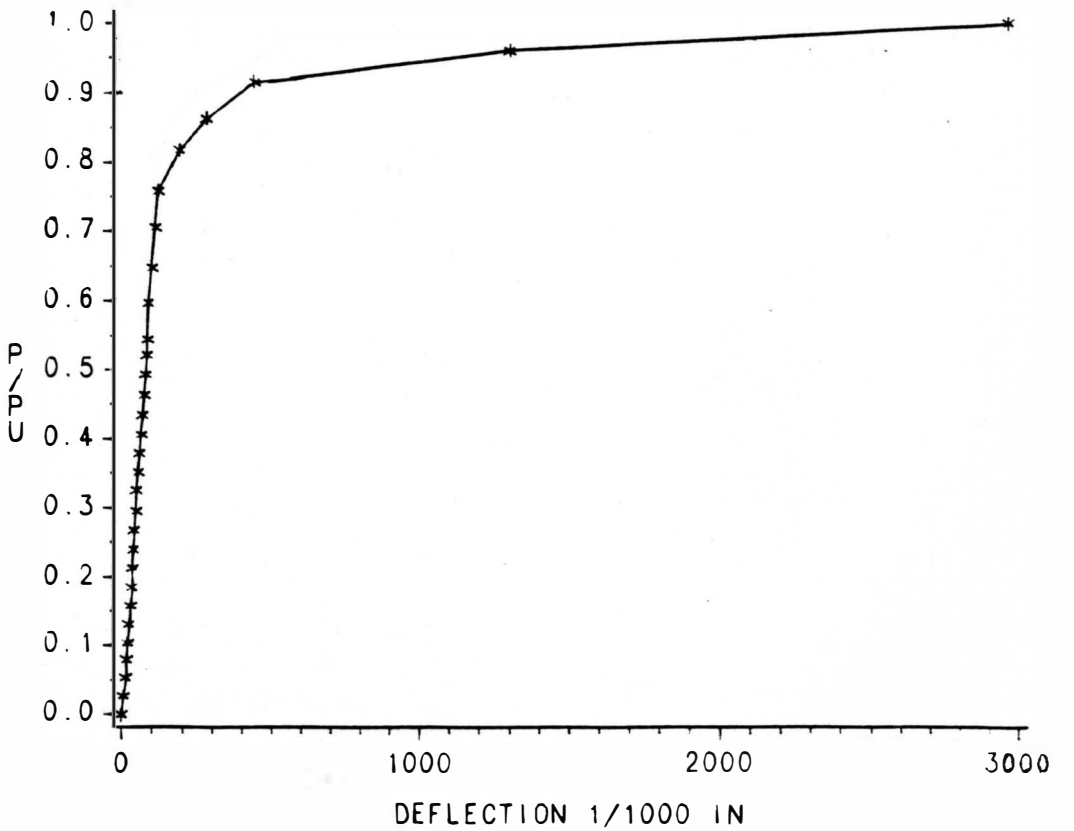

FIGURE 6.30 LOAD VS. DEFLECTION

FIGURE 6.31
P/PU-DEFLECTION RELATIONSHIP
MAIN STEEL-2#6 TOP STEEL-2#3 /STEEL FIBERS-1.2
BEAM #9

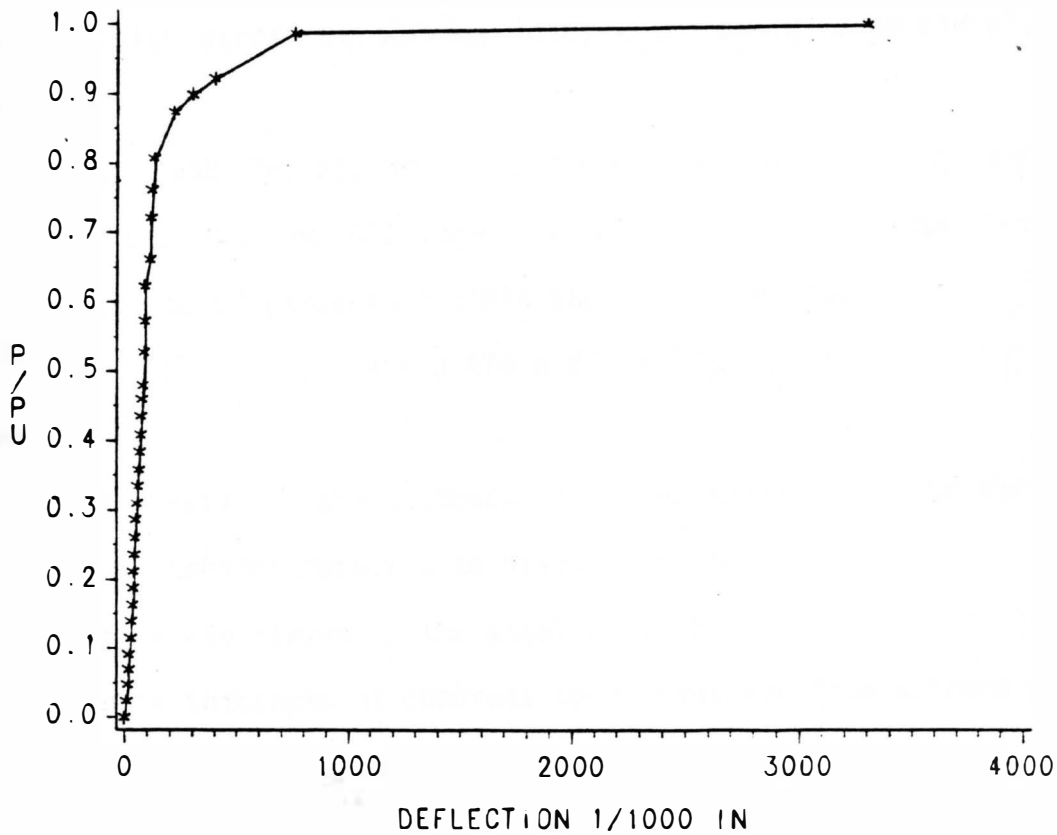

FIGURE 6.31 LOAD VS.DEFLECTION

specified value to prevent corrosion at the reinforcement and ensure water tightness of bridge decks and reservoirs.

Many factors influence the width of cracks, but the stress in the reinforcement, the bar diameter, the percentage of steel, and bond conditions are the principal ones. Therefore a high strength steel develops high stress at service load, which could cause visibly large cracks.

In 1968 Gergely and Lutz developed the following equation, which is used by the ACI code for limiting crack width for steel stresses up to 60 percent of yield stress of the steel:

$$W = 0.076\ \beta\ f_s \sqrt[3]{(A)(d_c)} \qquad (6.5)$$

where:

β = ratio of the distances from the neutral axis to the tension face and to steel centroid

f_s = the stress in the steel bars (ksi)

d_c = thickness of concrete cover measured from extreme tension fiber to the center of closest bar (in)

A = the effective tension area of concrete around the main reinforcing bars having the same reinforcement centroid, divided by the number of bars

The ACI Code adopted the preceding equation and used a value of $\beta = 1.2$ with the cross section proportional so that the formula $Z = f_s \sqrt[3]{Ad_c}$ is limited to 175 kips per inch for interior members and 145 kips per inch for exterior members. These limiting values allow a

maximum crack width of 0.016 in. for interior members and 0.013 in. for exterior members.

Crack Width and Crack Spacing Measurements

As explained in Chapter 4 the crack widths were measured at different loads by using a mechanical dial gage with an accuracy of one ten thousandth of an inch. The crack widths were determined at both the negative (over the middle support) and the positive sections (under the load). The difference between the strain readings before and after cracking was considered as the width of the crack. Calculated and experimental crack widths are shown in Table 6.14. The differential of all readings isrecorded in Tables C.1 through C.18 in Appendix C.

The first cracking load was noted and presented in Table 6.15. The spacings of the cracks were also measured. The maximum and minimum crack spacing as well as the number of cracks at each critical section at service load, and ultimate, are shown in Tables 6.16 and 6.17.

6.8.2 Calculations of Crack Widths at Service Load

B#1: A_s = 2#4 main steel, 2#3 top steel, and 0.0% steel fibers

b = 5 in h = 8 in d = 6.5 in f_y = 64.9 ksi

k_1d = 2.07 in (from Table 6.7) k_2d = 2.2 in (from Table 6.7)

$W = 0.076\ \beta f_s^3 \sqrt{d_c x A} \times 10^{-3}$

$\beta' = (h - k_1d)/(d-k_1d)$ (column 12 of Table 6.13)

$\beta' = (8 - 2.07)/(6.5 - 2.07) = 1.34$

$d_c = h - d = 8 - 6.5 = 1.5$ in (column 10 of Table 6.13)

$A = (2 \times d_c \times b)/n$ (column 11 of Table 6.13)

where:

n = number of bars in the section

$A = (2 \times 1.5 \times 5)/2 = 7.6$ in^2

$f_s = 0.6\, f_y = 0.6\,(64.9) = 38.94$ ksi (column 7 of Table 6.13)

$Z = f_s\sqrt[3]{Ad_c} = 38.94\sqrt[3]{1.5 \times 1.75} = 87.3$ k/in

$\beta'' = (h-k_2d)/(d-k_2d)$ (column 13 of Table 6.13)

$\beta'' = (8-2.2)/(6.5-2.2) = 1.35$

$W_1 = 0.076\, \beta' f_s\sqrt[3]{d_c x A_c} x 10^3$ (column 6 of Table 6.14)

where:

W_1 = calculated crack width when the top steel is considered

$W_1 = 0.076x10x1.34x38.94\, f_s\sqrt[3]{1.5x7.5x10^{-3}} = 89 \times 10^{-4}$ in

$W_2 = 0.076\, \beta' f_s\sqrt[3]{d_c x A_c} \times 10^{-3}$ (column 8 of Table 6.14)

where:

W_2 = calculated crack width when the top steel is neglected

$W_2 = 0.076x10x1.35(38.94)\sqrt[3]{1.5x7.5} \times 10^{-3} = 90 \times 10^{-4}$ in

B#2: A_s = 2#5 main steel, 2#3 top steel, and 0.0% steel fibers

b = 5 in h = 8 in d = 6.31 in f_y = 63.2 ksi

k_1d = 2.42 in (from Table 6.7) k_2d = 2.57 in (from Table 6.7)

$W = 0.076\, \beta f_s\sqrt[3]{d_c x A_c} \times 10^{-3}$

$\beta' = (h - k_1 d)/(d - k_1 d)$

$\beta' = (2 - 2.42)/(6.31 - 2.42) = 1.43$

$d_c = h - d = 8 - 6.31 = 1.69$ in

$A = (2 \times d_c \times b)/n$

where:

n = number of bars in the section

$A = (2 \times 1.69 \times 5)/2 = 8.45$ in^2

$f_s = 0.6\, f_y = 0.6\,(63.2) = 37.92$ ksi

$Z = f_s \sqrt[3]{Ad_c}$

$Z = 37.92\ \sqrt[3]{1.69 \times 8.45} = 92$ k/in

$\beta'' = (n - k_2 d)/(d - k_2 d)$

$\beta'' = (8 - 2.57)/(6.31 - 2.57) = 1.45$

$W_1 = 0.076 \times 10 \times 1.43 \times 37.92 \sqrt[3]{1.69 \times 8.45} \times 10^{-3} = 100 \times 10^{-4}$ in

$W_2 = 0.076 \times 10 \times 1.45 \times 37.92 \sqrt[3]{1.69 \times 8.45} \times 10^{-3} = 101 \times 10^{-4}$ in

B#3: A_s = 2#6 main steel, 2#3 compression steel and 0.0% steel fibers

b = 5 in h = 8 in d = 6.5 in f_y = 67.0 ksi

$k_1 d = 2.75$ in (from Table 6.7)

$W = 0.076\, \beta f_s \sqrt[3]{d_c \times A_c} \times 10^{-3}$

$\beta' = (h - k_1 d)/(d - k_1 d)$

$\beta' = (8 - 2.75)/(6.25 - 2.75) = 1.5$

$d_c = h - d = 8 - 6.25 = 1.75$ in

$A = (2 \times d_c \times b)/n$

where:

n = number of bars in the section

$A = (2 \times 1.75 \times 5)/2 = 8.75$

$f_s = 0.6\, f_y = 0.6\,(67) = 40.2$ ksi

$Z = f_s \sqrt[3]{A d_c}$

$Z = 40.2 \sqrt[3]{1.75 \times 8.75} = 99.8$ k/in

$W_1 = 0.076\, \beta'\, f_s \sqrt[3]{d_c \times A_c} \times 10^{-3}$

$W_1 = 0.076 \times 10 \times 1.5 \times 40.2 \sqrt[3]{1.75 \times 8.75} \times 10^{-3} = 114 \times 10^{-4}$ in

TABLE 6.13

CALCULATED BEAM PARAMETERS FOR CRACK WIDTH CALCULATIONS

Beam No. (1)	% Steel Fibers (2)	Tension Steel A_s (3)	Top Steel A'_s (4)	Actual Ultimate load kips (5)	Service load $P=0.6P_u$ kips (6)	$f_s = 06\ f_y$ ksi (7)	$k_1 d$ in (8)	$k_s d$ in (9)	d_c in (10)	A_{c_2} in^2 (11)	$\beta' = h-k_1 d/d-k_1 d$ (12)	$\beta'' = h-k_2 d/d-k_2 d$ (13)
1	0.0	2#4	2#3	21.80	13.08	38.94	2.07	2.2	1.5	7.5	1.34	1.35
4	0.8	2#4	2#3	24.80	14.88	38.94	2.12	2.27	1.5	7.5	1.34	1.35
7	1.2	2#4	2#3	28.90	17.34	38.94	2.22	2.42	1.5	7.5	1.35	1.37
2	0.0	2#5	2#3	28.00	16.8	37.92	2.42	2.57	1.69	8.45	1.43	1.45
5	0.8	2#5	2#3	32.40	19.44	37.92	2.48	2.64	1.69	8.45	1.44	1.46
8	1.2	2#5	2#3	34.50	20.70	37.92	2.6	2.81	1.69	8.45	1.46	1.48
3	0.0	2#6	2#3	35.00	21.0	40.2	2.75	---	1.75	8.75	1.50	---
6	0.8	2#6	2#3	38.28	22.97	40.2	2.81	---	1.75	8.75	1.51	---
9	1.2	2#6	2#3	43.4	26.04	40.2	2.94	---	1.75	8.75	1.53	---

TABLE 6.14

MAXIMUM ACTUAL AND CALCULATED CRACK WIDTH AT ASSUMED SERVICE LOAD (0.6 P_u)

				At Middle Support						At Midspan					
Beam No.	% Steel Fibers	Tension Steel A_s	Top Steel A'_s	Actual crack width $1x10^{-4}$ in	Calculated crack width $1x10^{-4}$ in	% Deviation (5) from (6)	Calculated crack width $1x10^{-4}$ in	% Deviation (5) from (8)	% Decrease in actual crack width from 0.0% Steel Fibers	Actual crack width $1x10^{-4}$ in	Calculated crack width $1x10^{-4}$ in	% Deviation (11) from (12)	Calculated crack width $1x10^{-4}$ in	% Deviation (11) from (14)	% Decrease in actual crack width from 0.0% Steel Fibers
(1)	(2)	(3)	(4)	(5)	(6)	(7)	(8)	(9)	(10)	(11)	(12)	(13)	(14)	(15)	(16)
1	0.0	2#4	2#3	87	89	-2.3	90	-3.3	---	80	89	-10.1	90	-10.1	---
4	0.8	2#4	2#3	68	89	-23.6	90	-3.3	-21.8	65	89	-27.0	90	-27.0	-18.8
7	1.2	2#4	2#3	55	90	-38.9	91	-39.6	-36.8	50	90	-44.4	91	-45.1	-37.5
2	0.0	2#5	2#3	104	100	+4.0	101	+3.0	---	98	100	-2.0	101	-3.0	---
5	0.8	2#5	2#3	84	101	-16.8	102	-17.6	-19.2	78	101	-22.8	102	-23.5	-20.4
8	1.2	2#5	2#3	78	102	-23.5	103	-24.3	-25.0	73	102	-28.4	103	-29.1	-25.5
3	0.0	2#6	2#3	107	114	-6.1	---	---	---	103	114	-9.6	---	---	---
6	0.8	2#6	2#3	92	115	-20.0	---	---	-14.0	85	115	-26.1	---	---	-17.5
9	1.2	2#6	2#3	87	116	-25.0	---	---	-18.7	80	116	-31.0	---	---	-22.3

TABLE 6.15

INITIAL CRACKING LOADS AND STRENGTHS

Beam No. (1)	% Steel Fibers (2)	Tension Steel A_s (3)	Top Steel A'_s (4)	Actual Load P_u (kips) (5)	Initial Cracking load (P_i) kips (6)	P_i/P_u (7)	Actual Initial Crack Strength For R.C. Beams (psi) (8)	ACI Code $f_r=7.5\sqrt{f'_c}$ (psi) (9)	% Deviation from ACI Code (10)	f_r for Small Concrete Beams psi (11)	% Deviation from ACI Code (12)	% Deviation (8) from (11) (13)
1	0.0	2#4	2#3	21.80	3.96	0.18	835	529	+57.8	508	-3.97	+64.4
4	0.8	2#4	2#3	24.80	6.02	0.24	1267	540	+134.6	610	+13.00	+107.7
7	1.2	2#4	2#3	28.90	8.13	0.28	1715	545	+214.7	715	+31.00	+139.9
2	0.0	2#5	2#3	28.00	4.68	0.17	987	529	+86.6	508	-3.97	+94.3
5	0.8	2#5	2#3	32.4	7.05	0.22	1487	540	+175.4	610	+13.00	+143.8
8	1.2	2#5	2#3	34.50	8.64	0.25	1823	545	+234.5	715	+31.00	+155.0
3	0.0	2#6	2#3	35.00	5.49	0.16	1158	529	+118.9	508	-3.97	+128.0
6	0.8	2#6	2#3	38.28	7.59	0.19	1601	540	+196.5	610	+13.00	+162.5
9	1.2	2#6	2#3	44.00	9.7	0.22	2046	545	+275.4	715	+31.00	+186.2

TABLE 6.16

MAXIMUM AND MINIMUM CRACK SPACINGS AT MIDDLE SUPPORT (NEGATIVE MOMENT REGION)
AT SERVICE LOAD (0.6 P_u)

Beam No. (1)	% Steel Fibers (2)	Tension Steel A_s (3)	Top Steel Steel A'_s (4)	Maximum Spacing (inches) (5)	Minimum Spacing (inches) (6)	Average Spacing (inches) (7)	Relative Average Spacing* (8)	Number of Cracks At Service Load (9)	Number of Cracks Before Failure (10)
1	0.0	2#4	2#3	6.0	6.0	6.0	1.0	3	4
4	0.8	2#4	2#3	4.0	2.5	3.5	0.58	6	6
7	1.2	2#4	2#3	3.5	2.0	3.0	0.50	7	8
2	0.0	2#5	2#3	5.0	2.8	3.6	1.0	4	6
5	0.8	2#5	2#3	3.5	2.5	2.7	0.75	6	10
8	1.2	2#5	2#3	3.5	1.5	2.4	0.67	7	10
3	0.0	2#6	2#3	5.5	2.0	3.0	1.0	5	7
6	0.8	2#6	2#3	3.5	1.5	2.5	0.83	7	10
9	1.2	2#6	2#3	3.0	1.0	2.2	0.73	8	11

*Relative Spacing = average crack spacing of beams with fibers/average crack spacing of beams without fibers

-Negative Moment Region is 16.34 from each side of center of middle support (Refer to Figure 5.3)

-Spacing of cracks were measured at distance 10' from each side of center of middle support.

TABLE 6.17

MAXIMUM AND MINIMUM CRACK SPACINGS AT MIDSPAN (POSITIVE MOMENT REGION) AT SERVICE LOAD (0.6 P_u)

Beam No. (1)	% Steel Fibers (2)	Tension Steel A_s (3)	Top Steel Steel A'_s (4)	Maximum Spacing (inches) (5)	Minimum Spacing (inches) (6)	Average Spacing (inches) (7)	Relative Average Spacing* (8)	Number of Cracks At Service Load (9)	Number of Cracks Before Failure (10)
1	0.0	2#4	2#3	8.0	5.0	5.0	1.0	6	8
4	0.8	2#4	2#3	3.0	1.0	2.5	0.5	7	12
7	1.2	2#4	2#3	2.5	0.8	2.0	0.4	8	10
2	0.0	2#5	2#3	5.0	2.8	3.8	1.0	7	9
5	0.8	2#5	2#3	4.5	2.5	2.8	0.8	7	9
8	1.2	2#5	2#3	4.0	1.0	2.0	0.57	8	13
3	0.0	2#6	2#3	3.5	3.0	3.1	1.0	7	10
6	0.8	2#6	2#3	4.5	1.5	2.8	0.9	9	13
9	1.2	2#6	2#3	2.9	1.0	2.3	0.74	7	10

*Relative Spacing = average crack spacing of beams with fibers/average crack spacing of beams without fibers

-Positive moment region has a length = 43.66 inches measured from each end of the beam (Refer to Figure 5.3)

CHAPTER 7

DISCUSSION OF RESULTS

7.1 Compressive Strength

Standard size concrete cylinders (6" x 12") were cast to determine the compressive strength of plain and fibrous concrete. The percentages of steel fibers used were 0.0, 0.8 and 1.2. Table 7.1 summarizes the compressive strength results. The percentage increase in compressive strength was 4.2 and 6.1 for 0.8 and 1.2 percentage of steel fibers respectively. It can be concluded from these results that the increase in compressive strength is not appreciable by the presence of steel fibers. Similar observations were reported by others (25,33,50,47,39) who found an insignificant increase or no increase in compressive strength when using steel fibers. Nevertheless, the type of failure varies with the addition of steel fibers. The plain concrete failed suddenly with some pieces falling apart (Figure 7.1); on the other hand, the failure of fibrous concrete produced a ductile mode of failure where the pieces did not fall apart (Figure 7.2)

7.2 Modulus of Elasticity

Six standard size cylinders were tested to determine the modulus of elasticity of plain and fibrous concrete. Table 7.2 summarizes the results of the actual plain and fibrous modulus of

TABLE 7.1

SUMMARY OF ACTUAL COMPRESSIVE STRENGTH RESULTS

% Steel Fibers	Compressive Strength (PSI)	% Increase from 0.0% Steel Fibers
0.0	4970	---
0.8	5180	4.2
1.2	5275	6.1

TABLE 7.2

SUMMARY OF ACTUAL MODULUS OF ELASTICITY RESULTS

% Steel Fibers	Actual $E_{ca} \times 10^6$ (psi) From Testing	Calculated $E_c \times 10^6$ (psi) ACI-Code (Eq. 6.1)	% Deviation From ACI-Code (Eq. 6.1)	% Decrease From From 0.0% Steel Fibers
0.0	4.0	4.11	-2.7	---
0.8	3.71	4.34	-14.5	-7.3
1.2	3.15	4.4	-28.4	-21.3

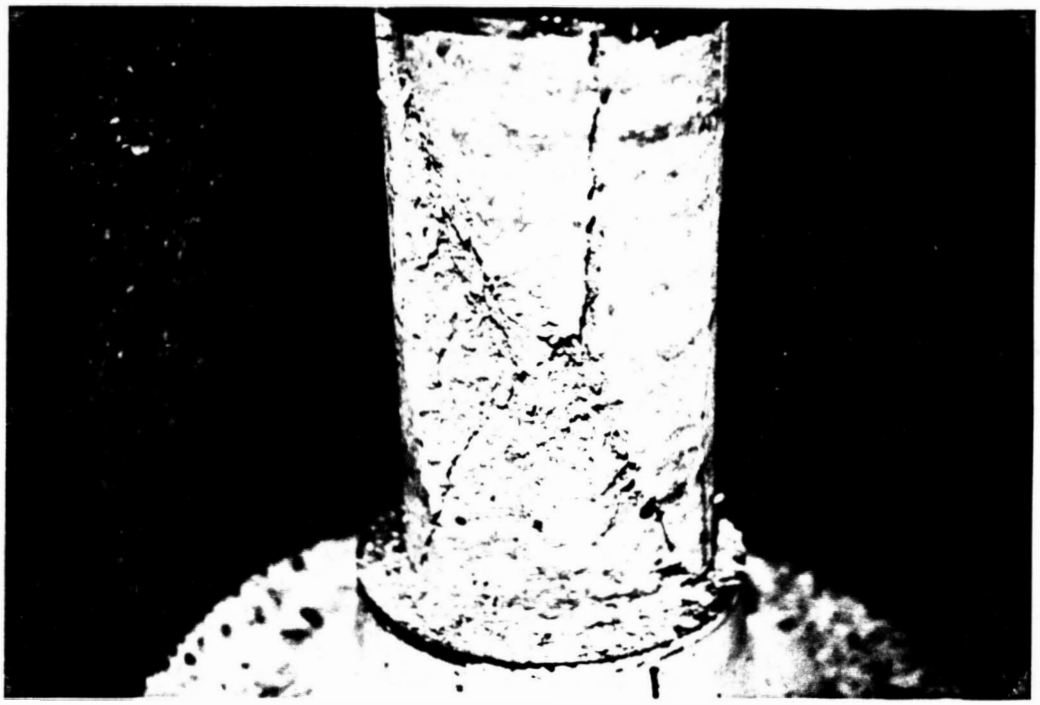

Figure 7.1. Failure of plain concrete in compression.

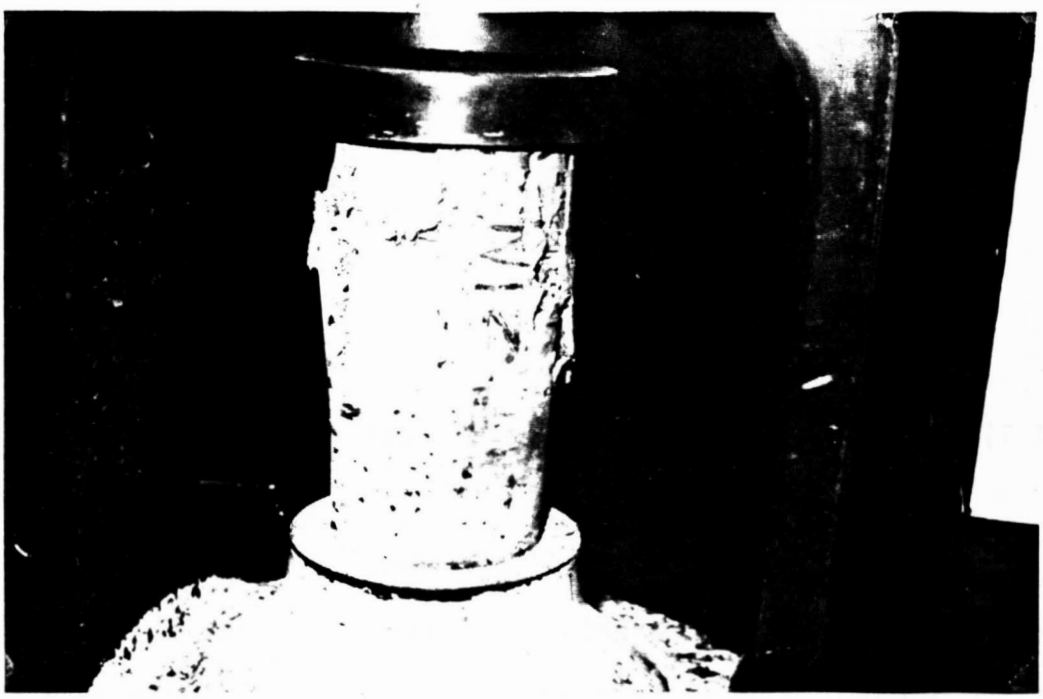

Figure 7.2. Failure of fibrous concrete in compression.

elasticity of concrete. A decrease in the modulus of elasticity of 7.3 and 2.13 percent was found when using 0.8 and 1.2 steel fibers percentage respectively. Similar observations were reported by others (50,39,5). It can also be concluded from Table 7.2 that the actual modulus of elasticity of fibrous concrete is considerably less than the one calculated by the ACI formula $E_c = 33w^{1.5}\sqrt{f'_c}$ (6.1). This percentage reduction in the modulus of elasticity of fibrous concrete cylinders was 14.5 and 28.4 compared to the ACI formula, when 0.8 and 1.2 percent steel fibers were used.

A statistical analysis of the data was done to the modify the ACI formula since the formula overestimates the fibrous concrete modulus of elasticity. A simple regression using the best fit line through the ratios $E_{ca}/33w^{1.5}\sqrt{f'_c}$ and volume percentage of steel fibers was evaluated (Figure 7.3). The ACI formula as shown by Equation 6.1 may be modified as follows:

$$E_{cc} = m\ 33w^{1.5}\sqrt{f'_c}$$

where:

$$m = 1 - 0.2\ \rho_s$$

or:

$$E_{cc} = (33 - 6.6\ \rho_s)w^{1.5}\sqrt{f'_c} \qquad (7.1)$$

where:

E_{cc} = modulus of elasticity of fibrous concrete (psi)

The correlation coefficient between 'm' and ρ_s was 0.93. This shows about 87 percent ($r^2 = 0.87$) of the variation is accounted for by the

FIGURE 7.3
MODULUS OF ELASTICITY VS.%STEEL FIBERS
CORRELATION COEFFICIENT=0.934

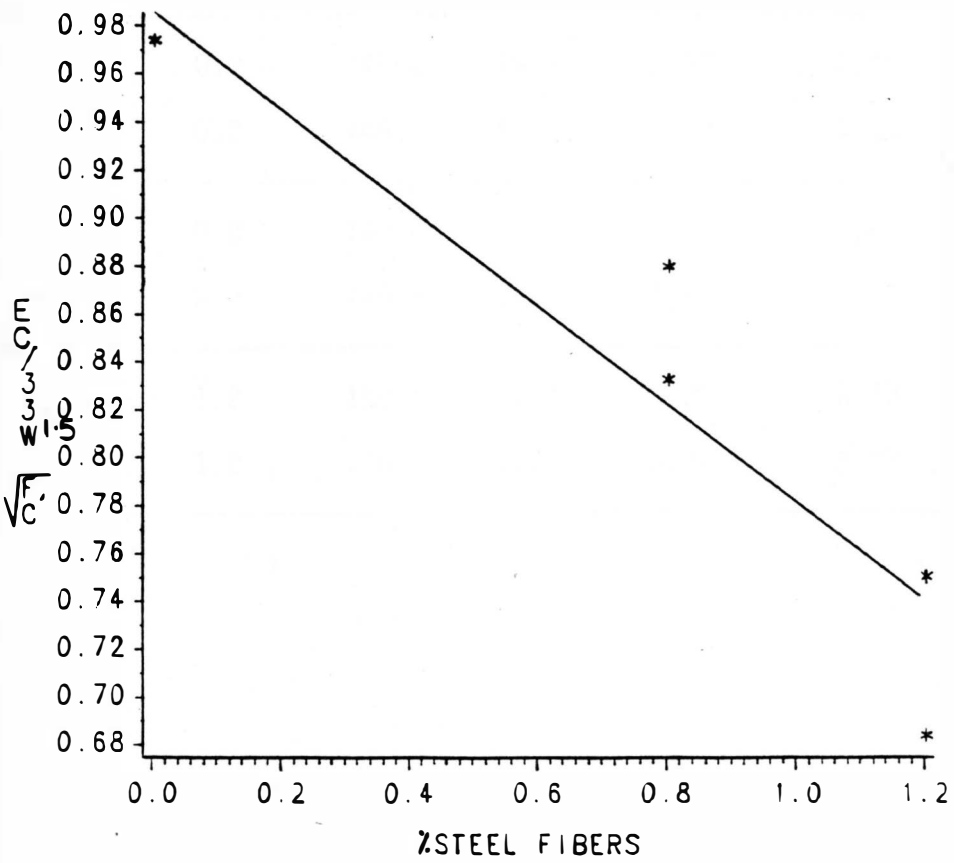

FIGURE 7.3 $E_C / 33\, w^{1.5} \sqrt{f'_c}$ VS.%STEEL FIBERS

TABLE 7.3

ACTUAL AND PREDICTED VALUES FOR MODULUS OF ELASTICITY

Cylinder Number	% Steel Fiber	Unit Weight (PCF)	f'_c (PSI)	$E_{ca} \times 10^6$ (PSI)	$E_{cc} \times 10^6$ (PSI) (Eq. 7.1)	% Deviation from Actual
C11	0.0	145.2	4986	3.97	4.08	+2.8
C12	0.0	146.0	5023	4.02	4.13	+2.7
C21	0.8	149.0	5182	3.80	3.63	+4.5
C22	0.8	149.5	5196	3.62	3.65	+0.83
C31	1.2	150.0	5234	3.00	3.33	+11.0
C32	1.2	150.5	5305	3.30	3.37	+2.12

linear relationship and an 'F' value of 35 indicates that the first order model (equation 7.1) is very useful for predicting the modulus of elasticity at highly significant level (Table D.1).

Actual and predicted values using Equation 7.1 are compared and presented in Table 7.3.

It can be seen from Equation 7.1 that the modulus of elasticity is a function of compressive strength; therefore, the slight increase in compressive strength due to the presence of steel fibers can only increase the modulus of elasticity theoretically since the addition of steel fibers decreases the actual modulus of elasticity.

From the results of this research, it is concluded that strains in fibrous concrete cylinders were higher than those of plain concrete at a given stress level (Figures 6.3 through 6.8). This increase in strain when steel fibers are used is further evidence of the large deformation and ductility of fibrous concrete over that of the plain concrete.

7.3 Split Cylinder

Six concrete cylinders with percentage of steel fibers varying from 0.0 to 1.2 percent were cast and tested in indirect tension (splitting test) according to ASTM Standards C-78.

Table 6.3 shows the initial and ultimate tensile strength results. It can be seen, at the ultimate stage, that the percentage deviation of actual values from the ACI Code formula for normal weight

concrete ($f_{ct} = 6.7\sqrt{f'_c}$) increases by 19.3 and 39.8 percent for 0.8 and 1.2 percent steel fibers respectively. Therefore a modified formula using statistical regression analysis is needed to account for the effect of steel fibers. The results also show that the indirect tensile strength of fibrous concrete is considerably greater than that for the plain concrete having the same mix proportions. That a 0.8 and 1.2 percent of steel fibers produced an improvement of 27 and 51 percent was noted. Similar observations were reported by others (50,47,39,5).

A linear regression statistical analysis was performed for the ratio $f_{ctu}/6.7\sqrt{f'_c}$ and the variable ρ_s resulting in the best fit line through the data (Figure 7.4). It was also found that the correlation coefficient between $(f_{ctu}/6.7\sqrt{f'_c})$ and (ρ_s) is 0.9849 (Table D.2), which means that 97.2 percent (r^2 = 97.2 percent) of the variation is accounted for by using the linear relationship with the variable ρ_s, and an F value of 139, which indicates that the first order model is very useful for predicting the tensile strength at highly significant level.

Therefore, the fibrous concrete split cylinder's strength can be calculated as

$$f_{cts} = (6.7 + 2.4\ \rho_s)\sqrt{f'_c} \qquad (7.2)$$

where:

f_{cts} = ultimate split cylinder strength of fibrous concrete (psi)

ρ_s = % steel fibers

f'_c = compressive strength (psi)

FIGURE 7.4
SPLIT CYLINDER TEST VS.%STEEL FIBERS
CORRELATION COEFFICIENT=0.982

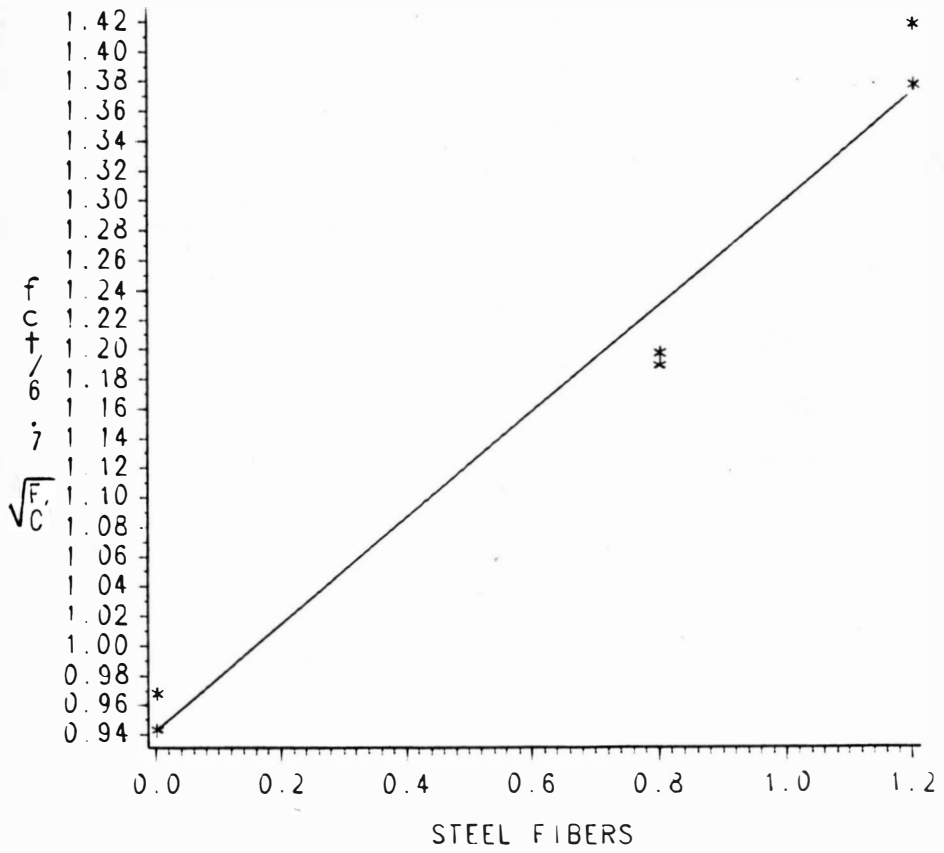

FIGURE 7.4 $f_{ct}/6.7\sqrt{FC'}$ VS.%STEEL FIBERS

TABLE 7.4

ACTUAL AND PREDICTED SPLIT CYLINDER'S STRENGTHS

% Steel Fibers	f'_c	Actual Average Ultimate f_{ctu} (PSI)	Calculated f_{cts} (PSI) (Eq. 6.2)	% Deviation From Actual Value
0.0	4970	451	472	+4.7
0.8	5180	475	620	+7.8
1.2	5275	681	696	+2.2

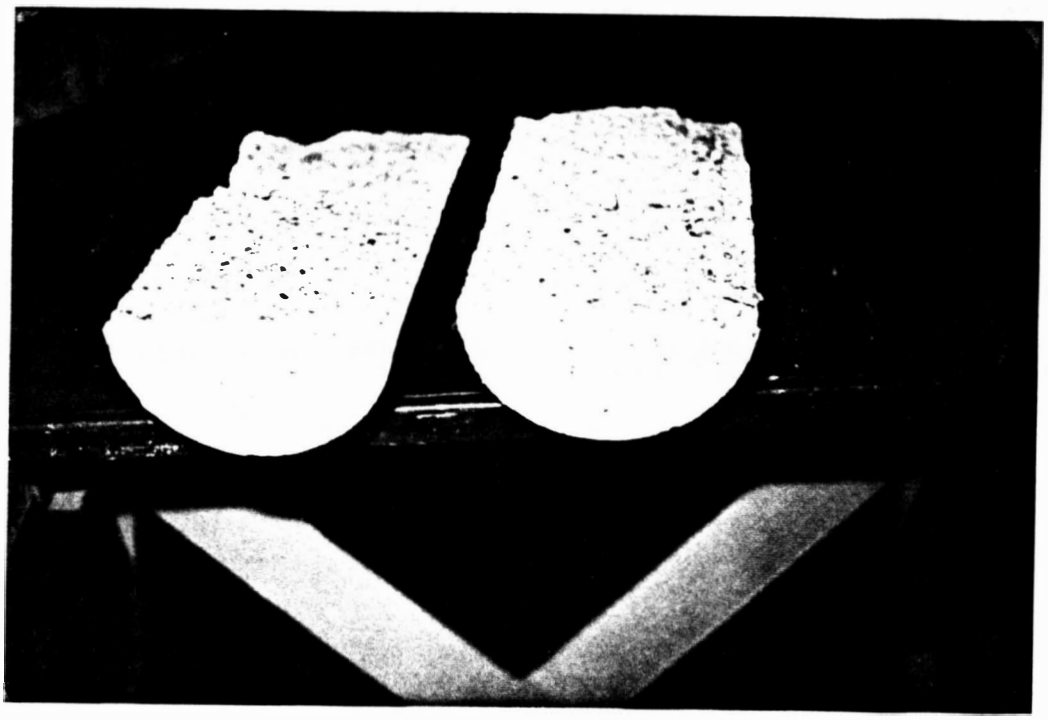

Figure 7.5. Failure of plain concrete in indirect tension.

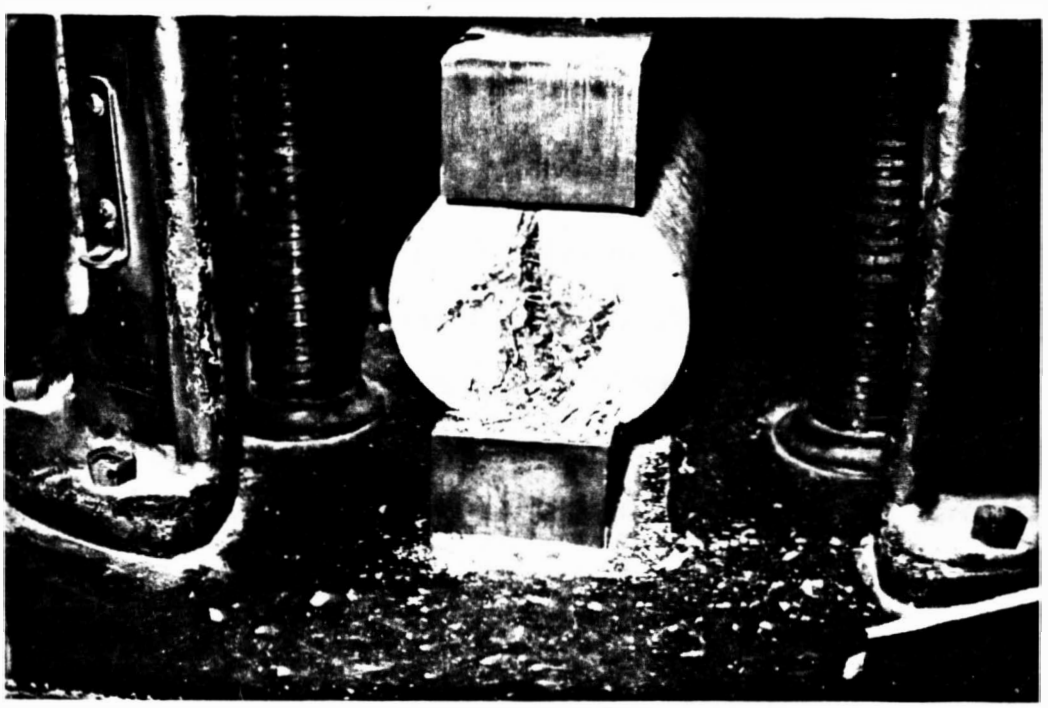

Figure 7.6. Failure of fibrous concrete in indirect tension.

A comparison of the predicted values using Equation 7.2 could be made with the measured values using the split tests for the concretes used in this research (Table 7.4).

It was found during the testing that the failure of the plain concrete cylinder was sudden. They failed with a single crack (Figure 7.5); on the other hand, fibrous concrete cylinders did not fail with a single crack: they had two stages a first crack and a ductile collapse (Figure 7.6).

7.4 Modulus of Rupture

Six 6" x 6" x 24" concrete beams having a fiber content varying from 0.0 to 1.2 percent were cast and tested in flexure in a two point loading and with a clear span of 18" in a testing machine according to ASTM Standards C-78.

It was observed during testing that the failure of beams without fibers was sudden with a single crack, which is characteristic of brittle materials (Figure 7.7). The failure of fibrous concrete beams went through two stages; a first crack stage followed by a ductile collapse (Figure 7.8). The first crack stage was clearly noticed when a first crack appeared and the load dropped a certain amount. Therefore the load prior to this drop indicated the first crack strength or an initial modulus of rupture (f_{ri}). After the formation of first crack, the beams were able to withstand an increase in load up to a failure, thus resulting in ultimate modulus of rupture f_{ru}.

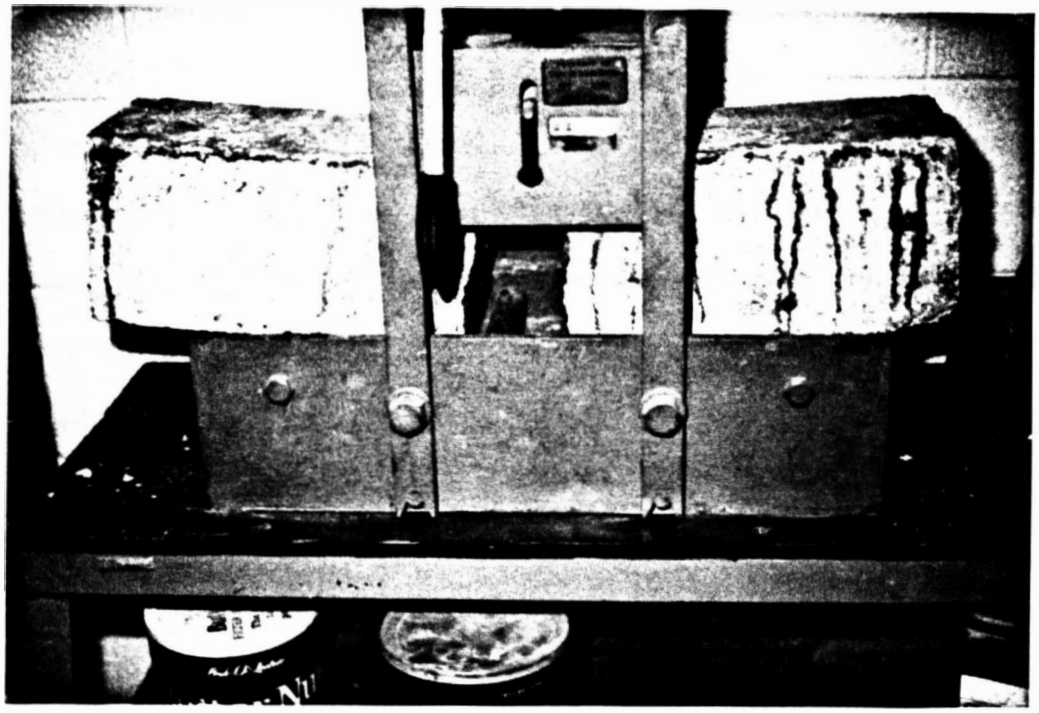

Figure 7.7. Failure of plain concrete in flexure.

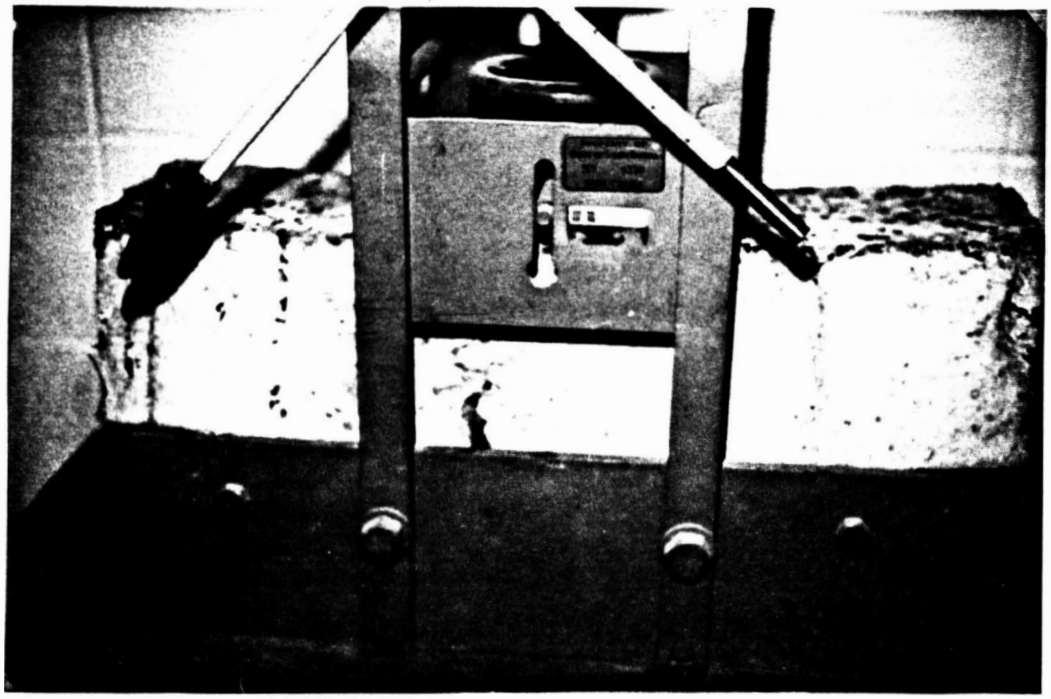

Figure 7.8. Failure of fibrous concrete in flexure.

Test results of both initial and ultimate modulus of rupture are shown in Table 6.4. It can be seen that both the initial and ultimate modulus of rupture increase with increase in fiber content. For a fiber content of 0.8 percent these values were 20 and 52 percent higher than those for the plain concrete respectively, and for a fiber content of 1.2 percent these values were 41 and 75 percent higher than those of plain concrete beams.

Actual test results were compared with ACI Code formula $f_r = 7.5\sqrt{f'_c}$ for normal weight concrete. The percentage deviation ranged from -3.97 to 31.0 percent. For the initial modulus of rupture and the ultimate modulus of rupture, the percentage deviation ranges from -3.97 to 63 percent. This noticeable deviation suggests that the ACI Code formula should be modified to account for the inclusion of steel fibers.

A regression analysis was performed separately for both ratios $f_{ri}/7.5\sqrt{f'_c}$ and $f_{ru}/7.5\sqrt{f'_c}$ and the volume of percentage of steel fibers.

a) Initial modulus of rupture can be modified as:

$$f_{rsi} = (7.5 + 2.1\ \rho_s)\sqrt{f'_c} \qquad (7.3)$$

where:

f_{rsi} = first modulus of rupture (psi)

ρ_s = percentage of steel fibers by volume

f'_c = compressive strength (psi)

Equation 7.3 indicated an intercept of 7.5 and a slope of 2.1 with a good correlation (correlation coefficient of 0.93) between the initial modulus of rupture and the steel fiber content (Table D.3).

b) Ultimate modulus of rupture can be modified to:

$$f_{rsu} = (7.5 + 4.2\ \rho_s)\sqrt{f'_c} \qquad (7.4)$$

where:

f_{rsu} = ultimate modulus of rupture (psi)

ρ_s = % steel fibers

f'_c = compressive strength (psi)

Equation 7.4 indicates an intercept of 7.5 and a slope of 4.2 with a good correlation (correlation coefficient of 0.97) between the ultimate modulus of rupture and fiber content (Table D.4).

Therefore, the modulus of rupture at first crack and ultimate moduls of rupture increased linearly with the volume percentage of steel fibers up to 1.2 percent. Similar observations were obtained by Musa (39), Sahebjam (50), Ajina (5), and Swamy (58).

Figures 7.9 and 7.10 show the trends of first and ultimate modulus of rupture as the percentage of steel fibers varies between 0.0 to 1.2 percent.

Comparisons between predicted values using Equations 7.3 and 7.4 and observed values of both initial and ultimate modulus of rupture are presented in Table 7.5.

7.5 Load Carrying Capacity of Beams

7.5.1 Yield and Ultimate Loads

A comparative study of theoretical and observed values regarding loads and moments of yield and ultimate stages can be made from

FIGURE 7.9
FIRST MODULUS OF RUPTURE VS.%STEEL FIBERS
CORRELATION COEFFICIENT=0.928

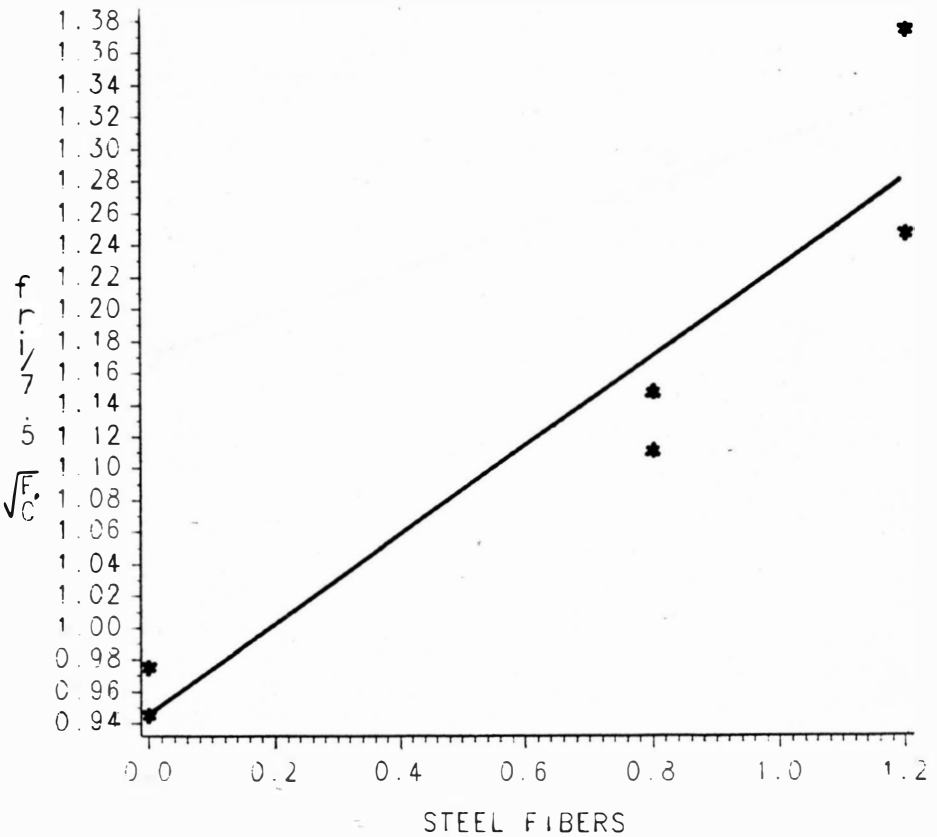

FIGURE 7.9 $f_{ri}/7.5\sqrt{FC'}$ VS.%STEEL FIBERS

FIGURE 7.10
ULTIMATE MODULUS OF RUPTURE VS %STEEL FIBERS
CORRELATION COEFFICIENT=0.974

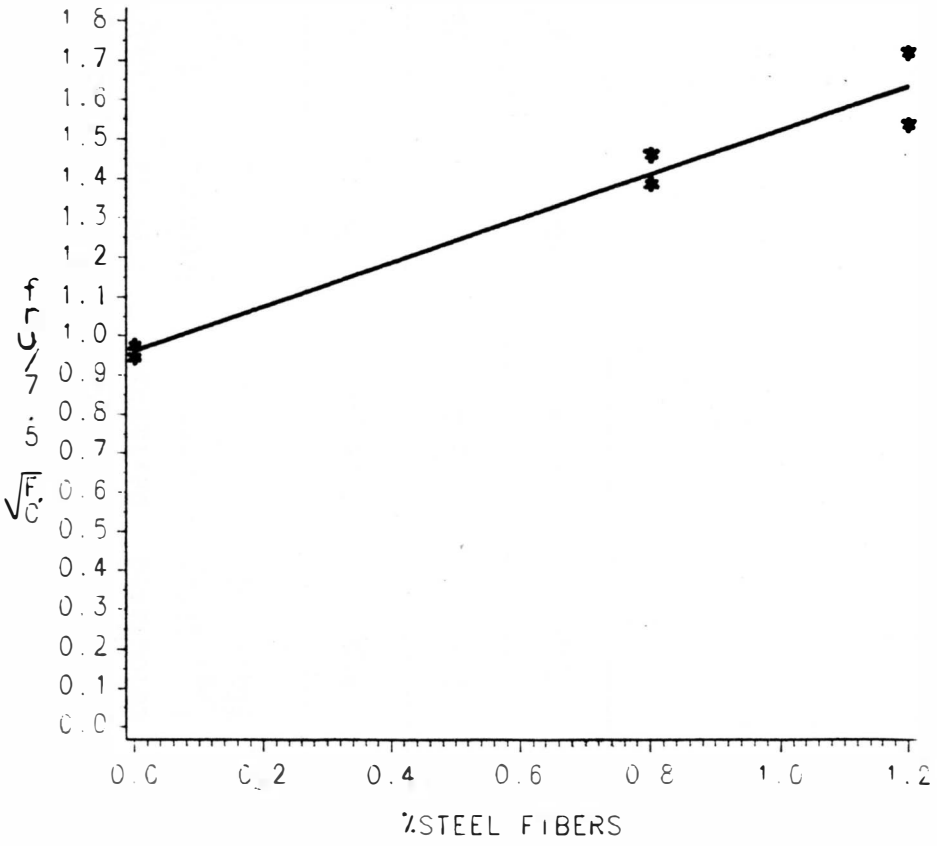

FIGURE 7.10 $f_{ru}/7.5\sqrt{FC}$ VS. %STEEL FIBERS

TABLE 7.5

ACTUAL AND PREDICTED INITIAL AND ULTIMATE MODULUS OF RUPTURE STRENGTHS

% Steel Fibers	f'_c (PSI)	Actual Average Initial f_{ri} (PSI)	Calculated f_{rsi} (PSI) (Eq. 7.3)	% Deviation From Actual	Actual Average Ultimate f_{ru} (PSI)	Calculated f_{rsu} (PSI) (Eq. 7.4)	% Deviation From Actual
0.0	4970	508	529	+4.10	508	529	+4.10
0.8	5180	610	661	+8.4	770	782	+1.6
1.2	5275	715	728	+1.8	890	911	+2.4

Tables 6.5 and 6.6. By examining Table 6.5, the following becomes apparent:

Experimental yield and ultimate loads are larger than theoretical ones (columns 11 and 12).

Full moment redistribution occurred in all cases since all the beams reached their ultimate loads, $P'_u/P_u > 1$ (column 12).

The yield and ultimate loads are found to be higher with the addition of higher percentages of steel fibers. This shows the advantage of fiber reinforced concrete versus non-fiber reinforced concrete in obtaining higher load carrying capacity.

The highest percentages of increase in yield and ultimate loads were obtained in beams reinforced with 2#4 tensile reinforcement and 2#3 top steel, and the lowest percentages of increase were obtained in beams reinforced with 2#6 tensile reinforcement and 2#3 top steel. This shows that the addition of steel fibers is most effective in obtaining higher loads when less tensile reinforcement is used. Similar conclusions were reported by Sahebjam (50), who concluded that the steel fibers are most effective when the percentage of main reinforcement is less than 1.

7.5.2 Load Redistribution Factor (r)

The redistribution factor (r) is defined as the ratio of ultimate to yield load. The values of the experimental distribution factor are summarized in Table 7.6. From examining Table 7.6 the following become apparent:

The load redistribution factor (r) is increased with the use of steel fibers.

The load redistribution factor (r) ranged from 1.17 to 1.28 for plain concrete beams and 1.25 to 1.39 for fibrous concrete beams. The highest load redistribution factors were obtained in beams reinforced with the least reinforcing ratio (Figure 7.11). This would mean that a greater ductility and greater reserve capacity is expected in those beams.

Sahebjam (50) used beams of similar design, without compression steel, and reported smaller values of load redistribution factors. They varied from 1.08 to 1.33 for plain concrete and 1.02 to 1.2. This would prove the superiority of beams with compression steel in greater reserve deformation capacity before failure over beams without compression steel. The ACI Code (section 8.4.3) requires that the redistribution of moments be permitted only if strict limits are placed on the net of tension reinforcement used at the critical section; it requires $\rho-\rho' < 0.5\ \rho b$.

7.6 Rotations

The theoretical values of the required and available plastic rotation were calculated for each beam tested and presented in columns 11 and 13 of Table 6.7. Whether such rotations will be developed or not is dependent on such important factors as: tension reinforcement ratio (50,19), compression reinforcement ratio (12,24,15), confinement

TABLE 7.6

LOAD REDISTRIBUTION FACTOR

Beam No.	% Steel Fibers	Main Steel A_s	Top Steel A'_s	$r' = \rho'_u/\rho'_y$
1	0.0	2#4	2#3	1.28
4	0.8	2#4	2#3	1.36
7	1.2	2#4	2#3	1.39
2	0.0	2#5	2#3	1.17
5	0.8	2#5	2#3	1.25
8	1.2	2#5	2#3	1.27
3	0.0	2#6	2#3	1.25
6	0.8	2#6	2#3	1.27
9	1.2	2#6	2#3	1.29

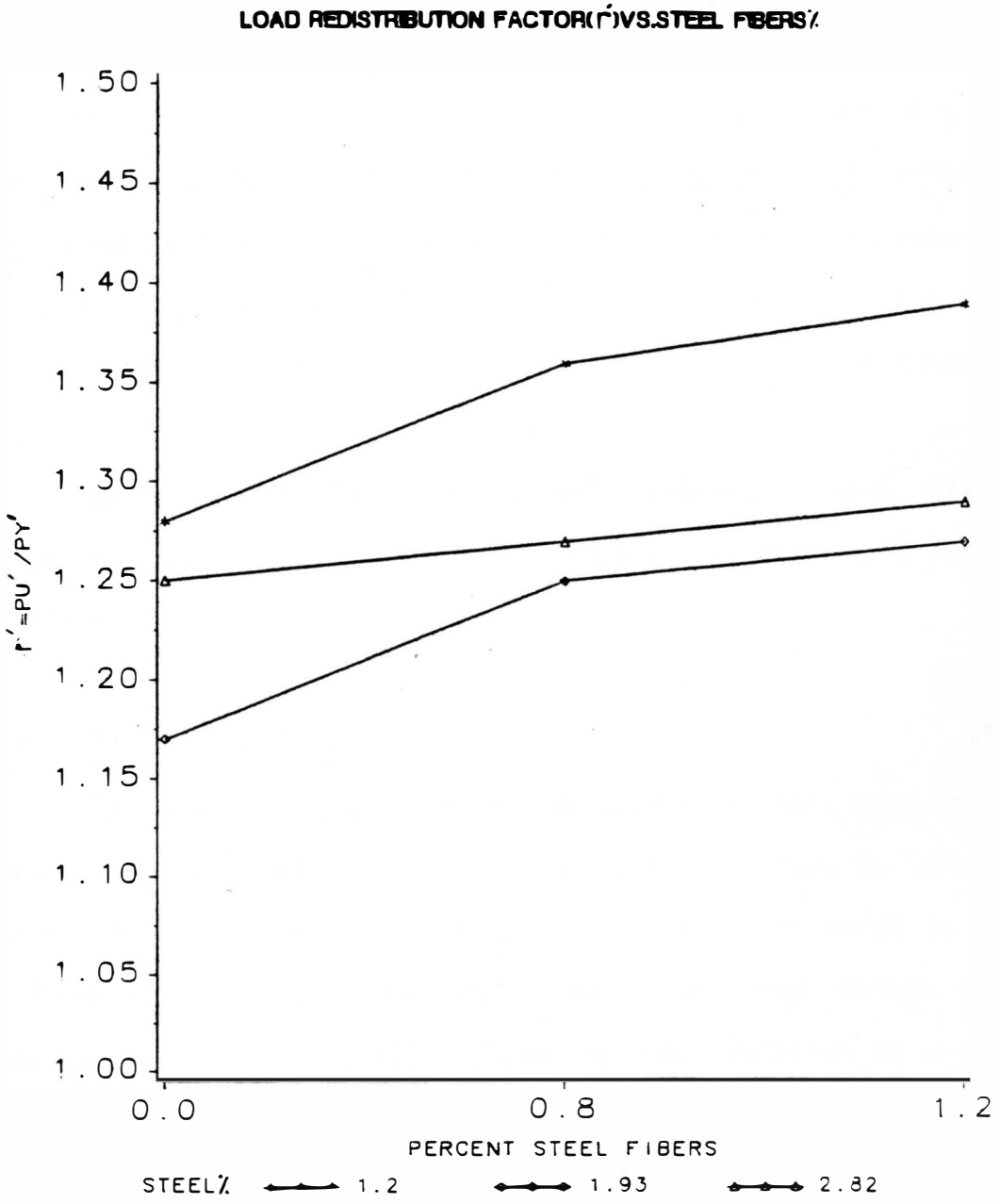
LOAD REDISTRIBUTION FACTOR(r')VS.STEEL FIBERS%
1.50
1.45
1.40
1.35
1.30
1.25
1.20
1.15
1.10
1.05
1.00
r'=PU'/PY'
0.0
0.8
1.2
PERCENT STEEL FIBERS
STEEL%
1.2
1.93
2.82

FIGURE 7·11

of concrete by lateral reinforcement (40), yield strength of the main steel (50,28), length over which plasticity or yield takes place (50,28), ductility index (50,28), and curvature distribution factor (50,28). Therefore the object of this section is to study some factors affecting the rotation capacity of reinforced concrete plastic hinges, particularly the effect of both steel fibers (ρ_s), reinforcements in the compression zone of plasticity and main reinforcements on the length of plastic hinges (H_L), the curvature distribution factor (β), and plastic rotations and the ductility of reinforced continuous beams.

The well-known SAS (Statistical Analysis System) will be utilized to analyze the collected data from actual testing to evaluate the affect of the preceding factors.

7.6.1 Plastic Hinge (H_L)

The lengths of plastic hinges deduced from tests were measured to the nearest one half inch and the results are shown in Table 6.9. Predicted locations of hinges in all the beams were found to agree well with the observed locations. The first hinge formed at the middle support (Figure 7.12), followed by the formation of a second hinge in the span (under concentrated load) Figure 7.13.

It can be seen from Table 6.9 that the lengths of plastic hinges varied from 6 to 9.5 in. Ratios of H_L/d varied from 0.92 to 1.04 for plain reinforced concrete beams, while for fibrous reinforced concrete they varied from 1.15 to 1.52.

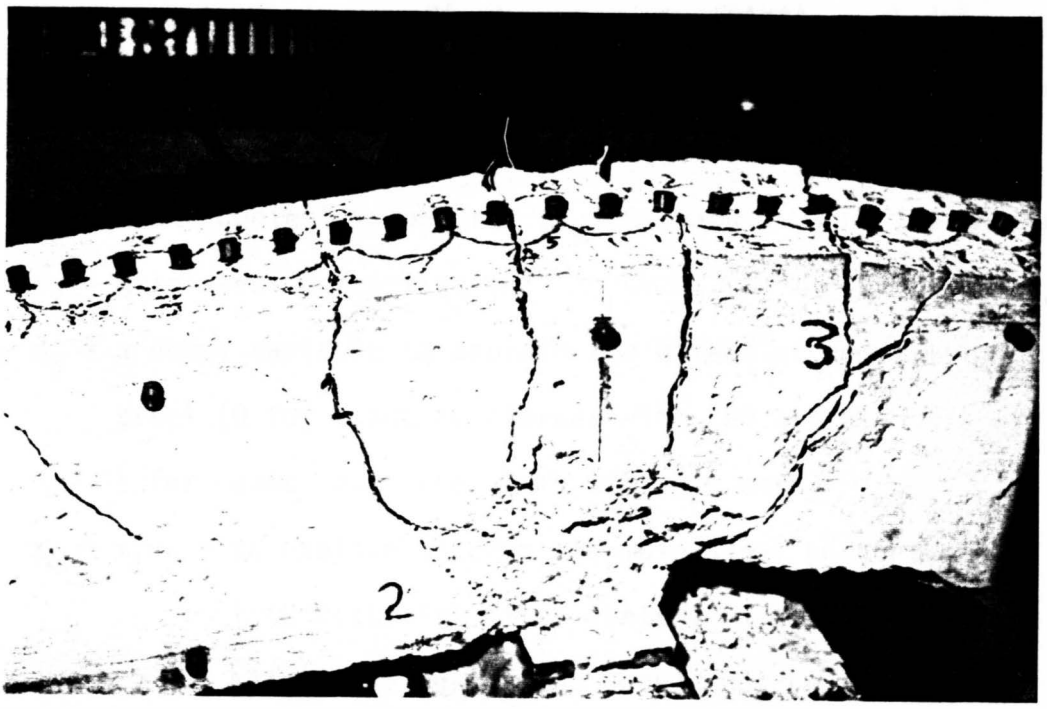

Figure 7.12. Formation of first plastic hinge at middle support.

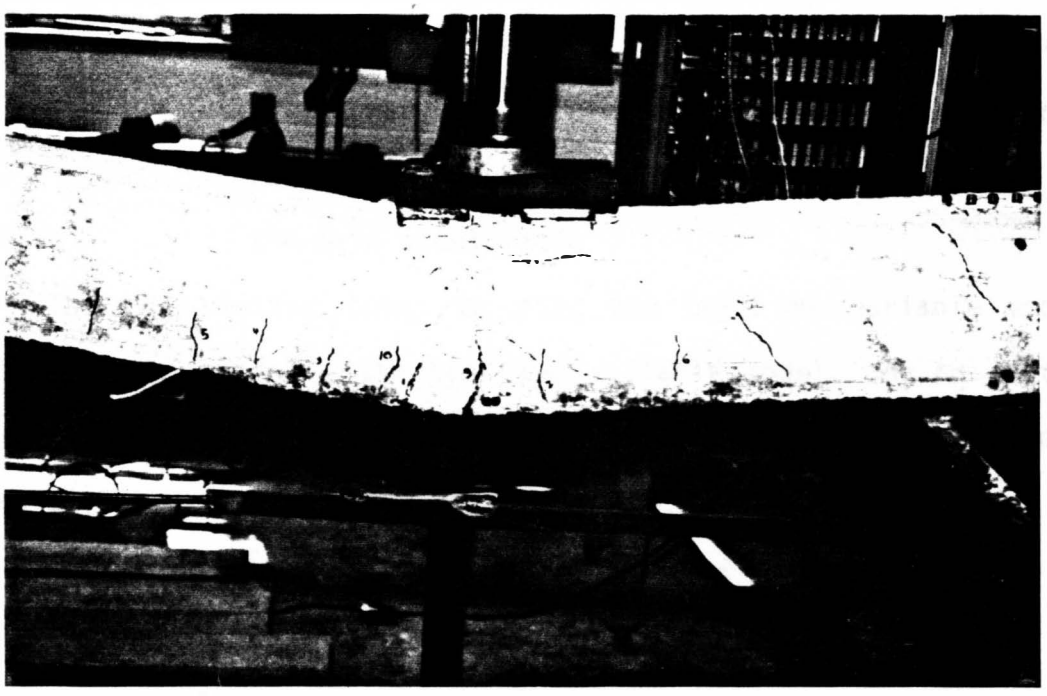

Figure 7.13. Formation of second plastic hinge at midspan.

The stepwise maximum R^2 improvement (MAXR) technique was performed on the experimental values of H_L/d and the following independent variables were included:

x_1 = fiber content in percent (ρ_s) between 0.0 and 1.2 percent

x_2 = main steel percentage (ρ)

x_3 = a dummy variable to explain the effect of compression steel (0 for beams reinforced with 2#4 and 2#5 main bars, 1 for beams reinforced with 2#6 main bars)

$x_4 = x_1x_2$ = to explain whether the main steel percentage interacts with fiber content, i.e., whether the main steel percentage should not be recommended without specifying the fiber content ($\rho\rho_s$)

$x_5 = x_1x_3$ = shows whether there is a difference between beams that have compression steel in the yield range and beams that have compression steel in the elastic range at various steel fiber content regardless of the main steel ratio

The MAXR method tries to find the best one variable model producing the highest R^2, the best two variable model, and so forth. In order to select the best regression model, the following F test statistic (38) was adopted for this purpose.

$$F = [(SSE_1-SSE_2)/(k-g)]/[SSE_2/n-(k+1)]$$

where:

F = F statistic to be compared with some critical value, F

SSE_1 = sum of squared errors for the reduced model

SSE_2 = sum of squared errors for the complete model

$k - g$ = number of variables being tested

$k + 1$ = number of variables in the complete model including the intercept

n = sample size

$\nu_1 = k - g$ = degrees of freedom for the numerator

$\nu_2 = N - (k + 1)$ = degrees of freedom for the denominator

The above test will test whether the complete model provides better predictions of Y than the reducedmodel.

In this research, it was found that H_L can be expressed in the following form:

$$H_L = \lambda . d$$

where:

$$\lambda = F(x_1, x_2, x_3)$$

By conducting the F test several times, a regression model was finally developed for plastic hinge length, and the best was decided to be an interaction model with (F = 156) (Table D-5). Therefore:

$$\lambda = 0.98 + 18\ \rho\rho_s$$

$$H_L = (0.98 + 0.18\ \rho\rho_s)d \qquad (7.5)$$

It can be noticed that the main steel percentage interacts with the steel fiber content. In other words, as the percent of steel

fibers increases, the effect of the percentage of the main steel on H_L becomes pronounced; therefore, one should recommend the percent of steel fibers when specifying the percent of main steel. This interaction is highly significant at $\alpha = 0.05$.

The above conclusion is in agreement with Sahebjam (50). Table 7.7 compares the observed and predicted values of H_L using Equation (7.6).

7.6.2 Curvature Distribution Factor (β)

Accepting an average constant value of the curvature along the plastic hinge, the rotation capacity may be deduced as:

$$\theta_{pc} = \beta(\phi_u - \phi_y)H_L = \beta\phi_p H_L$$

In this investigation experimental values ϕ_p, H_L and θ_{pc} were all measured for each beam and the results are shown in Table 6.9. The actual curvature distribution factor β was then calculated as follows: $\beta = \theta_{pc}/(\phi_u - \phi_y)H_L$ (column 9 of Table 6.10).

It was noted from Table 6.10 that values for the curvature distribution factor range from 0.24 to 0.45. It is also apparent that values of β for fibrous reinforced concrete beams are less than the values for plain reinforced concrete beams. A similar observation was reported by N. Hassoun and K.J. Sahebjam (28). The actual curvature distribution along the plastic hinge for each beam is plotted according to results in Table 6.9 as shown in Figure (7.14). The factor β represents the ratio of the area under each curve to the area of the rectangle ($\phi_p H_L$).

TABLE 7.7

ACTUAL AND PREDICTED PLASTIC HINGE LENGTH

Beam No.	% Steel Fibers ρ_s	Tension Steel A_s	Top Steel A'_s	Measured H_L (in)	Calculated H_L (in)	Deviation %
1	0.0	2#4	2#3	6.0	6.3	+5
4	0.8	2#4	2#3	7.5	7.5	0
7	1.2	2#4	2#3	8.0	8.0	0
2	0.0	2#5	2#3	6.0	6.2	+3
5	0.8	2#5	2#3	8.0	7.9	-1
8	1.2	2#5	2#3	9.0	8.8	-2
3	0.0	2#6	2#3	6.5	6.1	-6
6	0.8	2#6	2#3	9.0	8.6	-4
9	1.2	2#6	2#3	9.5	9.9	+4

It was suggested from this research that the curvature distribution factor for plain reinforced concrete would have an average value of 0.44. Therefore the β factor can be written as $\beta = \alpha\beta_o$.

where:

β_o = curvature distribution factor for plain reinforced concrete

Again, the stepwise maximum R^2 improvement (MAXR) technique was performed for the ratio m, several models were obtained by conducting the F test several times, and the best was decided to be a two variable model with F = 115 (Table 0.6).

Therefore, the magnitude of β can be evaluated from the following expression.

$$\alpha = 1 - 0.171\ x_4 + 0.106\ x_5$$

where:

x_4 and x_5 are defined in section 7.6.1.

$\beta = \alpha\beta_o = 0.44\alpha$

or $\beta = 0.44 - 0.075\ x_1x_2 + 0.047\ x_1x_3$ (7.6)

It can be noticed that the steel fiber content appears in each interaction beam. In other words, the effect of the percentage of main steel or the effect of compression steel becomes pronounced only in the presence of steel fibers; therefore substituting 0 for beams reinforced with 2#4 and 2#5 main steel and 1 for beams reinforced with 2#6 Equation (7.6) becomes:

$\beta = 0.44 - 0.075\ \rho\rho_s$ for beams reinforced with 2#4 and 2#5

$\beta = 0.44 - 0.075\ \rho\rho_s + 0.047\ \rho_s$ for beams reinforced with 2#6

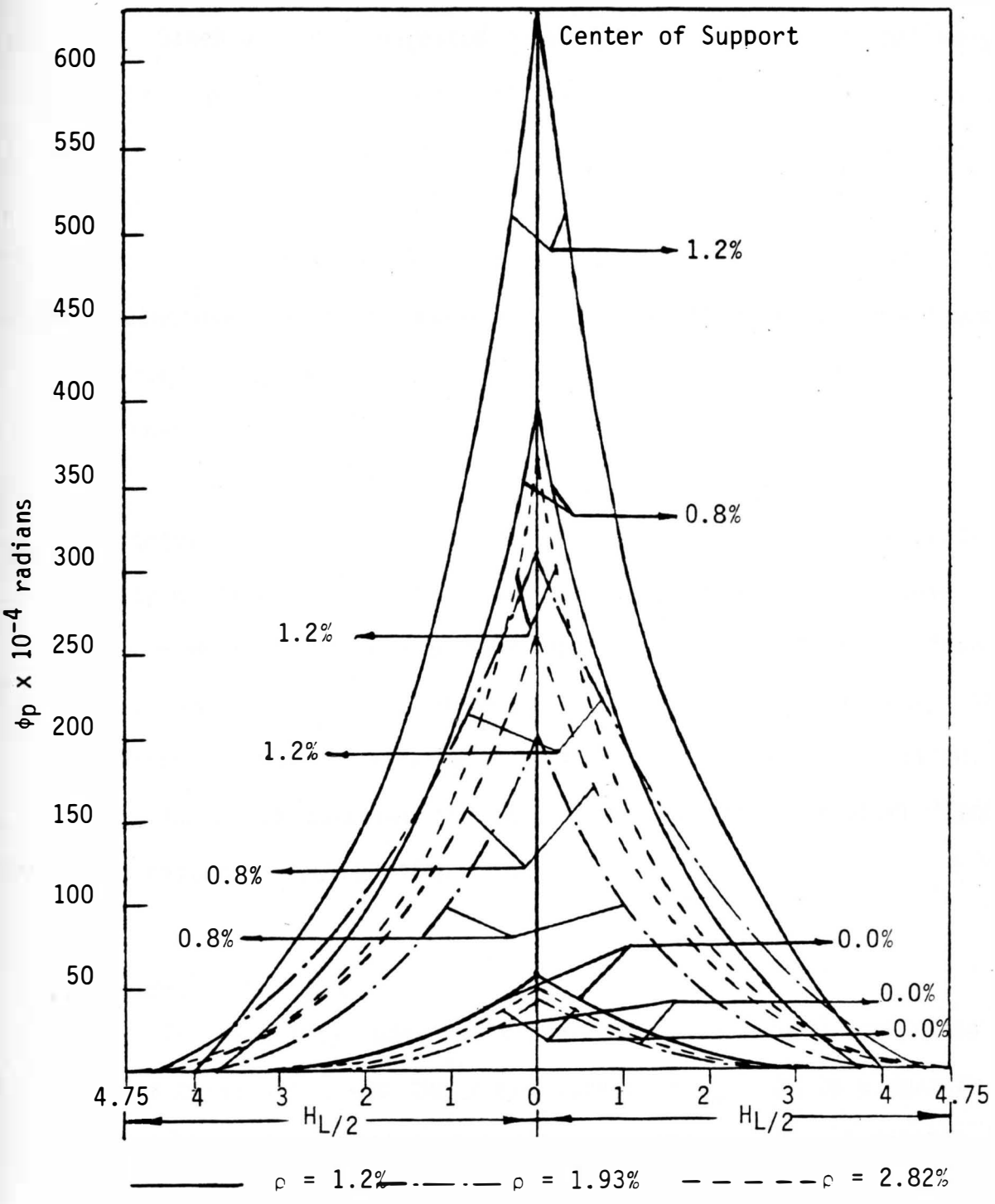

Figure 7.14. Actual curvature distribution along the plastic hinge.

Sahebjam (50) suggested a β value of 0.56 for normal weight concrete without steel fibers. In this research a 27 percent reduction in 'β' occurs when steel bars are provided in the compression side of flexural members. Chan (16) reported a 34 percent reduction in 'β' occurs when secondary reinforcement was used in concrete as has been concluded in this research. The value of β for non-fibrous reinforced concrete flexural members that were recommended by other researchers are shown in Table 7.8.

It is worth noting that the reduction of curvature distribution factor (β) of fibrous concrete does not imply that the rotation capacity of fibrous concrete is lower than that of plain concrete. It is apparent from Table 6.8 that the plastic rotation of fibrous concrete is substantially higher than that of plain concrete. This conclusion is found to agree well with Sahebjam's (50) observation.

Table 7.9 compares the actual and predicted curvature distribution factors using Equation (7.6).

7.6.3 Ductility Index

The ductility index (μ) of any cross section is the ratio of ultimate curvature ϕ_u to the yield curvature ϕ_y. It is a measure of the ductility of material in flexure. In other words, it denotes the rotation capability of the cross section. A large value of ductility index indicates a greater capacity to sustain further increases in curvature, and a lower value, the lack of it.

TABLE 7.8

COMPARISON OF β VALUES

Reference	β
Chan (16)	0.2
Chan (16)	0.35
Kaushik et al (32)	0.22 - 0.81
Cohn and Petcu (19)	0.34 - 0.97
Authors (8)	Recommended Value 0.5
Hassoun and Sahejam (28)	0.56

TABLE 7.9

ACTUAL AND PREDICTED 'β' VALUES

Beam No.	% Steel Fibers	Tension Steel A_s	Top Steel A'_s	Actual β	Predicted β	% Deviation From Actual Value
1	0.0	2#4	2#3	0.45	0.44	-2
4	0.8	2#4	2#3	0.39	0.37	-5
7	1.2	2#4	2#3	0.32	0.33	+3
2	0.0	2#5	2#3	0.44	0.44	0
5	0.8	2#5	2#3	0.33	0.32	-3
8	1.2	2#5	2#3	0.26	0.27	+4
3	0.0	2#6	2#3	0.42	0.44	+5
6	0.8	2#6	2#3	0.31	0.31	0
9	1.2	2#6	2#3	0.24	0.24	0

The ductility index for each tested beam was calculated and presented in Table 7.10. From an examination of Table 7.10, the following became apparent:

The ductility index of beams with steel fibers is higher than of that of plain concrete, but with steel fibers the ductility index increases with the increase of percentages of steel fibers.

Higher ductility index denotes higher plastic rotation capability.

This is true, since beams reinforced with 2#4 main steel have the highest rotation capacity.

A stepwise (MAXR) technique was performed on actual values of ductility index as follows:

$$\mu' = \gamma\mu$$

where:

μ = the ratio of ultimate to yield curvature for plain concrete (an average value of 5.8 was used)

μ' = ductility index of fibrous concrete

The ratio γ was entered with several independent variables (x_1, x_2, x_3) through regression model. By using the F test statistic the best model was found, with the three variables with an F value = 46 and coefficient of determination (R^2) = 97 percent (Table D.7). Therefore, the following expression was used to evaluate the ductility index:

TABLE 7.10

DUCTILITY INDEX

Beam No.	% Steel Fibers	Steel (A_s)	Steel (A'_s)	$\phi_y \times 10^{-4}$ (Radian)	$\phi_u \times 10^{-4}$ (Radian)	$\mu = \phi_u/\phi_y$
1	0.0	2#4	2#3	10.2	71.2	7
4	0.8	2#4	2#3	10.0	411.0	41
7	1.2	2#4	2#3	14.3	645.0	45
2	0.0	2#5	2#3	15.3	61.3	4
5	0.8	2#5	2#3	11.8	211.8	18
8	1.2	2#5	2#3	13.5	338.0	25
3	0.0	2#6	2#3	9.0	59.1	6.6
6	0.8	2#6	2#3	10.8	271.0	25
9	1.2	2#6	2#3	11.8	378.0	32

$$\mu' = 1.12 + 11.75\ x_1 - 4.76\ x_1x_2 + 1.14\ x_1x_3 \qquad (7.7)$$

It was found that steel fibers had a highly significant impact on the ductility index. Also the importance of steel fibers became evident since it appeared in each interaction term. Therefore the presence of steel fibers enhances the ductility. Therefore, substituting for x_1, x_2, x_3 as they are defined in Section 7.6.2., Equation (7.7) becomes:

$\mu' = 1.12 + 11.75\ \rho_s - 4.76\ \rho\rho_s$ for beams reinforced with 2#4 and 2#5 bars

$\mu' = 1.12 + 11.75\ \rho_s - 4.76 + 1.14\ \rho_s$

$= 1.12 + 12.89\ \rho_s - 4.76\ \rho\rho_s$ for beams reinforced with 2#6 bars

Burn (12) concluded that the use of compression steel increased the ductility of the beams as compared with beams without compression steel. Similar observations were reported by others (52). Sahebjam (50) found that ductility index values for beam reinforced with tension reinforcement only varied between 3 and 36. In this research on similar beams but with steel reinforcement in the compressive side, the ductility index values varied from 4 to 45. This conclusion supports observations in various references (15,52). Table 7.11 compares the actual and predicted ductility index using Equation (7.7).

TABLE 7.11

ACTUAL AND PREDICTED DUCTILITY INDEX

Beam No.	% Steel Fibers	Actual μ	Predicted μ Using Eq. 7.7	% Deviation From Actual
1	0.0	7	6.6	-6
4	0.8	41	35.0	-15
7	1.2	45	49.0	+8
2	0.0	4	6.6	+65
5	0.8	18	18.6	+3
8	1.2	25	24.7	-1
3	0.0	6.6	6.6	0
6	0.8	25	24.0	-4
9	1.2	32	32.7	+2

7.6.4 Plastic Rotation Capacity (θpc)

The rotation capacity of each tested beam is presented in column 13 of Table 6.7. Study of Table 6.7 indicates the following:

The plastic rotation capacity of beam with fibers is considerably higher than that of concrete without fibers.

The plastic rotations become larger, the greater the steel fiber percentage.

The highest plastic rotations were in beams reinforced with the least reinforcement (Beams #1, #4, #7).

It may be interesting to note that the plastic rotation of beams reinforced with 2#6 main steel is higher than that of beams reinforced with 2#5 main steel; this could be attributed to the fact that the top bars (2#3) reached the yield range in beams reinforced with 2#6.

In order to study factors affecting the plastic rotation a statistical analysis was performed. A MAXR technique was adopted and several models were obtained. After repeating the F test statistic, a three variable model with F = 287 and coefficient of determination R^2 = 0.99 was chosen (Table 0.8). Equation (7.8) can be used to estimate the plastic rotation of fibrous concrete:

$$\theta_{ps} = 150 + 2450x_1 - 1010x_1x_2 + 1020x_1x_3 \qquad (7.8)$$

where:

x_1, x_2 and x_3 are defined in section 7.6.2.

Therefore

$\theta_{ps} = 150 + 2450\ \rho_s - 1010\ \rho\rho_s$ for beams reinforced with 2#4 and 2#5

$\theta_{ps} = 150 + 2450\ \rho_s - 1010\ \rho\rho_s + 1020\ \rho_s$

$= 150 + 3470\ \rho_s - 1010\ \rho\rho_s$ for beams reinforced with 2#6.

It was found that the steel fiber percentage is a highly significant factor in increasing the plastic rotation of plain concrete. It is also clear that the steel fibers appear in each interaction term. This shows how much the steel fibers in the presence of other reinforcement affect the plastic rotation.

Table 7.12 compares the actual and predicted plastic rotation using Equation (7.8).

Tests reported by Sahebjam (50) have shown that the plastic rotation of similar beams reinforced with main steel, but without any reinforcement on the compressive side at the critical section, varied from 78 to 616 x 10^{-4} radians. However, in this research the values of plastic rotation were found to vary from 120 to 1615 x 10^{-4} radians. Therefore it can be concluded that beams reinforced with steel bars on the compressive side where the plasticity zone may occur have higher plastic rotation than those without any compressive reinforcement.

Several researchers (12,15) concluded that using compression steel can bring about significant increase in plastic rotation over beams that do not have compression steel.

Figures 7.15 through 7.16 show the rotation of plain and fibrous concrete.

TABLE 7.12

ACTUAL AND PREDICTED PLASTIC ROTATION CAPACITY

Beam No.	% Steel Fibers ρ_s	Main Steel A_s	Top Steel A'_s	Actual Plastic Rotation Capacity from Testing $1x10^{-4}$(radians)	Plastic Rotation Capacity Using Eq.(7.8) $1x10^{-4}$(radians)	% Deviation From Actual θ_{pc}
1	0.0	2#4	2#3	164	150	-8.5
4	0.8	2#4	2#3	1168	1139	-2.5
7	1.2	2#4	2#3	1615	1634	+1.2
2	0.0	2#5	2#3	120	150	+2.5
5	0.8	2#5	2#3	527	548	+4.0
8	1.2	2#5	2#3	762	748	-1.8
3	0.0	2#6	2#3	137	150	+9.5
6	0.8	2#6	2#3	722	644	-10.8
9	1.2	2#6	2#3	840	892	+6.2

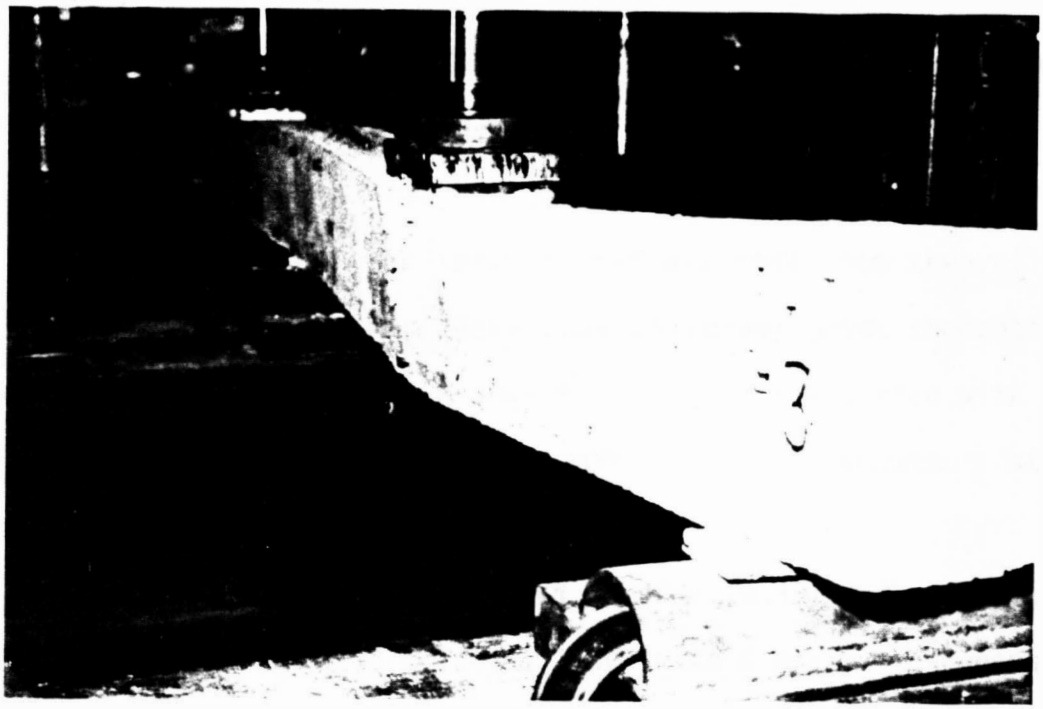

Figure 7.15. Rotation of plain concrete.

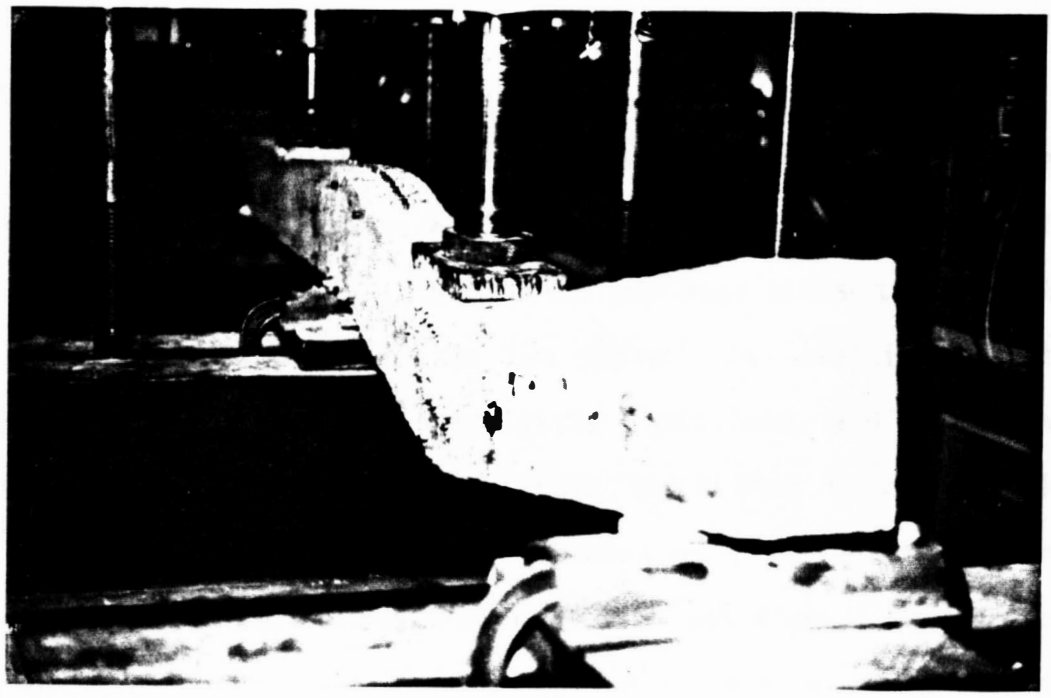

Figure 7.16. Rotation of fibrous concrete.

7.7 Deflections

Experimental and theoretical deflection of each tested beam was determined. A summary of the results is shown in Table 7.13.

By studying Table 7.13, the following become apparent:

Actual deflections at service load are less than theoretical ones (column 7). The maximum deviation of actual from theoretical ones was 39 percent, that is for beam #7, which is reinforced with the least volume of reinforcing bars, 2#4 main steel, 2#3 secondary steel and highest steel fiber content, 1.2 percent.

Beams with steel fibers showed smaller deflections than conventional beams at the actual service load, with a maximum decrease of 16 percent in beam #7, which is reinforced with 2#4 main steel, 2#3 secondary steel and 1.2 percent steel fibers. For the same service load the fibrous concrete beam deflections are much less than conventional ones.

Typical experimental load deflection curves for the tested beams were shown in Figures 6.23 through 6.31. Studying the deflection pattern at a critical section in any beam shows that the total deflection can be divided into two parts: (a) elastic deflection, which starts from zero load to elastic limit load, and (b) inelastic deflection, which starts from elastic limit load to collapse load. The observed ultimate deflection increased as the steel fiber content increased. The total inelastic deflection was highest for the lowest reinforcement percentage. This is true because of the greater ductility index.

Previous researchers (60,58,50) concluded that when steel fibers are used in conventional reinforced concrete beams, they increase the stiffness and can therefore result in a substantial reduction of deflections at service load. In this research the actual stiffness values of beams $E'_cI'_e$ (elastic modulus times effective moment of inertia) were calculated as follows:

E'_c actual = $0.5\ f'_c/\varepsilon$ (refer to Section 6.2)

I'_e actual = $(PL^3)/(100E_c\Delta$ actual) (refer to Section 6.7.2.)

Table 7.14 shows a comparison between the calculated effective moment of inertia based on ACI code's equation and the actual ones. Values of actual $E'_cI'_e$ are also presented in Table 7.13 (column 9).

From an examination of Table 7.14, the following can be made:

Actual stiffnesses of the beams are higher than calculated ones (column 12).

The presence of steel fibers in the conventional beams increases the effective moment of inertia column (13). This increase is mainly caused by: (a) the increase in the modulus of rupture which increases the cracking moment, and (b) the increase in modular ratio (n) which increases the cracking moment (I_{cr}).

The presence of steel fibers in the concrete is seen to increase the stiffness of the beams (column 14) and reduces deflections at working loads. The highest increase in stiffness is 57 percent and it is noticed in beam #7 which is reinforced with 2#4 main steel, 2#3 secondary steel and 1.2 percent steel fibers, and the

TABLE 7.14

EFFECTIVE MOMENT OF INERTIA AND STIFFNESS VALUES

Beam No. (1)	% Steel Fibers (2)	Main Steel A_s (3)	Calculated E_c $1x10^6$ psi (4)	Actual E'_c $1x10^6$ psi (5)	Calculated I_{e_4} (in^4) (6)	Actual I'_{e_4} (in^4) (7)	Calculated E_cI_e $1x10^6$ lb.in^2 (8)	Actual $E'_cI'_e$ $1x10^6$ lb.in^2 (9)	E'_c/E_c (10)	I'_e/I_e (11)	$E'_cI'_e/E_cI_e$ (12)	Ratio for I_e* (13)	Ratio for $E'_cI'_e$** (14)
1	0.0	2#4	4.11	4.00	72.98	73.9	300	296	0.97	1.01	0.90	---	---
4	0.8	2#4	4.34	3.71	77.62	101.0	337	375	0.85	1.30	1.12	1.37	1.27
7	1.2	2#4	4.40	3.15	88.00	148.0	387	466	0.72	1.68	1.21	2.00	1.57
2	0.0	2#5	4.11	4.00	93.36	106.0	381	424	0.97	1.14	1.11	---	---
5	0.8	2#5	4.34	3.71	100.45	134.0	433	497	0.85	1.34	1.15	1.26	1.17
8	1.2	2#5	4.40	3.15	111.55	171.0	487	539	0.72	1.54	1.11	1.61	1.27
3	0.0	2#6	4.11	4.00	117.00	119.0	481	476	0.97	1.02	0.99	---	---
6	0.8	2#6	4.34	3.71	123.75	151.0	536	560	0.85	1.22	1.10	1.27	1.18
9	1.2	2#6	4.40	3.15	138.75	205.0	609	646	0.72	1.48	1.10	1.72	1.36

*Ratio = effective moment of inertia of fibrous concrete/effective moment of inertia of plain concrete.

**Ratio = actual stiffness $E'_cI'_e$ of fibrous concrete/actual stiffness $E'_cI'_e$ of plain concrete.

percentage increase in stiffness varies from 20 to 60 percent compared to the beams without fiber reinforcement. Reference (60) reported a 50 to 70 percent increase in stiffness when steel fibers are used in conventional reinforced concrete beams.

Therefore, a modification of the ACI Code equation for calculation of the effective moment of inertia is required when fibrous concrete is used. The modification is as follows:

$$I_{ef} = \eta I_e$$

where:

I_e = effective moment of inertia based on ACI Code's equation

η = the factor that estimates I_{ef} for fibrous concrete.

In order to choose the best model for estimating η, the stepwise maximum R^2 improvement (MAXR) technique (defined in Section 7.6.1) was used on the collected data I'_e/I_e. The following independent variables were considered in the comparative analysis:

x_1 = fiber content in percent (ρ_s)

x_1^2 = shows whether the fiber content has a quadratic response curve (non-linear).

Two models for m were obtained. Therefore, the F test statistic was adopted in order to select which model is most useful. The best was found to be a one variable quadratic model with (F = 89.58), Table (D.9).

Therefore:

$$\eta = 1 + 0.37\rho_s^2$$

From the preceding, the effective moment of inertia can be predicted by using Equation (7.9):

$$I_{ep} = (1 + 0.37\ \rho_s^2)I_e$$

where:

$$I_e = (M_{cr}/M_a)^3 Ig + [1 - (M_{cr}/M_a)^3]I_{cr}$$

or:

$$I_e = (1+0.37\ \rho_s)\{(M_{cr}/M_a)^3 I_g + [1-(M_{cr}/M_a)^3]I_{cr}\} \qquad (7.9)$$

The above model showed a highly significant increase in the effective moment of inertia by the use of steel fibers up to 1.2 percent. A coefficient of determination of 93 percent was found, which means that 93 percent of the variability in the data is explained by the above model. It also shows the fiber content has a quadratic response curve.

Table 7.15 shows a comparison between actual and predicted effective moment of inertia, stiffness and deflection.

Sahebjam (50) studied the deflections of similar beams, but without the inclusion of compressive reinforcement. In order to perform a comparative study between tests reported in this research and tests reported by Sahebjam (50), the modification of the ACI code's equation for calculating of the effective moment of inertia becomes different than the preceding model. The stepwise maximum R^2 improvement (MAXR) technique was performed on the collected data I'_e/I_e. The following independent variables were considered in the comparative analysis:

TABLE 7.15

ACTUAL AND PREDICTED EFFECTIVE MOMENT OF INTERIA STIFFNESS AND DEFLECTION

Beam No. (1)	% Steel Fibers (2)	Main Steel (A_s) (3)	Top Steel (A'_s) (4)	Actual I'_e (in^4) (5)	Predicted l_{ef} Using Eq. 7.9 (in^4) (6)	Actual $E'_cI'_e$ $1x10^6$ lb.in^2 (7)	Predicted E_cI_e $1x10^6$ lb.in^2 (8)	Actual Deflection $1x10^{-3}$ (in) (9)	Predicted Deflection $1x10^{-3}$ E_cI_e (10)	% Deviation Column(6) from Column(5) (11)	% Deviation Column(8) from Column(7) (12)	% Deviation Column(10) from Column(9) (13)
1	0.0	2#4	2#3	73.9	73	296	300	95	94	-1	+1	-1
4	0.8	2#4	2#3	101.0	96	376	349	85	92	-5	-7	-4
7	1.2	2#4	2#3	148.0	135	466	452	80	83	-9	-3	+4
2	0.0	2#5	2#3	106.0	93	424	382	85	95	-12	-10	+12
5	0.8	2#5	2#3	134.0	124	498	451	84	93	-7	-9	+11
8	1.2	2#5	2#3	171.0	171	539	573	83	78	0	+6	-6
3	0.0	2#6	2#3	119.0	117	476	481	95	94	+2	+1	-1
6	0.8	2#6	2#3	151.0	153	562	557	88	89	+1	-1	+1
9	1.2	2#6	2#3	205.0	212	646	710	87	80	+3	+10	-8

$x_1 = \rho_s$ = steel fibers content in percent

x_2 = dummy variable = 1 for beams with compression steel; 0 for beams without compression steel

x_1^2 = shows whether the fiber content has a quadratic response curve (non-linear)

$x_1^2 x_2$ = explains whether the rate of curvature of the fiber content is different between beams with and without compression steel

After conducting the statistical analysis, several models were obtained and by using the F test statistic on these models, the best model was decided to be Step 2 model (Table D.10) with F value = 99.55 and R^2 value = 93 percent. Therefore, the effective moment of inertia for the combined data of both research is as follows:

$$I_{ef} = [1 + 0.26x_1^2 + 0.096x2x_1^2]I_e \qquad (7.10)$$

where:

$$I_e = (M_{cr}/M_a)^3 I_g + [1 - (M_{cr}/M_a)^3]I_{cr}$$

substituting x_1 and x_2 as defined above equation 7.10 becomes:

$I_{ef} = [1 + 0.26\ \rho_s^2]I_e$ for beam reported by reference 13

$I_{ef} = [1 + 0.37\ \rho_s^2]I_e$ for beams reported in this research

Therefore it can be noticed that beams with both compression steel and steel fibers content increases can bring a significant increase in the effective moment of inertia.

Table (7.16) shows a comparison between actual and predicted effective moment of inertia for tests reported by Sahebjam (50) and tests reported in this research.

TABLE 7.16

COMPARISON BETWEEN ACTUAL AND PREDICTED EFFECTIVE MOMENT OF INERTIA BETWEEN THIS RESEARCH RESULTS AND RESULTS REPORTED BY SAHEBJAM (Ref. 50)

Beam No. (1)	% Steel Fibers (2)	Service Load (kips) (3)	Main Steel A_s (4)	Top Steel A'_s (5)	Calculate I_e ACI Code (in^4) (6)	Actual Deflection 1×10^{-3} (in) (7)	Actual I'_e (in^4) (8)	Predicted I_{ef} (in) (9)	% Deviation From Actual I'_e (in) (10)
1	0.0	13.08	2#4	2#3	72.98	75	74	73	-1
4	0.8	14.88	2#4	2#3	77.62	85	101	96	-5
7	1.2	17.34	2#4	2#3	88.00	80	148	135	-9
2	0.0	16.80	2#5	2#3	93.36	85	106	93	-12
5	0.8	19.44	2#5	2#3	100.45	84	134	124	-7
8	1.2	20.70	2#5	2#3	111.55	83	171	171	0
3	0.0	21.00	2#6	2#3	117.25	95	119	117	-2
6	0.8	22.97	2#6	2#3	123.75	88	151	153	+1
9	1.2	26.04	2#6	2#3	138.73	87	205	212	+3
1	0.0	8.45	2#3	---	54.00	82	56	54	-4
4	0.8	9.6	2#3	---	60.20	70	75	70	-7
7	1.2	11.2	2#3	---	66.00	91	92	91	-1
2	0.0	11.0	2#4	---	77.00	87	81	77	-5
5	0.8	13.6	2#4	---	81.00	93	104	95	-9
8	1.2	14.0	2#4	---	91.00	--	129	125	-3
3	0.0	16.0	2#4	---	98.00	101	103	98	-5
6	0.8	18.0	2#5	---	104.00	106	130	121	-7
9	1.2	20.0	2#5	---	115.00	120	160	158	-1

Reference (50) also reported that maximum deflections of failure for plain concrete varied from 0.4 to 1 inch, and for fibrous concrete it varied from 2 to 5 inches. In this research of similar beams but with the inclusion of compressive steel, the maximum deflection of failure varied from 1.3 to 1.7 inch for plain concrete and from 3 to 6 inches for fibrous concrete beams. The higher ultimate deflection in this research is another indication of the greater ductility and strain energy absorption capacity that is caused by the secondary reinforcement in the compression zone of critical sections.

7.8 Cracks

7.8.1 Crack Widths at Service Load

Calculated and measured crack widths at a service load of 0.6 and ultimate load were shown in Table 6.14. Examining Table 6.14, the following can be concluded:

The addition of steel fibers to the conventionally reinforced concrete reduced the crack width, for a given load and a given reinforcement ratio ρ.

Actual cracks widths are less than calculated ones using the Gerely-Lutz formula.

1) At middle support

a) When 2#4 main steel and 2#3 top steel were used, the maximum cracks widths ranged from 87 to 55 x 10^{-4} inch for 0.0 to 1.2 percent steel fiber with a maximum decrease of 37 percent.

b) When 2#5 main steel and 2#3 top steel were used, the maximum cracks widths ranged from 78 to 104 x 10^{-4} inch for 0.0 to 1.2 percent steel fibers with a maximum decrease of 24 percent.

c) When 2#6 main steel and 2#3 compression steel were used, the maximum cracks widths ranged from 87 to 107 x 10^{-4} inch for 0.0 to 1.2 percent steel fibers with a maximum decrease of 25 percent.

2) At midspan

a) When 2#4 main steel and 2#3 top steel are used, the maximum cracks widths ranged from 50 to 80 x 10^{-4} in for 0.0 to 1.2 percent steel fibers with a maximum decrease of 37.5 percent.

b) When 2#5 main steel and 2#3 top steel were used, the maximum cracks widths ranged from 98 to 73 x 10^{-4} inch for 0.0 to 1.2 percent steel fibers with a maximum decrease of 28.4 percent.

c) When 2#6 main steel and 2#3 compression steel were used, the maximum cracks widths ranged from 80 to 103 x 10^{-4} inch for 0.0 to 1.2 percent steel fibers with a maximum decrease of 22 percent.

From the above discussion it can be concluded that the hooked end steel fibers proved their ability to reduce crack width. The reduction in crack width was highest for the lowest reinforcing bars. Therefore, the maximum reduction was obtained in beam #7, which is reinforced with 2#4 main bars, 2#3 top bars and 1.2 volume percent of steel fibers.

Figures 7.17 and 7.18 show the maximum actual crack width Vs. the steel fibers for a given main steel ratio ρ.

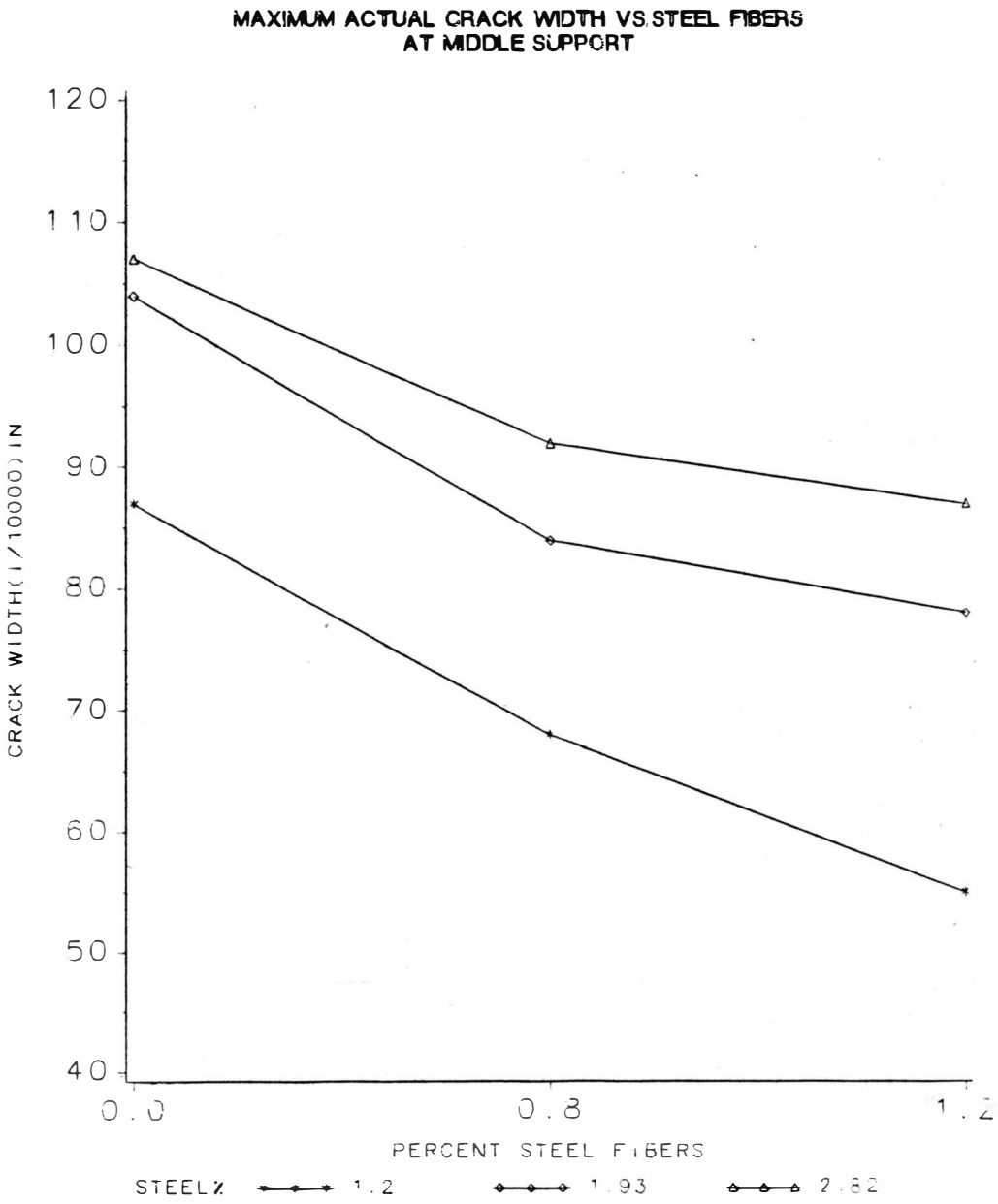
MAXIMUM ACTUAL CRACK WIDTH VS.STEEL FIBERS
AT MIDDLE SUPPORT
CRACK WIDTH(1/10000) IN
120
110
100
90
80
70
60
50
40
0.0
0.8
1.2
PERCENT STEEL FIBERS
STEEL%
1.2
1.93
2.82

FIGURE 7-17

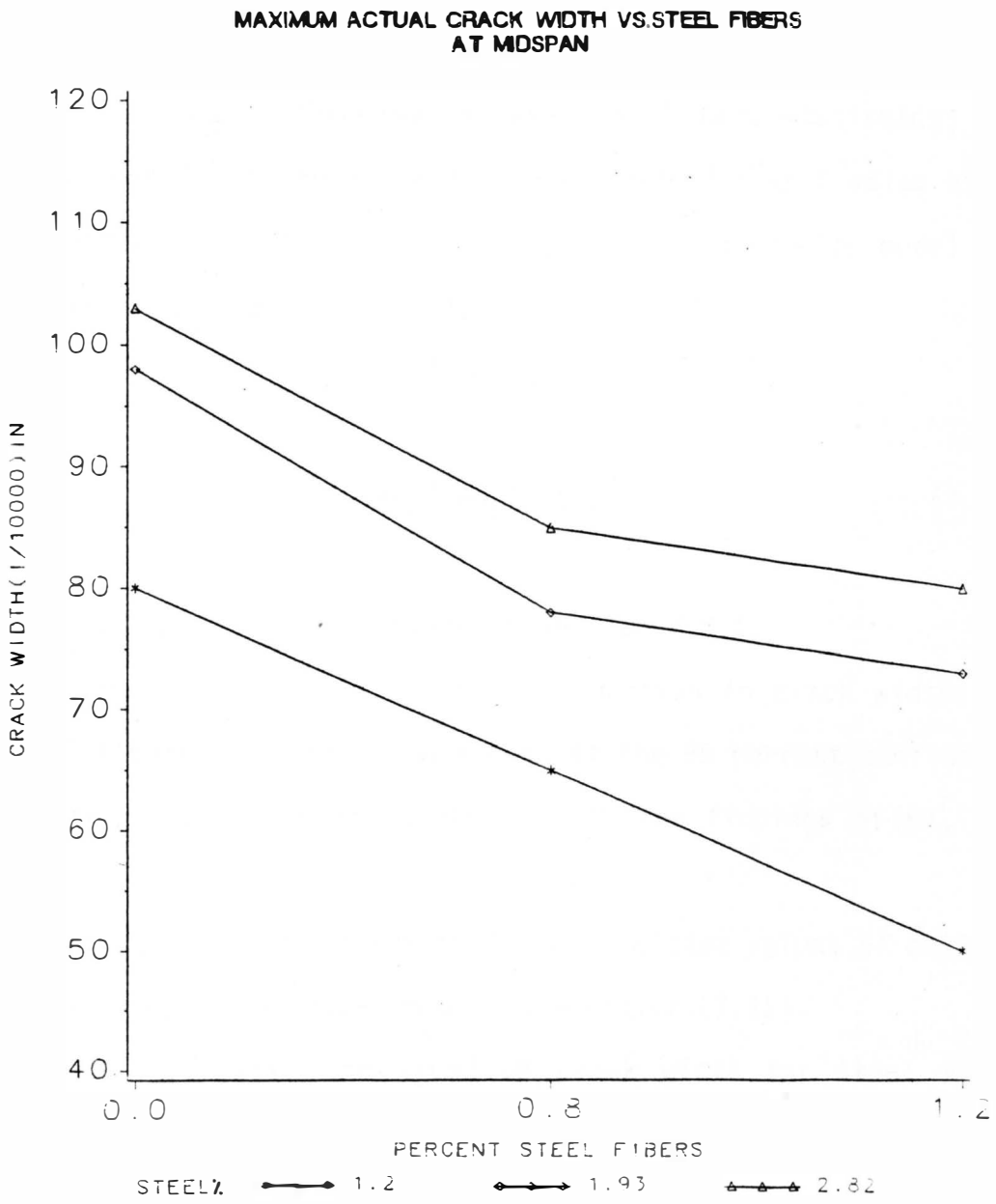
MAXIMUM ACTUAL CRACK WIDTH VS.STEEL FIBERS
AT MIDSPAN
120
110
100
90
80
70
60
50
40
CRACK WIDTH(1/10000) IN
0.0
0.8
1.2
PERCENT STEEL FIBERS
STEEL%
1.2
1.93
2.82

FIGURE 7-18

A statistical analysis using a stepwise (MAXR) technique was performed for the maximum crack width data given in Table 6.12. A form of the Gerely-Lutz equation was adopted, taking into consideration several independent variables. Different statistical models were tested, for one, two or three variables using F test statistics, and the best was decided to be a one variable model with an F value of 68 and R^2 of 81 percent (Table D.11). Therefore, the following model was adopted to evaluate the maximum crack width of concrete.

$$w = (1 - 0.23\ \rho_s)(0.076)\beta f_s \sqrt[3]{A d_c}$$

or,

$$w = (0.076 - 0.017\ \rho_s)\beta f_s \sqrt[3]{A d_c} \qquad (7.11)$$

where:

β, f_s, d_c and A_c are defined in section 6.8.1.

The above model showed that the reduction in crack widths by adding steel fibers is highly significant at the 95 percent confidence level. These results are in agreement with the findings of (59, 50, 58, 35).

Table 7.17 compares the actual and predicted values of maximum crack widths using the proposed modified equation (7.11).

Figure 7.19 shows the trend of crack width for steel fiber content which varies between 0.0 and 1.2 percent.

7.8.2 Initial Cracking Load

The visible first crack loads of all the beams were recorded and presented in column 6 of Table 6.15. Upon examining Table 6.15 the following becomes apparent:

TABLE 7.17

ACTUAL AND PREDICTED MAXIMUM CRACK WIDTHS AT MIDSPAN AND MIDDLE SUPPORT

Beam No.	% Steel Fibers	Tension Steel A_s	Top Steel A'_s	AT MIDDLE SUPPORT (1×10^{-4} in) Actual	Calculated	% Deviation From Actual	AT MIDSPAN (1×10^{-4} in) Actual	Calculated	% Deviation From Actual
1	0.0	2#4	2#3	87	85	-2.3	80	85	+6.3
4	0.8	2#4	2#3	68	69	+1.5	65	69	+6.2
7	1.2	2#4	2#3	55	62	+12.7	50	62	+24.0
2	0.0	2#4	2#3	104	96	-7.7	98	96	-2.0
5	0.8	2#4	2#3	84	78	-7.1	78	78	0.0
8	1.2	2#4	2#3	78	69	-11.5	73	69	-5.5
3	0.0	2#4	2#3	107	109	+1.9	103	109	+5.8
6	0.8	2#4	2#3	92	89	-3.3	85	89	+4.7
9	1.2	2#4	2#3	87	79	-9.2	80	79	-1.3

FIGURE 7.19
CRACK WIDTH VS.%STEEL FIBERS
CORRELATION COEFFICIENT=0.893

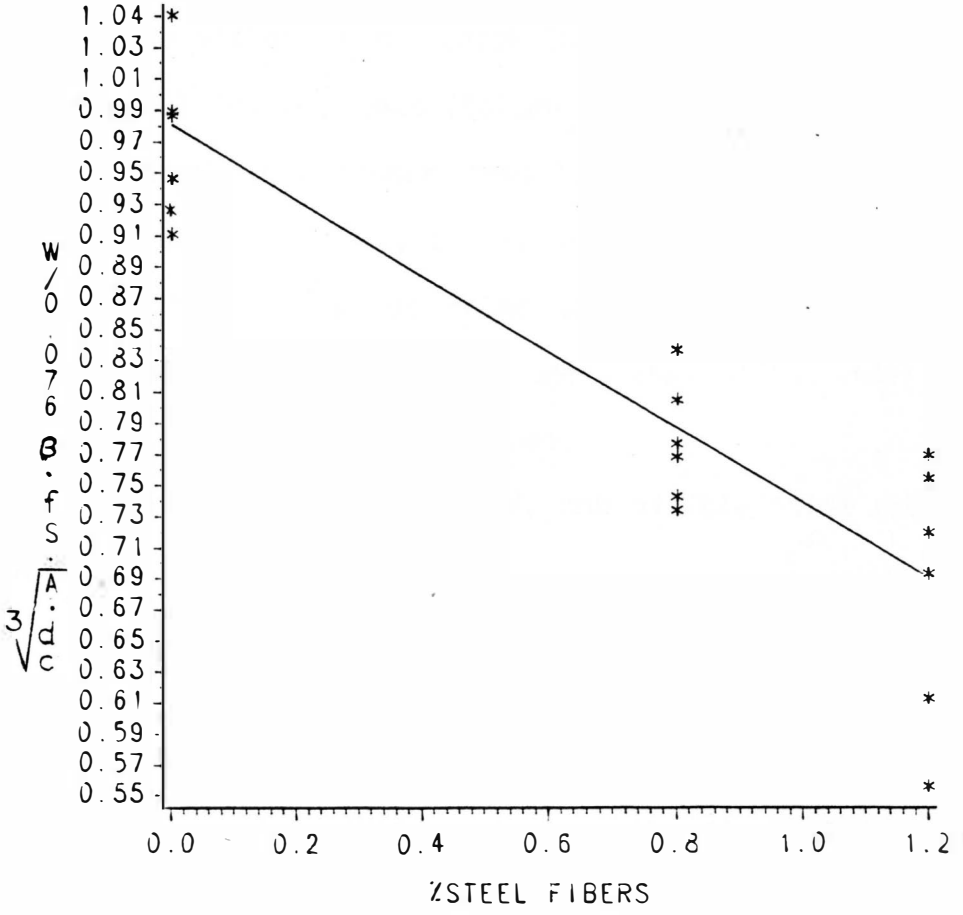

FIGURE 7.19

The loads at first crack for fibrous concrete beams are higher than that of conventional reinforced concrete beams.

Increasing the volume of fibers increases the first cracking loads.

The visible first crack load varied from 0.16 to 0.28 of the experimental failure loads (Column 7).

Beams with higher tensile reinforcement have higher first cracking loads. However, the ratio of first cracking load to experimental failure loads was found to be the highest at lower tensile reinforcement (column 7). This means that adding steel fibers is most effective with lower reinforcement.

In all the beams tested, the visible first crack appeared at the support section.

Similar observations were reported by Herager and Doherty (21).

Figure 7.20 shows the relation between the load at the first crack and the steel fiber content, while Figure 7.21 shows the relation between the ratio of the load at the first crack to the experimental failure load and the steel fiber content.

7.8.3 Cracks Spacings

Test results on spacings are shown in Tables 6.16 and 6.17. By studying these tables the following become apparent:

Adding steel fibers to the concrete mix reduces the average crack spacing. This can be attributed to a better strain distribution

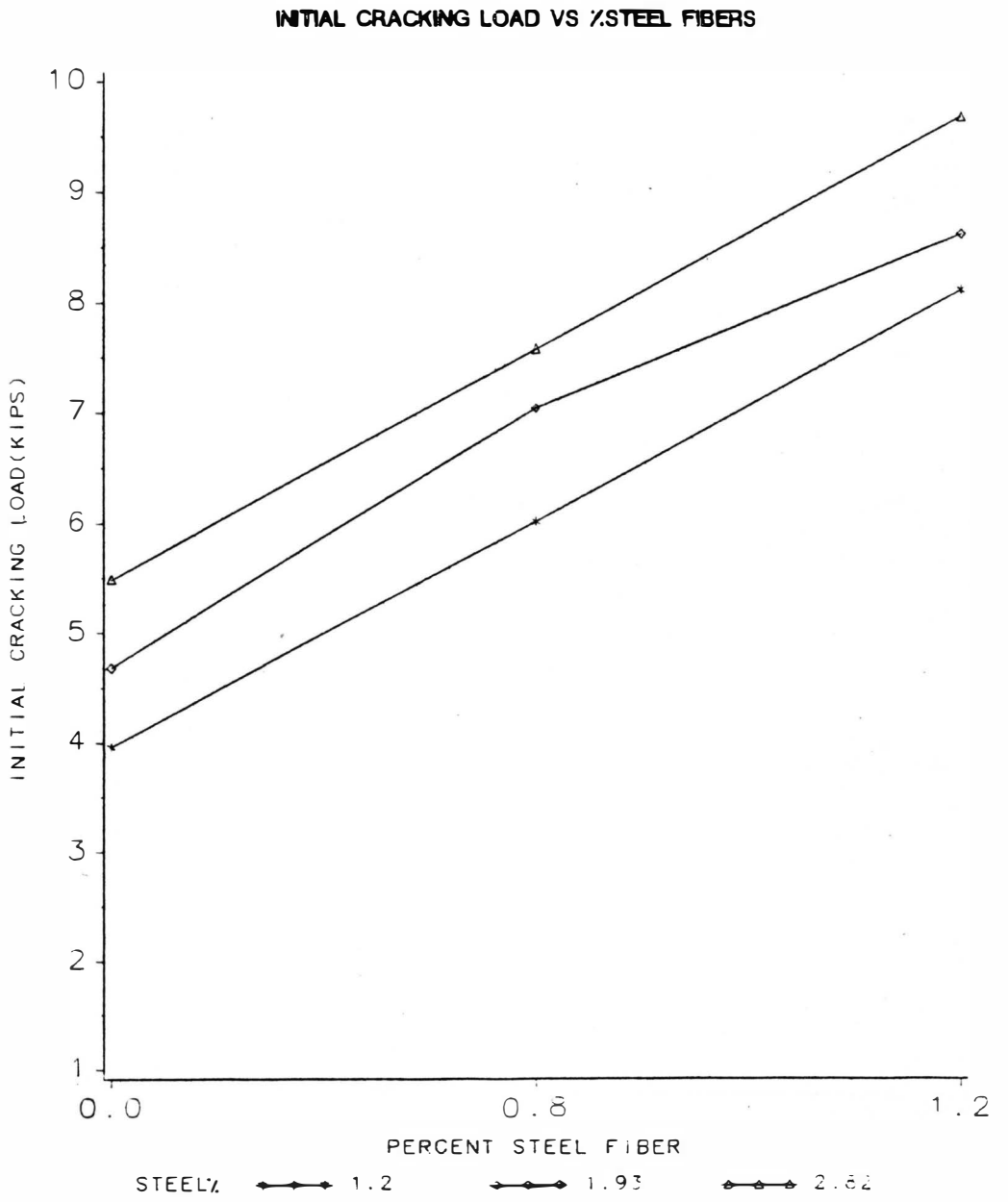
INITIAL CRACKING LOAD VS %STEEL FIBERS
INITIAL CRACKING LOAD(KIPS)
10
9
8
7
6
5
4
3
2
1
0.0
0.8
1.2
PERCENT STEEL FIBER
STEEL%
1.2
1.93
2.82

FIGURE 7·20

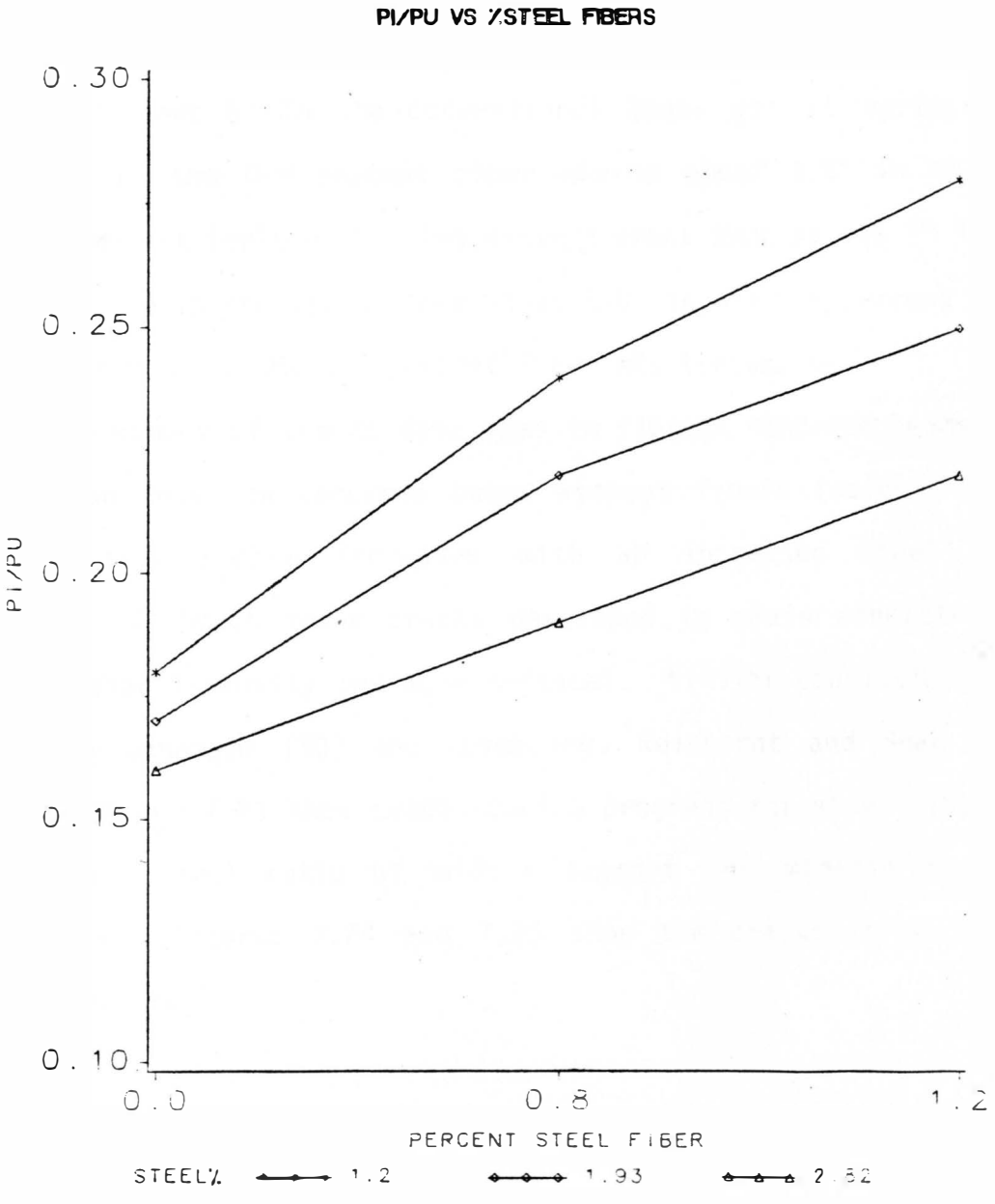
PI/PU VS %STEEL FIBERS
0.30
0.25
0.20
0.15
0.10
PI/PU
0.0
0.8
1.2
PERCENT STEEL FIBER
STEEL%
1.2
1.93
2.82

FIGURE 7-21

at the tension zone of the flexural member. The reduction was highest for the lowest volume of reinforcing bars (column 8). The higher the steel fiber content the lower the crack spacing; the higher the tensile reinforcement the lower the crack spacing. The maximum crack spacing was about 6" in the conventional beams and it varies from about 4.5" in the 0.8 percent fiber mix to about 3.5" in the 1.2 percent fiber mix (column 5). The minimum crack spacing was 2" in the conventional beams and varies from about 1.0" in the 0.8 percent fiber mix to about 0.8" in the 1.2 percent fiber mix (column 6).

The number of cracks developed in fibrous concrete beams were greater than those in concrete beams without fibers (columns 9 and 10), and this number increases with an increased steel fiber percentage. Although fewer cracks developed in plain concrete they were of higher intensity and more critical. Similar conclusions were reported by Sahebjam (50) and Kormeling, Reinhardt and Shah (35). Figures 7.22 and 7.23 show crack spacing progress for steel fiber for a given main steel ratio of middle support and midspan sections respectively. Figures 7.24 and 7.25 show the cracks in plain and fibrous concrete.

7.9 Strains

7.9.1 Steel Strains

Strains in the tension and compression steel for each beam were measured with electric strain gages. The values of various strains at service load are listed in Table 7.18.

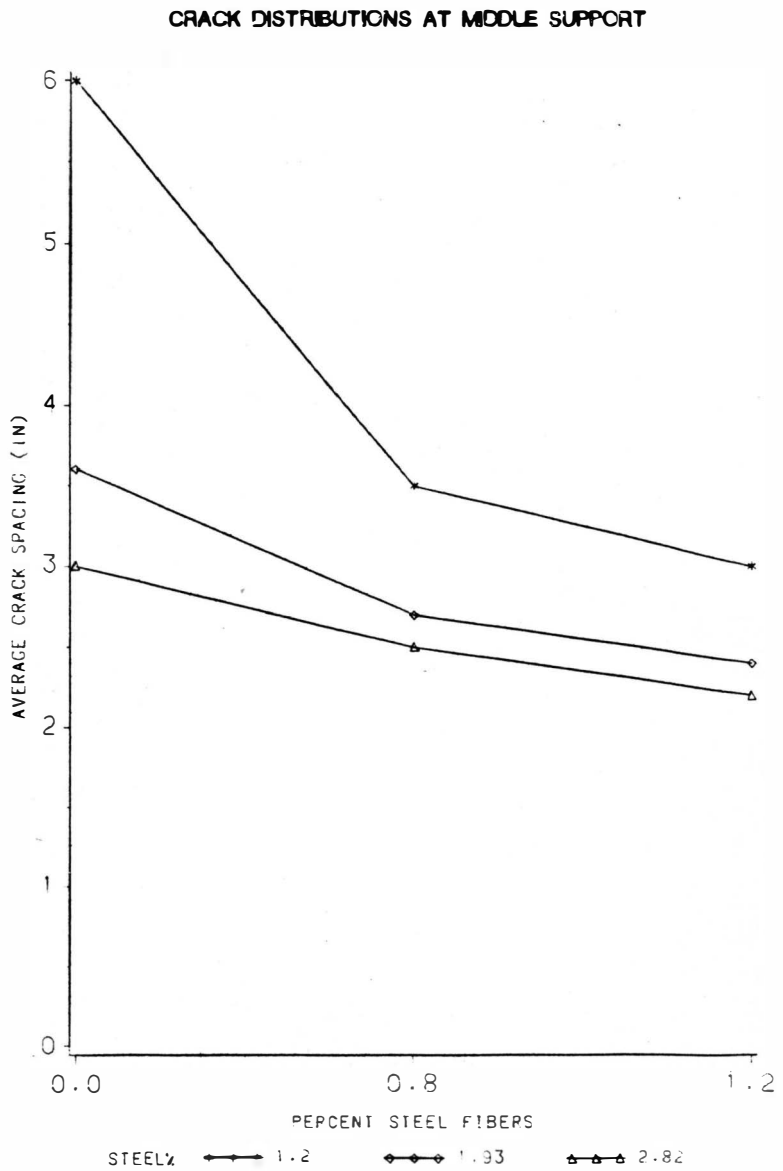
CRACK DISTRIBUTIONS AT MIDDLE SUPPORT
AVERAGE CRACK SPACING (IN)
6
5
4
3
2
1
0
0.0
0.8
1.2
PERCENT STEEL FIBERS
STEEL%
1.2
1.93
2.82

FIGURE 7-22

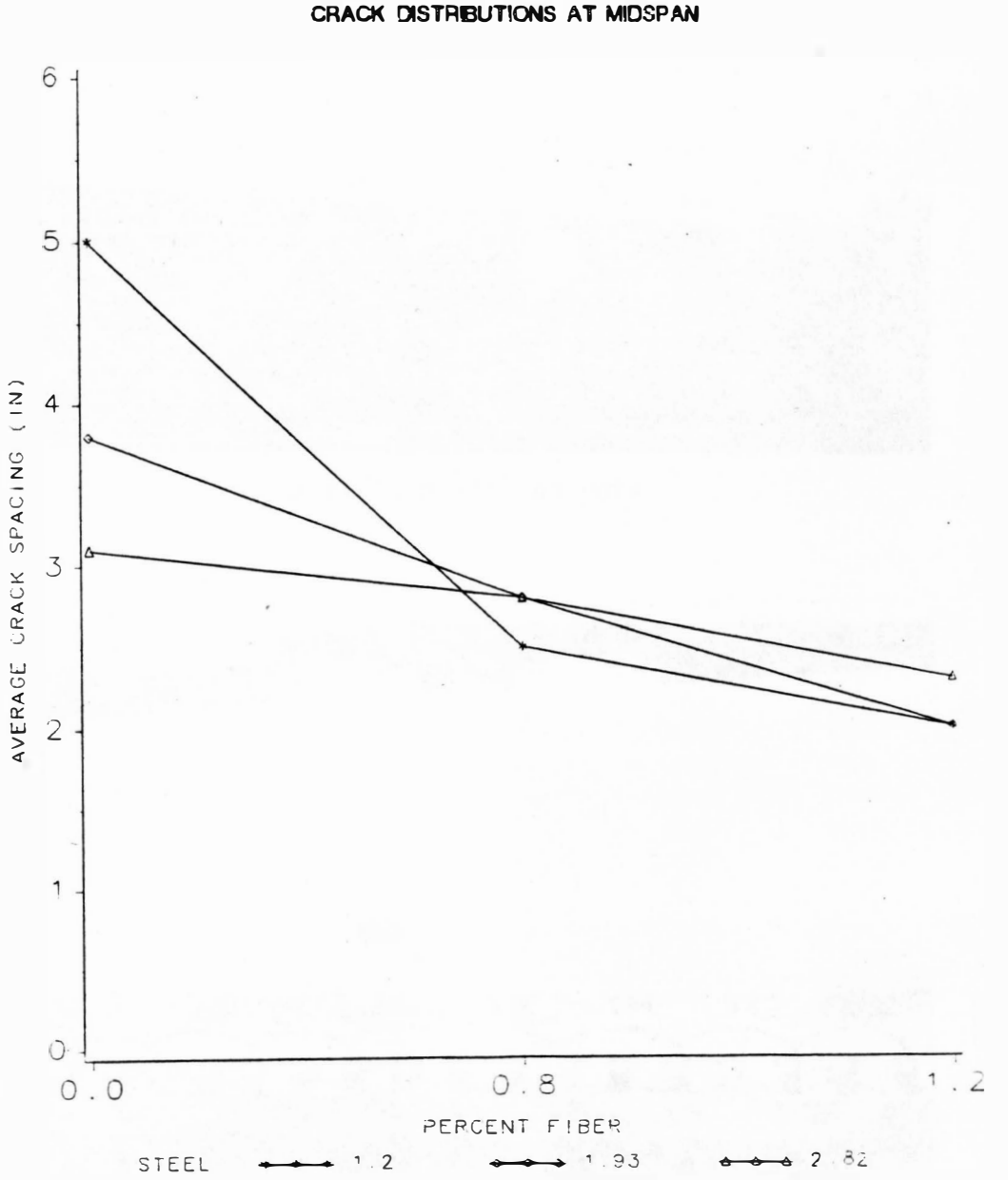
CRACK DISTRIBUTIONS AT MIDSPAN
AVERAGE CRACK SPACING (IN)
6
5
4
3
2
1
0
0.0
0.8
1.2
PERCENT FIBER
STEEL
1.2
1.93
2.82

FIGURE 7-23

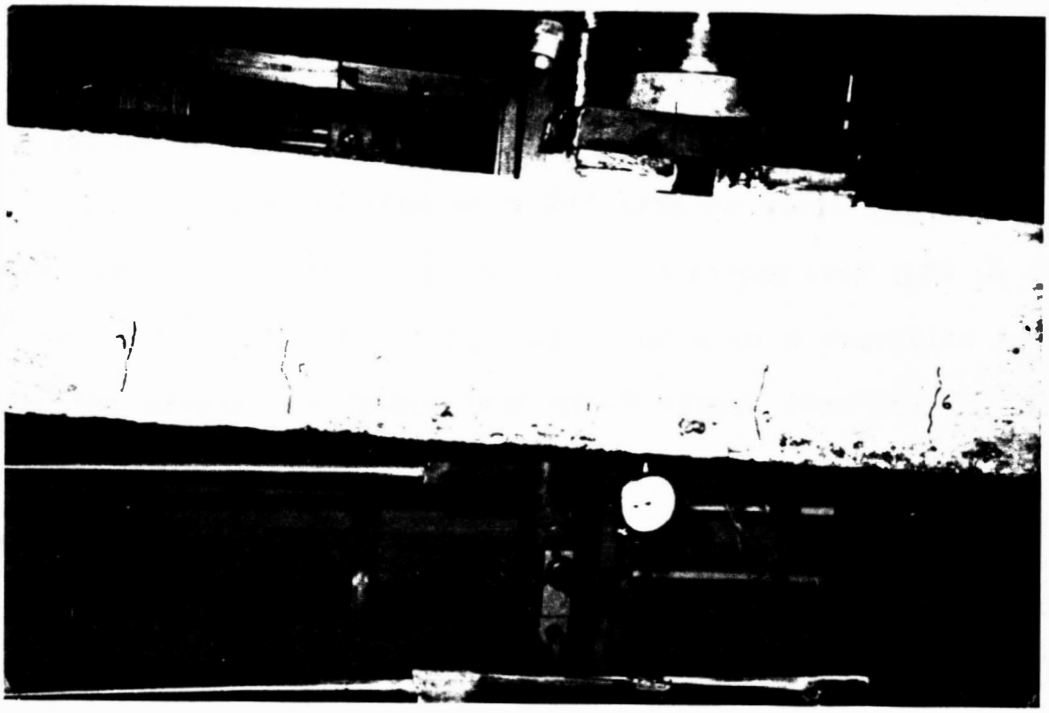

Figure 7.24. Cracks in plain concrete.

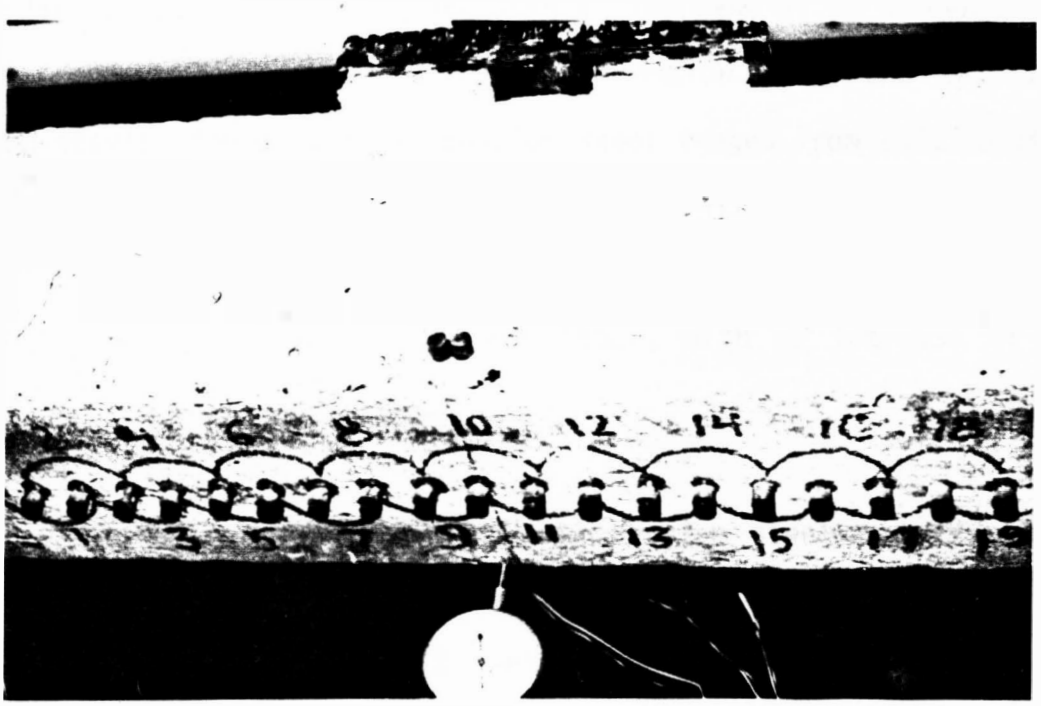

Figure 7.25. Cracks in fibrous concrete.

Upon examination of Table 7.18 the following become apparent:

1) At the middle support

a) Beams reinforced with 2#4 tension steel and 2#3 compression steel: The strains in tension steel ranged from 1680 to 1100 x 10^{-6} in/in for 0.0 and 1.2 percent fiber with a reduction of 35 percent; the strains in compression steel ranged from 301 to 465 x 10^{-6} in/in for 0.0 and 1.2 percent fiber with an increase of 54 percent.

b) Beams reinforced with 2#5 tension steel and 2#3 compression steel: The strains in tension steel ranged from 1600 to 1185 x 10^{-6} in/in for 0.0 and 1.2 percent fiber with a reduction of 26 percent; the strains in compression steel ranged from 496 to 694 x 10^{-6} in/in for 0.0 and 1.2 percent with an increase of 40 percent.

c) Beams reinforced with 2#6 tension steel and 2#3 compression steel: The strains in tension steel ranged from 1800 to 1410 x 10^{-6} in/in for 0.0 and 1.2 percent fibers with a reduction of 22 percent; the strains in compression steel ranged from 1400 to 1720 x 10^{-6} in/in for 0.0 and 1.2 percent fiber, with an increase of 23 percent.

2) At mid-span

a) Beams reinforced with 2#4 tension steel and 2#3 compression steel: The strains in the tension steel ranged from 1375 to 755 x 10^{-6} in/in for 0.0 and 1.2 percent fiber with a decrease of 45 percent; strains in compression steel ranged from 271 to 280 x 10^{-6} in/in for 0.0 and 1.2 percent fiber with an increase of 7 percent.

TABLE 7.18

ACTUAL STRAINS IN MAIN AND COMPRESSION STEEL AT SERVICE LOAD

Beam No.	% Steel Fibers	0.6 P_u (kips)	ACTUAL STRAINS AND STRESS IN MAIN STEEL MIDDLE SUPPORT ε_s μ in/in	f_s (ksi)	% Decrease in strain from 0.0% S.F.	MIDSPAN ε_s μ in/in	f_s (ksi)	% Decrease in strain from 0.0% S.F.	ACTUAL STRAINS AND STRESSES IN COMPRESSION STEEL MIDDLE SUPPORT ε'_s μ in/in	f'_s (ksi)	% Increase in strain from 0.0% S.F.	MIDSPAN ε'_s μ in/in	f'_s	% Increase in strain from 0.0% S.F.
1	0.0	13.1	1680	48.7	---	1375	39.9	---	301	9	---	271	8	---
4	0.8	14.9	1335	38.7	-21	1040	30.2	-24	401	12	+33	280	8	+3
7	1.2	17.3	1100	31.9	-35	755	21.9	-45	465	8	+54	290	8	+7
2	0.0	16.8	1600	46.4	---	1250	36.3	---	496	14	---	363	11	---
5	0.8	19.4	1395	40.5	-13	1200	34.8	-4	576	17	+16	480	14	+32
8	1.2	21.3	1185	34.4	-26	1080	31.3	-114	694	20	+40	508	15	+40
3	0.0	21.0	1800	52.2	---	1560	45.2	---	1400	41	---	1200	35	---
6	0.8	23.0	1600	46.4	-11	1260	36.5	-19	1600	46	+14	1450	43	+21
9	1.2	26.0	1410	40.9	-22	1200	34.8	-23	1720	50	+23	1600	46	+33

b) Beams reinforced with 2#5 tension steel and 2#3 compression steel: The strains in the tension steel ranged from 1250 to 1080 x 10^{-6} in/in for 0.0 and 1.2 percent fiber with a decrease of 14 percent; strains in compression steel ranged from 363 to 584 x 10^{-6} in/in for 0.0 and 1.2 percent fiber with an increase of 40 percent.

c) Beams reinforced with 2#6 tension steel and 2#3 compression steel: The strains in the tension steel ranged from 1560 to 1200 x 10^{-6} in/in for 0.0 and 1.2 percent fiber with a decrease of 23 percent; the strains in compression steel range from 1200 to 1600 x 10^{-6} in/in for 0.0 and 1.2 percent fiber with an increase of 95 percent.

From the preceding discussion, it can be concluded that the presence of steel fibers in concrete beams reduces the main steel strain at service load. The highest reduction was 45 percent for beam #7 which was reinforced with the highest percent of steel fiber, 1.2, and the lowest reinforcing bars 2#4 and 2#3. This reduction in main steel strain is attributed to the fact that fibrous concrete is more affective in withstanding tension than is plain concrete. The reduction in main steel strain confirms the crack control characteristics of the steel fibers; therefore, the steel fibers are able to mobilize the cracked section zone to resist deformation to a much greater extent than can plain concrete.

The conclusion supports the observation by Sahebjam (50), who reported a maximum decrease of 24 percent in the main steel strain. The reductions in main steel strain in this research were higher than

reductions reported by Reference (50) on similar beams, but without compression steel. This further supports the greater ductility of beams with compression steel over those without compression steel. Similar findings were reported by others (60,58).

7.9.2. Concrete Strains

The values of the various compressive concrete strains on the top of the beams were measured with electric strain gages. Table 7.19 shows concrete strains at service and ultimate load. By studying Table 7.19 the following becomes apparent:

The presence of steel fibers in the concrete beams increases compressive concrete strains at service load.

The ultimate compressive strain for fibrous concrete is higher than that of plain concrete. The ultimate concrete strain ranged from 3070 to 3205 x 10^{-6} in/in for plain concrete and from 4090 to 5525 x 10^{-6} in/in for fibrous concrete. The ACI Code (318-83) assumes a maximum compressive concrete strain of 3000 x 10^{-6} in/in, which is less than ultimate strain in fibrous concrete beams. Similar results were obtained by previous researchers (13,18,25) who reported that ultimate strains of fibrous concrete beams are much higher than those of plain concrete. Mosa (39) reported that the maximum compressive strain can reach up to 3055 x 10^{-6} in/in for plain concrete and 6237 x 10^{-6} in/in for fibrous concrete beams. Sahebjam (50) concluded that the maximum compressive strain can reach up to 2775 x 10^{-6} in/in for

TABLE 7.19

ACTUAL STRAINS IN CONCRETE AT SERVICE AND ULTIMATE LOAD

Beam No.	% Steel Fibers	Service Load 0.6 P_u (kips)	ACTUAL STRAINS AND STRESSES IN CONCRETE AT 0.6 ρ_u MIDDLE SUPPORT ε_c μ in/in	f_c (psi)	% Increase in ε_c from 0.01	MID-SPAN ε_c μ in/in	f_c (psi)	% Increase in ε_c from 0.0%	Concrete Strains ε_{cu} μ in/in	% Increase in Ultimate Strains
1	0.0	13.1	1055	3400	---	895	3580	---	3205	---
4	0.8	14.9	1405	3700	+33	950	3525	+6	4180	30
7	1.2	17.3	1630	3700	+55	980	3500	+9	4880	52
2	0.0	16.8	1290	3700	---	945	3400	---	3180	---
5	0.8	19.4	1690	3800	+31	1200	3400	+27	4090	29
8	1.2	21.3	1800	3800	+40	1510	3600	+60	4610	45
3	0.0	21.0	1360	3900	---	270	3000	---	3070	---
6	0.8	23.0	1775	4000	+31	1340	3700	+54	4995	63
9	1.2	26.0	2300	4100	+70	1700	3800	+95	5525	80

plain concrete beams and 5800 x 10^{-6} in/in for fibrous concrete, Swamy and Al-Taan (15) reported strains of up to 5780 x 10^{-6} in/in for plain concrete and 6620 x 10^{-6} in/in for fibrous concrete.

The visible difference between the non-fibrous concrete beams and fibrous concrete beams is that the visible damage in a non-fibrous concrete beam was in the form of spalling on the top of the beam at the critical sections (Figure 7.26 shows the appearance of plain concrete beams at ultimate). The fibrous concrete beams with compressive reinforcement showed a different mode of failure, which resulted in a very ductile failure. For beams without compressive reinforcement, the internal compressive force will be carried by the confined core and the crushing becomes very extensive. However, in beams with compressive reinforcement the internal compressive force will be carried by both the concrete and the compression steel. As crushing of the concrete progressed, the reinforcement was forced to pick up a larger proportion of the total compressive force. At ultimate stage the compression steel will act with the stirrups in confining the concrete core. Therefore compression steel is not only effective in increasing the ductility, but also it does not retard the cracking of compression concrete. (Figure 7.27 shows the appearance of a fibrous concrete at ultimate).

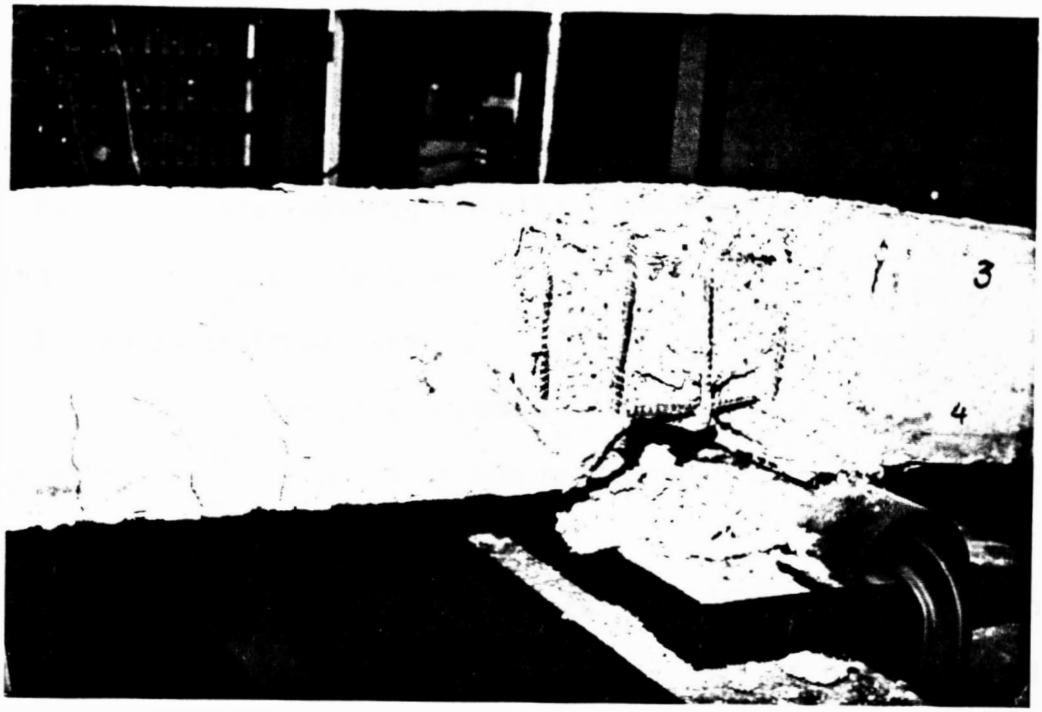

Figure 7.26. Failure of plain concrete.

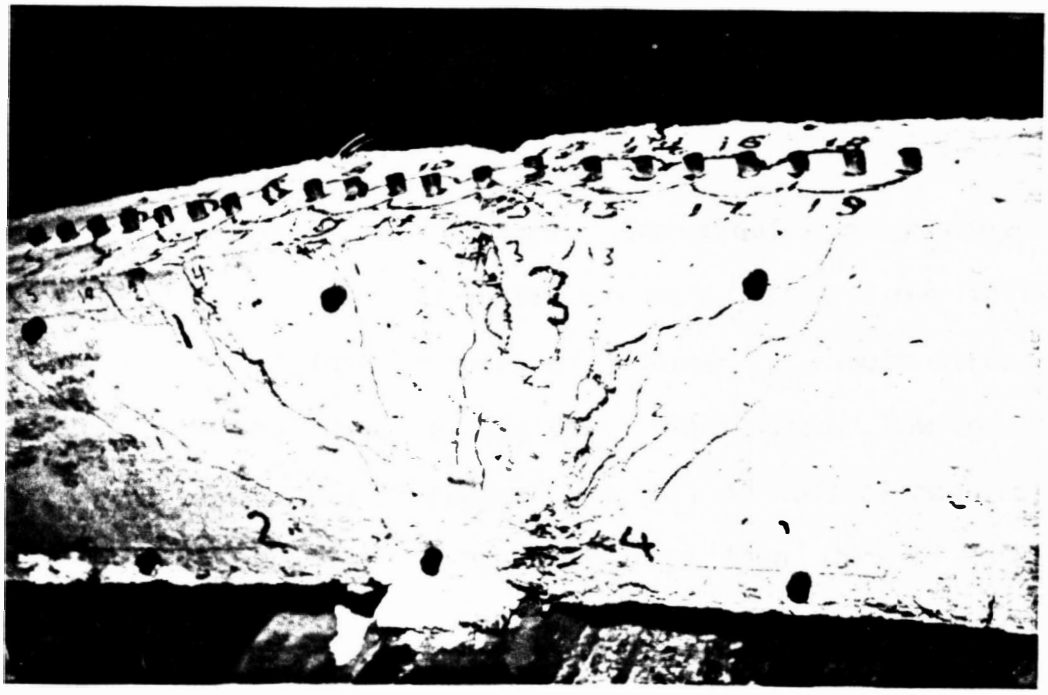

Figure 7.27. Failure of fibrous concrete.

CHAPTER 8

CONCLUSIONS AND RECOMMENDATIONS

Based on the results of this experimental research, the following conclusions can be made:

I. Physical Properties:

1) Compressive Strength: The increase in compressive strength of concrete cylinders by the presence of steel fibers was not appreciable (Section 7.1).

2) Modulus of Elasticity: The modulus of elasticity of fibrous concrete was found to be less than that of plain concrete. The reason for that decrease could be attributed to the higher deformation and strain of fibrous concrete (Section 7.2).

3) Tensile Strength: The inclusion of steel fibers in a concrete mix substantially increases the tensile strength of concrete (Section 7.3).

4) Modulus of Rupture: The modulus of rupture of fibrous concrete was found to have two main values, the initial modulus f_{ri} and the ultimate modulus of rupture f_{ru}. Both strengths are increased with the volume of the steel fibers used. However, for plain concrete, the modulus of rupture has only an initial modulus of rupture f_{ri}. It was found to be much less than that of fibrous concrete (Section 7.4).

II. Load Carrying Capacity of Beams (Section 7.5):

1) Ultimate and Yield Loads: Yield and ultimate loads of fibrous concrete beams were higher than those of plain concrete. Complete redistribution occurred in all the beams since the main steel yielded at the last critical section.

2) Load Redistribution Factor (r): Ultimate to yield load ratio of fibrous concrete beams were higher than those of plain concrete ones, with the inclusion of compression steel greater reserve capacity was attained (Section 7.5.2.).

III. Rotations:

1) Plastic Hinge Length: The length of the plastic hinge can be related to the effective depth of the section, and the percentages of main steel and steel fibers. The effect of compression steel on the length of the plastic hinge was minor, the magnitude of H_L increases with the increase of $(\rho\rho_s)$, and the length of the plastic hinge for plain concrete beams is equal 0.98 d (Section 7.6).

2) Curvature Distribution Factor: The fibrous concrete distribution factor is less than that of plain concrete even though the curvature of fibrous concrete is substantially higher than that of plain concrete. The value of β can be assumed to equal 0.44 for plain concrete beams with compression steel (Section 7.6.2.)

3) Ductility Index: The ductility index denotes the rotation capability. It is found that the ductility index for fibrous concrete is much higher than that for plain concrete, and it increases with the volume of the fibers used (Section 7.6.3).

4) Rotation Capacity: The inclusion of steel fibers in the concrete imparts a large rotation capacity and with the inclusion of compression steel it becomes substantially higher than that of conventional beams. This fact can be used effectively in the redistribution of moments in hyperstatic beams and frames (Section 7.6.4.).

IV. Deflections (Section 7.7):

1) The stiffness of beams of service load increased with the volume of steel fibers in the concrete. With the inclusion of compression steel the stiffness was higher than that of beams without compression steel, leading to a substantial reduction in deflections.

2) Beams with higher percentages of steel fibers underwent less deflections at service load, but higher deflections at ultimate loads.

3) Beams reinforced with compression steel had higher ultimate deflections than those without compression steel, therefore the beams possessed enormous ductility.

V. Cracks (Section 7.8):

1) The presence of steel fibers in concrete reduces the maximum crack width at service loads.

2) The initial cracks in the fibrous beams occurred at higher loads than in conventional concrete beams.

3) The cracks in the fibrous beams were more closely spaced than cracks in the conventional concrete beams.

VI. Strains (Section 7.9)

1) Addition of steel fibers substantially reduces the strains and stresses in the main reinforcement for a given load, thus leading to a greater inelastic deformation possessed by fibrous concrete beams.

2) Addition of steel fibers to concrete increases the ultimate strain capacity of concrete much greater than the assumed value of 0.003.

3) The presence of both steel fibers and compression steel preserved the structural integrity and minimized the crack retardation of the members after failure.

VII. Recommendations:

1) It is concluded the beneficial influences of steel fibers increases with the volume of fibers in the concrete; therefore, the use of 1.2 percent steel fibers is highly recommended, especially if it is used with the least volume of the conventional reinforcement.

2) The yielding of compression steel is recommended in all beams since it can bring higher ultimate deflections, curvature and plastic rotations.

BIBLIOGRAPHY

1. ACI Committee 318, "Building Code Requirements for Reinforced Concrete," American Concrete Institute, 1983.

2. ACI Committee 544, "Guide for Specifying, Mixing, Placing and Finishing Steel Fiber Reinforced Concrete," ACI Publication Sp. 81, American Concrete Institute, Detroit, Michigan, 1982, pp. 441-448.

3. ACI Committee 544, "Measurement of Properties of Fiber Reinforced Concrete," Concrete International, Common Report, May 1982.

4. ACI Committee 544, "State-Of-The-Art Report on Fiber Reinforced Concrete," Journal American Concrete Institute, 70, No. 11, Nov. 1973, pp. 729-744.

5. Ajina, Jamal, "Effect of Steel Fibers on Precast Dapped End Beam Connections," M.S. Thesis, S.D.S.U., 1986.

6. Ali, Mir M. and Grierson, Donald E., "Reinforced Concrete Design for Strength and Deformability," ASCE Journal, Mechanics Division, Vol. 100, No. EM5, Oct. 1974, pp. 839-859.

7. Baker, A.L.L., "Limit State Design of Reinforced Concrete," Cement and Concrete Association, London, 1970.

8. Baker, A.L.L., "The Ultimate Load Theory Applied to the Design of Reinforced and Prestressed Concrete Frames," Concrete Publications, London, England, 1956.

9. Beedle, Lynn S., "Plastic Design of Steel Frames," 1958.

10. Berwanger, C., "Limit Design of Reinforced Concrete Continuous Beams," The Engineering Journal, May 1962, pp. 42-49.

11. Burnett, E., "Flexural rigidity, Curvature and Rotation and Their Significance in Reinforced Concrete Design," Magazine of Concrete Research, Vol. 16, No. 46, March 1964, pp. 6772.

12. Burns, Ned H., and Siess, Chester P., "Plastic Hinging in Reinforced Concrete," ASCE Journal, Structural Division, Vol. 92, No. SI5, October 1966, pp. 45-63.

13. Bishara, Alfred G. and Londot, Larry and Au, Peter and Sastry, Majety V., "Flexural Rotational Capacity of Spandrel Beam," ASCE Journal, Structural Division, Vol. 105, No. ST1, January 1979, pp. 147-161.

14. British Standard Code of Practice, CP 110, 1972.

15. Chan, W.W.L., "The Rotation of Reinforced Concrete Plastic Hinges at Ultimate Load," Magazine of Concrete Research, Vol. 14, No. 41, July 1962, pp. 63-72.

16. Chan. W.W.L., "The Ultimate Strength and Deformation of Plastic Hinges in Reinforced Concrete Frameworks," Magazine for Concrete Research, November 1955, pp. 121-132.

17. Chen, W.F., and Carson, J.L., "Stress-Strain Properties of Random Wire Reinforced Concrete," Journal of the American Concrete Institute, Vol. 68, December 1971, pp. 933-936.

18. Cohn, M.Z., "Limit Design Solutions for Concrete Structures," ASCE Journal, Structural Division, Vol. 93, No. ST1, February 1967, pp. 37-57.

19. Cohn, M.Z., and Petca, V.A., "Moment Redistribution and Rotation Capacity of Plastic Hinges in Redundant Reinforced Concrete Beams," Indian Concrete Journal, August 1963, pp. 282-290.

20. Cohn, M.Z., "Rotation Compatibility in the Limit Design of Reinforced Concrete Continuous Beams," Flexural Mechanics of Reinforced Concrete, Proceedings of the International Symposium, Miami, FL, Nov. 10-12, 1964, pp.

21. Cohn, M.Z., and Ghosh, "The Flexural Ductility of Reinforced Concrete Sections, Vol. 33-11, 1972, pp. 53-83.

22. Desay, Prakash and Sundara Raja Iyegar, K.T. and Reddy, K. Nagi, "Ductility of Reinforced Concrete Sections with Confined Compression Zones," Earthquake Engineering and Structural Dynamics, Vol. 4, 1975, pp. 111-118.

23. Ernst, C.G., "A Brief for Limit Design," Transaction, ASCE, Vol. 121, 1956, p. 605.

24. Ernst, C.G., "Moment and Shear Redistribution in Two-Span Continuous Reinforced Concrete Beam," Journal American Concrete Institute, Proc. Vol. 55, Nov., 1958, pp. 563-589.

25. Halvorsen, Grant T. and Kesler, Clyde E., "Moment-Curvature Relationships for Concrete Beams with Plain and Deformed Steel Fibers," ACI Journal, Technical Paper, June 1979, pp. 697-706.

26. Hassoun, Nadim, "Design of Reinforced Concrete Structures," PWS Publishers, 1985.

27. Hassoun, Nadim, "Ultimate Design of Reinforced Concrete," A Practical Handbook, printed by J.B. Shears and Sons, Ltd.

28. Hassoun, Nadim and Sahebjam, K., "Plastic Hinging in Two-Span Reinforced Concrete Beams Containing Steel Fiber," Canadian Society for Civil Engineering, May 1985, pp. 119-139.

29. Henager, Charles H. and Doherty, Terrence J., "Analysis of Reinforced Fibrous Concrete Beams," ASCE Journal, Structural Division, Vol. 102, No. ST1, January 1976, pp. 177-188.

30. Hsu, Thomas, "Ductility of Reinforced Concrete Members and Shear Walls," Journal of the Chinese Institute of Engineering, Vol. 3, No. 1, Jan. 1980, pp. 1-20.

31. ICE, Institution of Civil Engineers, London, V. 21, Feb. 1962, pp. 400-422.

32. Kaushik, S.K. and Ramamurthy, L.N. and Kukuja, C.B., "Plasticity in Reinforced Concrete Continuous Beams with Parabolic Soffits," ACI Journal, September-October 1980, pp. 369-377.

33. Kar, Jitendra, Pal, Anil, "Strength of Fiber Reinforced Concrete," Journal Structure Division, American Society of Civil Engineers, Vol. 98, No. ST5, May 1982, pp. 1053-1068.

34. Kemp. A.R., "Ductility and Moment Redistribution in Reinforced Concrete Beams," The Civil Engineer in South Africa, May 1981, pp. 175-181.

35. Kormeling, H.A. and Reinhardt, H.W. and Shah, S.P., "Static and Fatigue Properties of Concrete Beams Reinforced with Continuous Bars and With Fibers," ACI Journal, January-February 1980, pp. 36-43.

36. Lenkei. P., "Local and Overall Specific Inelastic Rotation Capacities in Reinforced Concrete Beams," ACTA Technica Academiae Scientiarum Hungarical, Tomus 79 (3-4), 1974, pp. 451-463.

37. Mattock, Alan H., "Rotational Capacity of Hinging Regions in Reinforced Concrete Beams," Flexural Mechanics of Reinforced Concrete, Proceeding of the International Symposium, Miami, FL, November 10-12, 1964, pp. 143-181.

38. Mendenhall, William, and Terry Sinich, "Statistics for Engineering and Computer Sciences," Santa Carla, CA, Dellen Publishing Company, 1984.

39. Musa, Saadi, "The Effect of Steel Fibers on the Properties and Behavior of High Strength Reinforced Concrete Beam," M.S. Thesis, S.D.S.U., 1982.

40. Nawy, Edward, Danesi, Rodolfo, Grosk, John, "Rectangular Spiral Binders Effect on Plastic Hinge Rotation Capacity in Reinforced Concrete Beams," ACI Journal, December 1968, pp. 1001-1010.

41. Naville, Adam, "Fiber Reinforced Cement and Concrete," The Construction Press LTD, Rilem Symposium, 1975.

42. Noor, F.A., "Inelastic Behavior of Reinforced Concrete Frames," Magazine of Concrete Research, Vol. 28, No. 97, December 1976, pp. 209-223.

43. Rajagopalan, K., Parameswaran, V.S., and Ramaswamy, G.S., "Strength of Steel Fiber Reinforced Concrete Beams," Indian Concrete Journal, Vol. 48, No. 1, Jan. 1974, pp. 17-25.

44. Ramakrishnan, V., Brandshaug, Terje, Coyle, W.V., Schrader, Ernest K., "A Comparative Evaluation of Concrete Reinforced with Straight Steel Fibers and Fibers with Deformed Ends Glued Together into Bundles," ACI Journal, Vol. 77, No. 3, May-June 1980, pp. 135-143.

45. Ramakrishnan, V., and Blakrishnan, S., "Elastic and Limit State Deformation of Reinforced Concrete Space Frames," Indian Concrete Journal, March 1976, pp. 85-91.

46. Ramkrishnan, V., Coyle, W.V., Kulandaisamy, V., and Shrader, Ernest K., "Performance Characteristics of Fiber Reinforced Concrete with Low Fiber Contents," ACI Journal, Vol. 78, No. 5, Sept.-Oct 1981, pp. 388-394.

47. Ravindrarajah, S.R.I. and Tam, C.T., "Flexural Strength of Steel Fiber Reinforced Concrete Beams, "International Journal of Cement Composites and LIght Weight Concrete, Vol. 6, No. 6, Nov. 1984, pp. 273-278.

48. Richard, Rowland, Jr. and Lazard, Angel L., "Limit Analysis a Reinforced Concrete Frames," ACI Journal, October 1971, pp. 748-755.

49. Romualdi, J.P., and Batson, Gordon, B., "Behavior of Reinforced Concrete Beams with Closely Spaced Reinforcement," ACI, Vol. 60, No. 6, June 1963, pp. 750-790.

50. Sahebjam, K., "The Effect of Steel Fibers on Plastic Rotation of Reinforced Concrete Continuous Beam," M.S. Thesis, S.D.S.U., 1984.

51. Shaikh, M.F., Mirza, M.S., and McCutcheon, J.O., "Limit Analysis of Reinforced Frames," Engineering Institute of Canada, Vol. 14, No. A-6, July 1971, pp. I-VII.

52. Shah, Surendra P., and Rangan, B. Vijay, "Effects of Reinforcement on Ductility of Concrete," ASCE Journal, Structural Division, Vol. 96, No. ST6, June 1970, pp. 1167-1183.

53. Shah, S.P. and Winter, George, "Inelastic Behavior and Fracture of Concrete," ACI Journal, SEptember 1966, pp. 925-930.

54. Snyder, M.J., and Lamkard, D.R., "Factors Affective the Flexural Strength of Steel Fibrous Concrete," Journal of American Concrete Institute, Vol. 69, No. 2, Feb. 1972, pp. 96-100.

55. Subrahmanyam, B.V., "Prediction of the Inelastic Behavior of One-Way Continuous Slabs," ACI Journal, Technical Paper, pp. 621-631.

56. Sawuer, H.A., "Elastic-Plastic Design of Single Span Beams and Frames," Proc. Paper No. 551, ASCE, Vol. 81, Dec. 1955.

57. Swamy, R.M., and Mangat, P.S., "A Theory for Flexural Strength of Steel Fiber Reinforced Concrete," Cement and Concrete Research, Vol. 4, 1974, pp. 313-325.

58. Swamy, R.M., and Al-Taan, Saad, "Deformation and Ultimate Strength in Flexure of Reinforced Concrete Beams Made with Steel Fiber Concrete," Journal American Concrete Institute, Sept-Oct. 1981.

59. Swamy, R., and Al-Noori, K., "Flexural Properties of Steel Fiber Reinforced Concrete," Concrete (London), Vol. 9, No. 6, June 1975, pp. 30-31.

60. Swamy, R., Narayan, Al-Taan, Saad, A., and Ali, Sam A.R., "Steel Fibers for Controlling Cracking and Deflection," Concrete International, 1, No. 8, Aug. 1979, pp. 41-49.

61. Velazco, Visalyvanich K., and Shah, S.P., "Fracture Behavior and Analysis of Fiber Reinforced Concrete Beams," Cement and Concrete Research, Vol. 10, 1980, pp. 41-45.

62. Wright, D.T. and Berwanger, C., "Limit Design of Reinforced Concrete Beams, "ASCE Journal, Structural Division, Vol. 86, No. ST7, July 1960, pp. 1-36.

Appendix A

Actual Rotations and Strain at Critical Section

TABLE A.1

ACTUAL ROTATION AT THE CRITICAL SECTION USING METHOD 1 X 10^4 RADIANS

Main Steel = 2#4 Top Steel = 2#3 % Steel Fibers = 0.0 H_L = 6 inches

Load Kips	Moment Kip-in.	ϕ_1	ϕ_2	ϕ	θ
1.02	11.48	0.5	0.5	1.0	6.0
2.04	22.95	0.75	0.75	1.5	9.0
3.03	34.1	1.25	1.25	2.5	15.0
4.97	55.91	1.75	1.75	3.5	21.0
6.02	67.73	2.25	2.25	4.5	27.0
8.13	91.46	2.8	2.8	5.6	33.6
10.23	115.10	3.2	3.2	6.4	38.4
12.42	139.73	3.8	3.8	7.6	45.6
14.48	162.90	4.25	4.25	8.5	45.6
17.0*	191.25	5.1	5.1	10.2	61.2
17.72	191.25	15.0	20.0	35.0	210.0
21.8**	191.25	31.2	40.0	71.2	427.2

* = First yield of middle support
** = Second yield at midspan

TABLE A.2

ACTUAL ROTATION AT THE CRITICAL SECTION USING METHOD 1 X 10^4 RADIANS

Main Steel = 2#4 Top Steel = 2#3 % Steel Fibers = 0.8 H_L = 7.5 inches

Load Kips	Moment Kip-in.	ϕ_1	ϕ_2	ϕ	θ
1.02	11.48	0.5	0.5	1.0	7.5
2.04	22.95	0.8	0.95	1.75	13.1
3.03	34.10	1.25	1.25	2.5	18.8
3.96	44.55	1.8	1.8	3.6	27.0
4.97	55.91	1.8	2.2	4.0	30.0
6.02	67.73	2.2	2.3	4.5	33.8
7.05	79.31	2.7	2.8	5.5	43.0
8.13	91.46	3.0	3.0	6.0	45.0
9.16	103.1	3.0	3.5	6.5	48.8
10.23	115.1	3.2	3.55	6.75	50.6
11.29	127.0	3.6	3.7	7.5	54.8
12.42	139.73	3.7	3.8	7.5	56.3
13.43	151.08	4.0	4.0	8.0	60.0
14.48	162.9	4.1	4.1	8.2	61.5
15.53	174.71	4.2	4.3	8.5	63.8
16.63	187.1	4.4	4.6	9.0	67.5
17.72	199.35	4.8	5.0	9.8	73.5
18.4*	207.0	4.9	5.1	10.0	75.0
20.81	207.0	40.0	50.0	90.0	675.0
21.8	207.0	70.0	80.0	150.0	1125.0
22.85	207.0	110.0	140.0	250.0	1875.0
23.88	207.0	150.0	170.0	320.0	2400.0
24.8**	207.0	181.0	230.0	411.0	3083.0

* = First yield of middle support
** = Second yield at midspan

TABLE A.3

ACTUAL ROTATION AT THE CRITICAL SECTION USING METHOD 1 X 10^4 RADIANS

Main Steel = 2#4 Top Steel = 2#3 % Steel Fibers = 1.2 H_L = 8 inches

Load Kips	Moment Kip-in.	ϕ_1	ϕ_2	ϕ	θ
1.02	11.48	0.4	0.4	0.8	6.4
2.04	22.95	0.9	0.9	1.8	14.4
3.03	34.10	1.1	1.1	2.2	17.6
3.96	44.55	1.5	1.5	3.0	24.0
4.97	55.91	1.7	1.8	3.5	28.0
6.02	67.73	2.1	2.2	4.3	34.4
7.05	79.31	2.5	2.5	5.0	40.0
8.13	91.46	2.9	2.9	5.8	46.4
9.16	103.1	3.4	3.4	6.8	54.4
10.23	115.1	3.7	3.8	7.5	60.0
11.29	127.0	4.1	4.2	8.3	66.4
12.42	139.73	4.5	4.5	9.0	72.0
13.43	151.08	5.0	5.0	10.0	80.0
14.48	162.9	5.2	5.3	10.5	84.0
15.53	174.71	5.5	5.5	11.0	88.0
16.63	187.1	5.7	5.8	11.5	92.0
17.72	199.35	6.0	6.0	12.0	96.0
18.86	212.18	6.1	6.2	12.3	98.4
19.94	224.33	6.5	6.5	13.0	104.0
20.79*	233.89	7.1	7.2	14.3	114.4
21.8	233.89	45.0	50.0	90.0	720.0
22.85	233.89	65.0	85.0	150.0	1200.0
23.88	233.89	100.0	120.0	220.0	1760.0
24.8	233.89	130.0	170.0	300.0	2400.0
25.92	233.89	170.0	180.0	350.0	2800.0
27.0	233.89	180.0	220.0	400.0	3200.0
28.0	233.89	230.0	260.0	490.0	3920.0
28.9**	233.89	300.0	345.0	645.0	5160.0

* = First yield of middle support
** = Second yield at midspan

TABLE A.4

ACTUAL ROTATION AT THE CRITICAL SECTION USING METHOD 1 X 10^4 RADIANS

Main Steel = 2#5 Top Steel = 2#3 % Steel Fibers = 0.0 H_L = 6 inches

Load Kips	Moment Kip-in.	ϕ_1	ϕ_2	ϕ	θ
1.02	11.48	0.5	6.1	1.1	6.6
2.04	22.95	1.0	1.0	2.0	12.0
3.03	34.10	1.4	1.4	2.8	16.8
3.96	44.55	1.7	1.8	3.5	21.0
4.97	55.91	2.2	2.3	4.5	27.0
6.02	67.73	2.6	2.7	5.3	31.8
7.05	79.31	2.7	2.8	5.5	33.0
8.13	91.46	3.2	3.3	6.5	39.0
9.16	103.10	3.6	3.7	7.3	43.8
10.23	115.10	4.0	4.0	8.0	48.0
11.29	127.0	4.0	4.4	8.8	52.8
12.42	139.73	4.7	4.8	9.5	57.0
14.48	162.90	5.0	5.0	1.0	60.0
16.63	187.10	5.9	5.9	11.8	70.8
18.86	212.18	6.6	6.7	13.3	79.8
20.81	234.11	7.2	7.3	14.5	87.0
22.85	258.19	7.4	7.5	14.9	89.4
23.93*	269.21	7.6	7.7	15.3	91.8
24.8	269.21	12.0	18.0	30.0	180.0
25.92	269.21	20.0	25.0	45.0	270.0
28.0**	269.21	31.3	35.0	61.3	367.8

* = First yield of middle support
** = Second yield at midspan

TABLE A.5

ACTUAL ROTATION AT THE CRITICAL SECTION USING METHOD 1 X 10^4 RADIANS

Main Steel = 2#5 Top Steel = 2#3 % Steel Fibers = 0.8 H_L = 8 inches

Load Kips	Moment Kip-in.	ϕ_1	ϕ_2	ϕ	θ
1.02	11.48	0.25	0.25	0.5	4.0
2.04	22.95	0.5	0.5	1.0	8.0
3.03	39.10	0.75	0.75	1.5	12.0
3.96	44.55	1.0	1.0	2.0	16.0
4.97	55.91	1.2	1.3	2.5	20.0
6.02	67.73	1.42	1.48	2.9	23.2
7.05	79.31	1.75	1.75	3.5	28.0
8.13	91.46	2.0	2.0	4.0	32.0
9.16	103.10	2.25	2.25	4.5	36.0
10.23	115.10	2.5	2.5	5.0	40.0
11.29	127.0	2.75	2.75	5.5	44.0
12.42	139.73	3.0	3.0	6.0	48.0
13.43	151.1	3.2	3.3	6.5	52.0
14.48	162.90	3.4	3.6	7.0	56.0
15.53	174.71	3.7	3.8	7.5	60.0
16.63	187.10	3.9	4.1	8.0	64.0
17.72	199.35	4.3	4.5	8.8	70.4
18.86	212.18	4.6	4.7	9.3	74.4
19.94	224.33	4.8	5.0	9.8	78.4
20.81	234.11	5.1	5.2	10.3	82.4
21.8	245.25	5.2	5.6	10.8	86.4
22.85	257.1	5.3	5.8	11.3	90.4
23.88	268.68	5.7	5.9	11.6	92.8
24.8	279.0	5.8	6.0	11.8	94.4
25.92*	291.6	5.9	6.1	12.0	96.0
27.0	291.6	17.0	23.0	40.0	320.0
28.0	291.6	40.0	50.0	90.0	720.0
29.0	291.6	60.0	80.0	140.0	1120.0
30.0	291.6	80.0	95.0	175.0	1400.0
32.4**	291.6	91.81	120.0	211.8	1694.0

* = First yield of middle support
** = Second yield at midspan

TABLE A.6

ACTUAL ROTATION AT THE CRITICAL SECTION USING METHOD 1 X 10^4 RADIANS

Main Steel = 2#5 Top Steel = 2#3 % Steel Fibers = 1.2 H_L = 9 inches

Load Kips	Moment Kip-in.	ϕ_1	ϕ_2	ϕ	θ
1.02	11.48	0.31	0.32	0.63	5.67
2.04	22.95	0.55	0.55	1.1	9.9
3.03	34.10	0.9	0.9	1.8	16.2
4.97	55.91	1.45	1.45	2.9	26.1
7.05	79.31	2.1	2.2	4.3	38.7
9.16	103.10	2.65	2.65	5.3	47.7
11.29	127.0	3.1	3.2	6.3	56.7
12.42	139.73	3.2	3.3	6.5	58.5
14.48	162.90	3.7	3.8	7.5	67.5
16.63	187.10	4.2	4.3	8.5	76.5
18.86	212.18	4.7	4.8	9.5	85.5
20.81	234.11	5.1	5.2	10.3	92.7
21.8	245.25	5.3	5.3	10.6	95.4
22.85	257.10	5.6	5.6	11.2	101.0
23.88	268.68	5.8	6.0	11.8	106.0
24.8	279.0	6.1	6.2	12.2	111.0
25.92	291.60	6.2	6.3	12.5	113.0
27.16*	305.55	6.7	6.8	13.5	122.0
28.0	305.55	18.0	22.0	40.0	360.0
29.0	305.55	40.0	50.0	90.0	810.0
30.0	305.55	60.0	80.0	140.0	1260.0
32.4	305.55	85.0	105.0	190.0	1710.0
33.0	305.55	118.0	140.0	258.0	2322.0
34.5**	305.55	158.0	180.0	338.0	3393.0

* = First yield of middle support
** = Second yield at midspan

TABLE A.7

ACTUAL ROTATION AT THE CRITICAL SECTION USING METHOD 1 X 10^4 RADIANS

Main Steel = 2#6 Top Steel = 2#3 % Steel Fibers = 0.0 H_L = 6.5 inches

Load Kips	Moment Kip-in.	ϕ_1	ϕ_2	ϕ	θ
1.02	11.48	0.25	0.25	0.5	3.3
2.04	22.95	0.37	0.38	0.75	4.9
3.03	34.10	0.65	0.65	1.3	8.5
4.97	55.91	0.9	0.9	1.8	11.7
7.05	79.31	1.25	1.25	2.5	16.3
9.16	103.10	1.5	1.5	3.0	19.5
11.29	127.0	1.7	1.8	3.5	22.8
12.42	139.73	1.9	1.9	3.8	24.7
14.48	162.90	2.2	2.3	4.5	29.3
16.63	187.10	2.6	2.7	5.3	34.5
18.86	212.18	2.9	2.9	5.8	37.7
20.81	234.11	3.1	3.4	6.5	41.0
21.8	245.25	3.4	3.5	6.8	44.2
22.85	257.10	3.7	3.7	7.3	47.5
23.88	268.68	3.7	3.8	7.5	48.8
24.8	279.0	3.8	4.0	7.8	50.7
25.92	291.6	4.0	4.3	8.3	54.0
27.0	303.75	4.2	4.6	8.8	57.2
28.0*	315.0	4.3	4.7	9.0	58.5
29.0	315.0	8.0	12.0	20.0	130.0
30.0	315.0	12.0	18.0	30.0	195.0
32.4	315.0	18.0	22.0	40.0	260.0
33.0	315.0	23.0	27.0	50.0	325.0
35.0**	315.0	26.1	33.0	59.1	384.0

* = First yield of middle support
** = Second yield at midspan

TABLE A.8

ACTUAL ROTATION AT THE CRITICAL SECTION USING METHOD 1 X 10^4 RADIANS

Main Steel = 2#6 Top Steel = 2#3 % Steel Fibers = 0.8 H_L = 9 inches

Load Kips	Moment Kip-in.	ϕ_1	ϕ_2	ϕ	θ
1.02	11.8	0.25	0.25	0.5	4.5
2.04	22.95	0.5	0.5	1.0	9.0
3.03	34.10	0.5	0.65	1.3	11.7
4.97	55.91	1.05	1.05	2.1	18.9
7.05	79.31	1.4	1.4	2.8	25.2
9.16	103.10	1.75	1.75	3.5	31.5
11.29	127.0	2.15	2.15	4.3	38.7
12.42	139.73	2.25	2.25	4.5	40.5
14.48	162.90	2.65	2.65	5.3	47.7
16.63	187.10	2.9	3.1	6.0	54.0
18.86	212.18	3.4	3.6	7.0	63.0
20.81	234.11	3.8	3.8	7.8	70.2
21.80	245.25	4.1	4.2	8.3	74.7
22.85	257.10	4.2	4.3	8.5	76.5
23.88	268.68	4.5	4.5	9.0	81.0
24.8	279.0	4.7	4.8	9.5	85.5
25.92	291.60	4.8	5.0	9.8	88.2
27.0	305.55	4.9	5.1	10.0	90.0
28.0	315.0	5.2	5.3	10.5	95.0
29.0	326.25	5.3	5.5	10.8	97.2
30.0*	337.5	5.4	5.7	11.0	99.0
32.4	337.5	35.0	45.0	80.0	720.0
33.0	337.5	60.0	80.0	140.0	1260.0
35.0	337.5	80.0	110.0	190.0	1710.0
38.28**	337.5	100.0	171.0	271.0	

* = First yield of middle support
** = Second yield at midspan

TABLE A.9

ACTUAL ROTATION AT THE CRITICAL SECTION USING METHOD 1 X 10^4 RADIANS

Main Steel = 2#6 Top Steel = 2#3 % Steel Fibers = 1.2 H_L = 9.5 inches

Load Kips	Moment Kip-in.	ϕ_1	ϕ_2	ϕ	θ
1.02	11.8	0.37	0.38	0.75	7.1
2.04	22.95	0.75	0.75	1.5	14.3
3.03	34.1	1.0	1.0	2.0	19.0
4.97	55.91	1.4	1.4	2.8	26.6
7.05	79.31	1.75	1.75	3.5	33.3
9.16	103.10	2.2	2.3	4.5	42.8
11.29	127.0	2.5	2.5	5.0	47.5
12.42	139.73	2.6	2.7	5.3	50.4
14.48	162.90	2.8	3.2	6.0	57.0
18.86	212.18	3.6	3.7	7.3	69.4
21.80	245.25	4.0	4.0	8.0	76.0
22.85	257.10	4.2	4.3	8.5	80.8
24.8	279.0	4.5	4.5	9.0	85.5
25.92	291.60	4.7	4.8	9.5	90.3
27.0	305.55	4.8	5.0	9.8	93.1
28.0	315.0	5.0	5.0	10.0	95.0
30.0	337.5	5.2	5.3	10.5	99.8
32.4	364.5	5.6	5.9	11.5	109.0
33.6*	378.0	5.8	6.0	11.8	112.0
35.0	378.0	25.0	35.0	60.0	570.0
36.8	378.0	50.0	70.0	120.0	1140.0
39.0	378.0	80.0	110.0	190.0	1805.0
40.0	378.0	100.0	160.0	260.0	2470.0
43.4**	378.0	130.0	190.0	320.0	3040.0

* = First yield of middle support
** = Second yield at midspan

TABLE A.10

STEEL AND CONCRETE STRAINS AT CRITICAL SECTIONS

Main Steel = 2#4 Compression Steel = 2#3
Steel Fiber = 0.0 d = 6.5 inches

Load (kips)	Main Steel Strains μ in/in		Compression Steel Strains μ in/in		Concrete Strains μ in/in	
	Negative	Positive	Negative	Positive	Negative	Positive
2.04	240	160	55	30	90	80
3.96	480	400	90	60	220	240
6.02	700	600	130	80	270	320
8.13	920	800	175	120	420	400
10.23	1200	1020	220	150	560	580
12.42	1520	1260	280	200	800	800
13.43	1690	1375	301	271	1055	895
15.53	2000	1560	360	320	1380	1120
17.72	2237	1840	398	360	2000	1360
19.94	----	2080	500	400	2480	2080
21.80	----	2250	540	443	3205	2800

TABLE A.11

STEEL AND CONCRETE STRAINS AT CRITICAL SECTIONS

Main Steel = 2#4 Compression Steel = 2#3
Steel Fiber = 0.8 d = 6.5 inches

Load (kips)	Main Steel Strains μ in/in		Compression Steel Strains μ in/in		Concrete Strains μ in/in	
	Negative	Positive	Negative	Positive	Negative	Positive
2.04	200	160	50	40	160	80
3.96	360	320	80	65	360	160
6.02	440	420	140	100	560	240
8.13	580	540	200	115	720	400
10.23	900	660	260	145	880	480
12.42	1120	840	340	220	1120	640
14.9	1335	1040	401	280	1450	895
16.63	1680	1200	460	340	1760	1080
18.86	2240	1440	540	380	2080	1440
20.81	----	1760	600	420	2580	2000
27.85	----	1940	630	500	2960	7560
24.8	----	2270	730	600	4180	4100

TABLE A.12

STEEL AND CONCRETE STRAINS AT CRITICAL SECTIONS

Main Steel = 2#4 Compression Steel = 2#3
Steel Fiber = 1.2 d = 6.5 inches

Load (kips)	Main Steel Strains μ in/in		Compression Steel Strains μ in/in		Concrete Strains μ in/in	
	Negative	Positive	Negative	Positive	Negative	Positive
2.04	80	60	40	30	170	80
3.96	180	160	100	80	240	200
6.02	260	240	160	120	400	280
8.13	360	280	200	150	640	320
10.23	480	360	260	180	800	400
12.42	640	480	320	220	1040	560
14.9	880	590	380	260	1280	720
16.63	1040	630	410	280	1340	950
17.3	1100	755	465	290	1630	980
18.86	1540	880	490	310	1720	1200
20.81	2210	1120	560	340	2000	1600
22.85	----	1320	600	380	2320	2080
24.8	----	1600	660	420	2800	2620
27.0	----	2000	760	480	3840	3500
28.4	----	2240	800	500	4880	4600

TABLE A.13

STEEL AND CONCRETE STRAINS AT CRITICAL SECTIONS

Main Steel = 2#5 Compression Steel = 2#3
Steel Fiber = 0.0 d = 6.5 inches

Load (kips)	Main Steel Strains μ in/in		Compression Steel Strains μ in/in		Concrete Strains μ in/in	
	Negative	Positive	Negative	Positive	Negative	Positive
2.04	200	180	50	30	160	80
3.96	400	390	110	80	240	160
6.02	600	580	170	110	360	240
8.13	800	640	220	150	480	360
10.23	960	800	300	200	640	480
12.42	1200	960	380	260	860	640
14.48	1380	1120	440	300	1020	800
16.63	1600	1250	496	363	1290	945
18.86	1850	1480	560	410	1460	1040
20.81	1920	1640	640	460	1560	1280
22.85	2080	1800	700	520	1720	1520
23.93	2175	1880	730	540	1900	1680
24.8	----	2000	760	560	2000	1900
27.0	----	2150	840	620	2600	2240
28.0	----	2270	880	660	3180	2900

TABLE A.14

STEEL AND CONCRETE STRAINS AT CRITICAL SECTIONS

Main Steel = 2#5 Compression Steel = 2#3
Steel Fiber = 0.8 d = 6.5 inches

Load (kips)	Main Steel Strains μ in/in		Compression Steel Strains μ in/in		Concrete Strains μ in/in	
	Negative	Positive	Negative	Positive	Negative	Positive
2.04	120	140	20	20	160	80
3.96	280	260	80	70	320	160
6.02	400	390	115	105	480	240
8.13	440	420	180	180	640	320
10.23	640	630	260	240	800	420
12.42	720	690	340	300	960	570
14.48	880	860	420	360	1200	800
16.63	960	950	480	400	1360	880
18.86	1240	1120	540	450	1520	986
19.4	1395	1200	576	480	1690	1200
20.81	1480	1280	600	500	1720	1240
22.85	1780	1360	650	540	2320	1310
24.8	2080	1540	720	590	2160	1600
25.92	2224	1600	740	610	2240	2000
27.0	----	1820	810	670	2640	2240
29.0	----	1920	860	710	3050	2980
31.28	----	2080	915	750	3700	3290
32.4	----	2300	970	780	4090	4000

TABLE A.15

STEEL AND CONCRETE STRAINS AT CRITICAL SECTIONS

Main Steel = 2#5 Compression Steel = 2#3
Steel Fiber = 1.2 d = 6.5 inches

Load (kips)	Main Steel Strains μ in/in		Compression Steel Strains μ in/in		Concrete Strains μ in/in	
	Negative	Positive	Negative	Positive	Negative	Positive
2.04	160	120	40	30	160	120
3.96	260	230	100	80	320	200
6.02	380	320	170	120	460	320
8.13	480	400	240	180	600	460
10.23	560	440	300	220	800	590
12.42	760	560	360	300	960	800
14.48	820	720	470	380	1200	1000
16.63	930	800	540	420	1360	1200
18.86	1040	960	600	480	1600	1360
19.4	1120	1020	640	490	1720	1440
21.3	1185	1080	694	508	1800	1510
22.85	1440	1150	740	560	2000	1590
24.8	1760	1440	800	620	2360	1920
25.92	1820	1520	840	640	2400	2100
27.0	2170	1600	860	660	2480	2240
29.0	----	1760	920	720	2800	2640
31.28	----	1920	980	780	3600	3000
32.4	----	2080	1000	820	3780	3460
33.0	----	2120	1040	840	4200	3900
34.2	----	2200	1080	860	4610	4500

TABLE A.16

STEEL AND CONCRETE STRAINS AT CRITICAL SECTIONS

Main Steel = 2#6 Compression Steel = 2#3
Steel Fiber = 0.0 d = 6.5 inches

Load (kips)	Main Steel Strains μ in/in		Compression Steel Strains μ in/in		Concrete Strains μ in/in	
	Negative	Positive	Negative	Positive	Negative	Positive
2.04	240	120	180	100	160	80
3.96	360	260	280	240	280	160
6.02	560	420	400	320	400	240
8.13	720	600	560	480	480	320
10.23	880	800	620	560	640	400
12.42	1120	960	800	720	730	540
14.48	1280	1120	960	860	880	600
16.63	1440	1280	1100	970	990	760
18.85	1680	1440	1280	1120	1180	800
20.81	1800	1560	1400	1200	1360	870
24.8	2000	1880	1560	1420	1680	1080
27.0	2160	1920	1840	1680	1840	1240
28.0	2330	2000	1920	1720	1920	1320
29.0	----	2100	2000	1840	2080	1400
31.28	----	2160	2160	2000	2320	1600
33.0	----	2250	2370	2230	2690	2000
35.0	----	2350	2420	2280	3070	2980

TABLE A.17

STEEL AND CONCRETE STRAINS AT CRITICAL SECTIONS

Main Steel = 2#6 Compression Steel = 2#3
Steel Fiber = 0.8 d = 6.5 inches

Load (kips)	Main Steel Strains μ in/in		Compression Steel Strains μ in/in		Concrete Strains μ in/in	
	Negative	Positive	Negative	Positive	Negative	Positive
2.04	120	80	80	85	100	80
3.96	270	190	240	210	360	160
6.02	410	320	400	320	400	290
8.13	560	400	520	400	600	400
10.23	720	520	700	620	740	510
12.42	960	620	840	690	960	640
14.48	1000	800	940	800	1120	780
16.63	1120	880	1100	990	1280	880
18.85	1280	1040	1200	1100	1440	1000
20.81	1420	1120	1400	1400	1580	1120
23.0	1600	1260	1600	1450	1775	1340
24.8	1830	1400	1750	1500	1890	1460
27.0	2080	1520	1860	1580	2000	1520
29.0	2220	1700	2000	1600	2280	1680
30.0	2340	1860	2080	1840	2400	1860
33.0	----	2000	2300	2000	3200	2300
35.0	----	2160	2400	2200	3800	3000
38.3	----	2370	----	2420	4995	4800

TABLE A.18

STEEL AND CONCRETE STRAINS AT CRITICAL SECTIONS

Main Steel = 2#6 Compression Steel = 2#3
Steel Fiber = 1.2 d = 6.5 inches

Load (kips)	Main Steel Strains μ in/in		Compression Steel Strains μ in/in		Concrete Strains μ in/in	
	Negative	Positive	Negative	Positive	Negative	Positive
2.04	120	80	85	60	120	80
3.96	240	160	230	140	280	160
6.02	320	240	310	300	440	290
8.13	400	360	520	460	560	400
10.23	520	470	640	580	720	500
12.42	640	560	800	720	950	620
14.48	760	680	960	860	1100	800
16.63	880	740	1060	960	1280	960
18.85	970	880	1200	1120	1420	1120
20.81	1120	1000	1360	1240	1680	1280
23.0	1200	1080	1440	1400	1930	1500
24.8	1360	1120	1600	1520	2100	1600
26.0	1410	1200	1720	1600	2300	1700
29.0	1470	1440	1860	1720	2480	1910
33.0	2000	1640	2080	1890	2940	2400
34.0	2370	1690	2240	2080	3100	2880
37.9	----	1820	2000	2160	4000	3200
40.0	----	2000	2490	2200	4800	3900
43.4	----	2350	----	2300	5525	5000

Appendix B

Differential Level and Deflection Readings

TABLE B.1

DIFFERENTIAL LEVEL READINGS (INCHES) X 10^{-3}
AT CRITICAL SECTION (UNDER THE LOAD)

Load (kips)	Main Steel 2#4 Top Steel 2#3			Main Steel 2#5 Top Steel 2#3			Main Steel 2#6 Top Steel 2#3		
	0.0% S.F.	0.8% S.F.	1.2% S.F.	0.0% S.F.	0.8% S.F.	1.2% S.F.	0.0% S.F.	0.8% S.F.	1.2% S.F.
0	0	0	0	0	0	0	0	0	0
2.04	20	20	15	10	20	20	19	19	15
3.96	35	98	40	21	39	39	27	40	30
6.02	56	137	60	32	58	79	34	61	45
8.13	76	196	95	41	70	110	42	82	59
10.23	84	255	125	55	96	161	47	102	74
12.42	101	295	150	63	115	200	56	124	93
14.48	118	335	175	75	130	240	63	145	105
16.63	130	374	189	87	151	282	70	160	130
17.0	155	413	110	98	167	315	76	180	144
18.85	210	531	123	109	189	360	82	200	160
20.81	360	768	235	110	210	398	90	215	174
21.8	400	944	315	120	231	436	97	229	195
23.93	---	2145	433	129	249	481	103	241	215
24.8	---	2283	551	157	273	532	110	263	229
25.9	---	----	728	201	295	583	120	285	243
27.16	---	----	1535	276	391	629	129	325	253
28.0	---	----	2055	309	441	1003	140	350	267
28.9	---	----	2657	---	610	1102	160	375	283
30.0	---	----	----	---	760	1181	181	393	300
31.28	---	----	----	---	880	1240	211	450	314
32.4	---	----	----	---	1086	1300	242	669	330
33.6	---	----	----	---	----	1417	285	787	343
34.5	---	----	----	---	----	1771	310	1060	359
35.0	---	----	----	---	----	----	345	1162	379
35.7	---	----	----	---	----	----	---	1220	393
38.3	---	----	----	---	----	----	---	1476	893
40.0	---	----	----	---	----	----	---	----	1393
43.4	---	----	----	---	----	----	----	----	1653

TABLE B.2

ACTUAL DEFLECTIONS X 10^{-3} INCHES

Main Steel = 2#4 Top Steel = 2#3

load	0% Fibers			0.8% Fibers			1.2% Fibers		
(Kips)	Left	Right	Average	Left	Right	Average	Left	Right	Average
0	0	0	0	0	0	0	0	0	0
1.02	7	7	7	5	5	10	6	6	6
2.04	15	15	15	9	9	18	15	15	15
3.03	11	11	22	24	22	23	22	22	22
3.96	15	15	30	15	15	30	24	26	25
4.97	34	36	35	36	34	35	28	32	30
6.02	19	21	40	21	19	40	35	37	36
7.05	24	26	50	46	44	45	39	39	39
8.13	28	32	60	51	49	50	41	43	42
9.16	66	68	67	57	53	55	48	50	49
10.23	73	77	75	61	59	60	56	58	57
11.29	80	82	81	69	67	68	60	62	61
12.42	90	90	90	77	73	75	63	67	65
13.43	93	97	95	83	77	80	66	73	69
14.48	108	112	110	87	83	85	68	76	72
15.53	113	117	115	94	90	92	72	80	76
16.63	116	124	120	102	98	100	75	85	80
17.72	190	210	200	108	102	105	78	90	84
18.86	260	300	280	115	105	110	82	98	90
19.94	490	510	500	127	113	120	84	100	92
20.81	640	700	680	210	190	200	87	103	95
21.8	1300	1700	1500	315	285	300	110	130	120
22.85	-	-	-	650	550	600	145	175	160
23.88	-	-	-	1270	1130	1200	230	290	260
24.8	-	-	-	4300	4700	4500	340	460	400
25.92	-	-	-	-	-	-	520	680	600
27.0	-	-	-	-	-	-	1500	1700	1600
28.4	-	-	-	-	-	-	5600	5800	5700

TABLE B.4

ACTUAL DEFLECTIONS X 10^{-3} INCHES

Main Steel = 2#6 Top Steel = 2#3

load	0% Fibers			0.8% Fibers			1.2% Fibers		
(Kips)	Left	Right	Average	Left	Right	Average	Left	Right	Average
0	0	0	0	0	0	0	0	0	0
1.02	6	6	6	7	7	7	8	8	8
2.04	15	15	15	15	15	15	15	15	15
3.03	20	20	20	17	17	17	17	17	17
3.96	24	26	25	19	21	20	20	20	20
4.97	29	31	30	24	26	25	25	27	26
6.02	34	36	35	29	31	30	30	30	30
7.05	37	37	37	34	36	35	33	37	35
8.13	40	40	40	38	38	38	37	39	38
9.16	44	46	45	39	41	40	39	39	39
10.23	50	52	50	43	43	43	40	40	40
11.29	52	56	54	46	48	47	44	44	44
12.42	56	58	57	49	51	50	47	49	48
13.43	58	62	60	55	55	55	51	51	51
14.48	63	67	65	58	62	60	53	57	55
15.53	69	73	71	64	66	65	58	60	59
16.63	74	76	75	68	72	70	62	64	63
17.72	77	81	79	73	77	75	67	69	68
18.85	82	86	84	78	82	80	68	72	70
19.94	88	90	89	82	84	83	74	76	75
20.81	93	97	95	85	85	85	80	80	80
22.85	102	108	105	87	89	88	85	85	85
24.8	111	119	115	95	105	100	86	86	86
27.0	114	130	122	105	115	110	87	87	87
29.0	150	170	160	110	130	120	110	110	110
31.28	225	255	240	170	210	190	112	118	115
33.0	420	460	440	255	305	280	115	125	120
35.0	1300	1700	1570	410	470	440	123	137	130
37.9	-	-	-	2820	3000	2960	205	235	220
39.0	-	-	-	-	-	-	260	340	300
40.0	-	-	-	-	-	-	350	450	400
42.8	-	-	-	-	-	-	710	810	760
44.0	-	-	-	-	-	-	2850	3750	3300

TABLE B.3

ACTUAL DEFLECTIONS X 10^{-3} INCHES

Main Steel = 2#5 Top Steel = 2#3

load	0% Fibers			0.8% Fibers			1.2% Fibers		
(Kips)	Left	Right	Average	Left	Right	Average	Left	Right	Average
0	0	0	0	0	0	0	0	0	0
1.02	8	8	8	8	8	8	5	5	5
2.04	15	15	15	15	15	15	10	10	10
3.03	22	22	22	16	18	17	15	15	15
3.96	30	30	30	19	21	20	20	20	20
4.97	35	35	35	24	26	25	25	25	25
6.02	38	42	40	28	32	30	29	31	30
7.05	43	47	45	33	37	35	34	36	35
8.13	47	53	50	38	42	40	39	41	40
9.16	54	58	56	41	47	44	40	44	42
10.23	59	65	62	49	55	52	43	47	45
11.29	65	71	68	54	60	57	46	48	47
12.42	74	80	77	59	65	62	49	51	50
13.43	75	81	78	62	70	66	53	57	55
14.48	76	84	80	67	73	70	58	62	60
15.53	80	84	82	72	78	75	63	67	65
16.63	82	88	85	77	83	80	67	73	70
17.72	88	96	92	80	84	82	71	71	74
18.86	104	116	110	83	87	85	74	80	77
19.94	107	123	115	88	92	90	77	83	80
20.81	110	130	120	94	96	95	81	85	83
21.8	145	175	160	106	114	110	84	88	86
22.85	210	250	230	125	135	130	90	95	90
23.88	250	350	300	167	177	172	93	97	95
24.8	360	480	420	210	230	220	95	105	100
25.92	500	600	550	260	300	280	130	140	135
27.0	580	700	640	340	380	360	170	190	180
28.00	1120	1400	1260	400	460	430	200	240	220
29.0	-	-	-	450	590	520	265	315	280
30.0	-	-	-	600	780	690	315	395	370
31.28	-	-	-	840	1040	940	440	520	480
32.4	-	-	-	2570	2770	2670	1200	1600	1400
33.0	-	-	-	-	-	-	2060	2400	2280
34.2	-	-	-	-	-	-	3260	3500	3380

Appendix C

Crack Widths and Crack Patterns

TABLE C.1

CRACK READINGS AT NEGATIVE SECTION

Main Steel = 2#4 Top Steel = 2#3 % Steel Fibers = 0.0 f'_c = 4970 psi

Load (Kips)	P/P_u Ratio	ALL READINGS ARE IN 10^{-4} INCHES INTERVAL																			
		1	2	3	4	5	6	7	8	9	10	11	12	13	14	15	16	17	18	19	20
0.0	0	0	0	0	0	0	0	0	0	0	0	0	0	0	0	0	0	0	-	-	-
1.02	0.05	3	3	0	7	0	11	2	0	0	0	2	0	0	0	0	0	1	-	-	-
2.04	0.09	3	4	0	7	4	12	2	7	0	0	3	0	1	5	2	1	2	-	-	-
3.03	0.14	3	4	2	10	4	18	4	7	0	1	5	2	1	5	3	1	2	-	-	-
3.96	0.18	3	-	2	13	4	18	5	7	0	1	5	5	1	5	6	3	2	-	-	-
6.02	0.28	6	-	2	18	10	22	5	15	0	2	5	5	-	-	10	8	-	-	-	-
8.13	0.37	6	-	-	25	11	22	-	22	7	7	-	5	-	-	13	10	-	-	-	-
10.23	0.47	10	-	-	27	12	22	-	42	70	44	-	5	-	-	17	15	-	-	-	-
13.43	0.62	23	-	-	60	35	22	-	42	86	87	-	10	-	-	32	22	-	-	-	-
14.48	0.66	29	-	4	74	70	-	-	52	115	112	-	10	-	-	52	48	-	-	-	-
17.72	0.81	46	-	4	80	113	-	-	59	133	125	-	-	-	-	90	80	-	-	-	-

TABLE C.2

CRACK READINGS AT NEGATIVE SECTION

Main Steel = 2#4 Top Steel = 2#3 % Steel Fibers = 0.8 f'_c = 5180 psi

Load (Kips)	P/P_u Ratio	ALL READINGS ARE IN 10^{-4} INCHES INTERVAL																			
		1	2	3	4	5	6	7	8	9	10	11	12	13	14	15	16	17	18	19	20
0.0	0	0	0	0	0	0	0	0	0	0	0	0	0	0	0	0	0	0	0	0	-
1.02	0.04	0	0	0	0	0	0	0	0	0	0	0	7	0	0	0	0	0	0	0	-
2.04	0.08	0	0	0	0	0	3	2	0	1	0	1	9	0	0	0	3	0	1	-	-
3.96	0.16	0	1	2	2	1	4	-	1	3	2	1	9	5	-	0	3	-	2	-	-
6.02	0.24	-	-	-	-	-	-	-	-	13	-	-	-	-	-	-	-	-	-	-	-
8.13	0.33	-	-	-	-	-	-	20	-	18	34	-	-	30	-	-	-	-	-	-	-
10.23	0.41	-	-	-	-	-	-	55	-	21	48	-	-	47	-	32	-	-	-	-	-
12.42	0.50	-	-	-	-	-	-	61	-	33	60	-	-	60	-	32	23	-	-	-	-
14.48	0.58	-	-	-	-	-	34	67	-	41	68	-	-	62	-	35	33	-	-	-	-
16.63	0.67	62	-	-	-	-	55	80	-	53	100	-	-	80	-	35	63	-	-	-	-
19.94	0.8	97	-	-	-	-	102	87	-	24	140	-	-	105	-	35	190	-	-	-	-

TABLE C.3

CRACK READINGS AT NEGATIVE SECTION

Main Steel = 2#4 Top Steel = 2#3 % Steel Fibers = 1.2 f'_c = 5275 psi

Load (Kips)	P/P_u Ratio	ALL READINGS ARE IN 10^{-4} INCHES INTERVAL																			
		1	2	3	4	5	6	7	8	9	10	11	12	13	14	15	16	17	18	19	20
0.0	0	0	0	0	0	0	0	0	0	0	0	0	0	0	0	0	0	0	0	0	-
1.02	0.04	0	0	0	2	0	0	2	0	0	0	0	0	0	0	0	0	0	0	0	-
3.04	0.11	0	0	0	2	5	2	12	2	4	4	0	0	0	0	0	0	0	0	0	-
4.97	0.17	1	0	0	-	5	2	17	2	4	5	2	0	-	4	0	0	10	3	0	-
7.05	0.24	1	1	8	-	-	4	20	4	8	8	3	0	-	4	0	5	10	3	0	-
9.16	0.32	-	1	8	-	-	20	27	4	33	14	4	2	-	4	8	13	20	3	2	-
11.29	0.4	-	-	-	-	-	34	32	-	33	20	4	15	-	-	24	28	20	-	-	-
13.43	0.46	-	-	-	-	-	42	42	-	-	28	-	31	-	-	34	40	-	-	-	-
16.63	0.58	-	40	-	-	-	52	53	-	-	45	-	50	-	-	47	55	-	23	-	-
18.86	0.65	-	55	60	-	-	100	117	-	-	73	-	85	-	-	74	60	-	33	-	-
20.81	0.72	-	65	75	-	-	126	143	-	-	88	-	90	-	-	97	65	-	43	-	-

TABLE C.4

CRACK READINGS AT NEGATIVE SECTION

Main Steel = 2#5 Top Steel = 2#3 % Steel Fibers = 0.0 f'_c = 4970 psi

Load (Kips)	P/P_u Ratio	ALL READINGS ARE IN 10^{-4} INCHES — INTERVAL																			
		1	2	3	4	5	6	7	8	9	10	11	12	13	14	15	16	17	18	19	20
0.0	0	0	0	0	0	0	0	0	0	0	0	0	0	0	0	0	0	0	0	0	0
1.02	0.04	-	-	0	0	1	0	0	2	0	0	0	0	0	0	0	0	0	0	0	-
2.04	0.07	-	-	0	0	8	0	0	2	0	0	0	0	4	2	-	0	0	0	2	-
3.03	0.11	-	-	0	3	8	4	-	2	-	3	0	9	6	2	-	2	0	-	2	-
3.96	0.14	-	-	1	3	22	7	-	-	-	3	2	27	19	-	-	7	-	-	2	-
4.97	0.18	-	-	-	3	22	19	-	-	1	-	2	35	37	-	-	-	-	-	-	-
6.02	0.22	-	-	-	-	33	24	-	-	-	-	4	45	42	-	-	-	-	-	-	-
8.13	0.29	-	-	-	-	54	42	-	-	2	-	4	65	-	-	-	-	-	-	-	-
10.23	0.37	-	-	-	-	69	55	-	-	-	-	-	85	-	-	-	-	-	-	-	-
13.43	0.48	-	-	-	-	81	77	-	-	-	-	-	95	-	-	-	-	-	-	-	-
16.63	0.6	-	-	-	-	104	100	-	-	66	-	-	99	-	-	-	-	-	-	-	-
18.86	0.67	-	-	-	-	204	167	-	-	91	-	-	120	-	-	-	-	-	-	-	-
20.81	0.74	-	-	-	-	264	347	-	-	187	-	-	175	-	-	-	-	-	-	-	-

TABLE C.5

CRACK READINGS AT NEGATIVE SECTION

Main Steel = 2#5 Top Steel = 2#3 % Steel Fibers = 0.8 f'_c = 5180 psi

Load (Kips)	P/P_u Ratio	ALL READINGS ARE IN 10^{-4} INCHES — INTERVAL																			
		1	2	3	4	5	6	7	8	9	10	11	12	13	14	15	16	17	18	19	20
0.0	0	0	0	0	0	0	0	0	0	0	0	0	0	0	0	0	0	0	0	0	-
2.04	0.06	2	2	0	0	2	3	1	3	2	0	0	1	0	0	0	0	0	0	2	-
3.95	0.12	2	2	3	2	4	3	2	5	4	2	0	2	4	1	1	2	2	1	8	-
6.02	0.19	2	2	4	2	6	-	4	5	24	12	1	2	4	2	4	2	4	5	8	-
8.13	0.25	-	-	-	5	6	-	-	-	29	27	-	-	-	-	-	-	-	5	-	-
10.23	0.32	-	-	-	-	32	-	22	-	-	28	-	-	-	42	-	-	-	-	-	-
12.42	0.38	-	-	-	-	54	-	30	-	-	45	-	-	-	47	-	16	-	-	-	-
14.48	0.45	-	-	-	-	64	-	36	-	-	55	-	-	-	57	-	34	-	-	-	-
16.63	0.51	-	29	-	-	69	-	42	-	-	64	-	-	-	67	-	44	-	-	-	-
18.86	0.58	-	45	-	-	84	-	52	-	-	79	-	-	-	82	-	54	-	-	-	-
20.81	0.64	-	55	-	-	119	-	57	-	-	147	-	-	-	102	-	84	-	-	-	-
22.85	0.71	-	65	-	-	129	-	62	-	-	180	-	-	-	117	-	102	-	-	-	-
24.80	0.77	-	75	-	-	136	-	67	-	-	243	-	-	-	147	-	107	-	-	-	-

TABLE C.6

CRACK READINGS AT NEGATIVE SECTION

Main Steel = 2#5 Top Steel = 2#3 % Steel Fibers = 1.2 f'_c = 5275 psi

Load (Kips)	P/P_u Ratio	ALL READINGS ARE IN 10^{-4} INCHES INTERVAL																			
		1	2	3	4	5	6	7	8	9	10	11	12	13	14	15	16	17	18	19	20
0.0	0	0	0	0	0	0	0	0	0	0	0	0	0	0	0	0	0	0	0	0	0
2.04	0.06	0	5	0	0	1	0	0	0	2	0	0	0	0	0	0	0	0	0	0	-
3.96	0.11	0	8	0	0	2	2	1	3	4	6	0	0	0	1	0	0	2	0	0	-
6.02	0.17	5	7	2	5	8	8	6	15	9	7	2	3	4	2	2	0	2	5	0	-
8.13	0.24	5	7	2	5	8	8	6	25	19	7	2	10	16	6	2	3	10	5	2	-
10.23	0.30	-	-	-	-	-	-	-	35	28	-	-	30	26	6	-	5	-	-	-	-
12.42	0.36	-	-	-	-	-	-	-	50	36	-	-	45	39	-	-	-	-	-	-	-
14.48	0.42	-	-	-	-	30	43	-	65	45	-	-	58	46	-	27	-	-	-	-	-
16.63	0.48	-	-	-	-	44	58	21	70	51	-	-	64	55	-	32	-	-	-	-	-
18.86	0.55	-	-	-	-	55	73	26	72	62	-	-	66	66	-	32	-	-	-	-	-
20.81	0.60	-	-	-	-	70	78	36	78	74	-	-	73	71	-	52	-	-	-	-	-
22.85	0.66	-	-	-	-	90	118	46	145	128	-	-	104	101	-	57	-	-	-	-	-
24.8	0.72	-	-	-	-	95	133	46	227	233	-	-	149	136	-	102	-	-	-	-	-

TABLE C.7

CRACK READINGS AT NEGATIVE SECTION

Main Steel = 2#6 Top Steel = 2#3 % Steel Fibers = 0.0 f'_c = 4970 psi

Load (Kips)	P/P_u Ratio	ALL READINGS ARE IN 10^{-4} INCHES — INTERVAL																			
		1	2	3	4	5	6	7	8	9	10	11	12	13	14	15	16	17	18	19	20
0.0	0	0	0	0	0	0	0	0	0	0	0	0	0	0	0	0	0	0	0	0	0
1.02	0.03	3	0	2	0	0	0	2	0	1	1	0	0	0	0	0	0	0	2	0	-
2.04	0.06	3	1	8	1	1	0	4	1	2	1	0	-	2	0	0	2	2	3	1	-
3.03	0.09	3	2	8	1	1	2	4	8	5	1	5	-	2	0	0	2	2	5	3	-
3.96	0.11	3	3	9	-	2	-	-	35	5	2	5	-	2	2	2	2	6	-	5	-
6.02	0.17	3	6	13	-	-	-	-	58	-	-	9	-	23	17	-	-	-	-	-	-
8.13	0.23	-	16	16	-	-	-	-	68	-	-	-	-	45	33	-	-	-	-	-	-
10.23	0.29	-	32	46	-	-	-	-	73	-	-	-	-	68	43	-	-	-	-	-	-
12.42	0.35	-	48	67	-	-	-	-	78	-	-	-	-	73	60	-	-	-	-	-	-
14.48	0.41	-	73	71	-	-	-	-	81	-	-	-	-	78	70	-	-	-	-	-	-
16.63	0.48	-	80	74	-	-	-	-	93	-	-	-	-	83	75	-	-	-	-	-	-
18.86	0.54	-	88	83	-	-	-	-	104	-	-	-	-	88	75	-	-	-	-	-	-
20.81	0.57	-	98	91	-	-	-	-	107	-	-	-	-	103	94	-	-	-	-	-	-
22.85	0.65	-	103	203	-	-	-	-	254	-	-	-	-	243	185	-	-	-	-	-	-
24.9	0.71	-	216	214	-	-	-	-	267	-	-	-	-	261	205	-	-	-	-	-	-

TABLE C.8

CRACK READINGS AT NEGATIVE SECTION

Main Steel = 2#6 Top Steel = 2#3 % Steel Fibers = 0.8 f'_c = 5180 psi

Load (Kips)	P/P_u Ratio	ALL READINGS ARE IN 10^{-4} INCHES INTERVAL																			
		1	2	3	4	5	6	7	8	9	10	11	12	13	14	15	16	17	18	19	20
0.0	0	0	0	0	0	0	0	0	0	0	0	0	0	0	0	0	0	0	0	0	0
1.08	0.03	0	1	7	1	5	0	2	2	1	-	0	0	0	0	0	2	0	0	0	-
3.03	0.08	1	1	14	10	9	1	2	7	2	-	1	0	1	0	0	2	0	0	0	-
4.97	0.13	1	-	17	13	9	2	2	12	6	-	5	6	2	0	2	5	0	0	3	-
7.05	0.18	4	-	19	13	9	2	3	22	22	-	5	18	6	4	7	5	1	1	3	-
10.23	0.27	-	-	21	18	25	2	3	42	36	-	33	38	8	9	22	10	-	1	-	-
14.43	0.38	-	-	24	23	30	-	-	49	47	-	48	38	-	-	32	25	-	-	-	-
15.53	0.41	-	-	24	28	35	-	-	57	52	-	58	-	-	-	42	30	-	-	-	-
17.72	0.46	-	-	-	38	39	-	-	65	62	-	68	-	15	-	-	35	-	-	-	-
20.81	0.54	-	-	-	48	47	-	-	80	66	-	83	-	23	-	57	40	-	-	-	-
23.88	0.62	-	-	-	75	47	-	-	92	85	-	92	-	33	-	84	50	-	-	-	-
27.0	0.70	-	-	-	102	65	-	-	135	85	-	143	-	33	-	111	60	-	-	-	-
30.21	0.79	-	-	-	137	100	-	-	149	95	-	168	-	38	-	126	70	-	-	-	-

TABLE C.9

CRACK READINGS AT NEGATIVE SECTION

Main Steel = 2#6 Top Steel = 2#3 % Steel Fibers = 1.2 f'_c = 5275 psi

Load (Kips)	P/P_u Ratio	ALL READINGS ARE IN 10^{-4} INCHES INTERVAL																			
		1	2	3	4	5	6	7	8	9	10	11	12	13	14	15	16	17	18	19	20
0.0	0	0	0	0	0	0	0	0	0	0	0	0	0	0	0	0	0	0	0	0	-
2.04	0.05	2	10	8	0	1	0	0	0	9	1	0	0	3	0	8	0	0	0	0	-
3.96	0.09	7	10	8	5	4	5	5	0	9	1	8	1	3	0	10	0	1	0	3	-
6.02	0.14	9	15	13	9	8	10	10	0	9	1	8	1	5	5	13	0	1	5	3	-
8.13	0.19	9	15	14	9	8	10	10	0	19	8	8	3	5	7	13	5	1	5	3	-
10.23	0.24	9	20	14	9	13	20	13	2	26	13	10	10	10	15	18	10	6	5	8	-
12.42	0.27	-	-	-	-	-	-	13	-	33	30	-	-	10	-	18	-	-	-	-	-
14.48	0.33	-	-	-	-	18	-	-	-	46	38	-	25	-	-	-	-	-	-	-	-
16.63	0.38	-	-	-	-	28	55	-	-	46	43	-	35	-	-	-	-	-	-	-	-
18.86	0.43	-	25	-	-	30	55	-	-	-	48	-	40	-	35	-	30	-	-	-	-
20.81	0.48	-	35	-	-	-	60	-	-	-	58	-	45	-	37	-	30	-	-	-	-
22.85	0.53	-	40	-	-	38	75	-	-	-	78	-	55	-	47	-	35	-	-	-	-
24.8	0.57	-	45	-	-	42	80	-	-	-	87	-	65	-	65	-	40	-	-	18	-
27.0	0.62	-	55	-	29	48	90	-	-	-	93	-	65	-	75	-	50	-	-	23	-
29.0	0.67	-	62	-	34	73	100	-	-	-	104	-	70	-	80	-	50	-	-	23	-
32.4	0.75	-	75	-	44	73	114	-	-	-	128	-	70	-	100	-	55	-	-	28	-

TABLE C.10

CRACK READINGS AT POSITIVE SECTION

Main Steel = 2#4 Top Steel = 2#3 % Steel Fibers = 0.0 f'_c = 4970 psi

Load (Kips)	P/P_u Ratio	ALL READINGS ARE IN 10^{-4} INCHES INTERVAL																			
		1	2	3	4	5	6	7	8	9	10	11	12	13	14	15	16	17	18	19	20
0.0	0	0	0	0	0	0	0	0	0	0	0	0	0	0	0	0	0	0	0	0	0
0.05	1.02	1	2	0	0	0	25	0	0	0	0	11	15	5	5	2	0	0	0	1	0
0.09	2.04	2	2	5	1	3	25	0	0	0	0	34	15	5	5	5	5	0	0	5	0
0.14	3.03	3	2	5	2	5	28	5	10	3	0	35	20	8	25	7	7	0	5	5	-
0.18	3.96	3	4	5	2	8	30	13	15	5	0	35	25	25	35	7	15	15	15	5	-
0.28	6.02	-	-	-	-	20	35	20	20	5	0	43	25	30	45	15	15	20	25	-	-
0.37	8.13	-	-	-	-	25	40	22	22	10	0	50	25	40	50	15	15	35	35	-	-
0.47	10.23	-	-	-	-	35	44	24	30	16	5	55	25	55	67	15	15	49	50	-	-
0.62	13.43	-	-	-	-	40	52	25	34	25	14	58	25	70	80	25	20	71	65	-	-
0.66	14.48	-	-	-	-	45	65	26	36	33	20	60	25	80	105	32	35	80	85	-	-
0.81	17.72	-	-	-	-	55	70	28	38	35	30	80	25	85	118	45	45	90	99	-	-

TABLE C.11

CRACK READINGS AT POSITIVE SECTION

Main Steel = 2#4 Top Steel = 2#3 % Steel Fibers = 0.8 f'_c = 5180 psi

Load (Kips)	P/P_u Ratio	ALL READINGS ARE IN 10^{-4} INCHES INTERVAL																			
		1	2	3	4	5	6	7	8	9	10	11	12	13	14	15	16	17	18	19	20
0.0	0	0	0	0	0	0	0	0	0	0	0	0	0	0	0	0	0	0	0	0	0
1.02	0.04	0	1	12	0	0	2	0	0	0	0	0	0	0	0	0	0	0	4	0	-
2.04	0.08	2	2	25	5	1	4	1	3	0	5	9	3	0	4	0	0	2	5	0	-
3.96	0.16	10	2	25	15	-	-	13	3	3	5	19	15	3	5	2	10	12	-	-	-
6.02	0.24	-	-	-	28	-	-	13	-	-	-	42	25	3	-	-	30	-	-	-	-
8.13	0.33	-	-	-	43	-	-	-	-	-	-	52	37	-	-	-	46	-	-	-	-
10.23	0.41	-	-	-	48	-	-	-	-	-	20	54	47	-	-	-	54	-	-	-	-
12.42	0.50	23	-	-	53	-	57	-	-	-	40	60	53	-	-	-	57	-	-	-	-
14.48	0.58	26	-	-	56	-	65	-	-	-	65	63	64	-	29	-	59	-	-	-	-
16.63	0.67	34	-	-	103	-	74	-	-	-	98	122	123	-	54	-	82	-	-	-	-
16.94	0.8	34	-	-	118	-	84	-	-	-	370	307	398	-	54	-	92	-	-	-	-

TABLE C.12

CRACK READINGS AT POSITIVE SECTION

Main Steel = 2#4 Top Steel = 2#3 % Steel Fibers = 1.2 f'_c = 5275 psi

Load (Kips)	P/P_u Ratio	ALL READINGS ARE IN 10^{-4} INCHES INTERVAL																			
		1	2	3	4	5	6	7	8	9	10	11	12	13	14	15	16	17	18	19	20
0.0	0	0	0	0	0	0	0	0	0	0	0	0	0	0	0	0	0	0	0	0	0
1.02	0.04	1	7	3	5	0	5	0	2	1	1	4	4	4	3	5	7	0	1	4	-
3.04	0.11	4	10	7	10	2	8	4	2	1	7	7	9	4	5	11	7	0	7	4	-
4.97	0.17	8	10	13	18	2	20	4	2	13	14	8	16	9	8	11	8	-	7	7	-
7.05	0.24	10	-	15	25	2	22	13	4	17	19	-	16	-	8	26	11	-	7	7	-
9.16	0.32	20	-	18	28	5	30	17	4	26	29	-	19	14	-	26	16	-	-	7	-
11.29	0.4	-	-	25	35	-	35	27	-	33	32	-	-	-	-	-	-	-	-	-	-
13.43	0.46	-	-	30	40	-	40	37	-	46	37	-	-	-	-	-	-	-	-	-	-
16.63	0.58	-	-	49	48	-	50	42	-	50	45	-	-	-	-	-	41	-	-	-	-
18.86	0.65	41	-	57	60	-	80	42	-	106	77	-	-	24	-	-	61	-	-	-	-
20.81	0.72	56	-	65	100	-	95	44	-	156	102	-	-	34	-	-	66	-	-	-	-

TABLE C.13

CRACK READINGS AT POSITIVE SECTION

Main Steel = 2#5 Top Steel = 2#3 % Steel Fibers = 0.0 f'_c = 4970 psi

Load (Kips)	P/P_u Ratio	ALL READINGS ARE IN 10^{-4} INCHES INTERVAL																			
		1	2	3	4	5	6	7	8	9	10	11	12	13	14	15	16	17	18	19	20
0.0	0	0	0	0	0	0	0	0	0	0	0	0	0	0	0	0	0	0	0	0	0
1.02	0.04	1	3	1	1	3	0	0	0	2	2	5	0	2	2	1	-	0	0	0	-
2.04	0.07	1	3	2	13	3	0	0	2	2	3	5	10	18	8	1	-	0	2	2	-
3.03	0.11	1	6	9	14	3	0	22	27	2	5	11	10	20	16	1	-	13	15	4	-
3.96	0.14	4	8	21	26	3	0	30	38	4	5	14	20	21	16	-	-	15	18	5	-
4.97	0.18	-	-	-	-	5	5	40	46	6	10	14	-	-	-	-	-	-	-	-	-
6.02	0.27	-	-	-	-	-	7	50	56	9	10	-	-	-	-	-	-	-	-	-	-
8.13	0.29	-	-	48	48	-	10	60	-	-	13	-	50	51	-	-	-	30	-	-	-
10.23	0.37	-	-	55	69	-	-	70	-	-	-	-	55	61	-	-	-	40	-	-	-
13.43	0.48	-	-	70	-	-	-	75	-	-	-	-	77	76	-	-	-	70	73	-	-
16.63	0.60	-	-	100	99	-	-	100	-	-	-	-	94	100	-	-	-	100	98	-	-
18.86	0.67	-	-	115	116	-	-	175	-	-	-	-	115	109	-	-	-	210	113	-	-
20.81	0.74	-	-	205	223	-	-	288	-	-	-	-	219	133	-	-	-	304	148	-	-

TABLE C.14

CRACK READINGS AT POSITIVE SECTION

Main Steel = 2#5 Top Steel = 2#3 % Steel Fibers = 0.8 f'_c = 5180 psi

Load (Kips)	P/P_u Ratio	ALL READINGS ARE IN 10^{-4} INCHES INTERVAL																			
		1	2	3	4	5	6	7	8	9	10	11	12	13	14	15	16	17	18	19	20
0.0	0	0	0	0	0	0	0	0	0	0	0	0	0	0	0	0	0	0	0	0	0
2.04	0.06	1	0	3	0	2	0	5	5	2	1	0	15	0	0	8	5	2	6	6	-
3.95	0.12	8	-	10	3	5	1	10	12	5	3	8	22	2	2	10	14	2	6	8	-
6.02	0.19	8	-	23	3	5	2	14	18	5	3	13	25	2	4	20	18	-	6	14	-
8.13	0.25	14	-	26	13	-	-	22	25	-	-	17	30	-	-	25	25	-	-	19	-
10.23	0.32	-	-	-	-	-	-	-	32	-	-	23	34	-	-	-	25	-	-	-	-
12.42	0.38	-	-	31	30	-	-	-	41	-	-	37	42	-	-	43	-	-	-	-	-
14.48	0.45	-	-	42	38	-	-	-	52	-	-	47	47	-	-	54	-	-	-	-	-
16.63	0.51	-	-	57	48	-	-	-	70	-	-	54	59	-	-	62	-	-	-	54	-
18.86	0.58	-	-	69	58	-	-	-	78	-	-	76	72	-	-	69	-	-	-	60	-
20.81	0.64	-	-	98	68	-	-	-	103	-	-	1--	92	-	-	85	-	-	-	78	-
22.85	0.71	-	-	112	78	-	-	-	125	-	-	112	127	-	-	95	-	-	-	83	-
24.8	0.77	-	-	132	92	-	-	-	130	-	-	148	245	-	-	100	-	-	-	88	-

TABLE C.15

CRACK READINGS AT POSITIVE SECTION

Main Steel = 2#5 Top Steel = 2#3 % Steel Fibers = 1.2 f'_c = 5275 psi

Load (Kips)	P/P_u Ratio	ALL READINGS ARE IN 10^{-4} INCHES INTERVAL																			
		1	2	3	4	5	6	7	8	9	10	11	12	13	14	15	16	17	18	19	20
0.0	0	0	0	0	0	0	0	0	0	0	0	0	0	0	0	0	0	0	0	0	-
2.04	0.06	0	5	0	2	0	1	0	3	7	0	5	5	0	1	9	0	0	0	0	-
3.96	0.11	5	5	7	5	5	7	0	3	8	0	8	8	5	6	9	0	0	5	10	-
6.02	0.17	10	5	17	10	15	11	23	28	16	8	7	8	10	6	9	2	2	15	20	-
8.13	0.24	10	-	17	15	25	17	23	30	16	8	12	9	15	8	17	9	2	15	20	-
10.23	0.30	-	-	-	15	30	17	23	38	21	-	17	-	25	-	17	24	-	-	20	-
12.42	0.36	-	-	-	-	35	-	-	43	21	-	24	-	31	-	-	29	-	-	-	-
14.48	0.42	-	-	-	-	40	-	-	48	21	-	36	-	38	-	-	34	-	-	-	-
16.63	0.48	-	-	-	-	49	-	-	58	26	-	42	-	45	-	-	39	-	-	-	-
18.86	0.55	-	-	-	-	60	-	-	68	31	-	52	-	50	-	-	49	-	-	-	-
20.81	0.60	-	-	-	-	68	-	-	73	51	-	71	-	63	-	-	65	-	-	-	-
22.85	0.66	-	-	-	-	80	-	-	78	61	-	169	-	100	-	-	89	-	-	-	-
24.8	0.72	-	-	-	-	80	-	-	83	69	-	277	-	160	-	-	109	-	-	-	-

TABLE C.16

CRACK READINGS AT POSITIVE SECTION

Main Steel = 2#6 Top Steel = 2#3 % Steel Fibers = 0.0 f'_c = 4970 psi

Load (Kips)	P/P_u Ratio	ALL READINGS ARE IN 10^{-4} INCHES — INTERVAL																			
		1	2	3	4	5	6	7	8	9	10	11	12	13	14	15	16	17	18	19	20
0.0	0	0	0	0	0	0	0	0	0	0	0	0	0	0	0	0	0	0	0	0	0
1.02	0.03	1	2	5	1	2	0	0	3	1	5	2	1	3	10	1	0	0	1	1	-
2.04	0.06	3	7	5	2	2	0	1	7	1	5	5	17	8	10	1	0	0	3	6	-
3.03	0.09	3	7	8	6	7	4	13	12	3	-	7	22	16	10	3	0	3	13	17	-
3.96	0.11	3	7	12	10	7	5	16	17	-	-	7	45	2-	11	3	1	5	23	33	-
6.02	0.17	11	-	-	-	-	7	20	30	-	-	-	50	48	12	-	-	-	37	46	-
8.13	0.23	21	-	-	-	-	10	30	-	-	-	-	65	60	16	-	-	-	47	48	-
10.23	0.29	27	-	-	-	-	10	50	35	-	-	-	78	68	16	-	-	-	47	56	-
12.42	0.35	31	-	39	37	-	-	50	-	-	-	-	80	73	-	38	39	-	58	56	-
14.48	0.41	48	-	47	45	-	-	55	-	-	-	-	85	-	-	38	49	-	63	-	-
16.63	0.48	48	-	52	50	-	-	65	-	-	-	-	90	78	-	-	59	-	83	66	-
18.86	0.54	53	-	67	65	-	-	67	-	-	-	-	90	83	-	-	69	-	93	81	-
20.81	0.59	58	-	74	75	-	-	72	79	-	-	-	95	103	-	-	83	-	103	96	-
22.85	0.65	123	-	97	108	-	-	110	105	-	-	-	255	206	-	-	124	-	128	146	-
24.9	0.71	268	-	207	215	-	-	225	201	-	-	-	265	310	-	-	143	-	158	216	-

TABLE C.17

CRACK READINGS AT POSITIVE SECTION

Main Steel = 2#6 Top Steel = 2#3 % Steel Fibers = 0.8 f'_c = 5180 psi

Load (Kips)	P/P_u Ratio	ALL READINGS ARE IN 10^{-4} INCHES INTERVAL																			
		1	2	3	4	5	6	7	8	9	10	11	12	13	14	15	16	17	18	19	20
0.0	0	0	0	0	0	0	0	0	0	0	0	0	0	0	0	0	0	0	0	0	0
1.08	0.03	2	1	11	0	1	1	2	3	0	0	1	0	4	5	0	0	0	0	0	-
3.03	0.08	3	8	15	10	7	1	6	15	3	0	7	10	20	0	0	0	5	7	2	-
4.97	0.13	5	17	21	18	7	2	12	17	3	0	12	15	34	0	5	4	17	19	2	-
7.05	0.18	5	25	35	18	7	3	32	35	3	3	12	20	60	0	5	4	25	25	2	-
10.23	0.27	-	35	41	18	-	14	32	35	32	23	17	30	60	7	15	15	37	35	-	-
13.43	0.38	-	42	-	-	-	-	37	35	32	-	27	40	62	7	15	15	39	45	-	-
15.53	0.41	-	58	41	-	-	-	42	-	-	-	27	50	73	-	-	-	50	55	-	-
17.72	0.46	-	58	51	-	-	-	52	-	-	-	-	50	-	-	-	-	57	60	-	-
20.81	0.51	-	-	71	-	-	-	57	-	-	25	-	-	80	-	-	-	70	73	-	-
23.88	0.62	-	-	81	-	-	-	78	-	-	35	-	-	85	-	-	-	75	81	-	-
27.0	0.70	-	-	31	-	-	-	102	-	-	58	-	-	130	-	-	-	125	100	-	-
30.21	0.79	-	-	36	-	-	-	102	-	-	73	-	-	145	-	-	-	145	110	-	-

TABLE C.18

CRACK READINGS AT POSITIVE SECTION

Main Steel = 2#6 Top Steel = 2#3 % Steel Fibers = 1.2 f'_c = 5275 psi

Load (Kips)	P/P_u Ratio	ALL READINGS ARE IN 10^{-4} INCHES INTERVAL																			
		1	2	3	4	5	6	7	8	9	10	11	12	13	14	15	16	17	18	19	20
0.0	0	0	0	0	0	0	0	0	0	0	0	0	0	0	0	0	0	0	0	0	0
2.04	0.05	5	4	4	9	10	8	4	0	7	8	0	5	2	5	5	5	0	0	5	-
3.96	0.09	8	10	5	11	20	8	10	10	10	18	0	27	2	10	5	15	4	2	5	-
6.02	0.14	15	11	7	11	25	8	15	2-	25	23	5	31	16	10	10	20	9	5	10	-
8.13	0.19	20	16	7	14	30	5	15	30	25	28	5	31	34	20	15	20	9	5	15	-
10.23	0.24	30	21	17	14	30	15	15	30	35	43	13	40	39	25	25	-	19	5	15	-
12.42	0.27	-	21	17	-	30	-	-	-	35	-	13	45	49	-	-	-	-	-	-	-
14.48	0.33	-	-	-	-	-	-	-	-	-	-	-	50	51	35	35	-	-	-	-	-
16.63	0.38	-	-	-	-	-	45	-	-	-	43	-	55	59	35	-	-	-	-	-	-
18.86	0.43	60	-	-	-	-	60	-	-	-	48	-	58	63	-	-	-	-	-	-	-
20.81	0.48	60	-	-	-	-	65	-	-	-	58	-	60	70	-	35	-	-	-	-	-
22.85	0.53	75	-	-	-	-	70	-	-	-	68	-	60	75	-	40	-	70	-	55	-
24.8	0.57	80	-	-	-	-	76	-	50	-	68	-	65	75	-	45	-	80	-	60	-
27.0	0.62	105	-	-	-	-	117	-	58	-	76	-	80	83	-	105	-	119	-	70	-
29.0	0.67	120	-	-	-	-	140	-	70	-	98	-	115	125	-	110	-	164	-	75	-
32.4	0.75	150	-	-	-	-	145	-	75	-	108	-	150	140	-	125	-	189	-	80	-

Initial crack appeared at 3.96 k ($0.18\ P_u$)

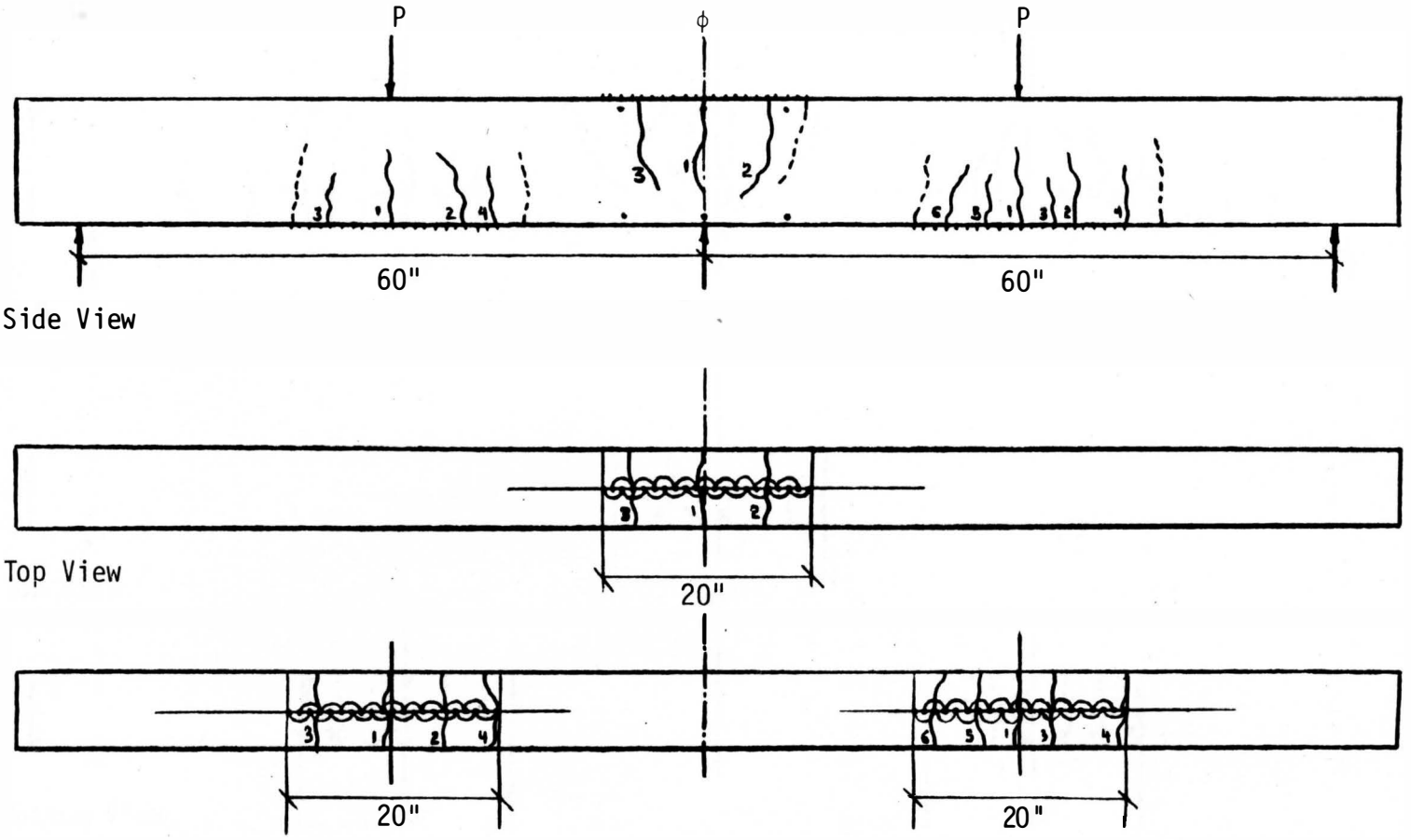

cracks appeared at service load cracks appeared at ultimate load

Figure C.1. Crack pattern in Beam No. 1.

Initial crack appeared at 4.68 k ($0.17\ P_u$)

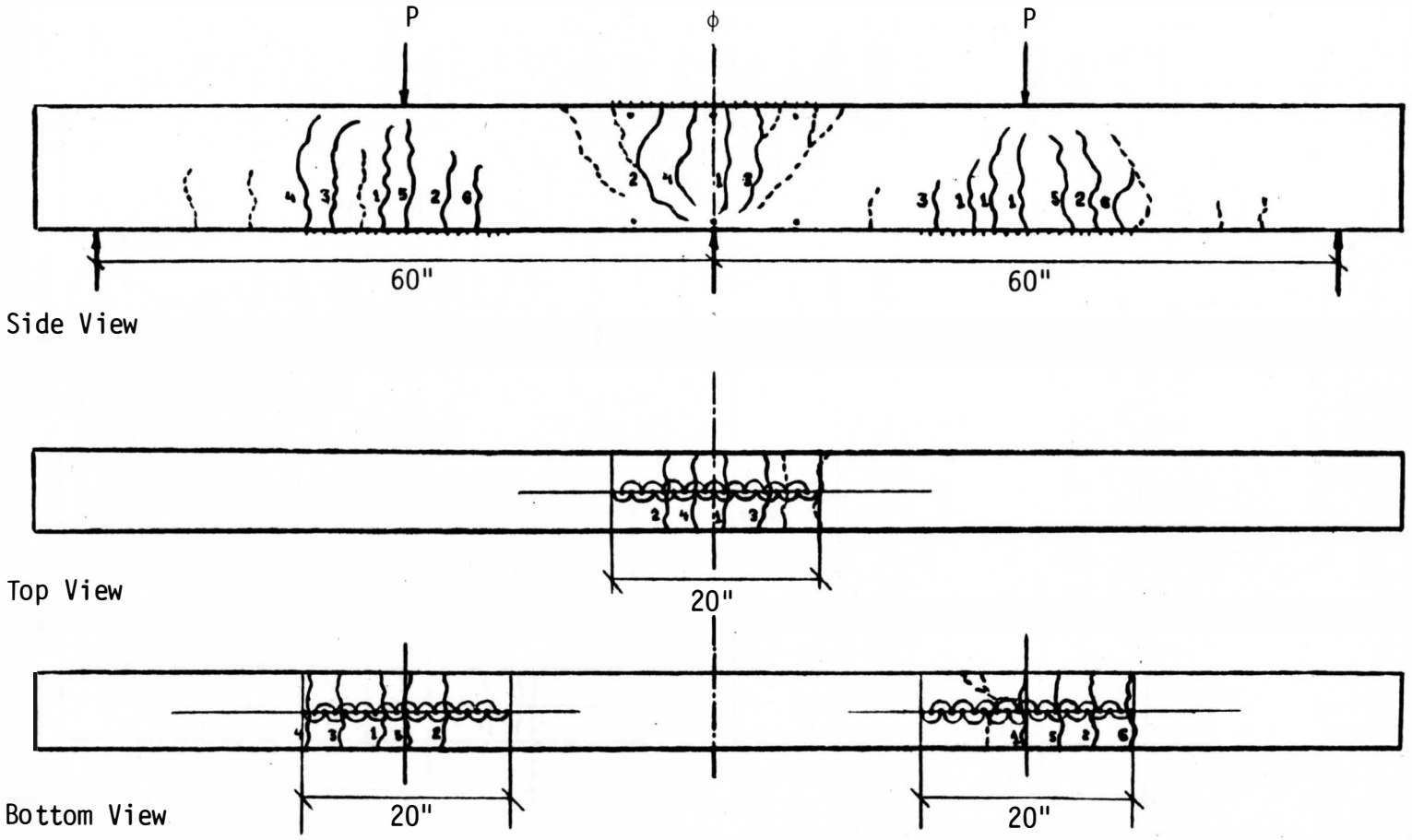

cracks appeared at service load

cracks appeared at ultimate load

Figure C.2. Crack pattern in Beam No. 2.

Initial crack appeared at 5.49 k (0.16 P_u)

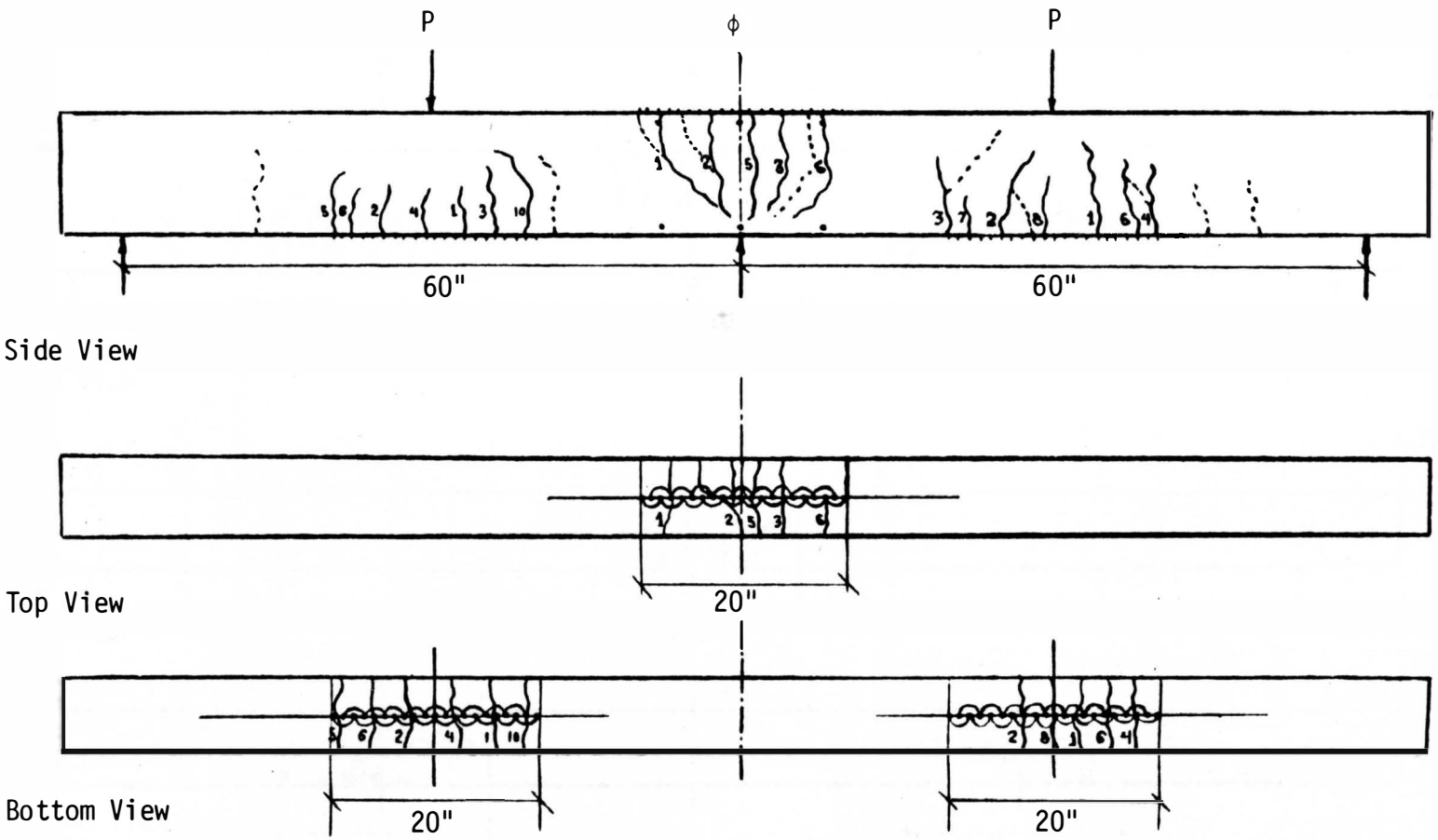

Figure C.3. Crack pattern in Beam No. 3

Initial crack appeared at 6.02 k (0.24 P_u)

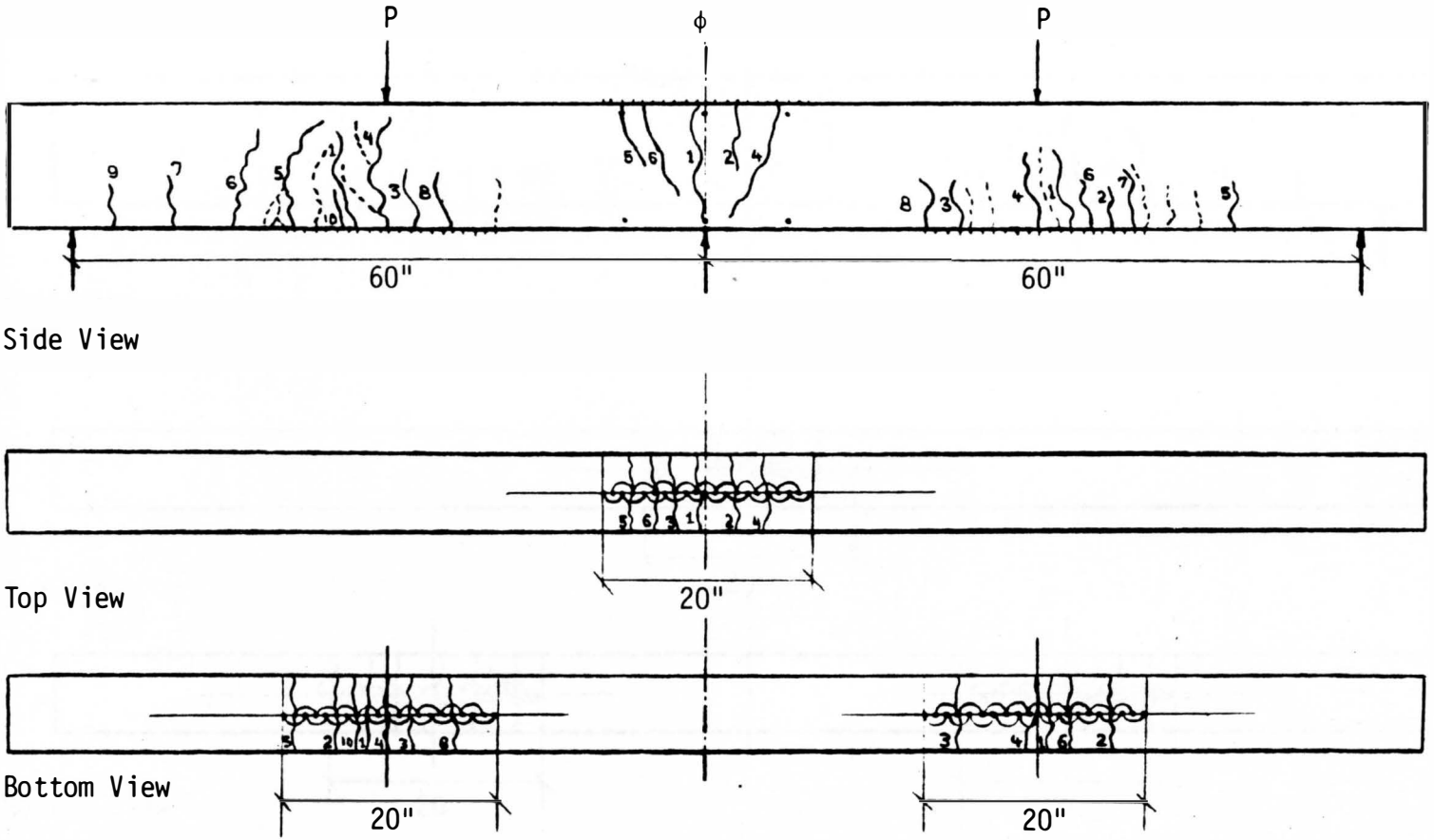

cracks appeared at service load

cracks appeared at ultimate load

Figure C.4. Crack pattern in Beam No. 4.

Initial crack appeared at 7.05 k ($0.22\ P_u$)

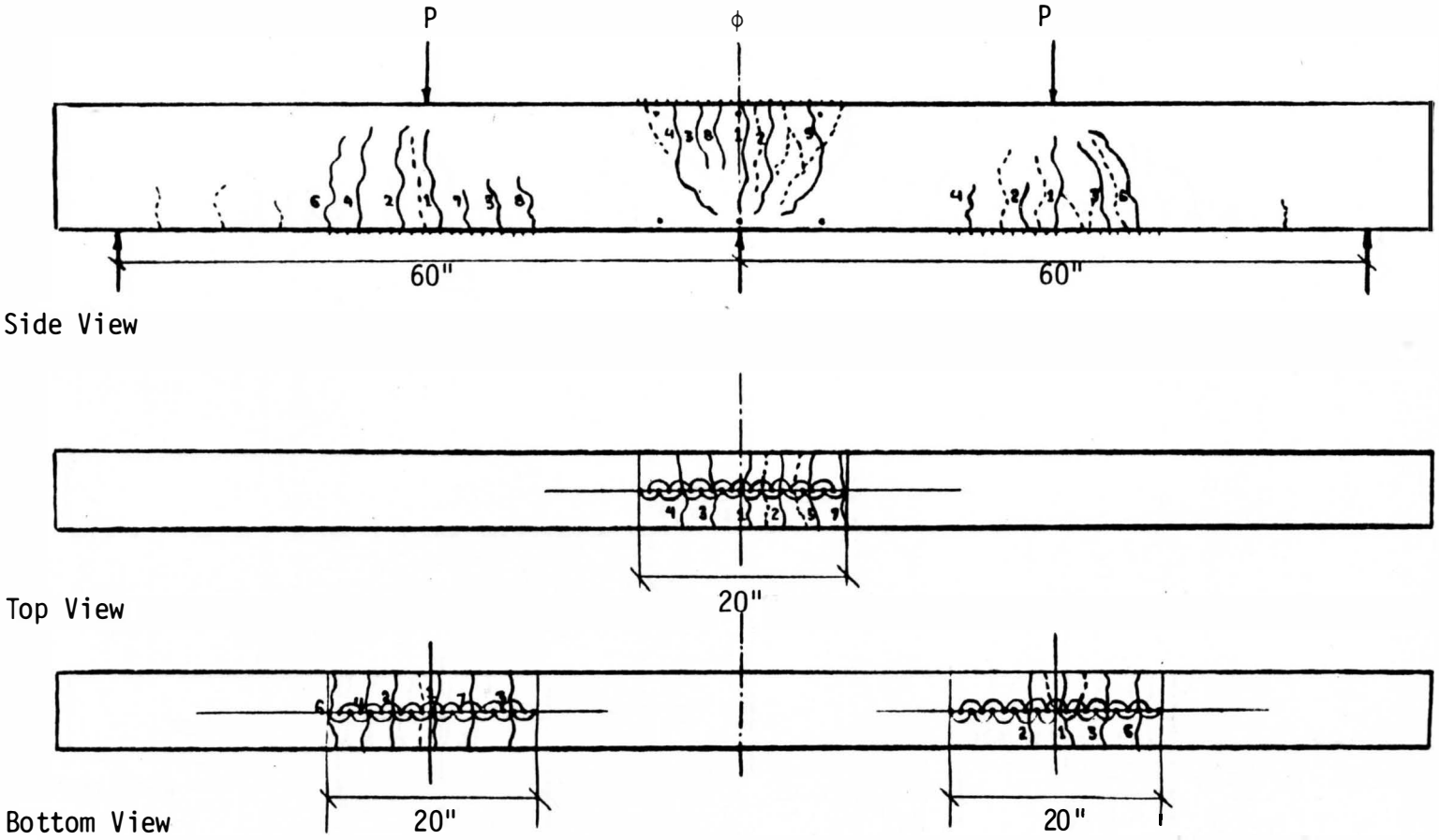

cracks appeared at service load

cracks appeared at ultimate load

Figure C.5. Crack pattern in Beam No. 5.

Initial crack appeared at 7.59 k (0.19 P_u)

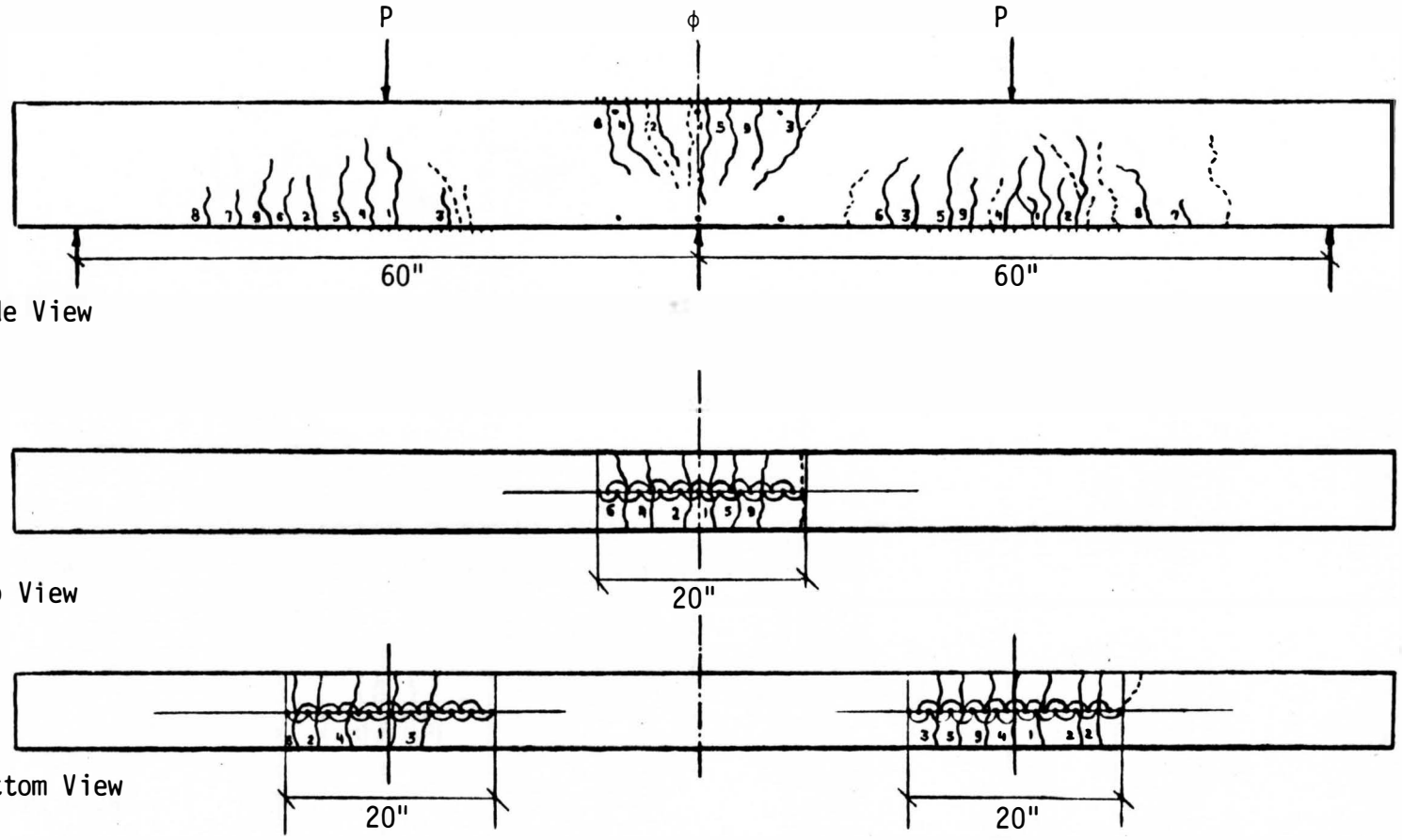

cracks appeared at service load

cracks appeared at ultimate load

Figure C.6. Crack pattern in Beam No. 6.

Initial crack appeared at 8.13 k (0.28 P_u)

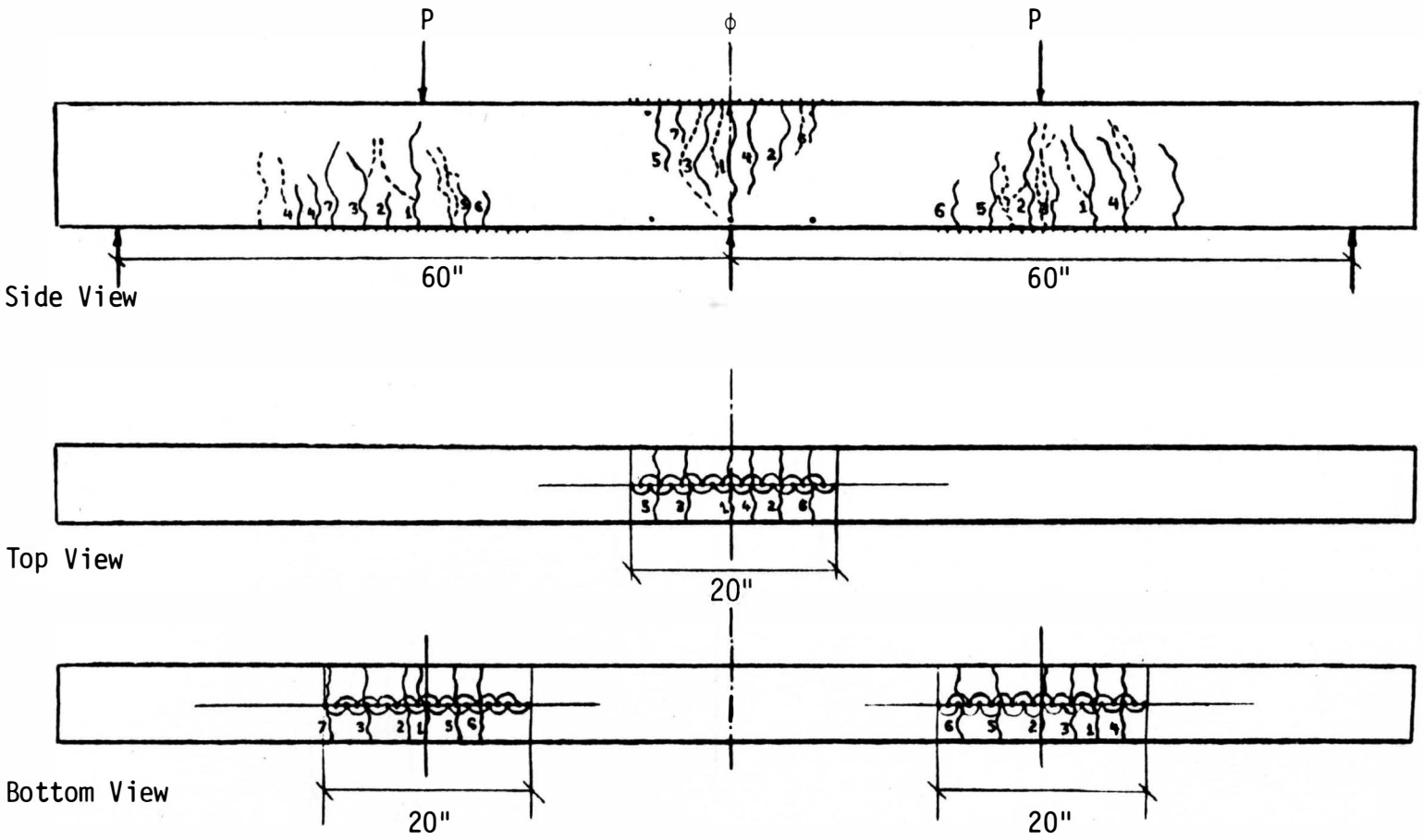

cracks appeared at service load

cracks appeared at ultimate load

Figure C.7. Crack pattern in Beam No. 7.

Initial crack appeared at 8.64 k (0.25 P_u)

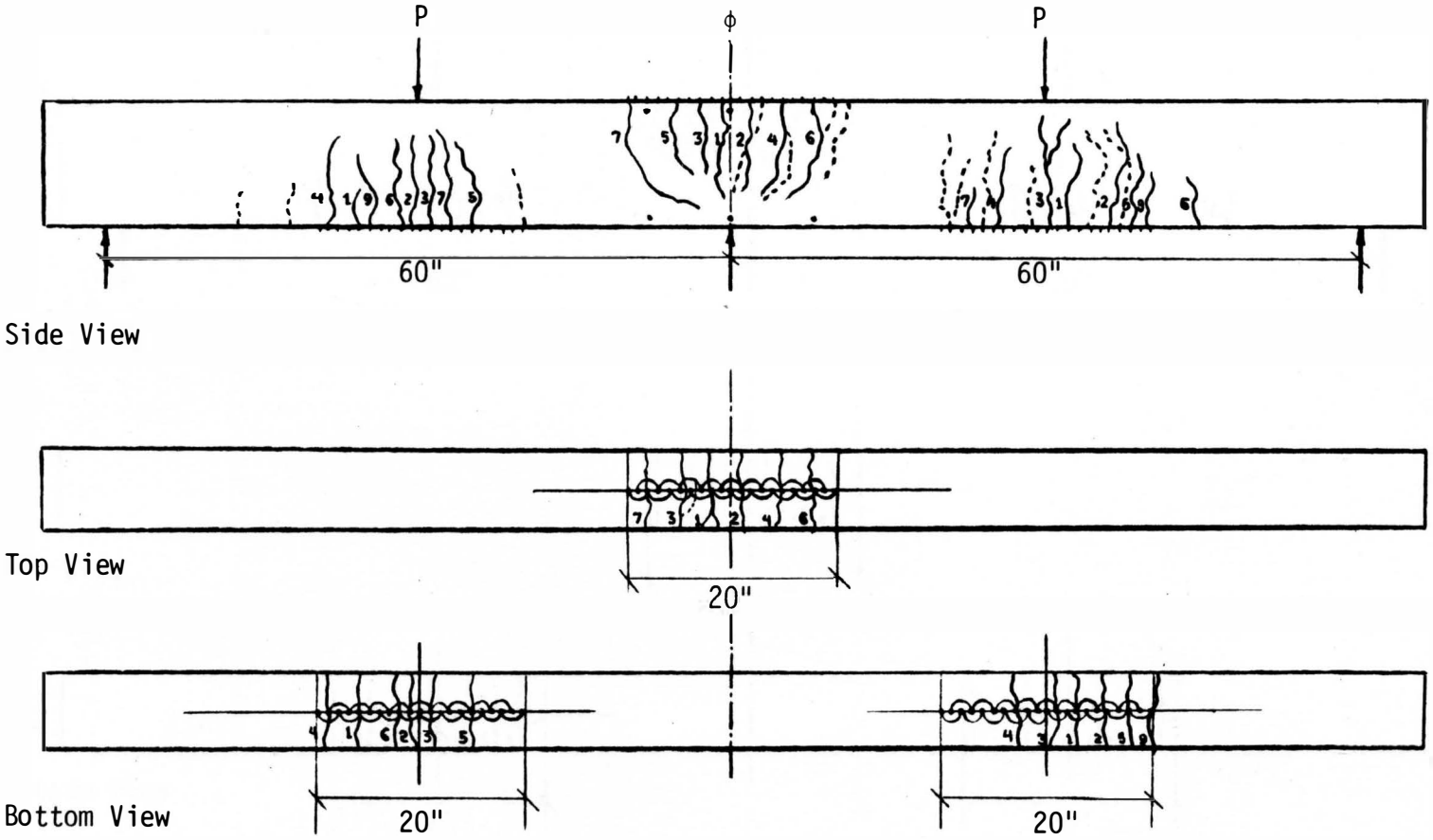

cracks appeared at service load

cracks appeared at ultimate load

Figure C.8. Crack pattern in Beam No. 8.

Initial crack appeared at 9.7 k ($0.22\ P_u$)

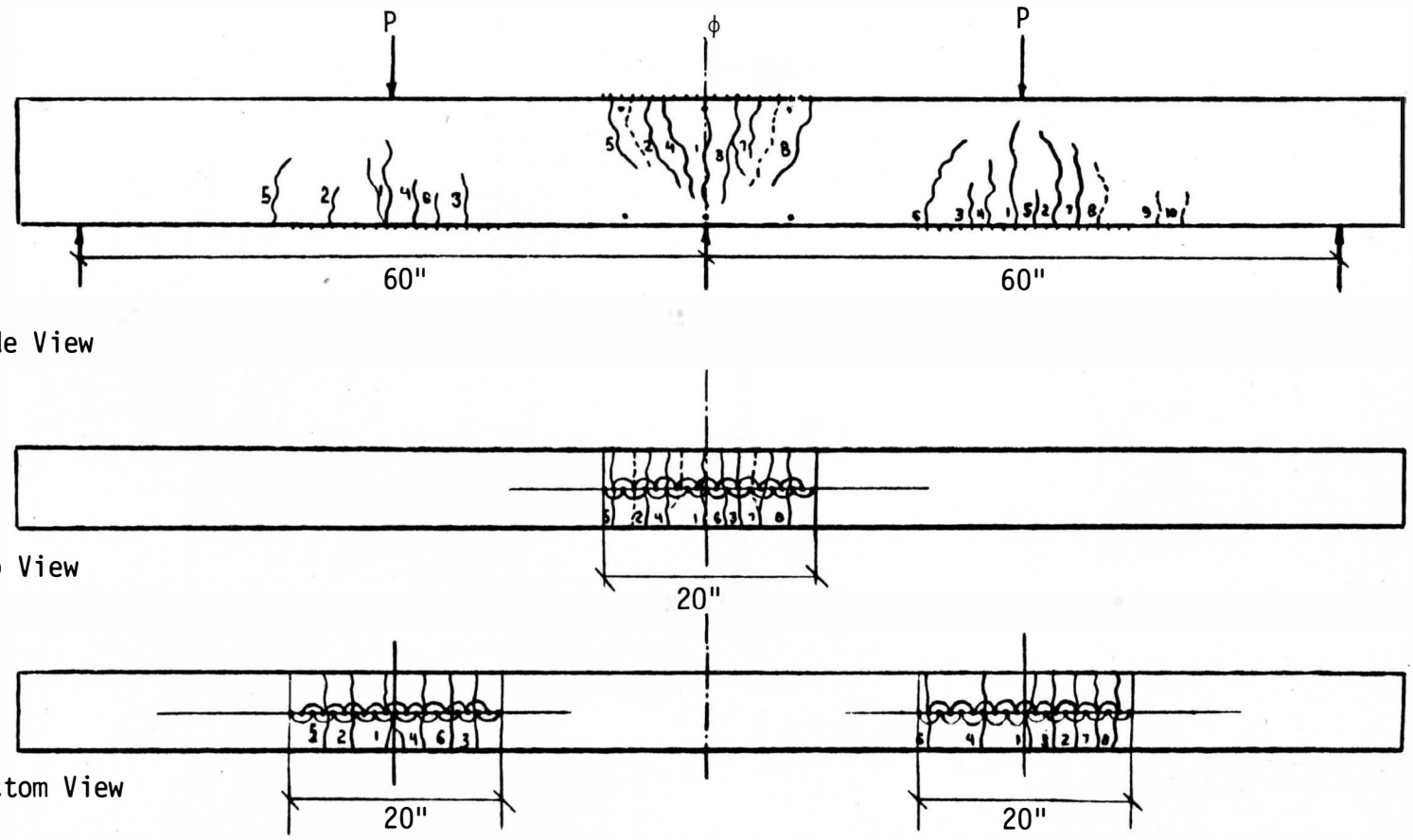

cracks appeared at service load

cracks appeared at ultimate load

Figure C.9. Crack pattern in Beam No. 9.

Appendix D

Statistical Analysis

TABLE D.1

STATISTICAL ANALYSIS FOR MODULUS OF ELASTICITY

DEP VARIABLE: Y

ANALYSIS OF VARIANCE

SOURCE	DF	SUM OF SQUARES	MEAN SQUARE	F VALUE	PROB>F
MODEL	1	0.06224452	0.06224452	35.322	0.0040
ERROR	4	0.007048841	0.001762210		
C TOTAL	5	0.06929336			

ROOT MSE	0.04197869	R-SQUARE	0.8983
DEP MEAN	0.8486	ADJ R-SQ	0.8728
C.V.	4.946817		

PARAMETER ESTIMATES

VARIABLE	DF	PARAMETER ESTIMATE	STANDARD ERROR	T FOR HO: PARAMETER=0	PROB > |T|
INTERCEP	1	0.98470714	0.02860366	34.426	0.0001
X1	1	-0.20416071	0.03435188	-5.943	0.0040

TABLE D.2

STATISTICAL ANALYSIS FOR SPLIT CYLINDER STRENGTH

DEP VARIABLE: Y

ANALYSIS OF VARIANCE

SOURCE	DF	SUM OF SQUARES	MEAN SQUARE	F VALUE	PROB>F
MODEL	1	0.19216563	0.19216563	139.896	0.0003
ERROR	4	0.005494519	0.001373630		
C TOTAL	5	0.19766015			

ROOT MSE	0.03706251	R-SQUARE	0.9722
DEP MEAN	1.182267	ADJ R-SQ	0.9653
C.V.	3.134869		

PARAMETER ESTIMATES

VARIABLE	DF	PARAMETER ESTIMATE	STANDARD ERROR	T FOR HO: PARAMETER=0	PROB > |T|
INTERCEP	1	0.94311786	0.02525384	37.346	0.0001
X1	1	0.35872321	0.03032889	11.828	0.0003

TABLE D.3

STATISTICAL ANALYSIS FOR FIRST MODULUS OF RUPTURE

DEP VARIABLE: Y

ANALYSIS OF VARIANCE

SOURCE	DF	SUM OF SQUARES	MEAN SQUARE	F VALUE	PROB>F
MODEL	1	0.11823002	0.11823002	31.884	0.0048
ERROR	4	0.01483267	0.003708168		
C TOTAL	5	0.13306269			

ROOT MSE	0.06089472	R-SQUARE	0.8885
DEP MEAN	1.133933	ADJ R-SQ	0.8607
C.V.	5.370221		

PARAMETER ESTIMATES

VARIABLE	DF	PARAMETER ESTIMATE	STANDARD ERROR	T FOR HO: PARAMETER=0	PROB > |T|
INTERCEP	1	0.94635000	0.04149276	22.808	0.0001
X1	1	0.28137500	0.04983119	5.647	0.0048

TABLE D.4

STATISTICAL ANALYSIS FOR ULTIMATE MODULUS OF RUPTURE

DEP VARIABLE: Y

ANALYSIS OF VARIANCE

SOURCE	DF	SUM OF SQUARES	MEAN SQUARE	F VALUE	PROB>F
MODEL	1	0.47449711	0.47449711	92.967	0.0006
ERROR	4	0.02041571	0.005103927		
C TOTAL	5	0.49491281			

ROOT MSE	0.07144177	R-SQUARE	0.9587
DEP MEAN	1.339767	ADJ R-SQ	0.9484
C.V.	5.332404		

PARAMETER ESTIMATES

VARIABLE	DF	PARAMETER ESTIMATE	STANDARD ERROR	T FOR HO: PARAMETER=0	PROB > |T|
INTERCEP	1	0.96397500	0.04867936	19.803	0.0001
X1	1	0.56368750	0.05846202	9.642	0.0006

TABLE D.5

STATISTICAL ANALYSIS FOR PLASTIC HINGE LENGTH

MAXIMUM R-SQUARE IMPROVEMENT FOR DEPENDENT VARIABLE Y

STEP 1 VARIABLE X4 ENTERED R SQUARE = 0.95710217
C(P) = 4.74490881

	DF	SUM OF SQUARES	MEAN SQUARE	F	PROB>F
REGRESSION	1	0.36429722	0.36429722	156.18	0.0001
ERROR	7	0.01632800	0.00233257		
TOTAL	8	0.38062522			

	B VALUE	STD ERROR	TYPE II SS	F	PROB>F
INTERCEPT	0.98213858				
X4	0.17760108	0.01421134	0.36429722	156.18	0.0001

BOUNDS ON CONDITION NUMBER: 1, 1

THE ABOVE MODEL IS THE BEST 1 VARIABLE MODEL FOUND.

STEP 2 VARIABLE X2 ENTERED R SQUARE = 0.96397811
C(P) = 5.18293328

	DF	SUM OF SQUARES	MEAN SQUARE	F	PROB>F
REGRESSION	2	0.36691438	0.18345719	80.28	0.0001
ERROR	6	0.01371084	0.00228514		
TOTAL	8	0.38062522			

	B VALUE	STD ERROR	TYPE II SS	F	PROB>F
INTERCEPT	0.93512231				
X2	0.02795412	0.02612087	0.00261715	1.15	0.3257
X4	0.17122841	0.01527463	0.28715930	125.66	0.0001

BOUNDS ON CONDITION NUMBER: 1.179216, 4.716865

THE ABOVE MODEL IS THE BEST 2 VARIABLE MODEL FOUND.

STEP 3 VARIABLE X1 ENTERED R SQUARE = 0.98201809
C(P) = 3.08487023

	DF	SUM OF SQUARES	MEAN SQUARE	F	PROB>F
REGRESSION	3	0.37378085	0.12459362	91.02	0.0001
ERROR	5	0.00684437	0.00136887		
TOTAL	8	0.38062522			

	B VALUE	STD ERROR	TYPE II SS	F	PROB>F
INTERCEPT	0.81861079				
X1	0.17476729	0.07803240	0.00686647	5.02	0.0752
X2	0.08080368	0.03107309	0.00925671	6.76	0.0482
X4	0.09195407	0.03731757	0.00831148	6.07	0.0569

BOUNDS ON CONDITION NUMBER: 11.74973, 73.4984

THE ABOVE MODEL IS THE BEST 3 VARIABLE MODEL FOUND.

STEP 4 VARIABLE X3 ENTERED R SQUARE = 0.98239170
C(P) = 5.00000000

	DF	SUM OF SQUARES	MEAN SQUARE	F	PROB>F
REGRESSION	4	0.37392306	0.09348076	55.79	0.0009
ERROR	4	0.00670216	0.00167554		
TOTAL	8	0.38062522			

	B VALUE	STD ERROR	TYPE II SS	F	PROB>F
INTERCEPT	0.80123322				
X1	0.17476729	0.08633181	0.00686647	4.10	0.1129
X2	0.09271555	0.05342025	0.00504718	3.01	0.1576
X3	-0.01874292	0.06433683	0.00014220	0.08	0.7853
X4	0.09195407	0.04128661	0.00831148	4.96	0.0899

BOUNDS ON CONDITION NUMBER: 11.74973, 133.524

THE ABOVE MODEL IS THE BEST 4 VARIABLE MODEL FOUND.

TABLE D.6

STATISTICAL ANALYSIS FOR CURVATURE DISTRIBUTION FACTOR

MAXIMUM R-SQUARE IMPROVEMENT FOR DEPENDENT VARIABLE Y

STEP 1 VARIABLE X4 ENTERED R SQUARE = 0.94072233
C(P) = 9.47458307

	DF	SUM OF SQUARES	MEAN SQUARE	F	PROB>F
REGRESSION	1	0.23169266	0.23169266	111.09	0.0001
ERROR	7	0.01459963	0.00208566		
TOTAL	8	0.24629230			

	B VALUE	STD ERROR	TYPE II SS	F	PROB>F
INTERCEPT	0.98525211				
X4	-0.14163605	0.01343815	0.23169266	111.09	0.0001

BOUNDS ON CONDITION NUMBER: 1, 1

THE ABOVE MODEL IS THE BEST 1 VARIABLE MODEL FOUND.

STEP 2 VARIABLE X5 ENTERED R SQUARE = 0.97464207
C(P) = 3.19196963

	DF	SUM OF SQUARES	MEAN SQUARE	F	PROB>F
REGRESSION	2	0.24004683	0.12002342	115.31	0.0001
ERROR	6	0.00624546	0.00104091		
TOTAL	8	0.24629230			

	B VALUE	STD ERROR	TYPE II SS	F	PROB>F
INTERCEPT	1.00085246				
X4	-0.17132620	0.01414069	0.15279864	146.79	0.0001
X5	0.10645483	0.03757686	0.00835417	8.03	0.0298

BOUNDS ON CONDITION NUMBER: 2.21867, 8.87468

THE ABOVE MODEL IS THE BEST 2 VARIABLE MODEL FOUND.

STEP 3 VARIABLE X3 ENTERED R SQUARE = 0.98561789
C(P) = 2.51186321

	DF	SUM OF SQUARES	MEAN SQUARE	F	PROB>F
REGRESSION	3	0.24275009	0.08091670	114.22	0.0001
ERROR	5	0.00354220	0.00070844		
TOTAL	8	0.24629230			

	B VALUE	STD ERROR	TYPE II SS	F	PROB>F
INTERCEPT	1.01985001				
X3	-0.06049287	0.03096791	0.00270326	3.82	0.1082
X4	-0.18239618	0.01296945	0.14011722	197.78	0.0001
X5	0.17757151	0.04781686	0.00976985	13.79	0.0138

BOUNDS ON CONDITION NUMBER: 5.278662, 32.18485

THE ABOVE MODEL IS THE BEST 3 VARIABLE MODEL FOUND.

TABLE D.6 (Continued)

STATISTICAL ANALYSIS FOR CURVATURE DISTRIBUTION FACTOR

MAXIMUM R-SQUARE IMPROVEMENT FOR DEPENDENT VARIABLE Y

STEP 4 VARIABLE X2 ENTERED R SQUARE = 0.98624809
C(P) = 4.35797797

	DF	SUM OF SQUARES	MEAN SQUARE	F	PROB>F
REGRESSION	4	0.24290531	0.06072633	71.72	0.0006
ERROR	4	0.00338699	0.00084675		
TOTAL	8	0.24629230			

	B VALUE	STD ERROR	TYPE II SS	F	PROB>F
INTERCEPT	1.04071781				
X2	-0.01456242	0.03401293	0.00015521	0.18	0.6906
X3	-0.04029463	0.05806754	0.00040774	0.48	0.5259
X4	-0.18055363	0.01481776	0.12571906	148.47	0.0003
X5	0.17237551	0.05366668	0.00873565	10.32	0.0325

BOUNDS ON CONDITION NUMBER: 7.964218, 87.67259

STEP 4 X3 REPLACED BY X1 R SQUARE = 0.98767695
C(P) = 4.00907670

	DF	SUM OF SQUARES	MEAN SQUARE	F	PROB>F
REGRESSION	4	0.24325722	0.06081431	80.15	0.0005
ERROR	4	0.00303507	0.00075877		
TOTAL	8	0.24629230			

	B VALUE	STD ERROR	TYPE II SS	F	PROB>F
INTERCEPT	1.09371748				
X1	-0.07553683	0.07549279	0.00075965	1.00	0.3737
X2	-0.04726571	0.02313435	0.00316728	4.17	0.1106
X4	-0.13421500	0.04317296	0.00733310	9.66	0.0359
X5	0.11620759	0.05199548	0.00379007	5.00	0.0891

BOUNDS ON CONDITION NUMBER: 28.3713, 215.2375

THE ABOVE MODEL IS THE BEST 4 VARIABLE MODEL FOUND.

STEP 5 VARIABLE X3 ENTERED R SQUARE = 0.98771412
C(P) = 6.00000000

	DF	SUM OF SQUARES	MEAN SQUARE	F	PROB>F
REGRESSION	5	0.24326638	0.04865328	48.24	0.0046
ERROR	3	0.00302592	0.00100864		
TOTAL	8	0.24629230			

	B VALUE	STD ERROR	TYPE II SS	F	PROB>F
INTERCEPT	1.08635822				
X1	-0.06846062	0.11442282	0.00036107	0.36	0.5918
X2	-0.04222114	0.05928813	0.00051152	0.51	0.5278
X3	-0.00793748	0.08331406	0.00000916	0.01	0.9301
X4	-0.13906556	0.07120274	0.00384753	3.81	0.1458
X5	0.12383977	0.10005695	0.00154512	1.53	0.3039

BOUNDS ON CONDITION NUMBER: 58.05267, 654.4496

THE ABOVE MODEL IS THE BEST 5 VARIABLE MODEL FOUND.

NO FURTHER IMPROVEMENT IN R-SQUARE IS POSSIBLE.

TABLE D.7

STATISTICAL ANALYSIS FOR DUCTITILITY INDEX

MAXIMUM R-SQUARE IMPROVEMENT FOR DEPENDENT VARIABLE Y

STEP 4 VARIABLE X2 ENTERED R SQUARE = 0.96608546
C(P) = 4.68668552

	DF	SUM OF SQUARES	MEAN SQUARE	F	PROB>F
REGRESSION	4	50.69941334	12.67485334	28.49	0.0034
ERROR	4	1.77980888	0.44495222		
TOTAL	8	52.47922222			

	B VALUE	STD ERROR	TYPE II SS	F	PROB>F
INTERCEPT	1.46526371				
X1	11.41688289	1.82813223	17.35374686	39.00	0.0034
X2	-0.17216178	0.56022104	0.04202116	0.09	0.7739
X4	-4.59473380	1.04547577	8.59421363	19.31	0.0117
X5	5.38087460	1.25912174	8.12612832	18.26	0.0129

BOUNDS ON CONDITION NUMBER: 28.3713, 215.2375

THE ABOVE MODEL IS THE BEST 4 VARIABLE MODEL FOUND.

STEP 5 VARIABLE X3 ENTERED R SQUARE = 0.97240241
C(P) = 6.00000000

	DF	SUM OF SQUARES	MEAN SQUARE	F	PROB>F
REGRESSION	5	51.03092222	10.20618444	21.14	0.0152
ERROR	3	1.44830000	0.48276667		
TOTAL	8	52.47922222			

	B VALUE	STD ERROR	TYPE II SS	F	PROB>F
INTERCEPT	2.86565558				
X1	10.07035225	2.50330262	7.81267738	16.18	0.0276
X2	-1.13209393	1.29708499	0.36776071	0.76	0.4470
X3	1.51042074	1.82271596	0.33150888	0.69	0.4681
X4	-3.67172211	1.55774869	2.68214405	5.56	0.0997
X5	3.92854697	2.18901107	1.55491002	3.22	0.1706

BOUNDS ON CONDITION NUMBER: 58.05267, 654.4496

THE ABOVE MODEL IS THE BEST 5 VARIABLE MODEL FOUND.

NO FURTHER IMPROVEMENT IN R-SQUARE IS POSSIBLE.

TABLE D.7 (Continued)

STATISTICAL ANALYSIS FOR DUCTITILITY INDEX

MAXIMUM R-SQUARE IMPROVEMENT FOR DEPENDENT VARIABLE Y

STEP 1 VARIABLE X1 ENTERED R SQUARE = 0.71667753
C(P) = 25.79861118

	DF	SUM OF SQUARES	MEAN SQUARE	F	PROB>F
REGRESSION	1	37.61067937	37.61067937	17.71	0.0040
ERROR	7	14.86854286	2.12407755		
TOTAL	8	52.47922222			

	B VALUE	STD ERROR	TYPE II SS	F	PROB>F
INTERCEPT	1.12380952				
X1	4.09761905	0.97378073	37.61067937	17.71	0.0040

BOUNDS ON CONDITION NUMBER: 1, 1

THE ABOVE MODEL IS THE BEST 1 VARIABLE MODEL FOUND.

STEP 2 VARIABLE X4 ENTERED R SQUARE = 0.81044006
C(P) = 17.60614174

	DF	SUM OF SQUARES	MEAN SQUARE	F	PROB>F
REGRESSION	2	42.53126386	21.26563193	12.83	0.0068
ERROR	6	9.94795836	1.65799306		
TOTAL	8	52.47922222			

	B VALUE	STD ERROR	TYPE II SS	F	PROB>F
INTERCEPT	1.12380952				
X1	6.75630755	1.76690451	24.24238648	14.62	0.0087
X4	-1.34051521	0.77813465	4.92058450	2.97	0.1357

BOUNDS ON CONDITION NUMBER: 4.217853, 16.87141

THE ABOVE MODEL IS THE BEST 2 VARIABLE MODEL FOUND.

STEP 3 VARIABLE X5 ENTERED R SQUARE = 0.96528474
C(P) = 2.77372789

	DF	SUM OF SQUARES	MEAN SQUARE	F	PROB>F
REGRESSION	3	50.65739219	16.88579740	46.34	0.0005
ERROR	5	1.82183004	0.36436601		
TOTAL	8	52.47922222			

	B VALUE	STD ERROR	TYPE II SS	F	PROB>F
INTERCEPT	1.12380952				
X1	11.74520422	1.34241863	27.89221849	76.55	0.0003
X4	-4.76027397	0.81082923	12.55865000	34.47	0.0020
X5	5.38087460	1.13940983	8.12612832	22.30	0.0052

BOUNDS ON CONDITION NUMBER: 20.83942, 113.2369

THE ABOVE MODEL IS THE BEST 3 VARIABLE MODEL FOUND.

TABLE D.8

STATISTICAL ANALYSIS FOR PLASTIC ROTATION CAPACITY

MAXIMUM R-SQUARE IMPROVEMENT FOR DEPENDENT VARIABLE Y

STEP 1 VARIABLE X1 ENTERED R SQUARE = 0.67446250
C(P) = 229.67160594

	DF	SUM OF SQUARES	MEAN SQUARE	F	PROB>F
REGRESSION	1	1378669.84126984	1378669.84127	14.50	0.0066
ERROR	7	665431.71428572	95061.67347		
TOTAL	8	2044101.55555556			

	B VALUE	STD ERROR	TYPE II SS	F	PROB>F
INTERCEPT	149.76190476				
X1	784.52380952	206.00545402	1378669.84127	14.50	0.0066

BOUNDS ON CONDITION NUMBER: 1, 1

THE ABOVE MODEL IS THE BEST 1 VARIABLE MODEL FOUND.

STEP 2 VARIABLE X4 ENTERED R SQUARE = 0.85122586
C(P) = 104.24744469

	DF	SUM OF SQUARES	MEAN SQUARE	F	PROB>F
REGRESSION	2	1739992.11425450	869996.057127	17.16	0.0033
ERROR	6	304109.44130105	50684.906884		
TOTAL	8	2044101.55555556			

	B VALUE	STD ERROR	TYPE II SS	F	PROB>F
INTERCEPT	149.7619048				
X1	1504.9781742	308.93068798	1202865.17958	23.73	0.0028
X4	-363.2543015	136.05130925	361322.27298	7.13	0.0370

BOUNDS ON CONDITION NUMBER: 4.217853, 16.87141

THE ABOVE MODEL IS THE BEST 2 VARIABLE MODEL FOUND.

STEP 3 VARIABLE X5 ENTERED R SQUARE = 0.99422866
C(P) = 3.16040918

	DF	SUM OF SQUARES	MEAN SQUARE	F	PROB>F
REGRESSION	3	2032304.35409035	677434.784697	287.12	0.0001
ERROR	5	11797.20146521	2359.440293		
TOTAL	8	2044101.55555556			

	B VALUE	STD ERROR	TYPE II SS	F	PROB>F
INTERCEPT	149.7619048				
X1	2451.1852075	108.02481700	1214826.24942	514.88	0.0001
X4	-1011.8545838	65.24766377	567433.88462	240.50	0.0001
X5	1020.5505796	91.68863962	292312.23984	123.89	0.0001

BOUNDS ON CONDITION NUMBER: 20.83942, 113.2369

THE ABOVE MODEL IS THE BEST 3 VARIABLE MODEL FOUND.

STEP 4 VARIABLE X7 ENTERED R SQUARE = 0.99479650
C(P) = 4.75107088

	DF	SUM OF SQUARES	MEAN SQUARE	F	PROB>F
REGRESSION	4	2033465.06837606	508366.267094	191.18	0.0001
ERROR	4	10636.48717949	2659.121795		
TOTAL	8	2044101.55555556			

	B VALUE	STD ERROR	TYPE II SS	F	PROB>F
INTERCEPT	-604.7023810				
X1	2414.4924482	127.42037533	954799.476908	359.07	0.0001
X4	-981.2772844	83.30634508	368948.338217	138.75	0.0003
X5	948.6939259	145.95737634	112341.022774	42.25	0.0029
X7	11.6071429	17.56838255	1160.714286	0.44	0.5449

BOUNDS ON CONDITION NUMBER: 30.14273, 238.8344

THE ABOVE MODEL IS THE BEST 4 VARIABLE MODEL FOUND.

TABLE D.8 (Continued)

STATISTICAL ANALYSIS FOR PLASTIC ROTATION CAPACITY

MAXIMUM R-SQUARE IMPROVEMENT FOR DEPENDENT VARIABLE Y

STEP 5 VARIABLE X6 ENTERED R SQUARE = 0.99521999
C(P) = 6.44578707

	DF	SUM OF SQUARES	MEAN SQUARE	F	PROB>F
REGRESSION	5	2034330.72713928	406866.145428	124.92	0.0011
ERROR	3	9770.82841628	3256.942805		
TOTAL	8	2044101.55555556			

	B VALUE	STD ERROR	TYPE II SS	F	PROB>F
INTERCEPT	-1013.8564598				
X1	2348.4219975	190.55199905	494692.576263	151.89	0.0012
X4	-935.5224667	127.97166673	174056.771032	53.44	0.0053
X5	901.0953970	186.05681090	76394.224957	23.46	0.0168
X6	1.1217521	2.17584824	865.658763	0.27	0.6418
X7	17.3318846	22.39065536	1951.497953	0.60	0.4953

BOUNDS ON CONDITION NUMBER: 58.07406, 536.8273

STEP 5 X5 REPLACED BY X2 R SQUARE = 0.99710744
C(P) = 5.08517378

	DF	SUM OF SQUARES	MEAN SQUARE	F	PROB>F
REGRESSION	5	2038188.86424334	407637.772849	206.83	0.0005
ERROR	3	5912.69131221	1970.897104		
TOTAL	8	2044101.55555556			

	B VALUE	STD ERROR	TYPE II SS	F	PROB>F
INTERCEPT	-6297.1268276				
X1	3765.1700252	353.31732625	223822.254560	113.56	0.0018
X2	3808.7639786	596.88013461	80252.362061	40.72	0.0078
X4	-925.6764083	96.13513042	182733.470609	92.72	0.0024
X6	145.7470140	21.89445056	87336.378823	44.31	0.0069
X7	-91.0839225	32.38883758	15586.789790	7.91	0.0672

BOUNDS ON CONDITION NUMBER: 713.9066, 7324.69

THE ABOVE MODEL IS THE BEST 5 VARIABLE MODEL FOUND.

STEP 6 VARIABLE X5 ENTERED R SQUARE = 0.99722559
C(P) = 7.00000000

	DF	SUM OF SQUARES	MEAN SQUARE	F	PROB>F
REGRESSION	6	2038430.38190324	339738.396984	119.81	0.0083
ERROR	2	5671.17365232	2835.586826		
TOTAL	8	2044101.55555556			

	B VALUE	STD ERROR	TYPE II SS	F	PROB>F
INTERCEPT	-5223.8381969				
X1	3507.2745068	980.0389182	36315.817295	12.81	0.0700
X2	3088.7709511	2568.8191864	4099.654764	1.45	0.3522
X4	-934.7274658	119.4089537	173755.744803	61.28	0.0159
X5	181.7907849	622.9008072	241.517660	0.09	0.7979
X6	118.3411970	97.5083147	4176.683491	1.47	0.3488
X7	-71.7027741	76.9378108	2462.834437	0.87	0.4497

BOUNDS ON CONDITION NUMBER: 9190.841, 106539.5

THE ABOVE MODEL IS THE BEST 6 VARIABLE MODEL FOUND.

NO FURTHER IMPROVEMENT IN R-SQUARE IS POSSIBLE.

TABLE D.9

STATISTICAL ANALYSIS FOR EFFECTIVE MOMENT OF INERTIA

MAXIMUM R-SQUARE IMPROVEMENT FOR DEPENDENT VARIABLE Y

STEP 1 VARIABLE X2 ENTERED R SQUARE = 0.92752373
C(P) = 1.11705731

	DF	SUM OF SQUARES	MEAN SQUARE	F	PROB>F
REGRESSION	1	0.42099271	0.42099271	89.58	0.0001
ERROR	7	0.03289617	0.00469945		
TOTAL	8	0.45388889			

	B VALUE	STD ERROR	TYPE II SS	F	PROB>F
INTERCEPT	1.03655738				
X2	0.36714481	0.03879036	0.42099271	89.58	0.0001

BOUNDS ON CONDITION NUMBER: 1, 1

THE ABOVE MODEL IS THE BEST 1 VARIABLE MODEL FOUND.

STEP 2 VARIABLE X1 ENTERED R SQUARE = 0.92891065
C(P) = 3.00000000

	DF	SUM OF SQUARES	MEAN SQUARE	F	PROB>F
REGRESSION	2	0.42162222	0.21081111	39.20	0.0004
ERROR	6	0.03226667	0.00537778		
TOTAL	8	0.45388889			

	B VALUE	STD ERROR	TYPE II SS	F	PROB>F
INTERCEPT	1.03000000				
X1	0.06666667	0.19485407	0.00062951	0.12	0.7439
X2	0.31250000	0.16501886	0.01928571	3.59	0.1071

BOUNDS ON CONDITION NUMBER: 15.81481, 63.25926

THE ABOVE MODEL IS THE BEST 2 VARIABLE MODEL FOUND.

TABLE D.10

STATISTICAL ANALYSIS FOR EFFECTIVE MOMENT OF INERTIA
OF THIS RESEARCH DATA AND DATA REPORTED BY SAHIBJAM REF.(50)

MAXIMUM R-SQUARE IMPROVEMENT FOR DEPENDENT VARIABLE Y

STEP 1 VARIABLE X3 ENTERED — R SQUARE = 0.88933744, C(P) = 11.33737819

	DF	SUM OF SQUARES	MEAN SQUARE	F	PROB>F
REGRESSION	1	0.56936429	0.56936429	120.55	0.0001
ERROR	15	0.07084747	0.00472316		
TOTAL	16	0.64021176			

	B VALUE	STD ERROR	TYPE II SS	F	PROB>F
INTERCEPT	1.04807508				
X3	0.31727569	0.02889736	0.56936429	120.55	0.0001

BOUNDS ON CONDITION NUMBER: 1, 1

THE ABOVE MODEL IS THE BEST 1 VARIABLE MODEL FOUND.

STEP 2 VARIABLE X4 ENTERED — R SQUARE = 0.93430482, C(P) = 3.44796199

	DF	SUM OF SQUARES	MEAN SQUARE	F	PROB>F
REGRESSION	2	0.59815294	0.29907647	99.55	0.0001
ERROR	14	0.04205883	0.00300420		
TOTAL	16	0.64021176			

	B VALUE	STD ERROR	TYPE II SS	F	PROB>F
INTERCEPT	1.05028521				
X3	0.25956678	0.02964246	0.23035565	76.68	0.0001
X4	0.09607920	0.03103726	0.02878864	9.58	0.0079

BOUNDS ON CONDITION NUMBER: 1.654306, 6.617226

THE ABOVE MODEL IS THE BEST 2 VARIABLE MODEL FOUND.

STEP 3 VARIABLE X1 ENTERED — R SQUARE = 0.94305411, C(P) = 3.52378030

	DF	SUM OF SQUARES	MEAN SQUARE	F	PROB>F
REGRESSION	3	0.60375434	0.20125145	71.76	0.0001
ERROR	13	0.03645743	0.00280442		
TOTAL	16	0.64021176			

	B VALUE	STD ERROR	TYPE II SS	F	PROB>F
INTERCEPT	1.03666667				
X1	0.14281491	0.10105238	0.00560140	2.00	0.1811
X3	0.13911235	0.08991388	0.00671306	2.39	0.1458
X4	0.09911304	0.03006423	0.03047924	10.87	0.0058

BOUNDS ON CONDITION NUMBER: 16.30525, 99.55251

THE ABOVE MODEL IS THE BEST 3 VARIABLE MODEL FOUND.

STEP 4 VARIABLE X2 ENTERED — R SQUARE = 0.94543575, C(P) = 5.00000000

	DF	SUM OF SQUARES	MEAN SQUARE	F	PROB>F
REGRESSION	4	0.60527909	0.15131977	51.98	0.0001
ERROR	12	0.03493267	0.00291106		
TOTAL	16	0.64021176			

	B VALUE	STD ERROR	TYPE II SS	F	PROB>F
INTERCEPT	1.05093915				
X1	0.14399250	0.10296858	0.00569273	1.96	0.1873
X2	-0.02854497	0.03944165	0.00152475	0.52	0.4831
X3	0.12527557	0.09358124	0.00521682	1.79	0.2055
X4	0.12384259	0.04588898	0.02120185	7.28	0.0194

BOUNDS ON CONDITION NUMBER: 17.01546, 152.9229

THE ABOVE MODEL IS THE BEST 4 VARIABLE MODEL FOUND.

TABLE D.11

STATISTICAL ANALYSIS FOR MAXIMUM CRACK WIDTH

MAXIMUM R-SQUARE IMPROVEMENT FOR DEPENDENT VARIABLE Y

STEP 1 VARIABLE X1 ENTERED R SQUARE = 0.80995845
C(P) = 5.49600484

	DF	SUM OF SQUARES	MEAN SQUARE	F	PROB>F
REGRESSION	1	0.23579139	0.23579139	68.19	0.0001
ERROR	16	0.05532403	0.00345775		
TOTAL	17	0.29111542			

	B VALUE	STD ERROR	TYPE II SS	F	PROB>F
INTERCEPT	0.95641667				
X1	-0.22941667	0.02778164	0.23579139	68.19	0.0001

BOUNDS ON CONDITION NUMBER: 1, 1

THE ABOVE MODEL IS THE BEST 1 VARIABLE MODEL FOUND.

STEP 2 VARIABLE X3 ENTERED R SQUARE = 0.85892998
C(P) = 2.47210777

	DF	SUM OF SQUARES	MEAN SQUARE	F	PROB>F
REGRESSION	2	0.25004776	0.12502388	45.67	0.0001
ERROR	15	0.04106766	0.00273784		
TOTAL	17	0.29111542			

	B VALUE	STD ERROR	TYPE II SS	F	PROB>F
INTERCEPT	0.95641667				
X1	-0.33060922	0.05077046	0.11609579	42.40	0.0001
X3	0.05102146	0.02235902	0.01425637	5.21	0.0375

BOUNDS ON CONDITION NUMBER: 4.217853, 16.87141

THE ABOVE MODEL IS THE BEST 2 VARIABLE MODEL FOUND.

STEP 3 VARIABLE X2 ENTERED R SQUARE = 0.86353195
C(P) = 4.00000000

	DF	SUM OF SQUARES	MEAN SQUARE	F	PROB>F
REGRESSION	3	0.25138746	0.08379582	29.53	0.0001
ERROR	14	0.03972795	0.00283771		
TOTAL	17	0.29111542			

	B VALUE	STD ERROR	TYPE II SS	F	PROB>F
INTERCEPT	0.99952767				
X1	-0.37206210	0.07944423	0.06224068	21.93	0.0004
X2	-0.02173664	0.03163529	0.00133971	0.47	0.5032
X3	0.07192207	0.03799275	0.01016930	3.58	0.0792

BOUNDS ON CONDITION NUMBER: 11.74973, 73.4984

THE ABOVE MODEL IS THE BEST 3 VARIABLE MODEL FOUND.

Appendix E

Calibration of RAM vs. Testing Machine

TABLE E.1

CALIBRATION OF RAM VS. TESTING MACHINE

Observation	Ram Pressure (psi)	Average Machine Load Jack (1) (lbs)	Average Machine Load Jack (2) (lbs)	% Error	Average Machine Reading
1	0	0	0	0	0
2	100	1035	1005	2.98	1020
3	200	2025	2055	1.46	2040
4	300	3018	3042	0.79	3030
5	400	3990	3930	1.53	3960
6	500	4995	4945	1.01	4970
7	600	6000	6040	0.66	6020
8	700	7080	7020	0.85	7050
9	800	8145	8115	0.37	8130
10	900	9140	9180	0.44	9160
11	1000	10260	10200	0.59	10230
12	1100	11265	11315	0.44	11290
13	1200	12400	12440	0.32	12420
14	1300	13390	13470	0.59	13430
15	1400	14530	14430	0.69	14480
16	1500	15580	15480	0.65	15530
17	1600	16570	16690	0.72	16630
18	1700	17770	17670	0.57	17720
19	1800	18810	18910	0.53	18860
20	1900	19880	20000	0.6	19940
21	2000	20870	20750	0.58	20810
22	2500	25810	26030	0.85	25920
23	3000	31400	31160	0.77	31280
24	3500	36960	36640	0.87	36800
25	4000	42100	42460	0.85	42280
26	4500	47280	47612	0.91	47446